UNIVERSITY OF SOUTHAMPTON

FACULTY OF ENGINEERING, SCIENCE & MATHEMATICS

School of Chemistry

Studies of Stability and Catalytic Activity of Lead Dioxide Electrodes

by

Yusairie Mohd

Thesis for the degree of Doctor of Philosophy

March 2006

UNIVERSITY OF SOUTHAMPTON

ABSTRACT

FACULTY OF ENGINEERING, SCIENCE & MATHEMATICS

SCHOOL OF CHEMISTRY

Doctor of Philosophy

STUDIES OF STABILITY AND CATALYTIC ACTIVITY OF LEAD DIOXIDE ELECTRODES

by Yusairie Mohd

The electrodeposition of stable and active, thick layers of pure and doped β-lead dioxide (PbO_2) coatings from acidic nitrate baths onto gold and titanium substrates has been investigated. The morphology of the coatings has been analysed by Scanning Electron Microscopy (SEM) and the composition determined by Energy Dispersive X-ray Analysis (EDAX). In addition, the behaviour of the coated electrodes as anodes (using dimethylsulfoxide, DMSO, as a model substrate) and on open circuit has been defined.

The structure and morphology of the β-PbO_2 deposits on both Au and Ti substrates depend strongly on the deposition conditions including temperature, current density, deposition charge and the bath composition (Pb(II) concentration, H^+ concentration, concentration and choice of dopant ions). Satisfactory deposits on Ti require pre-etching of the Ti surface and very careful selection of the deposition conditions to avoid the presence of resistive TiO_2 layers. It was confirmed the activity of the β-PbO_2 electrodes for the oxidation of organic compounds was significantly enhanced by the incorporation of bismuth. Bi-PbO_2 on Au was easily produced but on Ti it required a strategy involving the deposition of two layers. The procedures could be employed to produce uniform coatings on fine Ti meshes, a first stage in the design of three dimensional PbO_2 electrodes. The preferred coating on the Ti meshes was produced by the deposition of (a) an underlayer of Fe-F-PbO_2 onto etched Ti using 5 mA cm^{-2} for 1800 s from 0.5 M $Pb(NO_3)_2$ + 0.1 M HNO_3 + 0.04 M NaF + 10 mM $Fe(NO_3)_3$ (b) a top layer of Bi-PbO_2 using a low current density ~ 0.5 mA cm^{-2} from 0.5 M $Pb(NO_3)_2$ + 1 M HNO_3 + 10 mM $Bi(NO_3)_3$. The coated Ti meshes were demonstrated to be suitable for the anodic decolouration of dyes (reactive blue 4, methyl orange, bromothymol blue and cresol red).

The deposition of α-PbO_2 from acetate baths was also investigated but the coatings were less satisfactory. High surface area PbO_2 coatings with a highly ordered and porous structure were produced on gold using polystyrene microspheres and the colloidal templating technique and they were shown to support a high rate of DMSO oxidation.

All the PbO_2 coatings were subject to degradation if left standing on open circuit in acid solutions, the rate of degradation being rapid if the medium contained an oxidisable organic species. While the rates of PbO_2 degradation depends on the electrolyte, the dopants in PbO_2 and the structure of the PbO_2 coating, clearly the lack of stability on open circuit imposes additional difficulties in the application of PbO_2 anodes.

Contents

Acknowledgements

I would like to express my gratitude to Professor Derek Pletcher for his guidance, encouragement and patience during my study under his supervision over the past three years at Electrochemistry Department.

I am also very grateful to my sponsors: Government of Malaysia and Universiti Teknologi Mara (UiTM) Malaysia for funding my study and financial support for myself and my family.

Many thanks also go to all members of the Pletcher group, especially to Clelia, Richard, Dima, Hartini, Maria, Jho and all Malaysian friends for their kind friendship during my time in Southampton. I am also indebted to Mr Alistair Clark for his assistance on the Scanning Electron Microscopy.

Finally, I would like to thank my deepest appreciation to my wife (Adeline), my children (Fatin Adriena, Farha Adeeba and Farheen Adeena) who are with me in Southampton and also to my family in Malaysia especially my parents (Halijah and Mohd) for their continuing and loving support.

List of Abbreviations and Symbols (with typical units)

A	Planar geometric area (cm^2)
A_e	Active surface area per unit volume of a three dimensional electrode (cm^{-1})
A_{geo}	Geometric surface area for three dimensional electrode (cm^2)
c	Concentration of species (mol dm^{-3} or M)
$c_{(0)}$	Concentration of species at time, t = 0 (mol dm^{-3} or M)
$c_{(t)}$	Concentration of species at time, t (mol dm^{-3} or M)
$c_{(In)}$	Concentration of species at cell inlet (mol dm^{-3} or M)
$c_{(Out)}$	Concentration of species at cell outlet (mol dm^{-3} or M)
E	Electrode potential (mV or V) vs a reference electrode either vs SCE or SHE
E_{cell}	Cell potential away from equilibrium (V)
E^e_{cell}	Equilibrium potential of a cell (V)
E^0_e	Formal potential (V)
E^A_e	Equilibrium potential at anode (V)
E^C_e	Equilibrium potential at cathode (V)
F	Faraday constant (96485 C mol^{-1})
j	Current density (mA cm^{-2})
j_L	Limiting current density (mA cm^{-2})
I	Current (mA or A)
I_L	Limiting Current (mA)
k_m	Mass transport coefficient (cm s^{-1})
n	Number of electrons per molecule of reactant in electron transfer reaction
η	Overpotential (mV or V)
$\|\eta_A\|$	Overpotential at anode (mV or V)
$\|\eta_C\|$	Overpotential at cathode(mV or V)
T	Temperature (K)
t	Time (s)
m	Amount of species (mol)
Q	Volumetric flow rate for solution flow (m^3 s^{-1})
Ve	Volume of three dimensional electrode (m^3)

V	Volume of solution (L or m^3)
R_{Cell}	Resistance in cell (Ω)
$R_{Circuit}$	Resistance of external circuit (Ω)
MW	Molecular weight ($g\ mol^{-1}$)
LWD	Long way dimension (cm)
SWD	Short way dimension (cm)
ρ	Density ($g\ cm^{-3}$)

Abbreviations:

BOD	Biological oxygen demand
COD	Chemical oxygen demand
TOC	Total organic carbon
TSS	Total suspended solid
AOP	Advanced oxidation process
BDD	Boron doped diamond
RVC	Reticulated vitreous carbon
DSA	Dimensionally stable anode
RDE	Rotating disc electrode
HIPE	High internal phase emulsion
MOCVD	Metal organic chemical vapour deposition
EDAX	Energy dispersive X-ray analysis
SCE	Saturated Calomel Electrode
SHE	Standard hydrogen electrode
SEM	Scanning electron microscopy
EDTA	Ethylenediaminetetraacetic acid
DMSO	Dimethyl sulfoxide
TCA	Thiophene carboxylic acid
PTFE	Polytetrafluoroethylene or Teflon
ppm	Part per million
COSSH	Control of substance harzadous to health regulations

Chapter 1: Introduction

1.0 Background: Electrochemistry and the Environment

Nowadays, there is an increasing awareness of the need to protect the environment and to preserve natural resources from pollution. Pollution of water resources is increasing steadily due to urbanization and industrial proliferation. The use and production of chemical compounds worldwide have increased tremendously and many of these compounds are toxic and non-biodegradable.

Wastewater can normally be classified by its sources; either from residential, commercial, agricultural or industrial. Residential and commercial wastewaters tend to contain concentrated organic wastes that are readily biodegradable in a conventional municipal wastewater treatment plant. On the other hand, wastewaters produced from agricultural and industrial sites may contain any number of man-made or synthetic compounds that are often non-biodegradable and must be treated by special treatment processes before they can be safely discharged into the environment. Improper discharge of the wastewater is a major source of toxic organic compounds in aquatic environments. The presence of these hazardous compounds in water systems represents a major threat to the environment. In particular, organic pollutants which are carcinogenic such as organo-chlorinated compounds. Faster treatment, more efficient and more economical techniques are demanded for the treatment of these residues since conventional methods cannot cope with them. There is already the requirement to ensure that the legal limits of the pollutants discharged in water bodies set by law are not exceeded.

In wastewater treatment technology, the objective may be the complete oxidation of all organic pollutants to CO_2, the removal of particular toxic compounds, modification to decrease toxicity or just decolouration of the effluent. There are many established technologies used to treat these pollutants. But almost all methods have drawbacks in overcoming the problems. New methods known as advanced waste treatment techniques for removing pollutants are being studied and developed. One of the promising approaches to use electrochemical methods. Here, electrochemistry can play a significant role in treating the organic wastes either biodegradable or non-biodegradable. Electrochemistry, a link between physical chemistry and electronic

science, has proved to be a clean, versatile and powerful tool for the development of new advanced methods for water treatment. In recent years, the possible use of electrochemical methods in wastewater treatment for the removal of organic pollutants has attracted considerable attention [1-4].

1.1 Wastewater Treatment

Generally, effluents discharged from chemical processes have high amounts of contaminants which are often toxic and harmful to the environment. Various types of contaminants from wastewaters can be categorized as listed in figure 1.1. They are categorized according to their increasing solubility in aqueous solution. The presence of each contaminant in the effluents is dependent on the nature of the chemical processes.

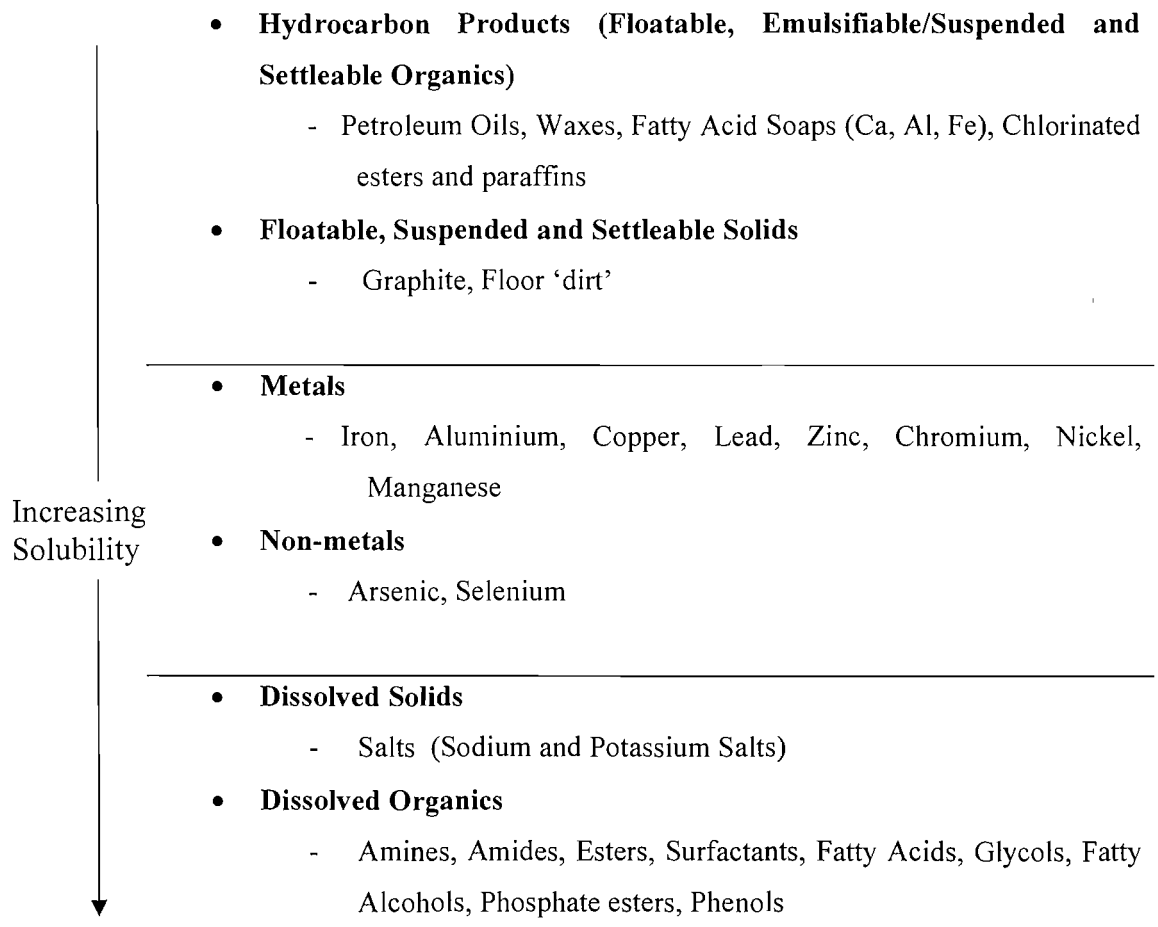

Figure 1.1: List of possible types of contaminants in wastewaters

Several parameters are generally used to monitor the quality of water such as biological oxygen demand (BOD), chemical oxygen demand (COD) and total organic carbon (TOC). BOD is a laboratory measurement of wastewater that is used to measure the amount of oxygen that will be consumed by microorganisms during biological reaction of oxygen with organic material. COD is used as a measure of oxygen requirement of a sample that is susceptible to oxidation by a strong chemical oxidant. TOC is the sum of all organic carbon present in water. Most industrial wastewater treatment plants have primary, secondary and tertiary treatments as shown in figure 1.2. The first stage is a physical method which is used to remove floatable and settleable solids only, which generally removes 40% of the suspended solids and 30-40% of the BOD in the wastewater.

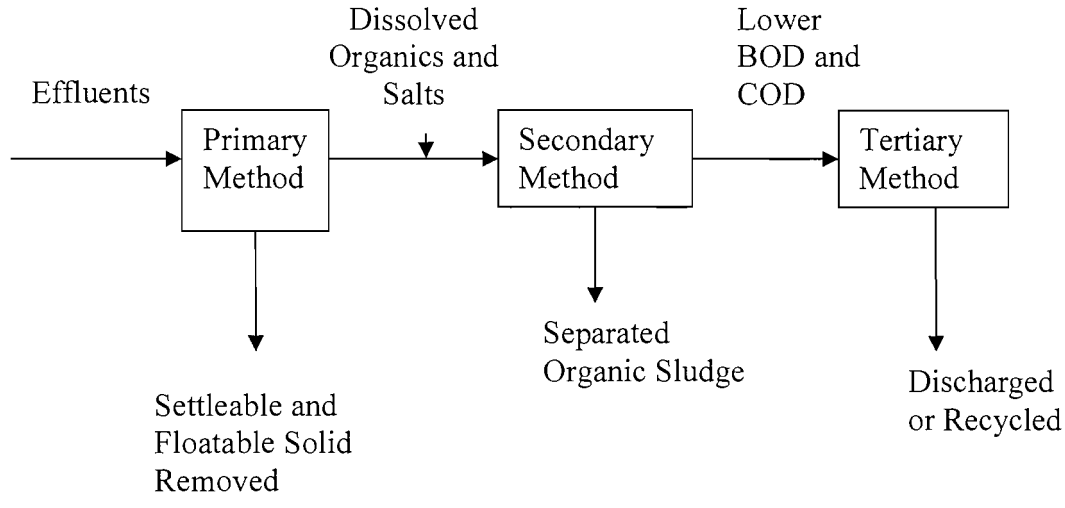

Figure 1.2: Schematic diagram of conventional wastewater treatments

Secondary treatment normally utilizes biological treatment processes in order to convert dissolved organics and salts and also suspended pollutants into a form that can be removed by producing a relatively highly treated effluent. Approximately 85% of the BOD and total suspended solid (TSS) was removed at this stage. Conventional biological processes have been used in industrial waste treatment for many years and utilise either aerobic or anaerobic digestion processes. Aerobic digestion is a bacterial process that runs in the presence of oxygen while anaerobic process runs in the absence of oxygen. Most industrial plants treat the wastewater using aerobic biological processes; under aerobic conditions, bacteria rapidly consume organic matter and

convert it into CO_2. Because the aerobic digestion occurs much faster than anaerobic digestion, the capital costs of aerobic digestion are lower than anaerobic processes. Biological oxidation techniques are the most frequently used among the different technologies for wastewater treatment. This technique is the most economical process and usually used for treatment of readily degradable or biocompatible organic pollutants present in the wastewater. However, biological treatment becomes ineffective when wastewater containing stable and toxic substances which cannot be decomposed by microorganisms under normal conditions or known as non-biocompatible pollutants such as organo-chlorine compounds, phenols, etc.

Effluents from secondary treatment which contain low level of contaminants such as non-biodegradable organic compounds, metals and nutrients will be separated and treated in the tertiary treatment plant. This final stage of treatment before discharge or recycle is also known as advanced treatment and normally employed either chemical or physical processes. This treatment typically utilizes one of the following current, established technologies for the removal of the dissolved organic pollutants.

- activated carbon adsorption
- chemical oxidation
- membrane separation

The organic pollutants can be removed from wastewater by adsorption onto a solid adsorbent, commonly activated carbon. There are a few types of activated carbon used in adsorption process; which are granular, powdered and extruded activated carbon. Different organic compounds adsorb differently on activated carbon. Adsorption depends on the different retention of the dissolved organic molecules in the wastewater on the surface of the activated carbon. The less water-soluble a compound, the more likely it will load well on the activated carbon.

The adsorbed organic waste on activated carbon can then be destroyed by incineration. Plattner and Comninellis have described the various incineration processes involved [5]. Used activated carbon can either be regenerated by pyrolysis or steam treatment or be destroyed by burning in an incinerator with its organic load. Although the processes are effective, they have high investment costs, high energy consumption and high operating costs. They are best suited for handling highly toxic and heavily

contaminated wastes. These processes produce large volumes of hot flue gases which may be toxic and need to be treated to reduce air pollution problems.

Those non-biodegradable organic pollutants have to be treated using other techniques, usually chemical oxidation. Chemical oxidation method uses oxidants to destroy the organic pollutants usually by conversion to carbon dioxide. Traditional oxidants include chlorine and sodium hypochlorite and more recent oxidants used are chlorine dioxide, hydrogen peroxide and ozone [5,6]. Chlorine based oxidants have the disadvantage that they may potentially evolve chlorine and act not only as oxidising agent, but also as chlorinating agents for organic substances. This is clearly a problem, since chlorinated derivatives are generally toxic and difficult to decompose.

Hydrogen peroxide (H_2O_2) does not have this disadvantage and it is a very strong oxidising agent. However, H_2O_2 is more expensive than chlorine based oxidants. Moreover, it requires the addition of $FeCl_2$ to the solution in the treatment of wastewater by a method known as Fenton process [7], which, in turn, invokes consecutive separation steps and this increases the cost of treatment.

Ozone (O_3) is the strongest oxidant. It attacks organic compounds and converts them mainly to aliphatic acids. But, it is not effective on some compounds such as halogenated organic compounds because of the stability of carbon-halogen bonds. Also, the investment and operating costs of this technique are very high [5]. Generally, complete removal of the principal organic pollutants can be easily carried out by the chemical oxidation but complete elimination of total organic carbon (TOC) is hardly achievable.

Another established technique used for the treatment of organic compounds is membrane separation. Membrane separation techniques can be divided into four types according to their particles size; which are microfiltration (0.01 – 0 microns), reverse osmosis (up to 100 Daltons), nanofiltration (100 – 500 Daltons) and ultrafiltration (100 – 500 Daltons). Ultrafiltration is the most widely used membrane due to its effectiveness in treating wastewater and it can operate at very low pressure. Nonetheless, these separation techniques have a few disadvantages such as very high investment and operating costs and also fouling problem. Fouling is an important phenomenon that limits the applicability of the separation techniques. Such fouling can be caused by cake or gel formation, pore plugging and pore narrowing [8].

The use of a single process for the secondary treatment is limited in reducing the organic contaminants especially for highly concentrated organic (ie: high COD). By combining the above listed methods, a substantial reduction of COD and BOD can be achieved. Combined technologies such as the combination between chemical and biological, chemical and adsorption, ultrafiltration and adsorption, or ultrafiltration and biological methods are gaining in popularity for wastewater treatment. Banata and Al-Bastakib [9] investigated the use of integrated process of adsorption using activated carbon and ultrafiltration for treating dye wastewater. The results obtained showed that the combined process achieved better rejection of dye that the ultrafiltration process alone. Combined biological and membrane treatment also has produced a superior effluent quality of food-processing wastewater [10]. Mohammadi and Esmaeelifar [11] compared the effectiveness of various treatments for vegetable oil factory wastewater. The results show that ultrafiltration is better than conventional biological method and combined of ultrafiltration and powdered activated carbon is better than that ultrafiltration alone.

A new option for the wastewater treatment known as Advanced Oxidation Process (AOP) technology is proposed to be used in producing cleaner water and efficient treatment. Wastewaters contaminated with organic pollutants can be treated by using AOP method which generates reactive substance such as hydroxyl radicals as the effective oxidant for converting organic molecules to simple acids or CO_2 and water [12]. One of the methods categorized in this AOP technology is electrochemical oxidation.

The electrochemical oxidation method appears to be more attractive for wastewater treatment. The electrochemical combustion or degradation of organics offers considerable advantages. It can be carried out at moderate temperatures and under clean conditions. Also, it provides a means for the total destruction of the pollutants, promoting their oxidation all the way down to CO_2 and no by-products are left in the effluent.

Electrochemical processes use electron transfer to initiate chemical reactions. For example, as shown in figure 1.3, direct electron transfer to the anode surface plus the production of mixed oxidants such as hydroxyl radicals ($OH\cdot$), hydrogen peroxide and ozone (O_3) caused by discharge of water molecules from direct surface reactions are believed leading to chemical reactions of reactants.

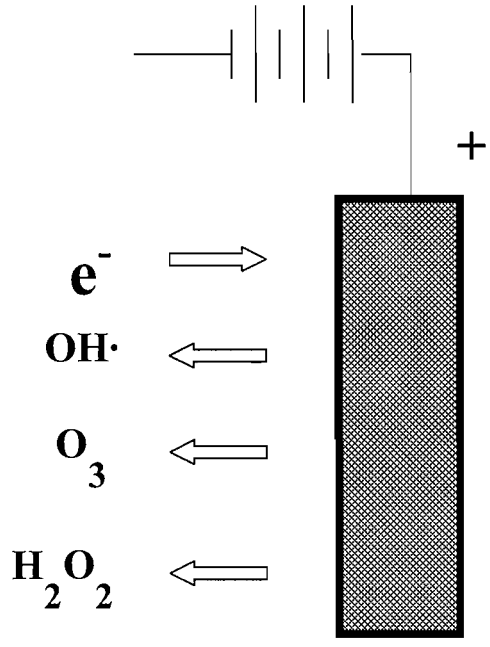

Figure 1.3: Schematic diagram of anode surface reactions

By controlling the electrode potential and the environment at the surface of the electrodes, the conditions necessary to initiate and control chemical reactions are created. The freedom of choice in adjusting the electrode potential and electrode material makes electrochemistry an extremely selective and flexible technique. One of its advantages is the fact that electrons released from or consumed by the electrode are a clean reagent that does not contribute to a further increase in the amount of chemicals in the environment as is the case in other chemical processes [13]. The direct application of the electron as a reagent is seen as an intrinsically clean processing method. Electrochemical technology which operates without generation of waste products is known as a clean technology. However, the wide application of this technique is still limited by problems related to the stability of the electrode materials. Recently, the use of electrochemical methods for the removal of organic and toxic pollutants present in wastewater, especially for dilute solutions of biorefractory organics such as phenols or stable halogenated organic compounds. Such molecules cannot be decomposed by biological treatment (ie: microorganisms) under normal conditions or by chemical oxidation method but can be degraded by electrochemical methods (ie: anodic oxidation). The electrolytic approach has attracted considerable attention and has been widely studied [14-18]. It has been reported that phenols can be

anodically oxidized using metal oxide anodes such as iridium oxide, lead dioxide, tin dioxide, etc. [19-21] as well as diamond.

1.1.1 Anodic Oxidation for Wastewater Treatment

Anodic oxidation is a powerful tool for the removal of organic wastes in industrial effluents. The main objective of this process is to oxidise all organic compounds to CO_2 and H_2O. Many electrochemical processes for wastewater treatment involve the direct reaction of species at electrode surfaces known as direct electrolysis, while others involve indirect electrolysis. Figure 1.4 shows a comparison of these two different approaches.

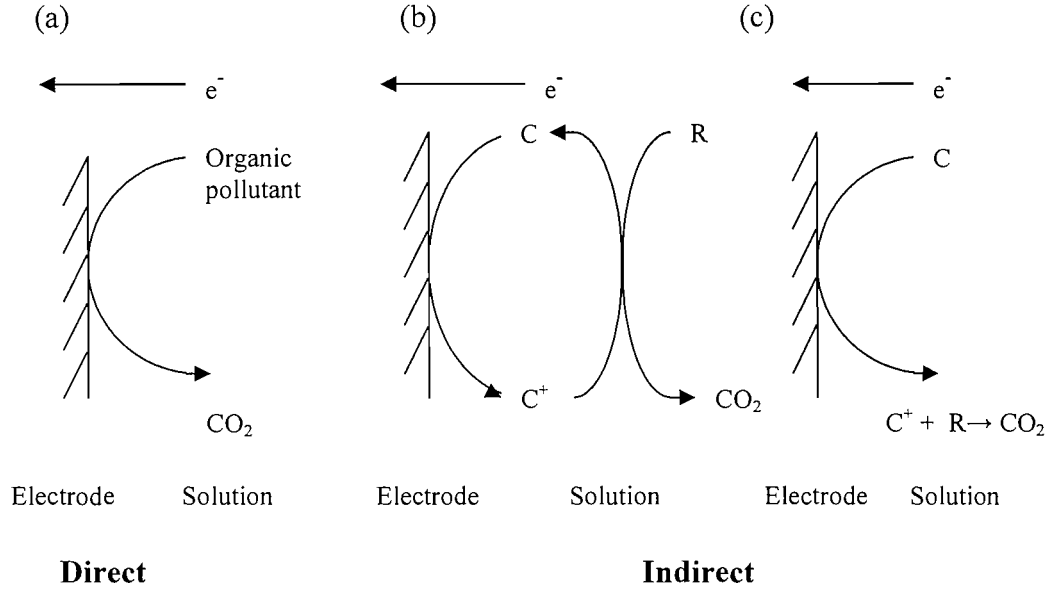

Figure 1.4: Schemes for direct (a) and indirect oxidation of organic pollutants. The latter can be carried out both with reversibly (b) and irreversibly (c) electrogenerated reagents. R is a pollutant, O is the oxidation product and C is a reagent or catalyst.

Indirect electrolytic processes are used to convert pollutants to less harmful products by using a mediator or an electron transfer agent. The mediator is electrochemically formed or generated either in a reversible or irreversible manner (as shown in figure 1.4b and 1.4c) at the electrode surface and acts as an intermediary for shuttling electrons between the pollutant substrate and the electrode.

There is a variety of reversible reagents that have been successfully used for pollutant treatment such as Ag(II) , Co(III) , Ce(IV) and Fe(III). Silver (II) is a powerful oxidant with a formal potential of E^{o}_{e} = 1.99 V vs SHE in 1 M HNO_3 [22]. Silver (II) is one of the most powerful oxidizing agents in acidic media and some organic pollutants such as ethylene glycol, benzene, tributyl phosphate and kerosene [23, 24] have been successfully treated using this reagent. It acts as a reusable catalyst and no silver waste is generated. AEA Technology has developed a process to generate Ag(II) species anodically via the oxidation of Ag(I) in a nitric acid solution [24]. The developed technology was originally used to solubilize PuO_2 during the treatment of nuclear wastes. The disadvantages of using silver as the reagent are total recycling and regeneration of this catalyst must be achieved as silver ions are considered a hazardous waste and the overall destruction efficiency of the pollutants is reduced when chloride ion precipitates Ag^+ as AgCl.

An alternative to silver is the Fe(II/III) redox couple which is non-toxic reagent but this has a much less positive formal potential (E^{o}_{e} = 0.77 V vs SHE). Oxidation efficiencies up to 100% of carbonaceous wastes have been reported [25,26] by using this oxidising agent in sulphuric acid. Organic compounds including polycyclic aromatic, coal and coke were completely oxidised at 150° C. But, there are a few difficulties with Fe(II/III) based processes, particularly low current densities and relatively high temperatures (~ 100° C) are required for efficient operation.

In irreversible electrolysis processes, generation of strong oxidants such as hypochlorite/chlorine, ozone, hydrogen peroxide are generated in situ and are utilized immediately [27]. The pollutants are destroyed in the bulk solution by oxidation reaction of the generated oxidant. The electrochemical generation of hypochlorite/chlorine in a solution containing chloride ions is given by the following reaction:

$$\mathbf{2Cl^- \rightarrow Cl_2 + 2e^-} \qquad \textbf{(1.1)}$$

$$\mathbf{Cl_2 + H_2O \rightarrow HOCl + H^+ + Cl^-} \qquad \textbf{(1.2)}$$

$$\mathbf{HOCl \rightarrow H^+ + OCl^-} \qquad \textbf{(1.3)}$$

The application of hypochlorite/chlorine for indirect electrochemical oxidation of various industrial effluents has been investigated by several investigators. Kuhn has

reported that cyanides can be destroyed by these oxidants [28]. Other organic compounds such as phenols, thiocyanides, sulphides, etc. can also be destroyed by this technique. This technique also was successfully used in the treatment of various wastewaters such as tannery wastewater [29,30], textile wastewater [31,32] and olive oil wastewater [33].

Ozone (O_3) is among the most powerful oxidants with formal potential of E^{o}_{e} = 2.07 V vs SHE and the advantage of generating this oxidant is its non-polluting property since it decays rapidly to oxygen. A method for ozone generation has been patented by Foller et al. [34,35] and developed by ICI and OxyTech Inc. Another electrolytic ozone generator known as Membrel process [36] was commercialised by Asea Brown Boveri. Both are based on the electrochemical oxidation of water to ozone (with competing with oxygen evolution) as shown below:

$$\mathbf{3H_2O - 6e^- \rightarrow O_3 + 6H^+} \qquad \textbf{(1.4)}$$

Hydrogen peroxide (H_2O_2) is a strong oxidising agent (E^{o}_{e} = 1.77 V vs SHE) and, like ozone, does not leave a secondary pollution problem. It may be manufactured and regenerated with only electricity and air or O_2 as feedstocks. An important advantage of in-situ electrochemical generation is that its transportation over long distances is avoided; it is a hazardous substance and unstable on long-term storage. The electrochemical in-situ generation of H_2O_2 is done via the reduction of oxygen on the cathodic surface through the following reaction:

$$\mathbf{O_2 + 2H^+ + 2e^- \rightarrow H_2O_2} \qquad \textbf{(1.5)}$$

A maximum current efficiency for the cathodic reduction of O_2 to H_2O_2 of up to 94 % has been reported by Do and Chen [37] on a graphite cathode in 0.5 M Na_2SO_4 and at pH 13. They found that one of the main factors affecting the cathodic reduction of oxygen for the production of hydrogen peroxide was the pH. The current efficiency of the production of H_2O_2 was lower in acidic solutions than in basic solutions. This was a consequence of the different pathways for the cathodic reduction of oxygen at different pH values. The reaction involved in alkaline solution was verified in the literature [38]:

$$O_2 + H_2O + 2e^- \rightarrow HO_2^- + OH^- \quad (1.6)$$

In acid solution, H_2O_2 effectiveness can be greatly increased by the addition of Fe(II) as a catalyst, which converts it into hydroxyl radicals in a chemical reaction shown below:

$$H_2O_2 + Fe^{2+} \rightarrow OH^{\cdot} + OH^- + Fe^{3+} \quad (1.7)$$

The production of hydroxyl radical ($OH^{\cdot}$) can then start the destruction of organic substances. The oxidising power of the hydroxyl radical (E^0_e = 2.85 V vs SHE) is as high as that of fluorine [39].

There is substantial literature [37,40-46] on the oxidation of aromatic hydrocarbons using Fe(III) and O_2 in aqueous acid solution to produce active H_2O_2/Fe(II) composition at a plate cathode or known as 'electrogenerated Fenton's reagent'. Do and Chen [37] investigated the use of electrogenerated H_2O_2 at a flat cathode surface together with the presence of Fe(II) for the degradation of phenol. It was shown that phenol could be effectively oxidized and largely converted to CO_2; at pH 1-4, with a final COD, 400 ppm from initial concentration as high as 2600 ppm. However, the current densities were low typically 0.4 mA cm^{-2} and obviously this is not sufficient for practical effluent treatment technology.

The main problems in electrosynthesis of H_2O_2 are the relative slowness of the O_2 reduction reaction due to the mass transport limitations that result from the low solubility of O_2 in the electrolyte solution. Commercial applications have required the development of a technology to overcome this problem. Recently, methods have been developed for the production of H_2O_2 using three dimensional electrodes such as beds of carbon particles or reticulated vitreous carbon [47-49] and gas diffusion cathode fabricated from carbon powders without metal catalysts [50,51] which allow the reduction of oxygen to H_2O_2 at an efficient rate and a practical current density. Both types of electrodes have increased the rate of H_2O_2 production by a factor of 100-1000. However, the developments are limited to the generation of H_2O_2 in concentrated alkaline solutions. The use of gas diffusion electrodes for the effluent treatment processes was first introduced by Brillas and co-workers [52]. They were able to reduce

COD of alkaline solutions containing aniline and 4-chloroaniline from 100 ppm to < 5 ppm with a current density as high as 200 mA cm^{-2}.

More recently, however, both three-dimensional electrodes [53] and gas diffusion electrodes [54] have been used in both neutral and acid solutions to reduce O_2 to H_2O_2. Alvarez-Gallegos and Pletcher [53] used reticulated vitreous carbon cathode to enhance the oxidation of formaldehyde. It was confirmed that the three dimensional electrode has greatly accelerated the rate of formaldehyde removal; with oxygen saturated solutions, current densities could reach > 20 mA cm^{-2}. In alkaline solution, the oxidation of formaldehyde (5-200 ppm) could be easily achieved by using H_2O_2 generated from three dimensional electrode without catalyst; but in neutral and acid solution, the presence of Fe(II) was essential to achieve complete oxidation to CO_2. Harrington and Pletcher [54] showed that the gas diffusion electrode could be used to remove phenol, aniline, acetic acid, formaldehyde and three azo dyes (amaranth, fat brown RR and methyl orange) from aqueous sulphate solution at pH 2 containing Fe(II) ions. COD of the solutions containing such organics may be reduced by 90 % with a current efficiency > 50 % and using a current density of ~ 20 mA cm^{-2}, leading to acceptable energy consumption. Even though the current density can be increased by using the three dimensional electrode, the presence of Fe(II) is still required in this process in order to oxidise organic compounds completely to CO_2, otherwise the reaction stopped at an intermediate stage; for example formaldehyde oxidation stopped at formic acid in the absence of Fe(II).

The direct anodic oxidation method has a number of advantages compared to the indirect approach such as (a) no need to add catalyst such as Ag(II) or Fe(III), (b) more direct control of the oxidation rate, (c) continuous operation and (d) simpler treatment plant can be designed. Basically, industrial wastewaters with low concentration of organic pollutants produced from chemical processes are treated in-situ before the treated water can be recycled or discharged into the water systems. Figure 1.5 shows various possibilities of treating contaminated process water:

- only electrochemical treatment, then recycle to the process
- pre-treatment by electrochemical and followed by biological treatment, then recycle to the process
- only electrochemical treatment, then discharged into water systems

- electrochemical pre-treatment and biological treatment, then discharged into water systems

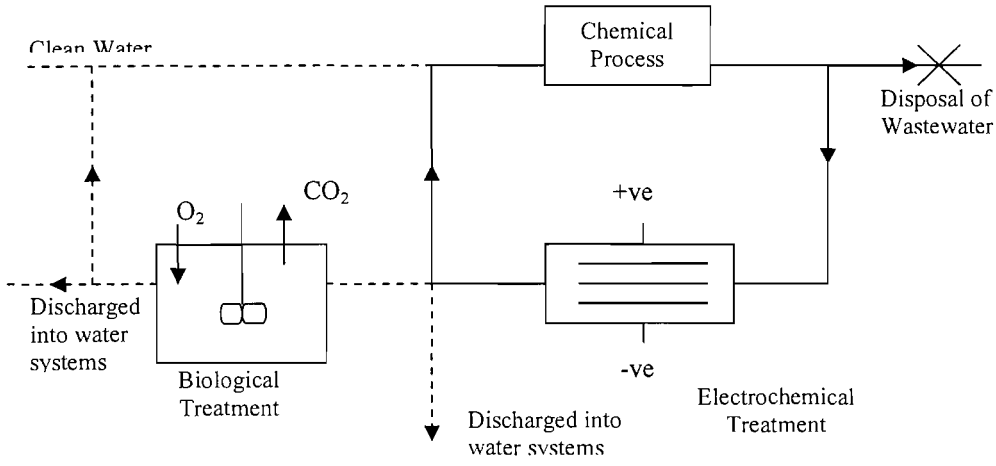

Figure 1.5: Recycling of chemical process water: treatment of organic contamination with an electrochemical or / and biological methods

In conclusion, it has been shown that there is a great need for the treatment of industrial wastewaters containing bio-refractory organic compounds which are non-biodegradable, toxic and harmful to the environment. The use of electrochemical method for the treatment is one of the most promising ways in order to achieve this goal since it is clean, simple and cost effective technology especially in treating diluted organic pollutants.

Both indirect and direct electrolytic approaches have their advantages; however, while indirect electrolysis has been studied widely and used in commercial processes, the great potential of direct oxidation method has not yet been realised, mainly due to the lack of suitable electrode materials. The choice of anode material plays an important role: it should be stable over a wide range of potentials and should present high overpotential for oxygen evolution, which constitutes the main side reaction in anodic oxidation.

1.2 Electrode Materials for Anodic Oxidation of Organic Compounds

The choice of electrode material as the anode for direct oxidation of organic compounds is a crucial factor; the electrode should be stable over a wide range of

anodic potentials and should present high overpotential for oxygen evolution, which constitutes the main side or competing reaction in anodic oxidation. The electrode reactions in electrochemical cell are shown in figure 1.6. The desired reaction on the anode surface is the oxidation of organic substances (eg: $HCOO^-$) entirely to carbon dioxide (CO_2), however, the competing reaction (O_2 evolution) can occur simultaneously reducing the efficiency of the anode for the oxidation of target pollutants.

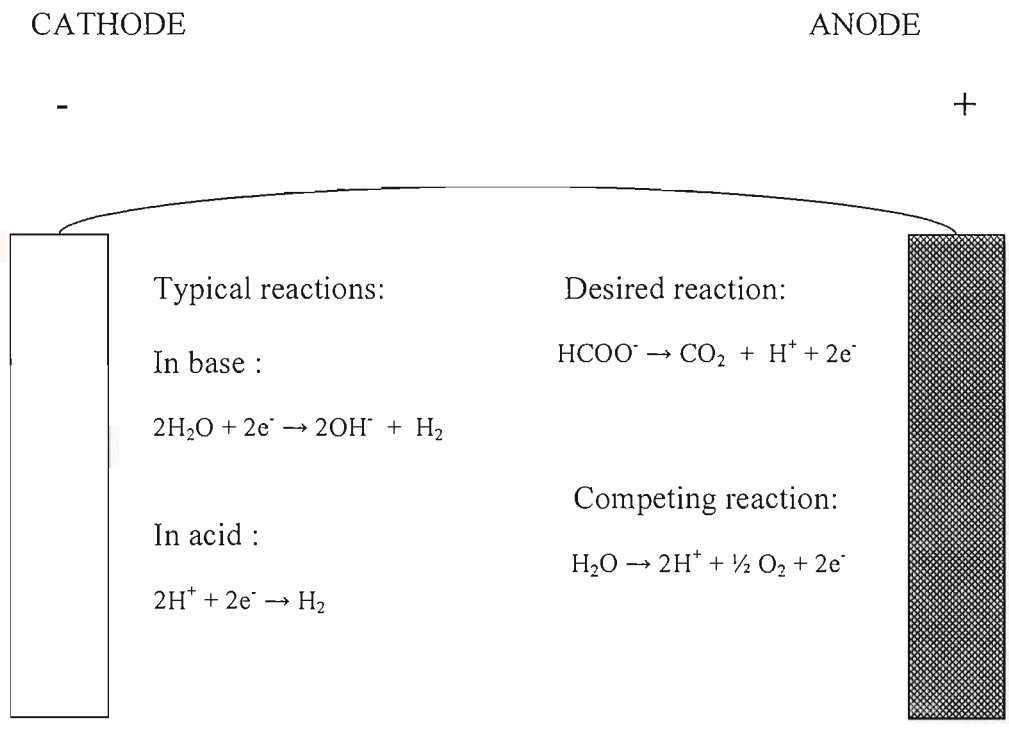

Figure 1.6: Electrodes reactions in aqueous solution

The right choice of electrode materials for such applications is related to its ability to limit the competing reactions, good faradaic efficiency, stability both during oxidation and on open circuit and economic feasibility. The performance of the material for electrochemical reaction depends on several parameters such as electrode potential (or current density), the concentration of electroactive species, electrolyte, pH, temperature, solvent, mass transport and cell design. Since there are many factors influencing the behaviour of the electrode on a practical basis, it is impossible to find

the optimum electrode to be used in a given process on a theoretical basis. It is a challenge to find the conditions where the oxidation of organic compounds is maximum with minimum oxygen evolution reaction and also stable over extended electrolysis time. Couper et. al [55] have listed some considerations in selecting a good electrode material :

- Physical stability: the electrode material must have adequate mechanical strength, must not be prone to erosion by the electrolyte, reactants or products and must be resistant to cracking.
- Chemical stability: the electrode material must be resistant to corrosion, unwanted oxide and hydride formation and the deposition of inhibiting organic films under all conditions experienced by the electrode.
- Suitable physical form: it must be possible to fabricate the material into the form demanded by the reactor design in order to facilitate sound electrical connections and to permit easy installation and replacement at a variety of scales.
- Rate and product selectivity: the electrode material must support the desired reaction and, in some cases, significant electrocatalytic properties are essential. The electrode material must promote the desired chemical change while inhibiting all competing chemical changes.
- Electrical conductivity: this must be reasonably high throughout the electrode system including the current feeder, electrode connections and the entire electrode surface exposed to the electrolyte. However, higher resistant material may be used as coatings on a low-resistivity metal.
- Cost/lifetime: a reasonable and reproducible performance including a lifetime probably extending over several years must be achieved for an acceptable initial investment.

The development of electrolytic processes for the direct oxidation of organic compounds has been limited by the availability of anode materials for such application. Intensive research has been carried out with the aim of producing more efficient and stable anode materials. In practice, the materials with large O_2 overpotential are commonly chosen as the anode and for most situations the choice is limited to precious

metal coatings (eg: Pt/Ti), carbon/ graphite/ diamond or oxides coatings (eg: PbO_2 or SnO_2).

a) Noble Metals

Platinum (Pt) has been used in the manufacture of persulfate. It is very stable to corrosion and has high oxygen overpotential. Nevertheless, Pt is obviously very expensive. The cost can be reduced by electroplating on to a cheap conducting substrate such as titanium. The coatings of Pt on Ti are smooth with low porosity, well-adhered to the substrate and have good stability and high oxygen overpotentials. Pt can also be coated on titanium by using MOCVD technique [56]. It is a natural choice for organic reactions that do not go well on PbO_2 electrodes. The synthesis of inorganic compounds such as perchlorate, periodate and persulfate can also be done on Pt/ Ti anode.

Pt electrodes were found to perform poorly for the oxidation of phenol since a blocking film of high molecular weight unreactive material rapidly built up at the electrode surface [57]. Pre-oxidation of the Pt electrodes only led to a slight improvement.

Marinerc and Lectz [58] have found that the direct electrooxidation of ammonia on Pt and platinized titanium (Pt/ Ti) anodes proceeded well to release N_2 as expressed by the following equation:

$$\mathbf{2\,NH_3 + 6OH^- \rightarrow N_2 + 6\,H_2O + 6e^-} \qquad \mathbf{(1.8)}$$

Apart from Pt, other thin layers of noble metals such as ruthenium [18] and rhodium [59] electrodeposited on titanium substrates have been used as electrocatalyts for destruction of biorefractory organics in wastewater such as phenols and surfactants. Gold (Au) is also used as the anode material and usually employed as thin coating on titanium substrate due to its inherent cost.

Nickel (Ni) is normally used in basic solution either as the anode or as the substrate for deposition of other materials. In acid media, however, Ni would not withstand anodic polarization therefore a different material had to be chosen as the substrate or the anode.

b) Carbon / Graphite/ Diamond

Carbon is another alternative that can be used as an anode in the destruction of organic compounds. Usually, glassy and vitreous carbons are used in very oxidizing conditions because of their inertness and high oxygen overpotentials. It has been reported that glassy carbon can be used for the generation of ozone [47]. However, on carbon electrode, similarly as on Pt, phenols are weakly oxidised since phenols cause anode inactivation by oligomer deposition on the surface [16,20,57]. For this reason other materials are sought to solve the problems.

Diamond, a type of carbon, is also used as the anode usually in the form of a thin coating on Ti or Si. Recently, many studies have been focused on boron doped diamond (BDD) as the anode material for a wide range of electrochemical applications [60-62] especially in electrosynthesis. BDD electrode offers advantages over other types of carbon-based electrode materials, due to its mechanical and chemical robustness, wide potential window and low background interference. Okino et al [63] proposed the use of BDD for anodic fluorination processes. Marken et. al [64] deposited PbO_2 on BDD and used microwave activation of electrochemical processes for the enhancement and control of processes at the electrode/solution interfaces. The increase in current for the electrocatalytic oxidation of ethylene glycol at the electrode was observed in the presence of microwave radiation. Saterlay et. al [65] employed ultrasound to enhance the efficiency of the PbO_2 deposition on BDD and the electrolysis rate of ethylene glycol oxidation at the electrode. The main problem encountered with the BDD is its high price therefore it is not ideal to be the anode material for a large scale of reactor especially in wastewater treatment.

c) Metal oxides

Metal oxides are probably the most interesting material for use in electrocatalysis. There are a number of oxides electrodes (RuO_2, IrO_2, SnO_2 and PbO_2) that may be used as anode materials for the oxidation of organic compounds. RuO_2 and IrO_2 are oxides with low overpotential for O_2 evolution and used when the minimization of the cell voltage is the key factor. Meanwhile oxides with high overpotential such as SnO_2 and PbO_2 are the most common electrodes studied and used in electrosynthesis, ozone production, waste water treatment, etc. Titanium is the most

common choice as substrate for these metal oxide anode coatings even though it has a quite high electrical resistivity.

Tin dioxide (SnO_2) has been widely studied by Stucki et. al [14,15] and Comninellis groups [16,66,67]. SnO_2 is said to have high chemical and electrochemical stability, and high electrical conductivity especially when doped with antimony. Phenol and benzoic acid were efficiently oxidised on SnO_2/Ti electrodes [14,15]. Comninellis and Pulgarin [66] have compared the oxidation of phenol on SnO_2 and Pt. They found that SnO_2 has performed better; 90% oxidation of phenol oxidation occurred at SnO_2 electrodes as compared to 40% at Pt. The catalytic activity of SnO_2 electrode is also increased by the incorporation with antimony (Sb). Lipp and Pletcher [68] have prepared the doped electrode (Sb doped SnO_2) on Ti substrate using thermal decomposition method. They found that high rate was achieved for the oxidation of EDTA at Sb-SnO_2/Ti electrode.

In chloride containing electrolytes, however, SnO_2 is poorer catalyst for chlorine evolution as compared to Pt electrode. Halogenated organic compounds were slowly dehalogenated on SnO_2 electrodes [66]. Winograd [69] describes Sb-SnO_2 surface as a poor electronic conductor in highly alkaline pH because of surface degradations but not in acid media

While SnO_2 may be considered an active and a reasonable material as anode for the direct oxidation of organic compounds, PbO_2 seems to have advantage on its higher potential for oxygen evolution than SnO_2.

Of the metal oxide electrodes available, β-PbO_2 has received extensive attention both in industrial and academic applications [3,36,39,66,70-81]. PbO_2 anodes (often in the form of a lead electrode oxidised in situ) are used in a number of electrosynthesis processes such as the production or regeneration of perchlorate, dichromate and ozone [36,70,71]. The anodes are also used in the oxidative destruction of organic pollutants such as cyanide ions [72]. PbO_2 has also been investigated as an electrocatalyst for the oxidation of organic compounds especially phenol by many researchers [3,39,66,73-81]. The use of high overpotential anode such as PbO_2 favours the degradation of phenols [78,79]. Electrodeposited PbO_2 was found to be corrosion resistant and superior for phenol removal. Good current efficiencies up to 60% were reported for the oxidation of 1000 ppm phenol on PbO_2 electrode at an applied current density of 50 mA cm^{-2} [73]. The destruction of the compound is believed to occur via

adsorbed hydroxyl radicals produced by anodic discharge of H_2O. The production of OH· can be expressed as the following:

$$H_2O - e^- \rightarrow OH_{ads} + H^+ \quad (1.9)$$

which then attack the phenol molecules [3,66].

Tahar and Savall [78] studied the phenol oxidation on PbO_2 electrodes using different substrates (ie: Ti, Ta and Pb). They found that there was a relation between the nature of the substrate used and the decreasing of total organic carbon (TOC). On the other hand, some studies have used doped PbO_2 (ie: other ions incorporated into the PbO_2) electrodes for the oxidation of phenol. Johnson et al [80] compared the electrocatalysis of phenol oxidation on doped and pure lead dioxide electrodes focusing their study on the influence of the doping ions. Bi-doped PbO_2 has been found to have higher catalytic activity for the oxidation of phenol than pure PbO_2. Fe-doped PbO_2 was also used as the anode for phenol degradation [81] and the final COD values reported were near zero when the electrolysis was done at pH 5.

In conclusion, the requirements for anode materials and types of anode materials for the direct oxidation of organic compounds have been discussed. The performance for such applications of the most common materials used as anodes such as Pt, carbon and oxides mainly PbO_2 and SnO_2 has been discussed and compared. From the literature, PbO_2 clearly emerges as an attractive material as an anode for the direct oxidation of organic compounds due to its high oxygen evolution potential, low price, relatively stable under the high positive potentials required, stability at high temperatures and ease of preparation [82]. Its high overpotential for O_2 evolution permits application of potentials to ca. 2.0 V vs SCE in acidic media without vigorous O_2 evolution [83]. The PbO_2 electrodes have some disadvantages which they are corrode at high rate under reducing conditions and in some acids, particularly hydrochloric acid; as well as their poor mechanical properties. While general conclusions of the various workers are similar, there remain discrepancies, which are partly caused by variations in the sample preparation. In the present work, PbO_2 will be the subject and further investigated. Details of the properties and preparation of lead dioxide electrodes will be discussed in the next section.

1.3 Electrodeposition of Lead Dioxide (PbO_2)

PbO_2 films can be electrochemically deposited on various substrates using either galvanostatic technique (constant current density), potentiostatic technique (constant potential) or pulsed current technique [84-87]. Optimization of electrodeposited PbO_2 can be carried out either by controlling the deposition parameters [88], or by adding different ions in the deposition bath [89,90] or by co-depositing with other oxides [91-93].

1.3.1 The choice of substrate for PbO_2 deposition

Lead dioxide anode can be prepared on a variety of substrates: lead [47], gold [87,94,95], carbonaceous substrate (ie: glassy carbon, graphite) [96], platinum [56,97-99], titanium [87,100], tin oxide [101] and ceramic materials (ie: Ti_4O_7 or Ebonex®) [102,103]. The factors influencing the choice of the materials to be the substrate for PbO_2 deposition are that the material must be at least a moderately good conductor, cheap, must possess good mechanical properties and must not corrode in the event of a pinhole in the covering layer of PbO_2. Lead substrates usually have poor performances. Precious metals such as Au or Pt are too expensive. The electrodeposition of PbO_2 on C or reticulated vitreous carbon (RVC) has been suggested for the production of alternative composite electrodes in lead-acid batteries [104,105]. PbO_2 anodes are also frequently formed by anodic electrodeposition on Ti and Ebonex® substrates [106]. PbO_2 on ceramic materials such as Ebonex® substrates leads to good adherent coatings but it is difficult to obtain cheap large electrodes.

In early years, graphite, iron silicide and magnetite were used as the substrates since all are reasonably conducting and corrosion-resistant. However, all of these substrates are fragile, heavy and available only in thick section or cylindrical form and thus incompatible for the fabrication of modern electrolytic cell designs. Therefore, valve metals such as Ta, Nb or Ti were considered since they possess good physical and mechanical properties which allow thinner and mechanically superior cell designs. Nb and Ta are more expensive substrates than Ti and only used when Ti shows deficiencies. Ti is the most common choice as substrate material for various metals and metal oxide coatings and also it is the most widely studied for the anodes useful for many kinds of industrial applications [107]. In the 1960s, Beer [108] proposed the use

of titanium as a substrate for dimensionally stable anodes (DSA) for such applications. The use of a titanium electrode coated with active oxides (eg: PbO_2) for wastewater treatments is very popular because of its stability, performance, cost and lifetime [109]. For practical reasons, PbO_2 on titanium and on platanized titanium (Pt/Ti) are the most widely used.

Titanium has several advantages in its use as substrate for PbO_2 deposition; it is a reasonably good conductor and therefore suitable for a current feeder, it is relatively cheap and has good mechanical strength and can easily be machined and shaped, ensuring flexibility in electrode and cell designs. Nonetheless, it has a disadvantage; Ti may passivate by forming TiO_2 under the polarisation conditions required for PbO_2 deposition. This passive layer of TiO_2 on the Ti surface acts as a barrier for electrons on anodic polarization. It is impossible to pass a few mA cm^{-2} at a titanium anode covered with TiO_2 layers in an aqueous medium unless the voltage applied was very high to break the oxide film. For this reason the passive layer must be removed before application of the PbO_2 onto the Ti substrate. Many attempts have been made to inhibit the formation of the oxide layer during deposition. Some studies have suggested carrying out some pre-treatments on the Ti surface before deposition. The pre-treatments are crucial in order to obtain a conductive and lasting PbO_2 anode for industrial purposes. There are a number of studies concerning the pre-treatment of titanium substrate prior to application of a coating [110-112].

Some studies have suggested depositing some intermediate layer between Ti substrate and PbO_2 coating so to prevent the growth of TiO_2 from spreading on the Ti surface. Normally, Pt is used as the plating interlayer on the clean Ti surface before any coatings were carried out; this interlayer coating is called platanized titanium (Pt/Ti).A very thin layer of gold was also used as the interlayer or undercoat for the deposition of stable PbO_2 on Ti [113,114]. Other alternative interlayers that can be used are carbides or borides of tantalum or titanium which form a conducting layer which inhibits the oxide formation [115]. Wabner et.al [116] have proposed a method for the preparation of PbO_2 coated titanium anodes where the clean titanium surface was covered with a film of an electron-conducting substance. They have treated the clean Ti surface with a solution containing Ti(IV). Recently, Gonzalez-Garcia et.al [117] have modified the pre-treatment method from Wabner's work. They have prepared a thin film of adsorbed 'C=O species' on the Ti surface by immersion the Ti substrate in a boiling oxalic acid

containing Ti(IV) oxalate which appeared to protect the titanium surface from the formation of the oxide film. Feng and Johnson [17] also have used the same chemical treatment (ie: using Ti(IV)) before PbO_2 deposition. Besides that they have also coated an interlayer (ie: F-PbO_2 layer) on the treated Ti surface to make the electrode conducting prior to Bi-PbO_2 deposition.

Physical and chemical pre-treatment methods are employed for the removal of thick TiO_2 film on the Ti surface. Wabner et. al [116] have physically treated the titanium surface by sandblasting the substrate and polishing with emery paper and alumina slurries; and then followed by the chemical treatment where the polished Ti substrate was immersed in an etching solution (ie: a boiling oxalic acid solution). These physical and chemical treatments lead to a clean, rough and free TiO_2 of titanium surface. Lipp and Pletcher [68] have used a boiling solution of strong hydrochloric acid for the chemical treatment. Good results for SnO_2 deposition on Ti have been achieved with this etching solution.

They all come to the conclusion that the removal of TiO_2 from or the inhibition of TiO_2 formation on the Ti surface is essential for successful coating, but they suggest different ways of achieving the goal.

1.3.2 PbO_2 Coatings

There are two forms of PbO_2; α-PbO_2 (orthorhombic structure) and β-PbO_2 (tetragonal structure) [117,118]. Electrochemically α-PbO_2 is prepared in weakly acidic or alkaline solution by the oxidation of Pb(II) whilst β-PbO_2 can be easily prepared by the electrooxidation of Pb(II) from acidic solutions usually of the perchlorate ($HClO_4$) or nitrate (HNO_3) [82,119-121]. β-PbO_2 also has higher stability in acid solutions than α-PbO_2 [122]. The redox activity of PbO_2 is related to the morphology and the structure of the produced deposit either α-PbO_2 or β-PbO_2. The α-PbO_2 has a more compact structure than porous β-PbO_2, resulting in a better contact between the particles [84,123]. In lead-acid batteries, however, the more compact α-PbO_2 is more difficult to discharge compared with the β-PbO_2 [124]. A porous structure of β-PbO_2 provides a greater surface area for anodic applications; therefore, the increased in the active surface area will increase the formation of OH radicals and will favour the degradation of organic compounds.

Different electrocatalytic activities of α and β forms of PbO_2 were reported in many studies [125-127]. It was concluded that porous, structured PbO_2 with high degrees of crystallinity is more active and has influenced the electrocatalytic properties of the material. Velichenko et al [99] reported that higher crystallinity increased the electrochemical activity of PbO_2 electrode. Abaci et. al [128] found that β surfaces have higher performance than α surfaces on phenol degradation; and higher crystallinity of the β increased the efficiency of the phenol degradation process. PbO_2 surfaces with high β content provided fast aromatic ring oxidation of phenol to benzoquinone and maleic acid and decreased the electrolysis time for phenol degradation. The degradation can be briefly shown as below:

$C_6H_5OH \rightarrow C_6H_4O_2 \rightarrow C_4H_4O_4 \rightarrow$ aliphatics products + CO_2
(Phenol) (Benzoquinone) (Maleic Acid)

Ho et. al [129] studied the evolution of O_2 on PbO_2 electrodes. They have carried out a comparative analysis of adsorbed reaction intermediates - $OH\cdot$ and $O\cdot$, at α and β of PbO_2. It is concluded that the structure of the PbO_2 has a strong influence on the behaviour of the adsorbed species and also on the electrocatalytic activity for O_2 evolution. Mostly, β-PbO_2 coatings have been used as anode materials in many applications including the electrochemical degradation of organic compounds.

There have been a number of papers describing studies of the nucleation and growth of the β-PbO_2 coatings on Pt, gold, vitreous carbon and titanium substrates from aqueous acid solutions [94,96,112,130,131]. They found that the behaviour of the nucleation as well as the dissolution of PbO_2 on Ti substrate is different than that shown on other substrates such as gold, Pt or vitreous carbon.

It is generally accepted that the electrodeposition of PbO_2 on Ti substrates is more difficult to form stable coatings than on other substrates. The electrodeposition of PbO_2 on Ti substrate is found to be dealing with two different competing processes:

i. electrodeposition of lead dioxide from Pb(II)
ii. passivation of the titanium surface

Yellowish TiO_2 is formed before PbO_2 deposition between +1.70 V and + 1.90 V vs SCE in 1 M $HClO_4$ [87], since TiO_2 is stable at anodic potentials up to +1.95 V vs SCE

[132] the PbO_2 film is deposited onto TiO_2 substrate. The TiO_2 produced on the Ti substrate can disturb the electrochemical deposition of PbO_2 [17,133]. However on a gold substrate, it was reported AuO species are formed above +1.0 V vs SCE in 1 M $HClO_4$ [120], but this oxide layer does not result in significant change in PbO_2 deposition.

A number of different mechanisms have been proposed by several workers for the formation of PbO_2 [95,119,130,134]. They come to conclusion that the electrodeposition process involves soluble species as reaction intermediates; these are likely to be Pb(III) and/or a Pb(IV) oxygen complex. Velichenko et al [99,120] suggested that the rate of electrodeposition of PbO_2 in nitric acid can be limited by an electron transfer or a diffusion stage and the reaction mechanism is described as follows:

$$H_2O \rightarrow OH_{ads} + H^+ + e^- \quad (1.10)$$

$$Pb^{2+} + OH_{ads} \rightarrow Pb(OH)^{2+} \quad (1.11)$$

$$Pb(OH)^{2+} + H_2O \rightarrow PbO_2 + 3H^+ + e^- \quad (1.12)$$

According to them, the first stage of the PbO_2 electrodeposition is the formation of oxygen-containing species such as chemisorbed OH, followed by a chemical stage in which these particles interact with the lead (II) species forming a soluble intermediate species (ie: $Pb(OH)^{2+}$), which is then oxidized electrochemically forming PbO_2.

At lower overpotentials, the lead dioxide electrodeposition is controlled by electron transfer with a growing diffusion zone adjusted to the surface topography. As potential increases, mixed control begins. The diffusion zone, independent from surface topography, appears with an area that is approximately the geometric surface area at full mass transport control.

Lead dioxide has often been expressed as a nonstoichiometric oxide with general formula $PbO_{2-x}.\ mH_2O$, where x denotes on oxygen deficiency and m the structural water content [122]. In view of the extensive defect structure of the PbO_2, the PbO_2 matrix is expected to be moderately tolerant of the incorporation of other foreign ions. Pure PbO_2 was demonstrated to exhibit a moderate electrocatalytic activity toward various anodic reactions in acidic media. However, the catalytic activity of the PbO_2 can be enhanced by the incorporation of some ions [135]. The incorporation of foreign

ions can activate the PbO_2 surface for O-transfer reaction. The existence of active sites in the oxide matrix will assist the oxidative discharge of water to produce OH· radicals and reduce the production of O_2 at the surface.

Several doping ions; both cations (eg: Fe^{3+}, Bi^{5+} , As^{5+}, Sb^{5+}, Co^{2+}) and anions (eg: Cl^- , OAc^- and F^-) have been used to dope pure PbO_2 electrodes for the oxidation of organic and inorganic compounds with promising results [17,72,80,113,136]. The electrocatalytic activity of pure PbO_2 electrodes, as well as their stability, can often be considerably enhanced by the incorporation of these foreign ions added to the electrodeposition solution. Feng and Johnson [17] have concluded that the incorporation of dissimilar metal cations into the PbO_2 can produce unfilled-p and/or d-orbitals which assist adsorption of ·OH radicals and reactants.

PbO_2 electrodes prepared with Bi(V) have a significant increase in rate constants for the oxidation of Mn^{2+} to MnO_4^- , phenol to benzoquinone and DMSO to $DMSO_2$ [17,113,137]. The creation of defect sites by the incorporation of Bi(V) into PbO_2 films produces an electrocatalytic effect for the oxidation of the organic compounds. Iniesta et al [138] used Bi-doped PbO_2 for phenol degradation in alkaline medium with the presence of chloride. Structural analyses of the Bi-doped PbO_2 films by X-ray diffractometry confirm the presence of bismuth and support the conclusion that Bi ions are substituted for Pb^{4+} in the slightly distorted rutile structure of the PbO_2 [137]. It is estimated that Bi sites at the PbO_2 surface are present as the +5 state and because the oxygen stoichiometry for pure Bi_2O_5 is greater than for PbO_2, it is speculated that the Bi^{5+} sites in the Bi-doped PbO_2 can adsorb hydroxyl radicals which generated by anodic discharge of H_2O (see equation 1.9). PbO_2 electrodes doped with arsenic (As-doped PbO_2) also exhibit an O-transfer activity which is greater than that of pure PbO_2 electrodes but not as great as for Bi-doped PbO_2 electrodes [139]. Many anodic O-transfer reaction rates of organic compounds at PbO_2 film electrodes are increased substantially by doping with Bi^{5+}. However, some reactions do not occur at either pure PbO_2 or Bi-doped PbO_2 electrodes. For example, neither formaldehyde nor cyanide (CN^-) is oxidized at a substantial rate. The doping of transition metal with PbO_2 (ie: Fe-doped PbO_2) has been reported to be substantially more effective than pure PbO_2 or Bi-PbO_2 electrodes for the oxidation of CN^- [17]. The oxidation product is CNO^- and then $CO_2 + N_2$. Even so, Fe_2O_3 incorporated into PbO_2 lattice has a smaller stoichiometry than PbO_2; it is predicted that a neighbouring Pb^{4+} site becomes activated

for the adsorption of OH· [80]. The Fe-doped PbO_2 electrode also has good activity for the oxidation of various thiophene derivatives such as 3-thiophene carboxylic acid (3-TCA). The incorporation of Fe^{3+} sites in PbO_2 electrode lattice has a more dramatic effect than Bi^{5+} for the oxidation of 3-TCA [80]. The Fe-doped PbO_2 is an anodic material with high electrocatalytic activity for the evolution of O_3 [135].

The incorporation of anions into PbO_2 has also improved the catalytic activity of pure PbO_2 electrodes. Johnson et al [80] speculate that anions that form slightly insoluble salts with Pb^{2+} (and Pb^{4+}) are most easily incorporated into PbO_2 films during the electrodeposition process. Hsiao et al [76] found little activity of pure PbO_2 film electrodes in the oxidation of toluene and p-xylene since the reactions were under extreme kinetic control. The incorporation of acetate (OAc^-) has performed significantly better but the surface was fouled by organic films after prolonged oxidation. Cl-doped PbO_2 electrode catalysed the oxidation of toluene to benzyl alcohol in acidic media [140]. Velichenko et al [89] studied the influence of fluoride and iron ions on the PbO_2 electrodes. The incorporation of iron and the presence of F^- into PbO_2 electrodes has enhanced the activity for ozone formation and reduced the O_2 evolution.

Much of the earlier work, however, employed very thin lead dioxide coatings prepared from low concentration of Pb(II) and their works focus on electroanalytical applications of the coated PbO_2 electrodes with low reactant concentrations and short timescale experiments where stability may not be an issue. In general, the PbO_2 electrodes produced have insufficient stability and wide range of activity. Therefore, in this study the ultimate aim is at producing PbO_2 anodes with improved electrocatalytic activity and stability for the use in industrial applications.

1.3.3 Porous PbO_2

A variety of three-dimensional and porous electrodes such as reticulated vitreous carbon, stacked meshes and perforated plates as well as particulate electrode beds have been used for many electrochemical processes, including water treatment, organic and inorganic synthesis, fuel cells and batteries. The advantage of using of such electrodes is their high surface area and high mass transfer coefficient and hence high rate of electrochemical conversion.

Casellato et al [141] have prepared porous PbO_2 electrodes with high surface roughness by anodic codeposition of β-PbO_2 particles with an electrochemically grown α-PbO_2 matrix; or called α-PbO_2 + β-PbO_2 composites. The steady-state oxygen evolution current density for the porous α-PbO_2 + β-PbO_2 composites was found to be 15-18 times higher than α-PbO_2 deposits. The codeposition technique was also employed for the preparation of porous PbO_2 electrodes as dispersed phase with other composites such as Co_3O_4 [91,92,142,143] or RuO_2 [144] as the matrix. The generation of porous and rough electrodes by codeposition of conducting particles might produce interesting materials for oxidative degradation of organic compounds.

Another approach of producing porous structure of PbO_2 is by using surfactants or emulsions. Blood et al [145] have prepared porous PbO_2 via anodic electrodeposition from a stationary high internal phase emulsion (HIPE) on carbon electrode substrates. The resulting deposits are organized in 10-50 μm high pyramidal aggregates, pitted with smaller pores. They reported that the deposits produced by this technique show at least a threefold increase in electroactive surface area per mass of deposit from those produced by normal or plain electrodeposition.

Colloidal crystal templated synthesis technique has recently been developed to enable the chemical preparation of macroporous metal oxides with three-dimensionally ordered arrays of regular and sub-micron diameter pores [146,147].The general concept of this technique is to form a colloidal crystal template of close-packed with uniform sized spheres and the interstitial spaces are filled with a fluid precursor which capable of solidification and the template is removed to obtain a porous inverse replica. Macroporous α- and β-PbO_2 films arranged in a highly ordered close-packed structure were prepared by electrochemical deposition through self-assembled polystyrene spheres (500 or 750 nm in diameter) assembled on gold and indium tin oxides (ITO) substrates via colloidal crystal templating technique [148]. The macroporous PbO_2 frameworks were found to be highly polycrystalline, self-supporting and free from defects.

Generally, when the focus of research is the use of PbO_2 as an anode, efforts are directed at improving the electrode stability and electrocatalytic activity. In conclusion, it can be said that many attempts have been made in order to improve the properties of PbO_2 films. Much research is required before PbO_2 can have commercial significance

for electrolytic degradation of organic compounds such as the optimization of the electrodeposited PbO_2 on inexpensive substrate materials.

1.4 Cell Designs

The engineering aspects of cell design for efficient mass transport is equally crucial for practical applications in wastewater treatment besides the fundamental aspects of an electrochemical process such as the choice of electrode material and the electrode reaction.

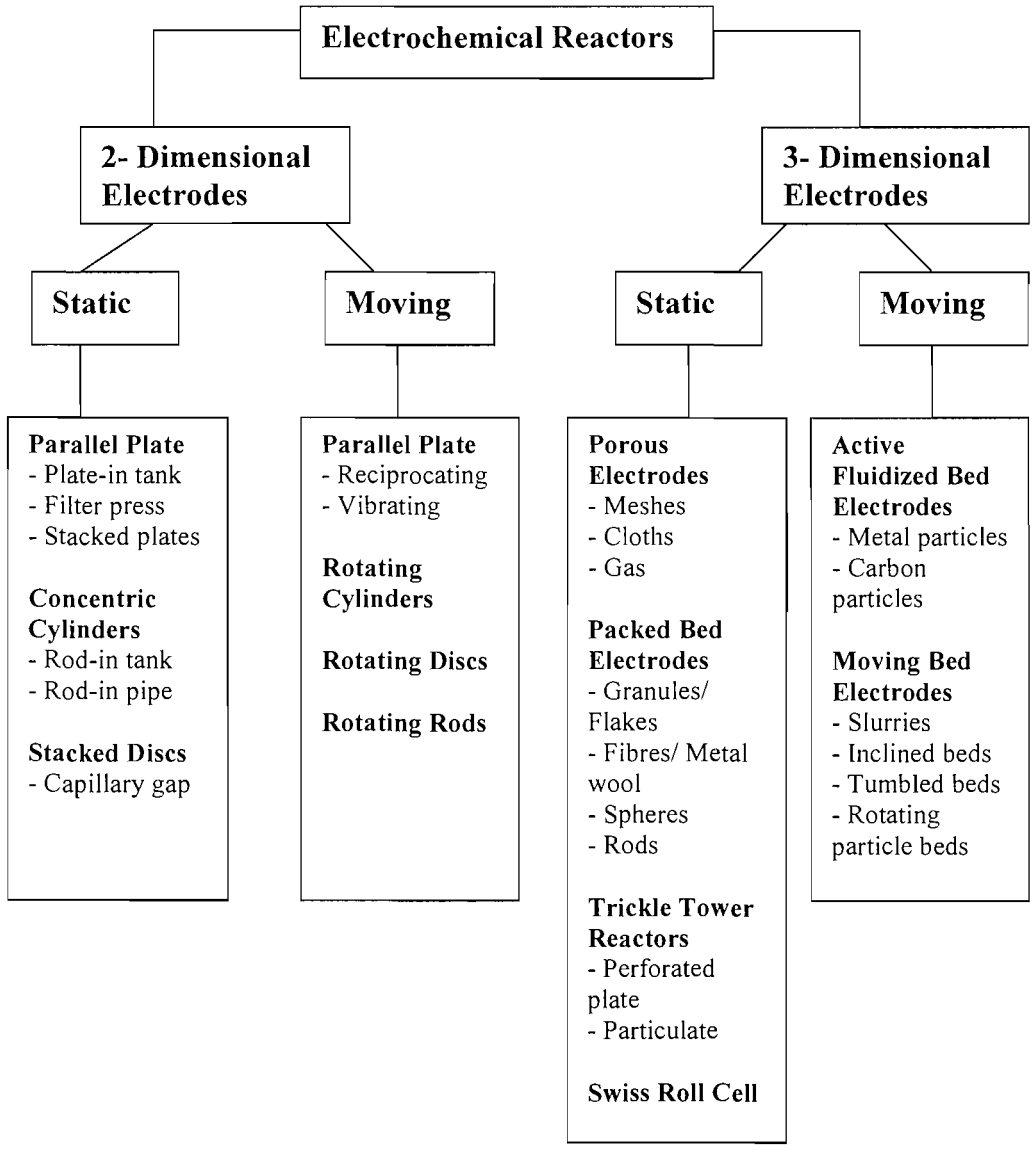

Figure 1.7: Classification of electrochemical reactors in terms of the electrode geometry and motion (adopted from Walsh [149]).

There are two types of two dimensional (2-dimensional) electrodes as listed in figure 1.7; static and dynamic (moving). For laboratory experiments or small scale electrolysis, a simple set up such as the use of a cylinder electrode in a beaker cell without forced convection is sufficient. But, there are a number of factors needs to be considered for larger scale or industrial cell design as proposed by Pletcher and Walsh [47] :

- Simplicity
- Operational convenience and reliability
- Integration and versatility
- Reaction engineering parameters
- Running costs

In wastewater treatment, the electrochemical processes are based on flow cells, since they are well suited for continuous operation. Normally, parallel plate flow cells are the convenient and popular choice for the purpose due to the following reasons [47]:

- Simplicity of construction with regard to features such as frames and electrode connections
- A choice of commercial filterpress cells is available from various manufacturers in a range of different sizes
- Mass transport may be enhanced or adjusted using a variety of turbulence promoters and control of the mean linear electrolyte velocity
- The potential distribution is reasonably uniform
- Scale-up is readily achieved by a suitable combination of increased electrode size and using more electrodes
- Three dimensional electrodes may be incorporated

Mass transport rates within a parallel plate reactor may be increased by increasing the fluid velocity or by the use of turbulence promoters. Forcing the electrolyte through the cell at a higher velocity will reduce the diffusion boundary layer thickness and thus increase mass transport to the electrode, but at the expense of higher energy requirements for pumping and lower conversion per pass. Placing inert turbulence promoters (usually plastic polymers) in the path of the electrolyte is a

convenient and cost effective way of increasing mass transport, since their presence increases the local fluid velocity and turbulence.

Mass transport in an electrochemical cell can occur via migration, diffusion and convection. Migration of the reactant species is usually negligible when a large excess of inert electrolyte is present. In unstirred solutions, diffusion is the only mass transport mechanism; however, the timescale of such experiments should be kept short in order to avoid the interference of natural convection. Forced convection is the predominant mode of mass transport in stirred beaker cells and in flow cells, but diffusion remains important close to the electrode surface.

In order to obtain reliable mechanistic and quantitative kinetic information, the form of forced convection must be capable of exact description by mathematical equations. This is usually the case in flow cells, but is impossible in stirred beaker cells.

When the electron transfer from the electrode surface to the electroactive species in solution is fast (ie: the electrode overpotential is high enough), the rate of reaction becomes limited by the supply of reactant to the electrode surface. Under these conditions of limiting current, the performance of a reactor can be written in terms of a mass transport coefficient, k_m:

$$\mathbf{I_L = n F k_m A c} \qquad \textbf{(1.13)}$$

where I_L is the limiting current , n the number of electrons involved, F the Faraday constant (96485 C mol^{-1}), A the area of the electrode and c the concentration of the reactant.

For low energy consumption the current efficiency should be high (no side reactions) and the cell voltage as low as possible. The cell voltage is a function of the equilibrium potentials and overpotentials of both (anode and cathode) reaction as well as resistances in the cell (eg: in the electrolyte, electrode and current feeders) and the external circuit; and given by the following equation:

$$\mathbf{E_{Cell} = E_e^C - E_e^A - |\eta_C| - |\eta_A| - iR_{Cell} - iR_{Circuit}} \qquad \textbf{(1.14)}$$

where E_{cell} is the cell voltage, E_e^C the equilibrium potential at cathode, E_e^A the equilibrium potential at anode, $|\eta_C|$ the overpotential at cathode, $|\eta_A|$ the overpotential

at anode, iR_{Cell} the resistance in the cell and $iR_{Circuit}$ the resistance of the external circuit.

The difference in equilibrium potentials are determined by the cell chemistry, low overpotentials are determined by the selection of materials and low iR drop can be partly be achieved by good cell design.

1.5 Three Dimensional Electrodes

Three dimensional (3-dimensonal) electrodes are porous structures, which can have in various geometries such as particulate, foams or stack of meshes and can be made of different materials. Many are available in carbon and a range of metals such as stainless steel, aluminium, titanium etc. Both can be used as base materials for further deposition with more active coatings such as metal oxides or other composites. They can be either static or dynamic (moving) as listed in figure 1.7.

Electrochemical reactors based on a porous 3-dimensional electrode can have a very high surface area per unit electrode volume and also more turbulent mass transport conditions which can be produced adjacent to the electrode surface. This combination of properties leads to a great enhanced rate of electrolysis and contributes to substantial effect to the electrochemical approach to effluent treatment.

This can be quantitatively seen by comparing the mass transport controlled current, I_L at a two dimensional electrode as equation 1.13 and at a three dimensional electrode as shown below.

$$\mathbf{I_L = n F A_e V_e k_m c} \qquad \mathbf{(1.15)}$$

where A_e is the specific electrode area (units $m^2\ m^{-3}$) and V_e the volume of the three dimensional electrode.

There are two main types of reactors where 3-dimensional electrodes may be employed; the batch reactor and the plug flow reactor as shown in figure 1.8.

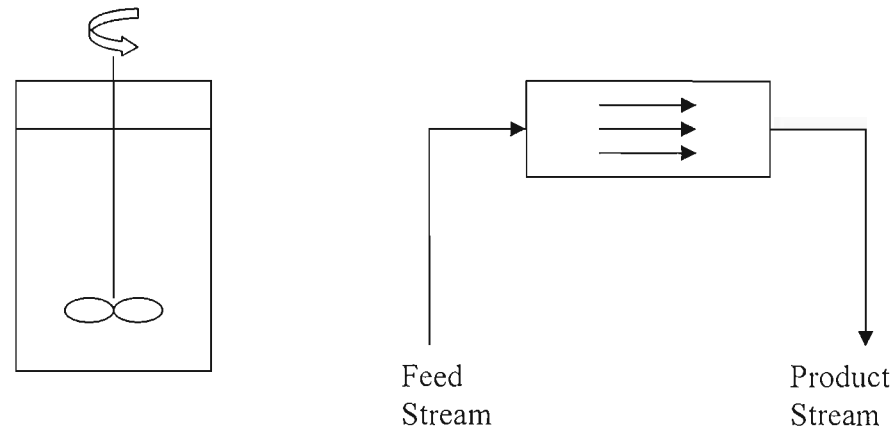

(a) (b)

Figure 1.8: Type of electrochemical reactors based on 3-dimensional electrodes; (a) batch reactor (b) plug flow reactor

The rate of electrolysis using this electrode can be expressed in terms of either the reduction in the concentration of reactant:

(a) for the batch reactor

$$\frac{c_{(t)}}{c_{(0)}} = \exp - \frac{k_m A_e V_e t}{V} \qquad (1.16)$$

where $c_{(0)}$ is the initial concentration of reactant, $c_{(t)}$ the concentration after time t and V the volume of the solution.

Or

(b) for the plug flow reactor

$$\frac{c_{(Out)}}{c_{(In)}} = \exp - \frac{k_m A_e V_e}{Q} \qquad (1.17)$$

where $c_{(Out)}$ and $c_{(In)}$ are the concentrations at the outlet and inlet to the cell respectively, and Q is the volumetric flow rate for the solution flow (units $m^3 s^{-1}$).

From these equations (ie: 1.15, 1.16 and 1.17), it is clear that with high values of k_m and $A_e V_e$, a high conversion of reactant to product is possible either in short time or during a single pass of a solution through the cell and even when very low concentration of reactant present. Therefore, 3-dimensional electrodes are ideally suitable for the removal of organic compounds from effluents before discharge.

In plug flow reactors, the 3-dimensional electrodes have two configurations, the flow-through mode and the flow-by mode. With the flow-through, current and electrolyte flow are parallel while for the flow-by mode; they are perpendicular; these are illustrated in figure 1.9.

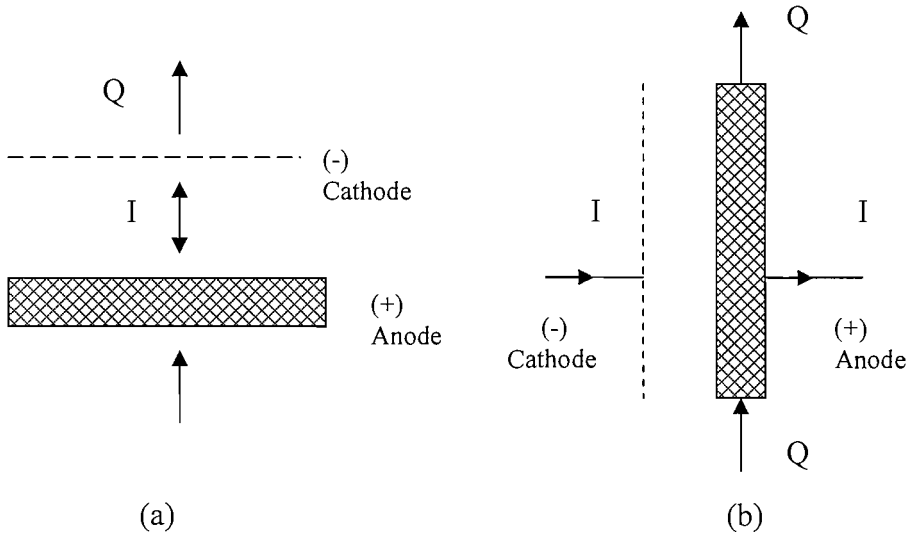

Figure 1.9: Configurations for 3-dimensional anode cells; (a) flow-through mode and (b) flow-by mode. I= Current flow, Q= Electrolyte Flow

Most of the porous and packed bed electrodes employ the flow-by mode configuration, in which high fractional conversions of reactants per pass are possible. The overall conversions can be increased by increasing the width or length of the porous electrode. In laboratory experiments, a higher conversion is achievable by plug flow reactor with batch recycle operation as shown in figure 1.10. In this system, the stirred tank is an additional advantage which facilitates temperature and composition (eg: pH) control, together with measurement and sampling facilities.

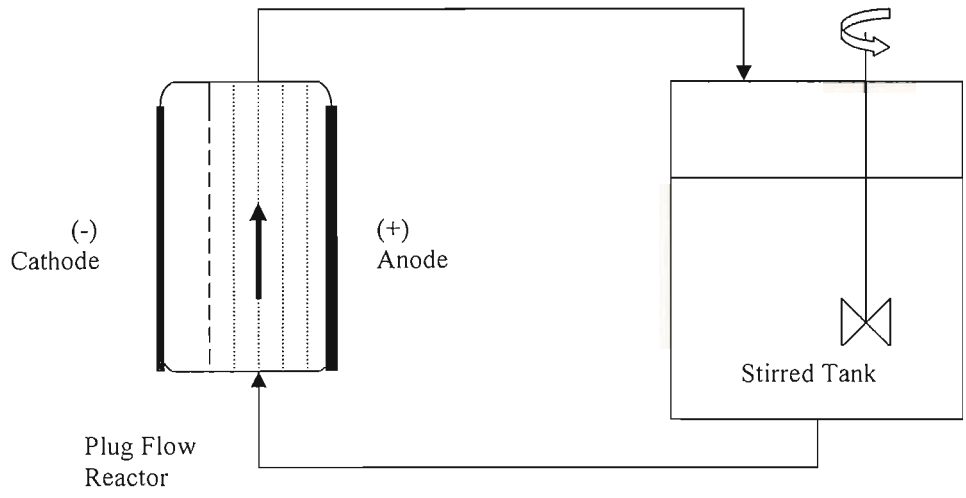

Figure 1.10: Plug flow reactor batch recycle operation.

1.6 Objectives

This present study is focused on the improvement of the stability and catalytic activity of lead dioxide (PbO_2) as an anode material for the use in the oxidation of organic compounds especially for wastewater treatment. PbO_2 anodes will be electrodeposited on gold and titanium substrates. Active PbO_2 anodes will be fabricated by the incorporation with potential dopant ions (eg: Fe^{3+}, Ag^{+}, Bi^{3+}) and the formation of high surface area electrodes by deposition as macroporous structures or deposition on Ti mesh to be used as the anode in a flow cell system. Deposition parameters will be adjusted and optimized in order to produce a highly stable and active PbO_2. It is envisaged that the fabricated anodes will remove organic compounds from wastewater.

Chapter 2: Experimental

2.0 Chemicals and Materials

All aqueous solutions were prepared with water from a Whatman Analyst purifier. The chemicals and materials used were supplied by the sources as shown in table 2.1.

Chemical / Material	Source	Grade / Purity
Alumina Powder	Buehler	1.0, 0.3 and 0.05 μm
Epoxy Resin + Hardener	Ciba-Geigy	Araldite (Fast setting)
Gold Wire (0.1 cm diameter)	Goodfellow	99.9 %
Titanium Rod (0.5 cm diameter)	Goodfellow	99.6 %
Expanded Titanium Mesh	Dexmet Corporation	99.5 %
Nitric Acid : HNO_3	Fisher Chemicals	70 %
Sulphuric Acid : H_2SO_4	Fisher Chemicals	98 %
Hydrochloric Acid : HCl	BDH Chemicals Ltd.	36.5 – 38 %
Oxalic Acid dihydrate	Avocado	98 %
Potasium Chloride : KCl	Fisher Chemicals	Analytical Reagent
Sodium Sulphate Anhydrous : Na_2SO_4	Hogg Chemicals	99 %
Sodium Acetate Anhydrous: CH_3COONa	FisherChemicals	Analytical Reagent 99 %
Sodium Fluoride : NaF	BDH Chemicals Ltd.	Analytical Reagent 99 %
Sodium Hydroxide : NaOH	Fisher Chemicals	Laboratory Reagent
Toluene : $C_6H_5CH_3$	Fisher Chemicals	Laboratory Reagent
Dimethyl Sulfoxide : CH_3SOCH_3	Fisher Chemicals	Analytical Reagent 99.96 %
3-Thiophenecarboxylic Acid : $C_5H_4O_2S$	Aldrich	99 %
3-Picoline: $C_6H_7N_1$	Avocado	99 %
Lead Nitrate : $Pb(NO_3)_2$	Alfa Aesar	99 %
Bismuth Nitrate : $Bi(NO_3)_3.5H_2O$	BDH Chemicals Ltd.	Analytical Reagent
Silver Nitrate : $AgNO_3$	Johnson Matthey Chemicals Ltd.	-
Ferric Nitrate : $Fe(NO_3)_3.9H_2O$	Hogg Chemicals	Laboratory Reagents

Ferrous Acetate : $Fe(CH_3COO)_2$	Aldrich	Laboratory Reagent 95 %
Lead Acetate trihydrate : $Pb(CH_3COO)_2.3H_2O$	Avocado	Analytical Reagent 99 %
Sodium Sulphide : $Na_2S.xH_2O$	Timstar Laboratory Suppliers	Laboratory Reagent
Polystyrene Latex Spheres (500 nm)	Alfa Aesar	2.5 % solutions in water
Reactive Blue 4 Dye $C_{23}H_{14}C_{l2}N_6O_8S_2$	Sigma-Aldrich	Dye content 35%
Methyl Orange $(CH_3)_2NC_6H_4N{:}NC_6H_4SO_3Na$	BDH	-
Bromothymol Blue $C_{27}H_{28}Br_2O_5S$	Aldrich	0.04 wt % solution in water
Cresol Red $C_{21}H_{17}O_5S$	Aldrich	0.04 wt % solution in water

Table 2.1: List of chemicals and materials supplied from manufacturers and also their grades.

Control of Substances Hazardous to Health Regulations (COSHH) assessment forms were filled in before using any chemical. All work involving hazardous chemicals or fumes was carried out in a fume cupboard and all experiments were carried out within a containing tray. Otherwise, good laboratory practice (GLP) was followed.

The majority of the project was using lead containing solutions as the bath solutions for PbO_2 electrodes production. The disposal of these solutions was achieved by using the following procedure:

Solutions were adjusted to pH 6 (with the addition of NaOH) and the Pb(II) reacted with sodium sulphide to form a black precipitate of lead sulphide (PbS) in a fume cupboard. The sodium sulphide was added in aliquots until no further precipitate was formed. The precipitate was allowed to settle and then separated from the liquid phase by filtration, dried and collected and the solid sent for disposal. The remaining, lead-free solution, was disposed off via the drain with plenty of water.

2.1 Preparation of PbO_2 Coatings

There were 2 types of substrates used for the deposition of PbO_2; gold and titanium. Both substrates underwent different surface treatment before deposition.

2.1.1 PbO_2 on Gold

For the preparation of PbO_2 coated Au electrode, two different size of RDE gold substrates were used; 0.008 cm^2 and 0.11 cm^2, respectively. Prior to each deposition, gold electrodes were gently polished on Buehler microcloth with alumina slurries (0.3 and 0.05 μm) and then rinsed with purified water until a mirror finish was obtained.

Pure and doped PbO_2 electrode depositions were carried out using constant current density (galvanostatic technique) in the range of 1 to 25 mA cm^{-2}. All depositions were done in a two-compartment glass cell.

As mentioned in section 1.3.2, PbO_2 occurs in two crystallographic forms; α-PbO_2 and β-PbO_2. The first was prepared from Pb(II) in acetate buffers. Lead acetate in sodium acetate was used as the bath for this study. Meanwhile, β-PbO_2 electrodes were prepared from solution containing lead nitrate in nitric acid. The majority of the preparations used acidic solutions which led to β-PbO_2 production.

Doped PbO_2 electrodes were prepared by the addition of metal cations or dopant ions such as Ag(I) , Ni(II) , Fe(III) and Bi(III). Mostly, 10 mM of the particular dopant ion was added into the bath solution containing Pb(II).

Between experiments, any remaining deposit was removed from the gold substrate by cathodic stripping at + 200 mV or by sequential polishing with slurries of 1.0, 0.3 and 0.05 micron alumina powder on microcloth (Buehler).

2.1.2 PbO_2 on Titanium

For the deposition of PbO_2 on titanium, the surface of the substrate needs to be treated prior to deposition in order to produce a good quality deposit and also to make the surface clean and free from TiO_2. High purity titanium discs of diameter 0.5 cm (area: 0.20 cm^2) were used as the substrates.

2.1.2.1 Surface Pre-treatment

The surface pre-treatment consist of two stages:

a) The first stage is a physical treatment where the Ti disc is abraded on silicon carbide emery paper (P 1200) and followed by polishing on a microcloth (Buehler) by alumina slurries 0.3 μm until a mirror finish is obtained.

b) The second stage is a chemical treatment where the polished surface is immersed in a boiling aqueous solution of either oxalic acid (1.6 M) or hydrochloric acid (11.5 M) until the TiO_2 dissolved.

2.1.2.2 Coating Procedure

Coating by pure and doped PbO_2 on the treated titanium was carried out immediately after pre-treatment in order to minimise the formation of a TiO_2 surface film.The electrodeposition of the PbO_2 electrodes was performed at constant current density ranging from 0.5 to 20 mA cm^{-2}. The process was carried out in a two-compartment electrochemical cell. A variety of deposition parameters such as Pb(II) concentration, acid concentration, temperature, etc. was manipulated and investigated to find the most suitable conditions for the production of the best quality deposit in terms on stability and catalytic activity.

2.1.3 Determination of Coating Thickness

The average coating thickness of PbO_2 on gold or titanium substrate was determined by the following equation:

$$\textbf{Average thickness} = \frac{j.t.MW}{n.F.\rho} \times \textbf{current efficiency} \qquad (2.1)$$

where j is the current density employed during deposition in A cm^{-2}, t is the deposition time in seconds, MW is the molecular weight of PbO_2 = 240 g mol^{-1}. While F refers to Faraday constant = 96485 C mol^{-1} and n is the number of electron involved for PbO_2

deposition is 2 . The density (ρ) of the electrodeposited PbO_2 was assumed to be 9.3 g cm^{-3}.

2.2 Preparation of Macroporous PbO_2 films

2.2.1 Assembly of Colloidal Templates

Monodispersed polystyrene latex spheres, with diameter of 500 nm ± 20 nm, were obtained from Alfa Aesar as 2.5% suspensions in water. Polystyrene sphere templates were assembled by sticking a 0.8 cm internal diameter Teflon ring using double gloss nail's polish onto the working electrode.

Approximately, 0.5 cm^3 of an aqueous suspension of the monodisperse polystyrene spheres diluted with water to 1 wt % was spread over the area of the substrate surrounded by the teflon ring. The sample was left undisturbed in a saturated humidity environment for 2 to 3 days in order to allow the spheres to sediment on to the substrate. A clear water layer subsequently appeared on top of the deposited spheres and this water layer was then allowed to slowly evaporate. Once all of the water had evaporated, the Teflon ring was removed to leave a circular area covered by the template.

2.2.2 Electrodeposition of Macroporous PbO_2

Macroporous PbO_2 films were deposited at constant current from a solution containing Pb(II) in nitric acid. The deposition was carried out in a short time depending on the thickness of film required corresponded to the radius of the template particles used. Calculation of charge required for the deposition of PbO_2 with half sphere layer of polystyrene template (diameter: 500 nm) on 0.008 cm^2 gold substrate is shown in Appendix A.

The polystyrene template was completely removed by soaking in toluene for 2 hours to leave behind a macroporous PbO_2 film with honey-comb structure as shown in figure 2.1.

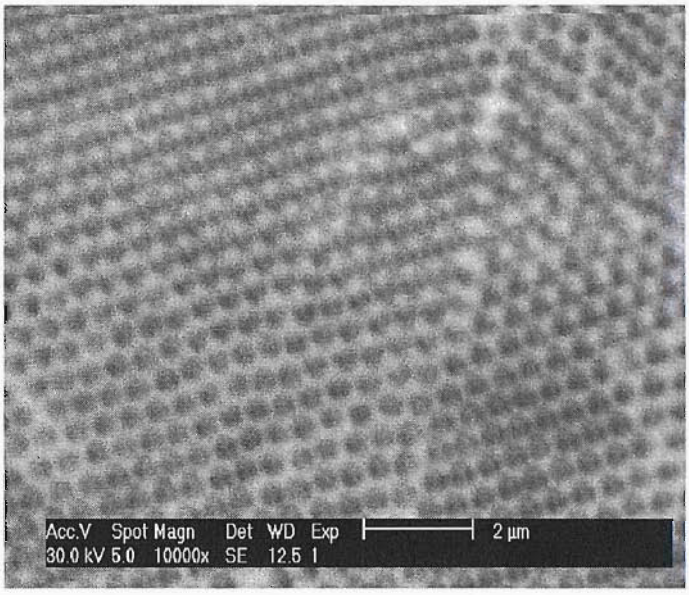

Figure 2.1: A honeycomb structure of macroporous PbO_2 film taken by scanning electron microscopy (SEM). The structure results by deposition into a self assembled monolayer of polystyrene spheres of 500 nm.

The schematic diagram of producing the macroporous PbO_2 film through colloidal templating electrodeposition is shown in figure 2.2.

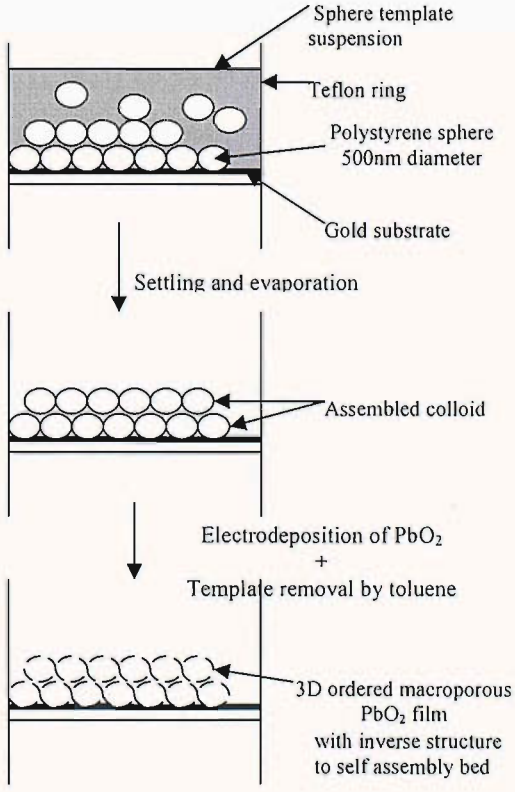

Figure 2.2: Schematic of the formation of ordered macroporous PbO_2 through colloidal templating of electrodeposition.

2.3 Preparation of PbO_2 on Expanded Titanium Mesh

The expanded Ti mesh was a gift from Dexmet/Delker Corporation. Table 2.2 summarizes the characteristics and dimensions of the meshes used in this work. The total exposed areas were calculated using formulae provided by Delker on their website (www.delkergrid.com/techinfo.html).

Mesh Type	Material	Density (g cm^{-3})	SWD (cm)	LWD (cm)	Strand width (cm)	Thickness (cm)	Overall dimension (cm)	A_{geo} (cm^2)
Fine	Ti	4.5	0.0533	0.0787	0.0127	0.0118	1x1x0.0118	1.6
Fine	Ti	4.5	0.0533	0.0787	0.0127	0.0118	3x5x0.0118	25

Table 2.2: Characteristics of fine expanded Ti meshes used in this work. LWD = long way dimension, SWD = short way dimension and A_{geo} = geometric surface area.

The product code supplied was 5.4 Ti 5-031. The first number represents nominal original thickness (5.4 = 0.0054 in or 0.118 mm). The number immediately following Ti represents strand width (5 = 0.005 in or 0.127 mm) and the last number indicates the long way dimension (LWD) (0.31 = 0.031 in or 0.787 mm). Figure 2.3 shows a sketch of one mesh of the expanded metal.

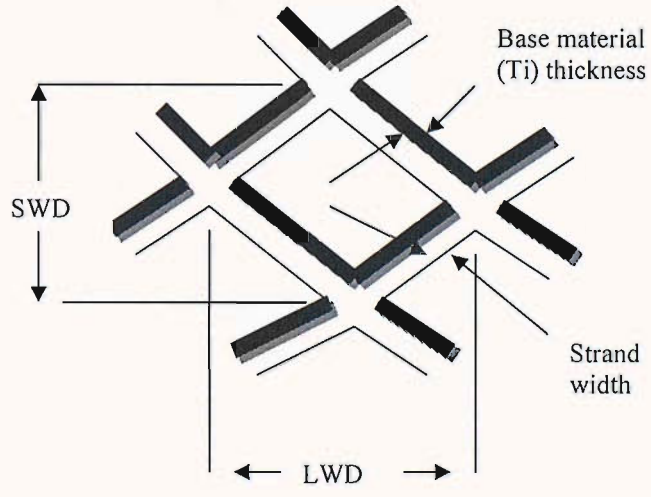

Figure 2.3: Sketch of one mesh of expanded Ti metal

There were two different dimensions of Ti mesh used in this study; 1 cm^2 and 15 cm^2. One centimeter square (1 cm^2) of the expanded mesh is shown in figure 2.4. The meshes were initially treated in boiling oxalic acid (1.6 M) for > 1 hour in order to remove TiO_2 and to produce high surface roughness. Figure 2.5 shows the images of titanium mesh surface before and after pre-treatment.

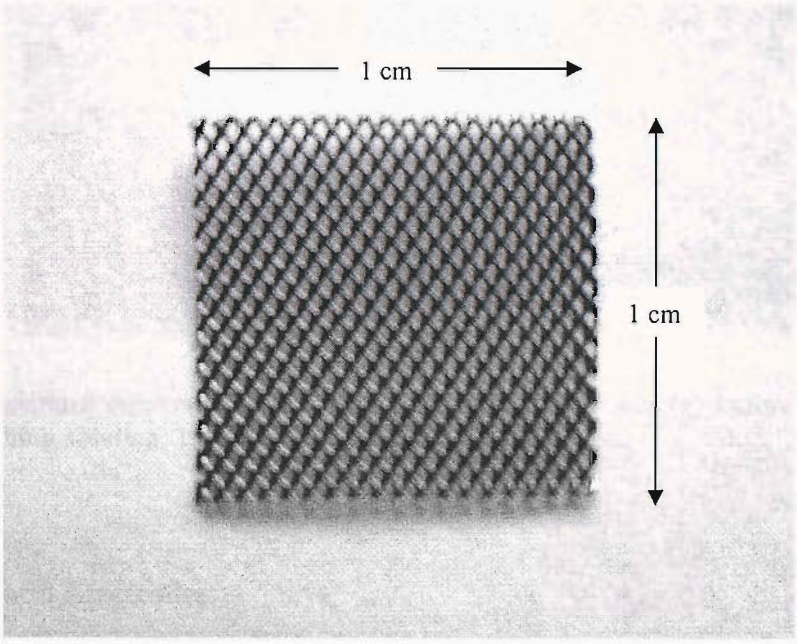

Figure 2.4: Photograph of 1 cm^2 expanded Ti mesh used in this work. Estimated geometric surface area: 1.6 cm^2.

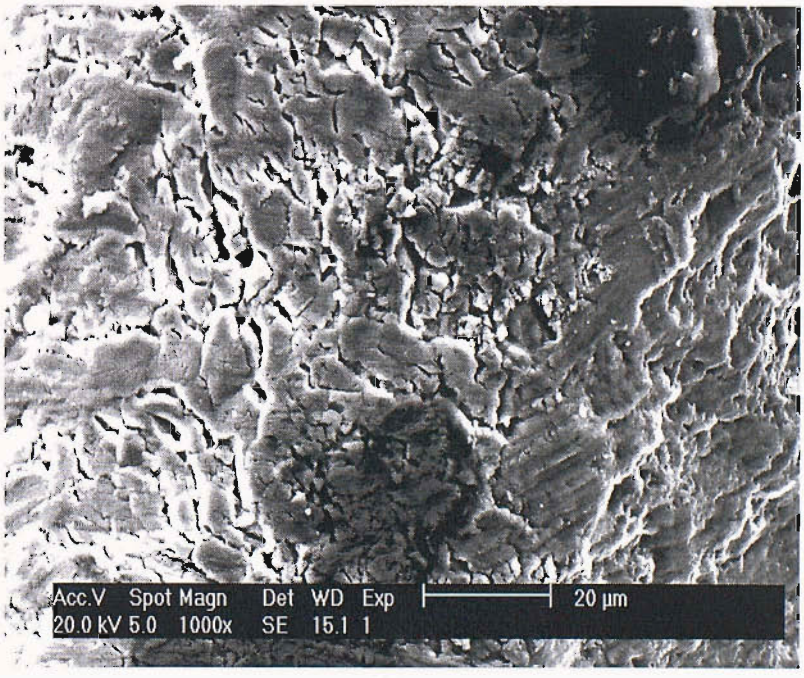

(a)

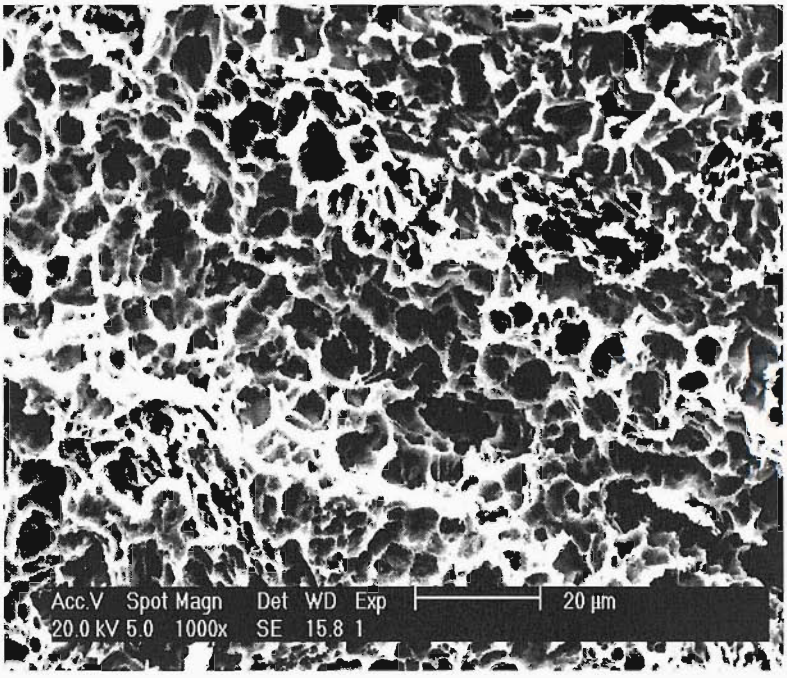

(b)

Figure 2.5: Scanning electron micrographs of fine titanium mesh (a) before (b) after pre-treatment. Etching solution: 1.6 M oxalic acid.

2.4 Cells and Electrodes

A two-compartment cell was used for electrodeposition and electrochemical studies of PbO_2 film electrodes on gold and titanium discs. The cell as shown in figure 2.6, is of the three electrode type with the working electrode and the counter electrode were separated from the reference electrode compartment. The reference electrode used was homemade saturated electrode calomel (SCE). All electrochemical potentials are quoted versus saturated calomel electrode as a reference. This gives a shift of -0.241 V compared to the widely used reference – standard hydrogen electrode (SHE). A platinum coil acted as the counter electrode.

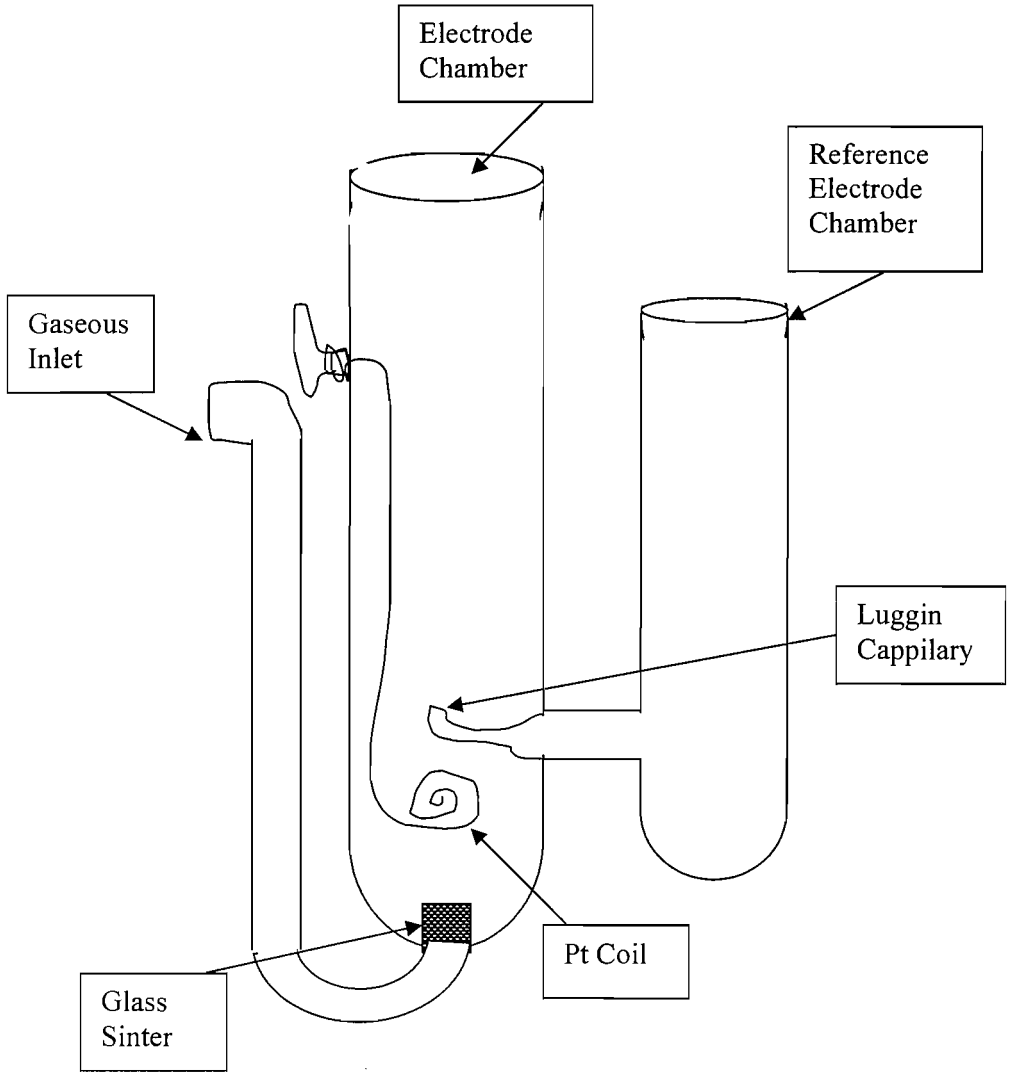

Figure 2.6: Two-compartment electrochemical cell

The working electrodes used were rotating disc electrodes (RDE) of gold with area of 0.11 cm^2 and also titanium (area: 0.20 cm^2). Each of the discs was mounted in a PTFE shroud as shown in figure 2.7(a) and (b). Figure 2.7 (c) shows the PbO_2 electrode deposited on titanium substrate.

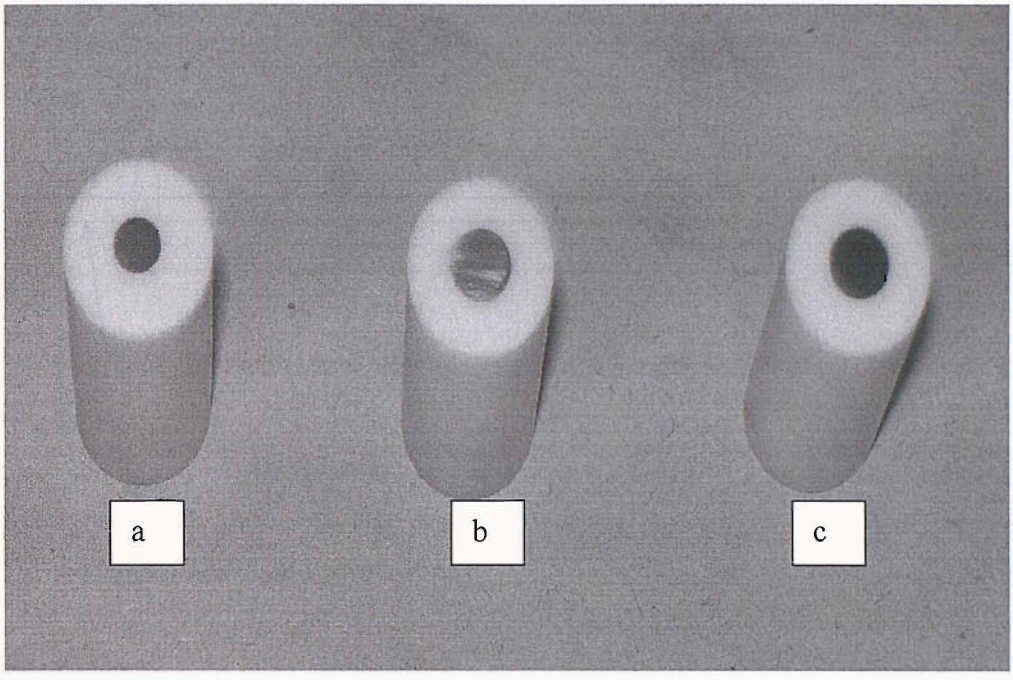

Figure 2.7: RDE working electrode of (a) gold (b) titanium and (c) PbO_2 on Ti

The surface of the working electrode disc was placed about 1 mm from the tip of a luggin capillary. The Luggin capillary is used to minimize any iR drop in the electrolyte associated with the passage of current in the electrochemical cell. A fine glass sinter was placed at the bottom of the cell to allow the efficient entry of gases into the electrolyte solutions.

Some experiments for the deposition of PbO_2 were carried out using smaller gold electrodes (area: 0.008 cm^2). The electrodes were home-made and prepared from 1 mm diameter gold wire as shown in figure 2.8.

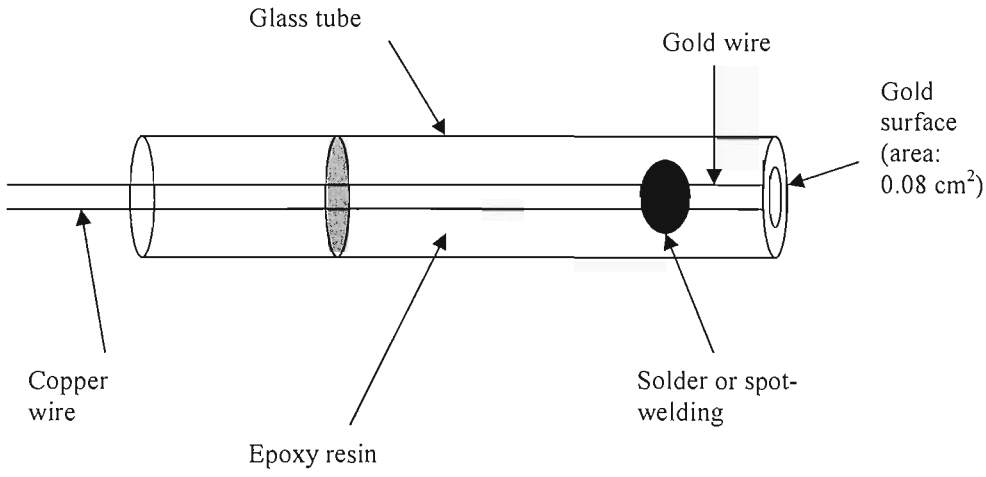

Figure 2.8: A Home-made Gold Electrode

The gold electrode was soldered or spot welded to a copper wire and fitted into a 10 cm long glass tube of 8 mm outer and 4 mm inner diameter. The end of the glass was sealed off with epoxy resin so that the gold electrode was firmly held at the middle with geometric surface area of 0.008 cm^2. The epoxy also avoided the solution from contacting the copper wire during an electrochemical experiment.

Meanwhile the electrodeposition and electrochemical studies of PbO_2 electrodes on Ti mesh was carried out in a small beaker cell as shown in figure 2.9. The cell has a volume of ~ 100 ml and has a removable Luggin capillary and reference electrode compartment. The counter electrodes are two Ni foils, 30 mm x 50 mm x 0.0118 mm, placed equidistant on either of the deposited Ti mesh. The cell is suitable for both cyclic voltammetry and electrolysis experiments of mesh electrodes.

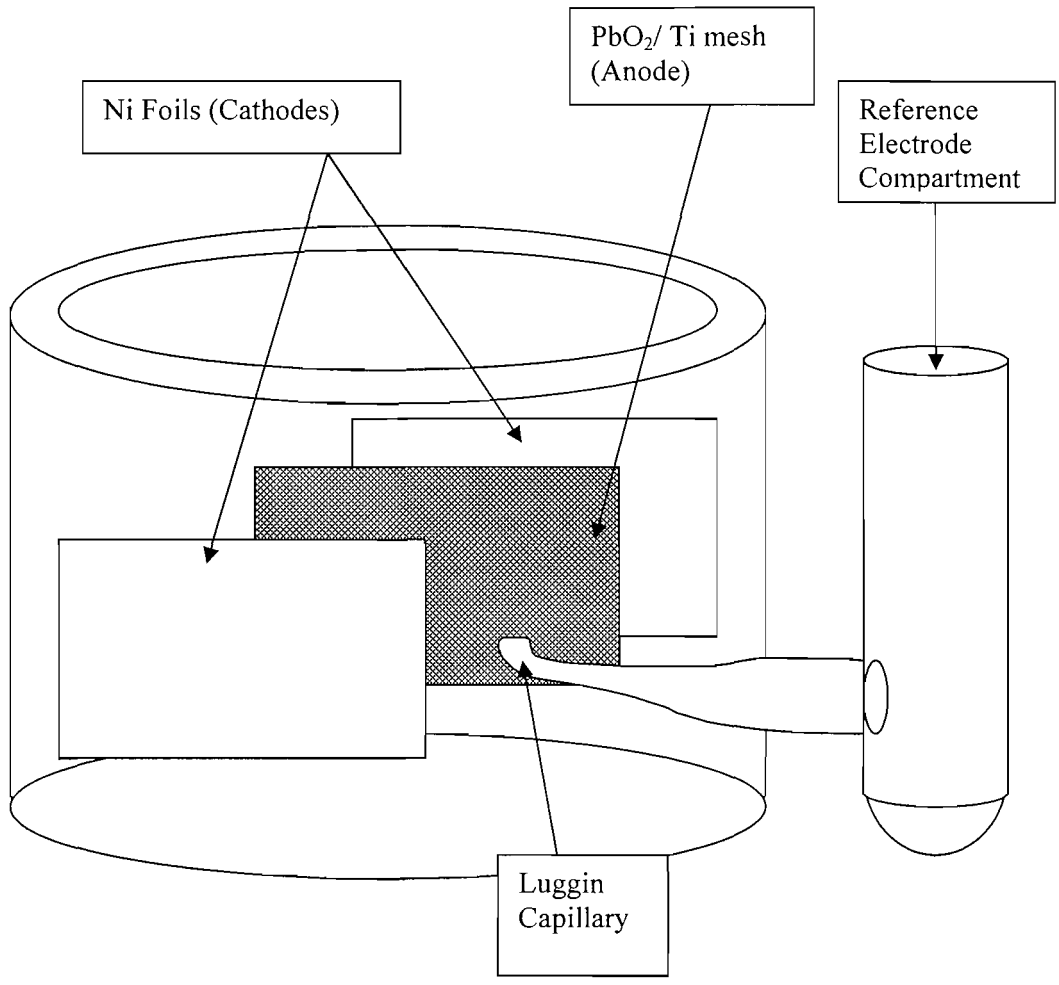

Figure 2.9: A beaker cell used for electrodeposition and electrochemical studies of PbO_2 electrodes on expanded Ti mesh.

2.5 Instrumentation

Voltammetric measurements were performed using one of these two equivalent sets of apparatus:

a) a Hi-Tek Instruments PPRI waveform generator coupled to a Hi-Tek Instruments type DT 2101 potentiostat. Results obtained from this apparatus were recorded with the use of a Bryans Instrument X-Y chart recorder.

b) a potentiostat coupled to a waveform generator supplied by T W Young and connected to a PC. Data were collected using in house data acquisition software.

Electrodeposition of PbO_2 coatings on gold and titanium substrates were carried out galvanostatically using the Hi-Tek instruments PPRI waveform generator coupled to the Hi-Tek instruments type DT 2101 potentiostat.

A rotator model 616 EG & G PARC was used to rotate the RDE working electrodes. To control the temperature for deposition, the electrochemical cell was immersed in a Camlab W 14 thermostatted water bath. Unless otherwise stated, voltammograms were recorded at 298 K.

2.6 Electrode Analyses

Several electrode analysis techniques were carried out to examine the characteristics and performance of the prepared PbO_2 deposits.

2.6.1 Adhesion Tests

The adhesion test was carried out for evaluating the adhesive quality of PbO_2 coatings on gold and titanium surfaces. The attractive force that exists between the coating and the substrate can be measured as the force required for separating the deposit from the substrate. The adhesion property on gold or titanium discs was categorized based on the following tests done as shown in table 2.3.

Test	Observation	Adhesion Property
Rubbed with tissue or pulled with adhesive tape	Easily removed	Poor
Sticked with adhesive tape or rubbed on microcloth with alumina slurries	Hardly removed or some removed	Medium
Rubbed on microcloth with alumina slurries or rubbed on emery paper	Very difficult to be removed	Good

Table 2.3: Classification of adhesion quality of PbO_2 coatings on gold or titanium substrates.

2.6.2 Scanning Electron Microscopy (SEM)

Morphology of electrodeposited pure and doped PbO_2 was examined using a scanning electron microscope (Model: Philips XL 30 ESEM). The microscope was operated with the sample chamber under high vacuum (chamber pressure of 10^{-5} mBar or lower). An electron accelerating voltage of 20 or 25 keV was typically used to observe bare electrodes (gold and titanium) and PbO_2 deposits. Sample was mounted on an adjustable stage within the microscope with a working distance of 10 mm between the probe detector and sample surface.

The SEM was also equipped with control software for energy dispersive analysis by X-rays (EDAX). This gives information about the elemental composition of the surface layers and the results are presented as plots of counts within the time measurement (or counts per second) against the x-ray quantum energy in keV.

2.6.3 Catalytic Activity Analysis

The catalytic activity of the pure and doped PbO_2 electrodes was defined by investigation of their ability to support the oxidation of organics. Most of the PbO_2 electrodes activity studies were performed using dimethyl sulfoxide (DMSO) dissolved in 1 M sulphuric acid. Anodic oxidation of DMSO to $DMSO_2$ (dimethyl sulfone) was used for intercomparison of electrode activities because of DMSO is unreactive at substrate materials (eg: Au, Pt or Carbon).The oxidation of the organic compound can be written as in equation 2.2.

$$(CH_3)_2SO + H_2O \longrightarrow (CH_3)_2SO_2 + 2H^+ + 2e^- \qquad (2.2)$$

Occasionally, other organic substance such as 3-thiophene carboxylic acid was used to examine the catalytic activity of PbO_2 electrodes. Decolouration of a few dyes (ie: Reactive Blue 4, Methyl Orange, Bromothymol Blue and Cresol Red) were also carried out in order to study the activity of PbO_2 deposited on Ti meshes.

2.6.4 Stability Analysis

The stability analysis on the produced PbO_2 electrodes (either on gold or Ti substrates) on open circuit was carried out by immersing the electrodes in several electrolytes solution with and without DMSO. The changes of the deposits after a period of time were observed by the naked eye and the change in morphology was examined by SEM.

The stability of the produced PbO_2 electrodes during electrolysis or on load was also investigated by passing the current at constant potential (ie: above the formal potential for Pb^{2+}/PbO_2). The changes were again observed by the naked eye and SEM.

Chapter 3: Electrodeposition of PbO_2 on Gold

3.0 Introduction

As discussed in the Introduction, many papers have discussed the electrodeposition of PbO_2 and several consider gold as the substrate [87,95,120]. While acidic nitrate solutions have been commonly used for the electrodeposition, there is little agreement between the published procedures as to the optimum conditions for the preparation of stable PbO_2 coatings. In this programme, the stability of the PbO_2 deposits, both on load and on open circuit were of particular interest and this is an aspect rarely considered by earlier workers. Here stability includes adhesion, resistance to abrasion, corrosion and chemical stability.

In this chapter, preliminary experiments to compare with the literature and to understand the relationship between deposition conditions and deposit characteristics are reported.

3.1 Cyclic Voltammetry Study

A series of experiments using cyclic voltammetry to study the deposition and dissolution of PbO_2 at a gold disk electrode was carried out to define the influence of Pb(II) concentration, acid concentration and temperature. The voltammograms were recorded from +0.40 to +1.90 V and back to +0.40 V vs SCE by scanning the potential at a scan rate 100 mV s^{-1}. All the potentials are quoted versus SCE.

3.1.1 Effect of Pb(II) Concentration

Figure 3.1 shows a voltammogram of PbO_2/Pb^{2+} couple at a gold electrode in solution containing 30 mM Pb(II) + 1 M HNO_3 at a scan rate of 100 mV s^{-1}. There is a range of potential where current is higher on reverse scan than on forward scan at E > + 1.60 V. This is evidence for phase formation involving nucleation and growth of PbO_2. The growth of the deposit is observed by a rapid increase in anodic current for E > +1.80V and continues until ca. +1.60 V on the reverse scan.

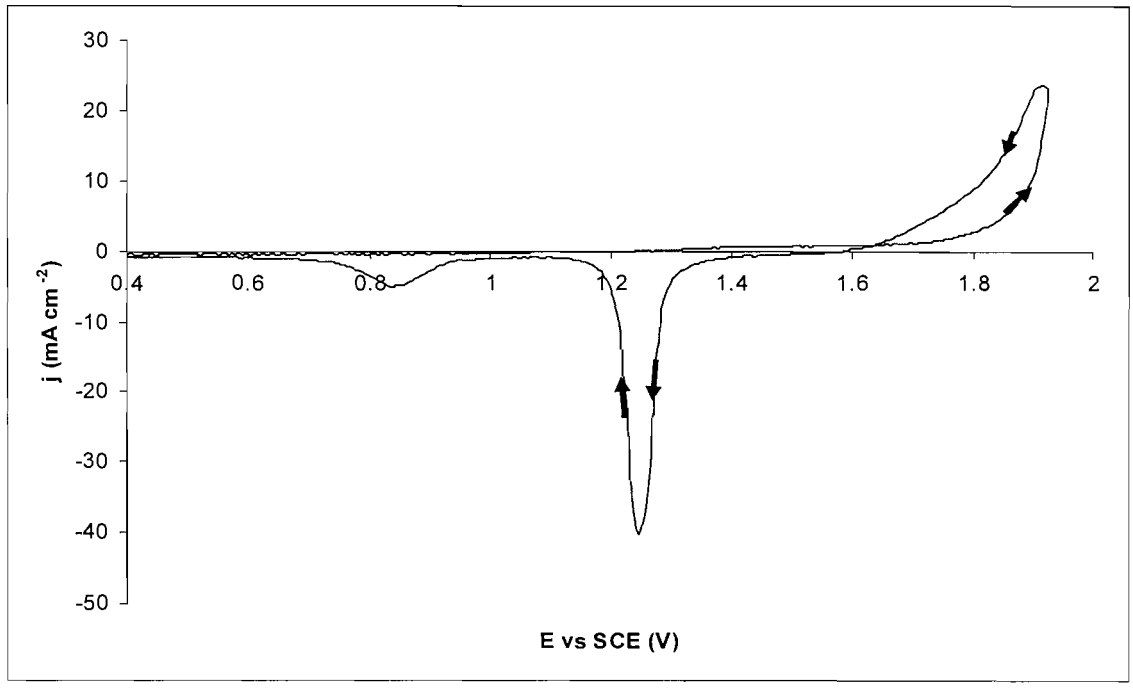

Figure 3.1: Cyclic voltammograms of gold electrode in 1 M nitric acid containing 30 mM Pb(II) at scan rate 100 mV s^{-1}.

The rapid increase in current at E > +1.80 V is due to the PbO_2 formation simultaneously with the O_2 evolution as a competing reaction [94]. This observation is according to the electrochemical reactions in equations 3.1 and 3.2.

$$Pb^{2+} + 2H_2O - 2e \longrightarrow PbO_2 + 4H^+ \quad (3.1)$$

$$2H_2O - 4e \longrightarrow O_2 + 4H^+ \quad (3.2)$$

Further on the reverse scan, a sharp symmetrical reduction peak appears at + 1.22 V which corresponds to the dissolution of PbO_2 back to Pb(II). The charge balance ($Q_{Cathodic}/Q_{Anodic}$) for the deposition and dissolution of PbO_2 is more than 90% which indicates that the current efficiency for $PbO_2 \leftrightarrow$ Pb(II) is high and the contribution of O_2 evolution to the current is small during PbO_2 deposition in this solution.

It can also be seen in the figure that a small increase in anodic current occurs at E > +1.30 V and an additional peak at +0.85 V on the cathodic scan. These are believed to be the formation and reduction of AuO. A cyclic voltammetry was carried out for the Au disc in 1 M nitric acid solution without the presence of Pb(II) ions in order to confirm these conclusions. As can be seen in figure 3.2, both features appear at the same potentials as in figure 3.1. This confirms the formation and dissolution of AuO on

the gold surface as reported by several workers [150,151]. In the figure, a rapid increase in current is seen at E > +1.80 V on the anodic scan is due to O_2 evolution on the gold oxide surface. These voltammograms are consistent with those reported by several workers for the deposition and dissolution of PbO_2 at gold electrodes in acidic media [87,94,123,131] and results previously presented in nitric acid [95,119].

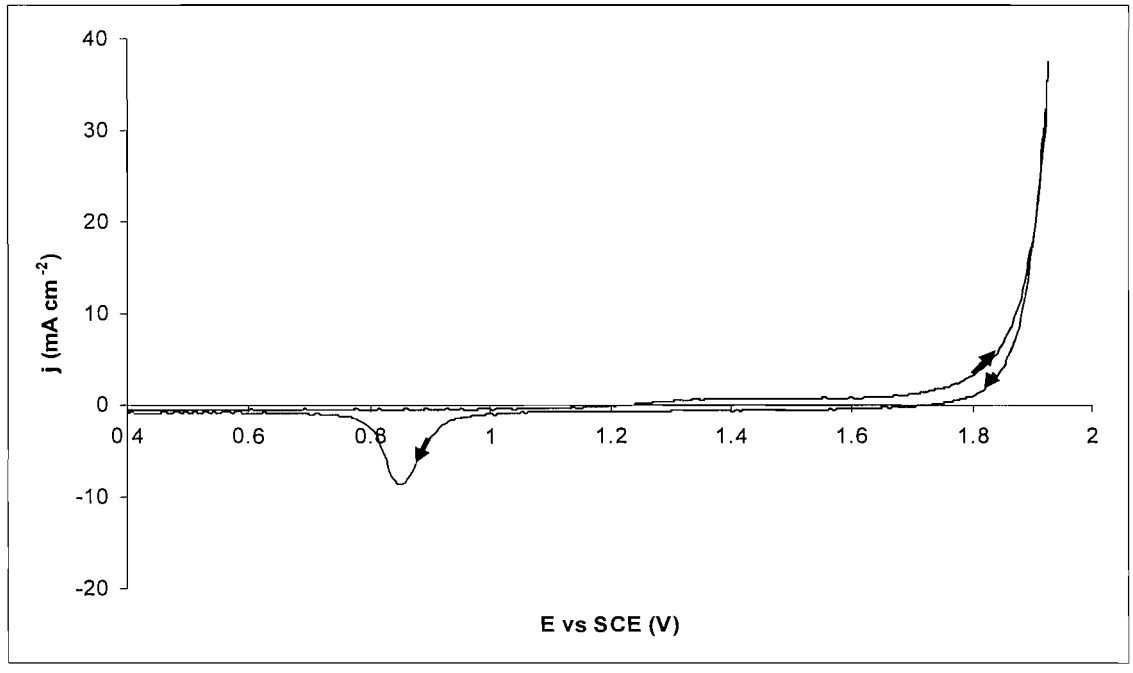

Figure 3.2: Cyclic voltammograms of gold electrode in 1 M nitric acid without the presence of Pb(II) at scan rate 100 mV s^{-1}.

In order to investigate the influence of Pb(II) concentration on the PbO_2/ Pb^{2+} couple, two further Pb(II) concentrations (ie: 100 mM Pb(II) and 500 mM Pb(II)) in 1 M HNO_3 were used. The same cyclic voltammetry experiment was carried out on each solution. Figure 3.3 shows the voltammetric curves corresponding to the deposition and dissolution processes of lead dioxide in 1 M nitric acid containing the two further Pb(II) concentrations. In this figure, the deposition and reduction of AuO species are not as clearly visible as in figure 3.1. This is due to higher concentration of Pb(II); more PbO_2 is deposited and reduced as shown by high anodic and cathodic current densities which dominate the response.

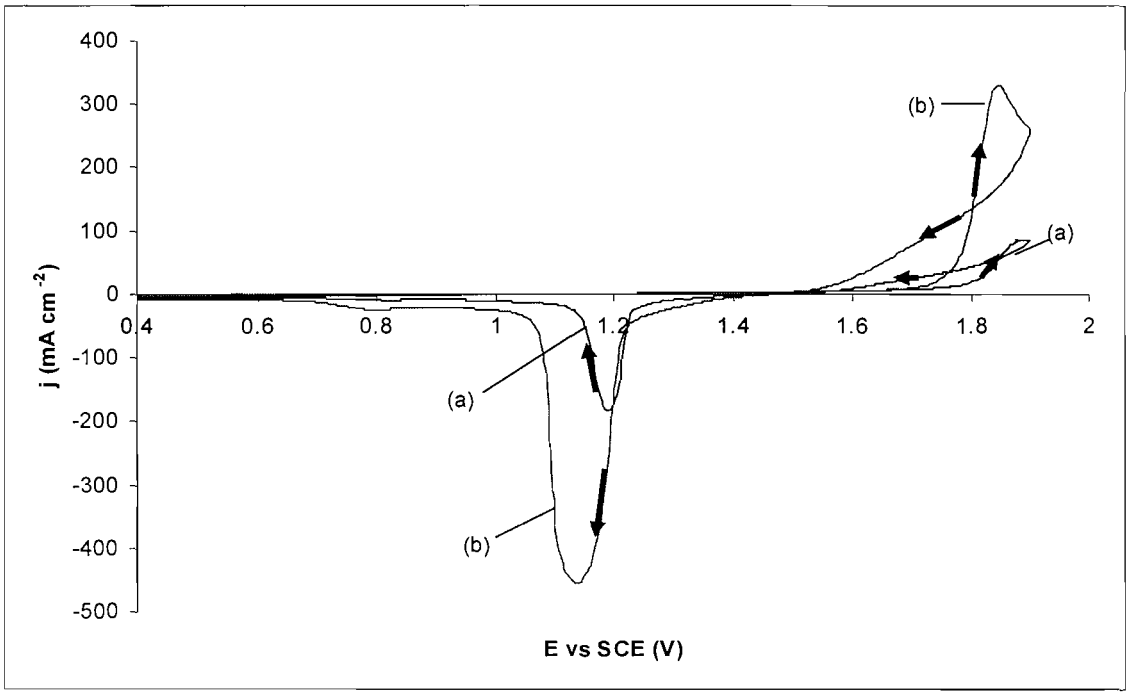

Figure 3.3: Cyclic voltammograms of gold electrode in 1 M nitric acid containing different Pb(II) concentration (a) 100 mM (b) 500 mM at scan rate 100 mV s^{-1}.

It should be noted that the current involved for the deposition and dissolution of PbO_2 is massive. On the current scale used, for the solution containing 100 mM Pb(II), anodic current is seen positive to +1.70 V. Again, as for 30 mM, there is a range of E where current is higher on negative going scan than on the forward scan due to the nucleation and growth of PbO_2. The peak at very high current density results from mass transport control by Pb(II), although the literature suggests that some O_2 evolution could also be occurring. Further, on the reverse scan towards less positive potentials, a well-defined cathodic peak is observed at +1.19 V due to the reduction of PbO_2 to Pb(II). The cathodic reduction of PbO_2 in this solution is initiated at negative to + 1.40 V.

It can clearly be seen that at + 1.80 V the current is much higher with 500 mM Pb(II) than with 100 mM Pb(II) or 30 mM Pb(II). Again, as in lower concentration of Pb(II), the growth of the PbO_2 deposit is represented by a rapid increase in anodic current at E > + 1.76 V and continues until ca. +1.50 V on the reverse scan. Further on the reverse scan, a cathodic peak appears at +1.11 V which is associated with the reduction and dissolution process of the anodically formed PbO_2 to Pb(II). From both figures (3.1 and 3.2), it was found that the potentials for PbO_2 deposition and dissolution shifted negative with increasing Pb(II) concentration. These findings are

related to Nernst equation below:

$$E_e = E^{\theta} + RT/2F \ln \frac{[H^+]^4}{[Pb^{2+}]} \quad (3.3)$$

The equilibrium potential for the PbO_2/Pb^{2+} couple will shift positive (120 mV / pH unit) with increasing acid concentration and negative (30 mV / 10 fold change in Pb^{2+}) with increasing Pb(II) concentration.

It is also noted that the deposition rate of PbO_2 from 500 mM Pb(II) onto the gold surface is faster and the current involved per unit area is much bigger (about five times bigger) than in 100 M Pb(II). This indicates that the current is proportional to the concentration of Pb(II). The cathodic peak is also increased greatly when the Pb(II) ion concentration increases.

The thicknesses of the PbO_2 deposits prepared from each solution can be estimated using Faraday law as shown below.

$$\text{Thickness of } PbO_2 \text{ deposit} = \frac{Q \times 10^{-3} \times MW \times \Phi}{n \times F \times \rho} \quad (3.4)$$

$$= (1.34 \times 10^{-7}) \times Q \times \Phi \quad (3.5)$$

Where Q is the charge passed for the deposition in mC cm^{-2}, Φ is the deposition efficiency, MW is the molecular weight of PbO_2 (240 g mol^{-1}), n is the number of electron involved, F is the Faraday constant (96485 C mol^{-1}) and ρ is the density of the PbO_2 (9.3 g cm^{-3}).

Based on the $Q_{Cathodic}$ the area under the reduction peak of each voltammogram, the thickness of the deposits prepared from 30 mM, 100 mM and 500 mM Pb(II) are estimated to be 0.04 μm, 0.14 μm and 0.61 μm, respectively. For all concentrations, the charge balance ($Q_{Cathodic}/Q_{Anodic}$) is more than 90% which corresponds to high current efficiency for $PbO_2 \leftrightarrow$ Pb(II) and it is believed that O_2 evolves only slowly during deposition.

3.1.2 Effect of Acid Concentration

Figure 3.4 shows cyclic voltammograms for lead dioxide deposition and dissolution in different concentrations of nitric acid containing 500 mM Pb(II) onto a

gold working electrode.

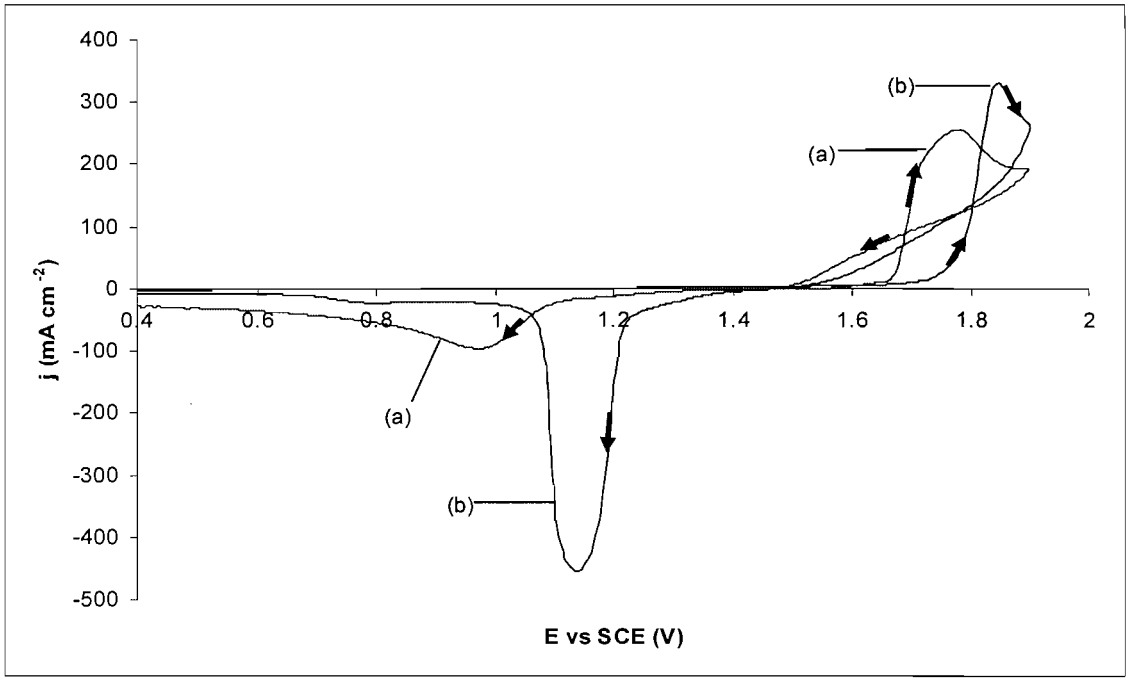

Figure 3.4: Cyclic voltammograms (j – E) of 500 mM Pb(II) in (a) 0.1 M HNO_3 (b) 1 M HNO_3 at gold disk electrode. Potential scan rate: 100 mV s^{-1}

With more dilute nitric acid solution (ie: 0.1 M HNO_3), the deposition of PbO_2 occurs at less positive potential. The lower deposition potential is largely due to the thermodynamics for PbO_2 deposition. It can be seen from equation (3.3) that the equilibrium potential for the PbO_2/Pb^{2+} couple will shift negative by 120 mV for an increase in pH by one unit. In addition, in 0.1 M, the cathodic peak occurs at less positive potential ca. +0.98 V and the peak is broad and smaller; in comparison in 1 M HNO_3, it is bigger and sharp as seen in the figure. It is believed that the shape of the reduction peaks for PbO_2 dissolution is related to the strength of the acid concentration used. The reduction of each PbO_2 molecule consumes four protons. With 0.1 M HNO_3 and a thick PbO_2 layer, protons close to the PbO_2 surface become depleted causing a shift in the pH and hence in the thermodynamics and kinetics of the reduction. It is also possible that some insulating PbO is formed. Thus, the reduction process occurs very slowly which leading to the formation of small and broad peak as in the figure. However, with 1 M HNO_3, more protons are present in the solution therefore the reduction of PbO_2 occurs faster leading to the big and sharp peak. The reduction of PbO_2 to Pb(II) in acidic media is shown in equation 3.6.

$$PbO_2 + 4H^+ \xrightarrow{+2e} Pb^{2+} + 2H_2O \qquad (3.6)$$

With decreasing acid concentration, the deposition and reduction peaks for PbO_2 are shifted to less positive potentials about 120 mV per pH unit as explained earlier for equation 3.3.

The charge balance calculated for deposition and reduction of PbO_2 in 0.1 M HNO_3 is < 70 %. A probable explanation for this is the incomplete conversion of PbO_2 to Pb(II) during dissolution and the formation of small quantities of lead oxide (PbO) at least on the timescale of voltammetry. A tetragonal form of PbO having a red colour is well known [124] and it has been observed on the gold surface following dissolution of PbO_2 after back scan until + 0.40 V. Velichenko et. al [95] reported that two cathodic peaks of PbO_2 dissolution from gold surface appeared at ca. + 1.20 V and at ca. +0.03 V vs Ag/AgCl, respectively. The latter peak was explained by the dissolution of an ultrathin film of lead oxide covered the gold electrode [152]. However, no red deposit was observed on the gold electrode for the dissolution of PbO_2 prepared from 1 M HNO_3 after scanning until +0.40 V and the Q_C/ Q_A calculated was > 90 %. It is believed that in 1 M HNO_3 almost all of the PbO_2 was converted to Pb(II) after scanning until +0.40 V. Therefore, in order to remove all of the PbO_2 deposits prepared from more dilute nitric acid from the gold surface the scan back potential must be extended to + 0.05 V vs SCE and held there for a few seconds.

3.1.3 Effect of Temperature

Figure 3.5 shows the cyclic voltammetric curves obtained for a gold electrode in a 500 mM Pb(II) + 1 M HNO_3 solution at different temperatures, 298K and 333K. It can be seen that, with increasing deposition temperature, the growth of PbO_2 deposits onto the gold surface occurs at less positive potential due to faster nucleation and deposition. More PbO_2 was deposited at 333 K.

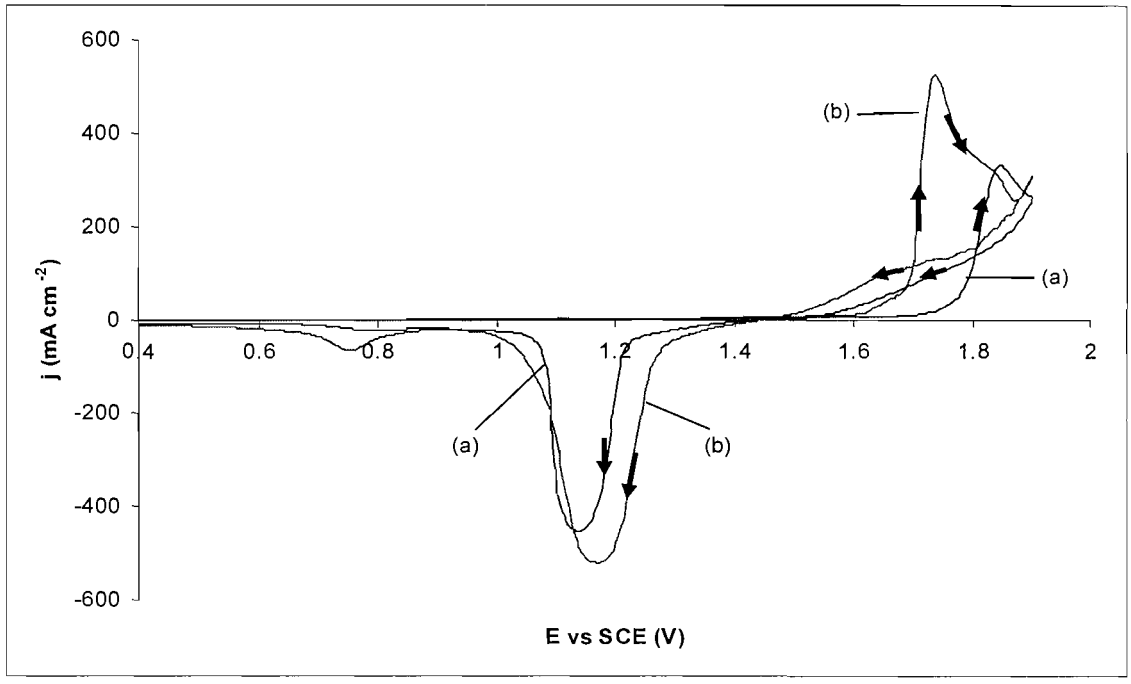

Figure 3.5: Current density (j) vs potential (E) for deposition and dissolution of PbO_2 onto gold disk electrode in 1 M HNO_3 at different temperature (a) 298 K (b) 333 K. Potential scan rate 100 mV s^{-1}.

It can be seen that at 333 K, bigger currents are recorded at all potentials than at room temperature. The increase in current density at all potentials results from an increase in rate constants for all the steps in the PbO_2/Pb^{2+} interconversion at the higher temperature. The current efficiency is also good for deposition and dissolution of PbO_2 at 333 K with a charge ratio > 90 %. Also, no red deposit was observed left on the gold surface after scanning back until +0.40 V. This means that at 333 K, the contribution of O_2 evolution remains small and almost all PbO_2 was converted back to Pb(II). At 333 K, a bigger peak for reduction of AuO to Au is observed at +0.78 V. This indicates that more Au is anodically oxidized at 333 K than at 298 K.

3.2 Scanning Electron Microscopic Study

The morphologies of all PbO_2 deposits prepared from various deposition conditions were observed and recorded by scanning electron microscopy (SEM). The experiments used both small discs (area: 0.008 cm^2) sealed into glass and discs (area: 0.11 cm^2) within a PTFE shroud. This section is a summary of a large number of experiments and the relationships between deposition conditions and structure were very reproducible.

3.2.1 Influence of Pb(II) Concentration

Figure 3.5 shows the scanning electron microscopic (SEM) images of PbO_2 deposits prepared from different concentrations of Pb(II) in 1 M HNO_3 using a constant current density (ie: 5 mA cm^{-2}) at 298 K for 300 s.

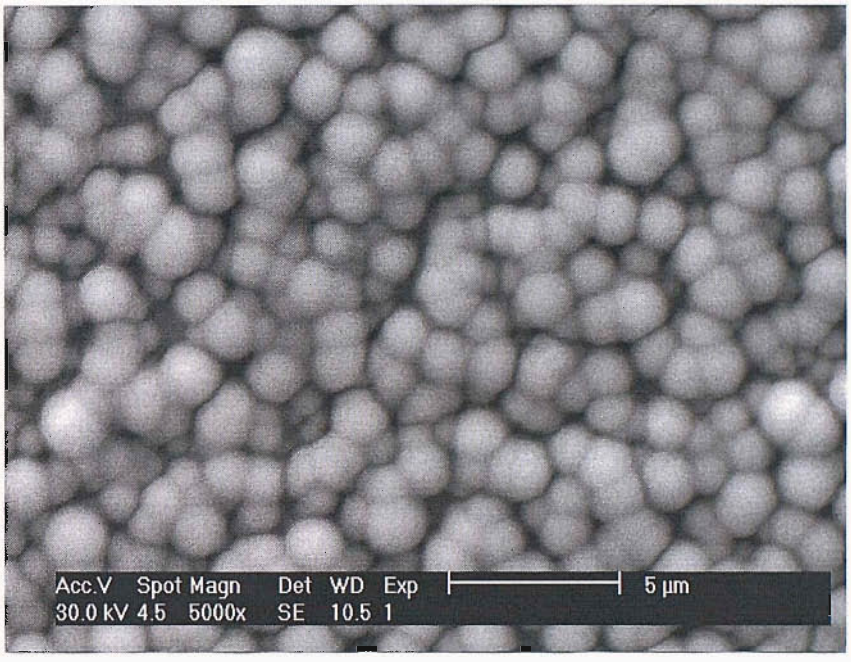

(a)

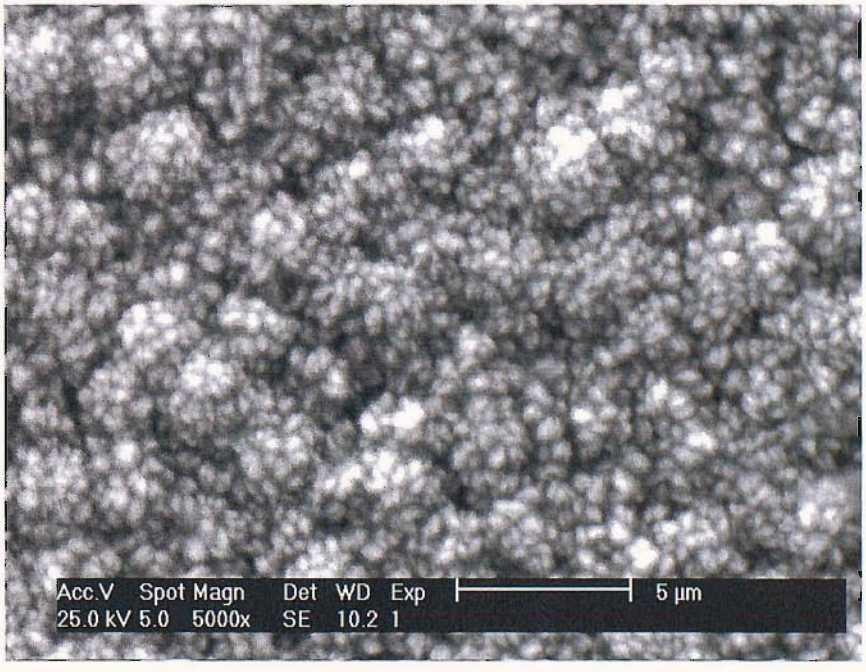

(b)

Figure 3.5: SEM images of PbO_2 prepared from different concentration of Pb(II) (a) 30 mM (b) 500 mM. Deposition conditions: 5 mA cm^{-2}, 300 s, 298 K

It was observed that the deposit prepared from 30 mM Pb(II), see figure 3.5a, consisted of hemispherical centers, not totally uniform in size but typically 1-2 μm in diameter. Moreover, although there is substantial overlap of the centers, there also appear to be significant voids in the structure between some centers. Meanwhile, under the same deposition conditions, PbO_2 deposits prepared from high concentration of Pb(II) (ie: 500 mM), the morphology was a more complex as shown in figure 3.4b. The deposits have hemispherical centers around 2-5 μm in diameter but these are clearly made up of agglomerates of much smaller centers.

The colour of the deposits prepared from 500 mM Pb(II) was black as compared to dark brown for 30 mM Pb(II). It is apparent that under the same charge passed (Q= 1500 mC cm^{-2}) more PbO_2 is formed or deposited on gold substrate from 500 mM than 30 mM of Pb(II) solution. Based on equation 3.5, the thickness of PbO_2 prepared with Q = 1500 mC cm^{-2} should be 2μm.

However, the thicknesses measured from SEM images taken at 8.1° tilt angle for the PbO_2 deposits prepared from 30 mM Pb(II) were less than 2μm. As can be seen in figure 3.6a, the thicknesses of the PbO_2 were in the range of 0.8 – 1.0 μm. Meanwhile, the thickness measured from the PbO_2 deposits prepared from 500 mM Pb(II) was approximately 2 μm as seen in figure 3.6b.

This indicates that for solution containing 30 mM Pb(II), under the deposition conditions used, only about 50 % of the charge was consumed in the oxidation of Pb(II) to PbO_2. It is believed that some of the currents are used for O_2 evolution during the deposition. This was consistent with the presence of a lot of bubbles on the electrode surface later in the deposition. By comparison with cyclic voltammetry of PbO_2/Pb^{2+}couple for solution containing 30 mM Pb(II) (as shown in figure 3.1), the thickness calculated from $Q_{cathodic}$ peak area of the cyclic voltammetry was higher and that measured on the SEM image lower. The lower result is believed to be due to the depletion of Pb(II) concentration close to the electrode surface during the deposition of the thicker deposit and more O_2 evolves.

(a)

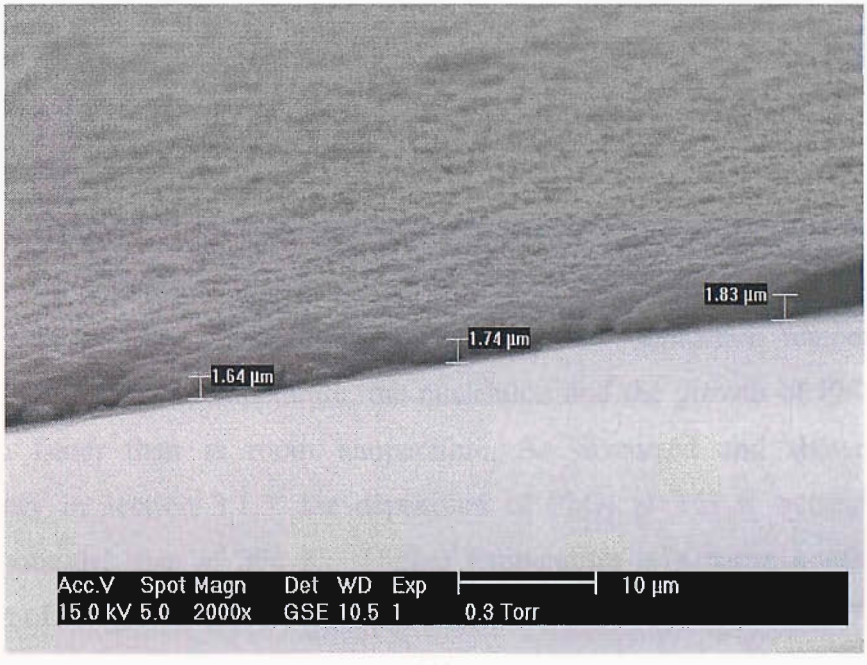

(b)

Figure 3.6: SEM images taken at 8.1° tilt angle using gaseous secondary electron (GSE) detector of PbO_2 prepared from (a) 30 mM Pb(II) and (b) 500 mM Pb(II). Deposition conditions: 5 mA cm^{-2}, 300 s, 298 K

On the other hand, for the solution with 500 mM Pb(II), there is semi quantitative agreement between the estimates PbO_2 thicknesses calculated from the charge passed during cyclic voltammograms (see equation 3.5) and that measured directly from the SEM image shown in figure 3.6b. The thicknesses measured from the SEM, figure 3.6b indicate that almost all the current was used for oxidation of Pb^{2+} to

PbO_2 with relatively little leading to O_2 evolution. Furthermore, there was no bubble observed on the electrode surface during the deposition. With increasing Pb(II) concentration, more nucleation centers are believed to be formed both on the gold substrate and the growing PbO_2 deposit and less O_2 evolves. The growth of PbO_2 becomes faster; resulting a thicker deposit. Also the deposit structure becomes more complex.

3.2.2 Influence of Temperature

An investigation into the influence of the deposition temperature on the morphology of PbO_2 was also carried out. Figure 3.7 compares the PbO_2 deposits prepared at two different deposition temperatures (ie: 298 K and 333 K) carried out using constant current density (ie: 5 mA cm^{-2}) for 600 s from solution containing 500 mM Pb(II) + 1 M HNO_3.

The deposits prepared at room temperature (ie: 298 K) have hemispherical clusters around 5 – 8 μm in diameter made up of small centers with gaps in the structure as shown in figure 3.7a. Figure 3.7b shows the PbO_2 deposit prepared at elevated temperature (ie: 333 K). At the higher temperature, the deposits were made up of closely packed angular grains with good uniformity of the grains. It shows that the change in morphology is strongly dependent on the deposition temperature. It is believed that at higher temperature, the nucleation and the growth of PbO_2 processes are much faster than at room temperature. As discussed and shown by cyclic voltammetry in section 3.1.3, the deposition of PbO_2 at 333 K occurred at a less positive potential than at 298 K. Higher temperature is a better condition for the deposition of PbO_2 in order to have a well-formed and uniform deposit.

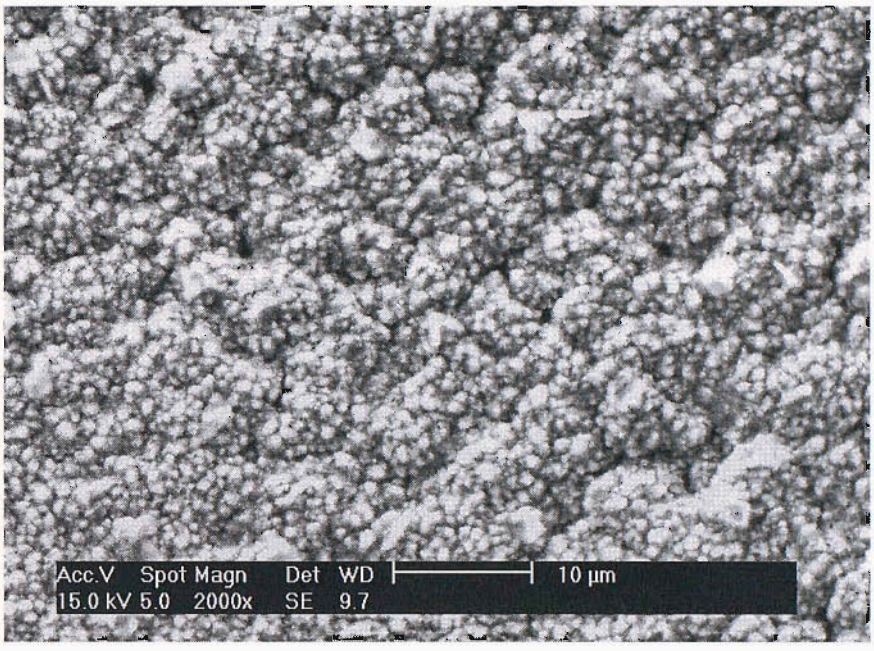

(a)

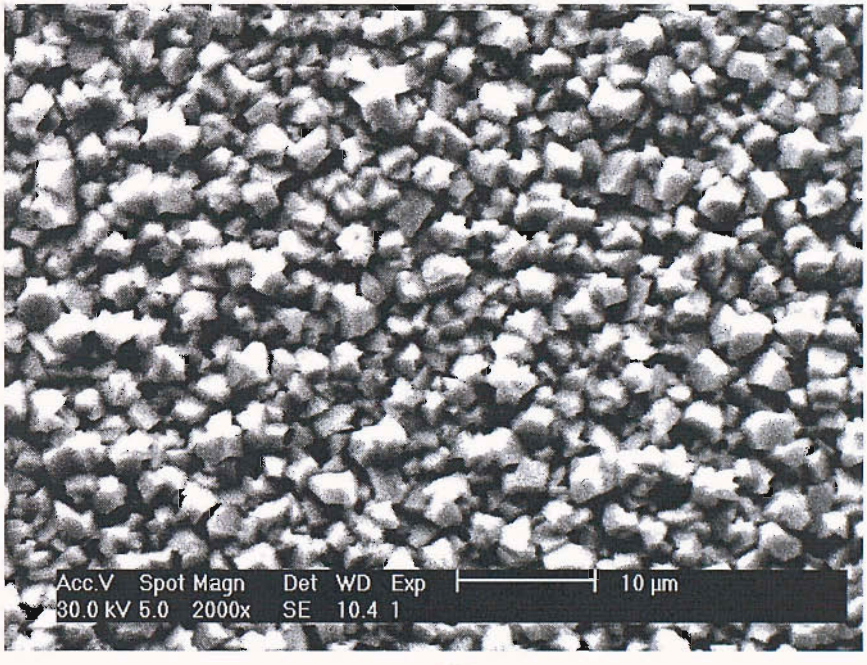

(b)

Figure 3.7: SEM images of PbO_2 prepared from 500 mM Pb(II) in 1 M HNO_3 using current density of 5 mA cm^{-2} for 600 s at (a) 298 K and (b) 333 K.

3.2.3 Influence of Current Density

The investigation on the effect of current density on the morphology of the formed PbO_2 was carried out. Initially, two different current densities (ie: 1 mA cm^{-2} and 5 mA cm^{-2}) were employed for the formation of PbO_2 deposits from the same solution (ie: 500 mM Pb(II) + 1 M HNO_3) at room temperature.

It was found that PbO_2 deposits prepared at 1 mA cm^{-2} had uniform hemispheres with around 1 μm in diameter for each hemisphere as seen in figure 3.8a. Meanwhile, at increased current density (ie: 5 mA cm^{-2}), the morphology of the top surface appeared to be much smaller centers collected together in larger hemispheres as in figure 3.8b.

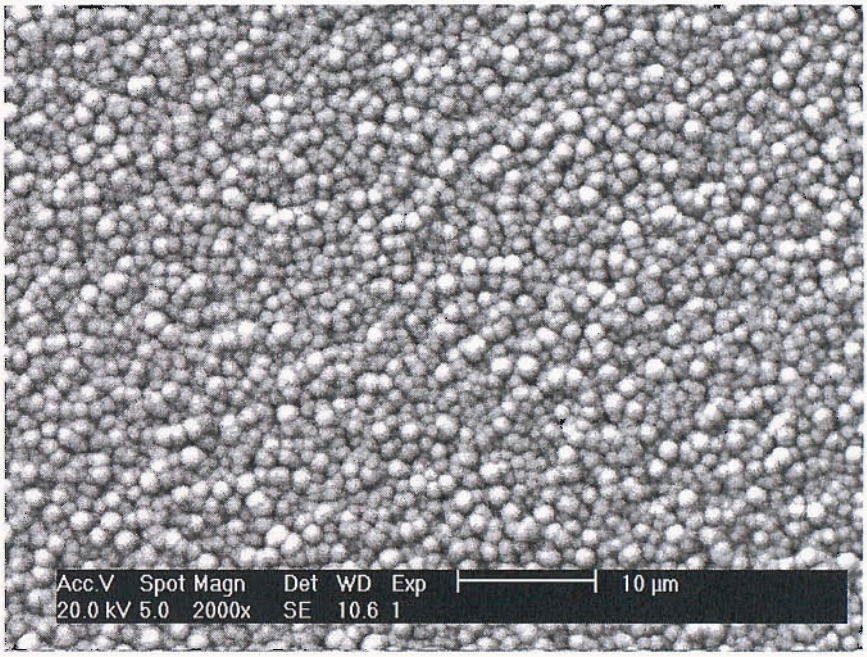

(a)

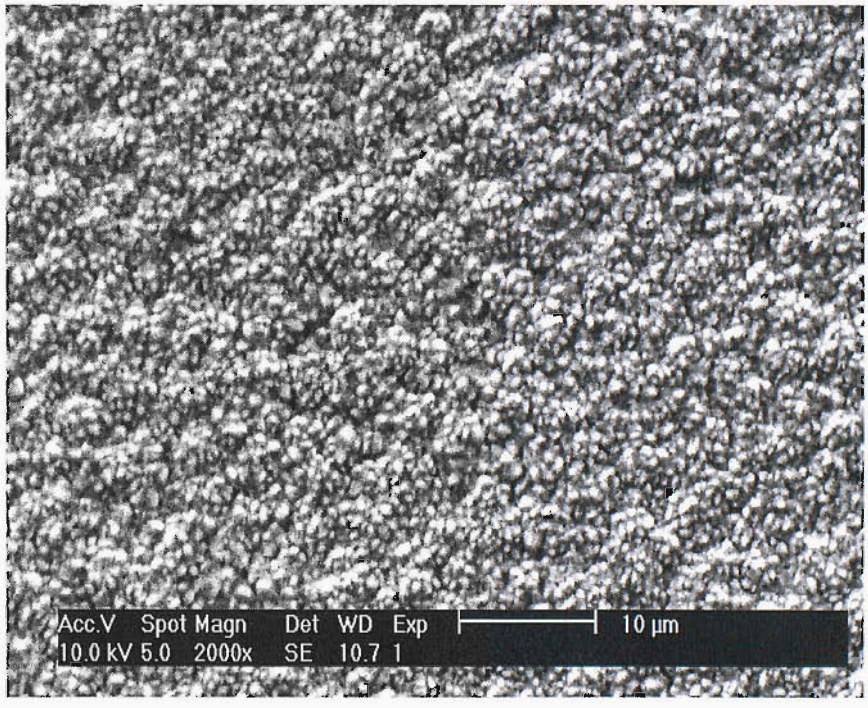

(b)

Figure 3.8: SEM images of PbO_2 prepared using current density of (a) 1 mA cm^{-2} (b) 5 mA cm^{-2} for 300 s at 298 K. Deposition solution: 500 mM Pb(II) in 1 M HNO_3

It is believed that many more nuclei are formed at 5 mA cm^{-2} during deposition than at the lower current density. The rate of nucleation and growth of the PbO_2 is sensitive to current density. At the higher current density, the deposition rate is faster than at 1 mA cm^{-2}.

On the other hand, if the deposition is carried out at extremely high current densities, some O_2 evolution is observed and this can also be seen to damage the surface. Figure 3.9 shows the damaged surface of the PbO_2 deposit with holes and cracks which has been prepared from 100 mM Pb(II) using a current density of 25 mA cm^{-2}.

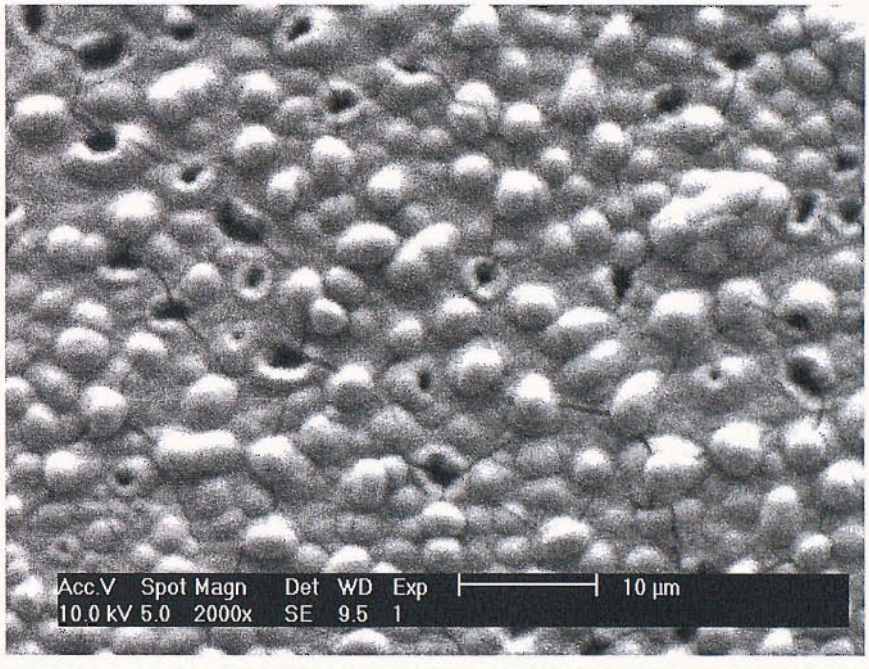

Figure 3.9: SEM image of PbO_2 prepared using current density of 25 mA cm^{-2} for 120 s at 298 K. Deposition solution: 100 mM Pb(II) in 1 M HNO_3

It should be noted that a porous morphology (less ordered and outward growth) can also be formed if high current density is used for a long time for the deposition of PbO_2. For example the PbO_2 deposits prepared at 25 mA cm^{-2} for 600s at 333 K from solution containing 100 mM Pb(II) + 1 M HNO_3 as shown in figure 3.10. Under these deposition conditions, the deposition rate is fast and at the same time some oxygen evolution occurs during the deposition leading to isolated nuclei of the PbO_2. These isolated nuclei are overlaid on a more uniform layer and the growth is favourable in vertical direction to form cauliflower-like crystals.

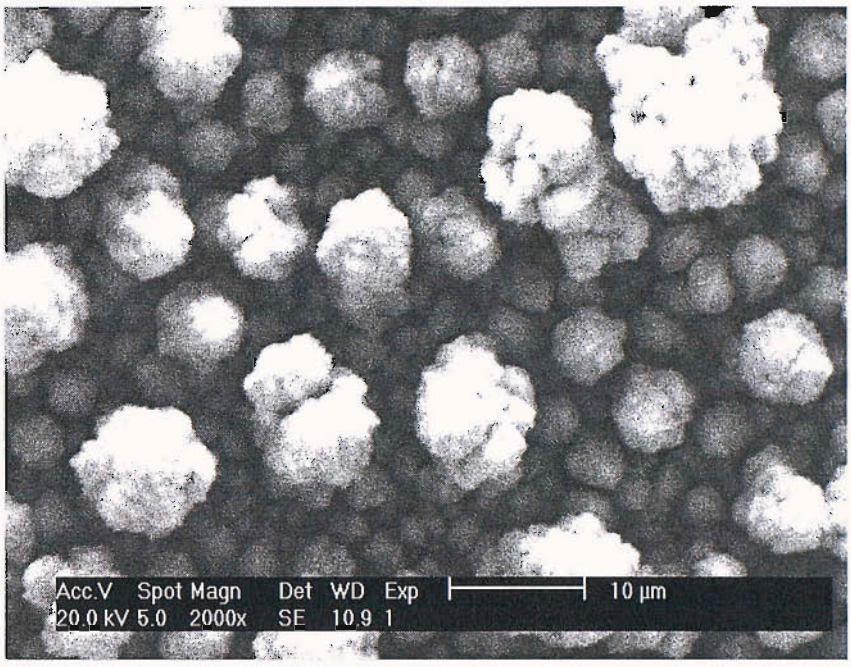

(a)

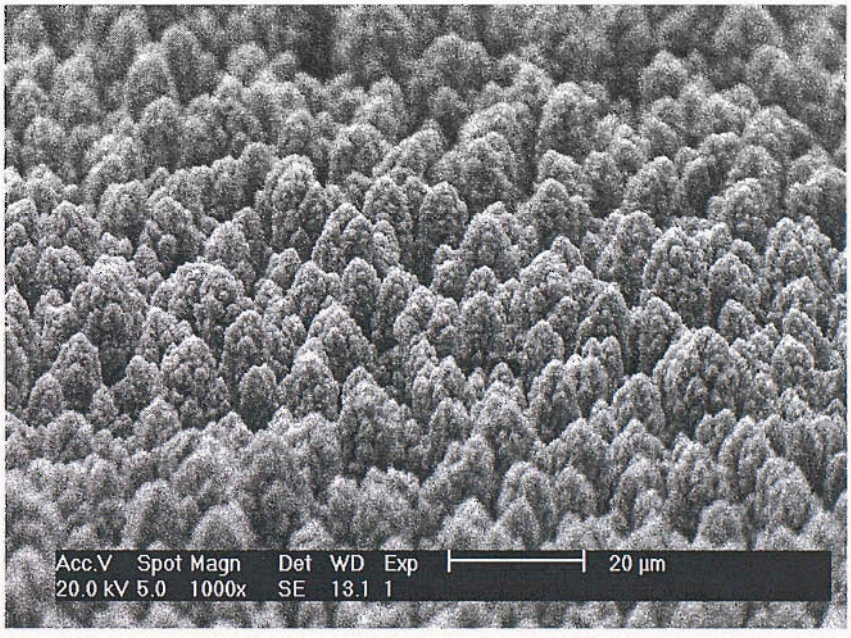

(b)

Figure 3.10: SEM images of PbO_2 from (a) top view (b) side view; prepared from 100 mM Pb(II) + 1 M HNO_3 using constant current density of 25 mA cm^{-2} for 600 s at 333 K.

Shen and Wei [123] reported that high current density employed is the main factor in the formation of high surface area or porous structured of PbO_2. This type of structure greatly increases its active area, which is a favourable property in view of a possible application as anode materials.

It was found that the density of nucleation is extremely sensitive to current density. Uniform and well-formed deposits can be formed at low current densities and

when high current densities used, which some O_2 evolution occurs, uneven and porous structure of PbO_2 deposits are formed.

3.2.4 Influence of Acid Concentration

The preparation of PbO_2 from different concentration of acid electrolytes was carried out and the morphology of the oxides was compared and investigated by SEM. It was found that, under similar conditions as with 1 M HNO_3, the formation of PbO_2 deposits with low acid concentration is closely packed angular crystals as seen in figure 3.11, as compared to hemispherical clusters with small centers (image shown in figure 3.5b) when higher acid concentration was used as the electrolyte.

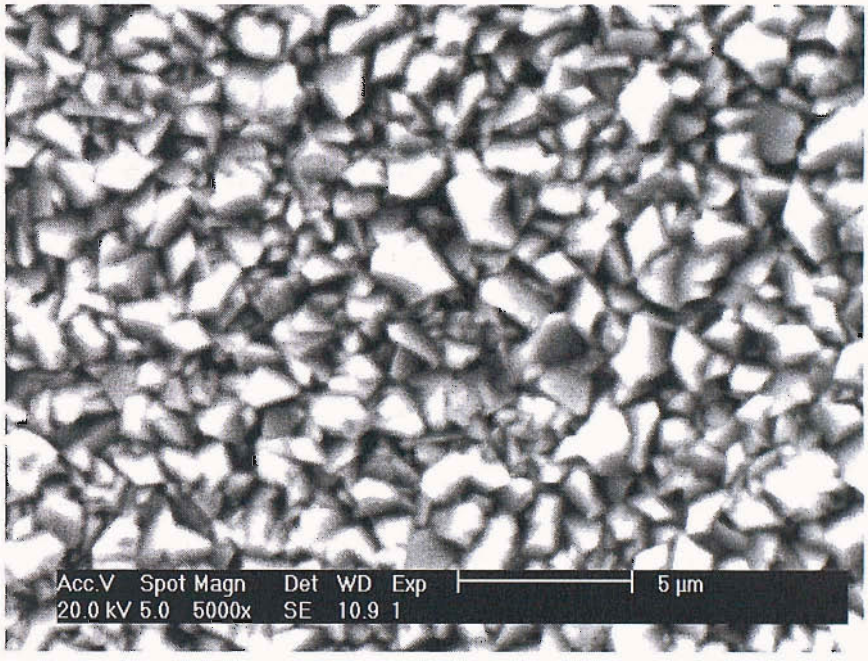

Figure 3.11: SEM images of PbO_2 prepared from 0.1 M HNO_3 solution containing 500 mM Pb(II) using current density of 5 mA cm^{-2} for 300 s at 298 K.

A significant change in morphology is apparent, as a result of using a different acid concentration, with an increase in the size of the crystallites and in the density of the deposits with decreasing acid concentration. This is related to the cyclic voltammetry curves shown in figure 3.4. The faster nucleation and growth of PbO_2 occur in low concentration of acid rather than in 1 M HNO_3; as indicated by a negative shift in the onset potential for the oxide deposition.

By increasing the deposition temperature to 333 K, the PbO_2 crystals prepared from 500 mM Pb(II) + 0.1 M HNO_3 solution became bigger as seen in figure 3.12.

Thus, temperature had a significant effect on producing a thicker and denser deposit. As discussed in section 3.2.2 for 1 M HNO_3 solution, at higher temperature, the nucleation and deposition rates are faster than that at room temperature; resulting a thicker deposit.

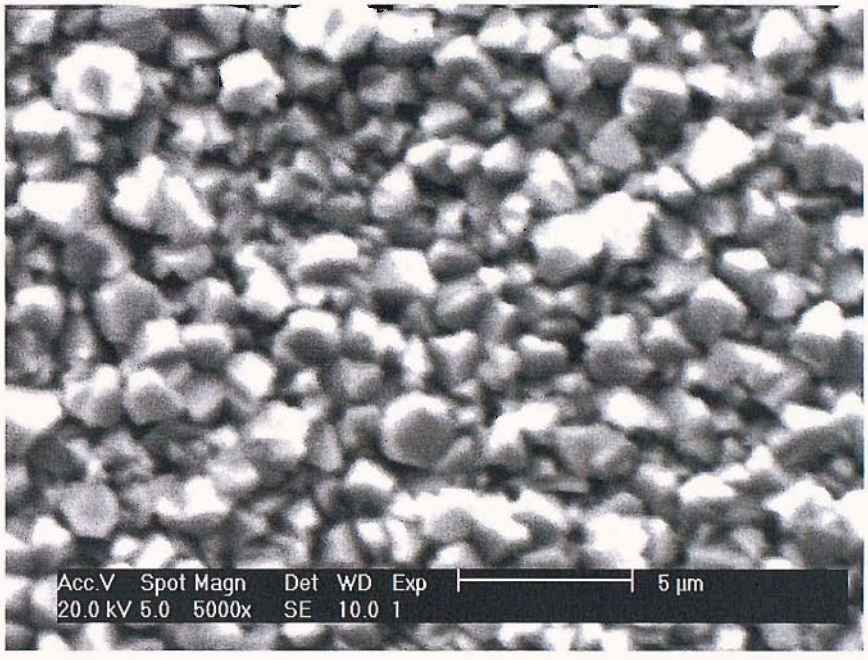

Figure 3.12: SEM images of PbO_2 prepared from 0.1 M HNO_3 solution containing 500 mM Pb(II) using current density of 5 mA cm^{-2} for 300 s at 333 K.

3.3 Adhesion Study

The adhesive quality of the prepared PbO_2 deposits towards abrasion was investigated and classified using methods listed in table 2.3. Table 3.1 shows the characteristics of lead dioxide deposits including their adhesion properties on gold substrates. The PbO_2 deposits were prepared using various deposition conditions.

Deposition solution	Deposition Conditions	Colour	Adhesion	Structure by SEM
30 mM Pb(II)/ 1 M HNO_3	5 mA cm^{-2}/ 120 s/ 298 K	brown	medium	As figure 3.5a
30 mM Pb(II)/ 1 M HNO_3	5 mA cm^{-2}/ 300 s/ 298 K	dark brown	medium	As figure 3.5a
30 mM Pb(II)/ 1 M HNO_3	5 mA cm^{-2}/ 600 s/ 298 K	black	poor	As figure 3.5a but deposit cracked and lifting from substrate
30 mM Pb(II)/ 1 M HNO_3	5 mA cm^{-2}/ 600 s/ 333 K	black	medium/good	As figure 3.7b but thinner

30 mM Pb(II)/ 1 M HNO_3	25 mA cm^{-2}/ 120 s/ 298 K	brown	medium	As figure 3.5a
30 mM Pb(II)/ 1 M HNO_3	25 mA cm^{-2}/ 120 s/ 333 K	dark brown	medium/good	As figure 3.5a
100 mM Pb(II)/ 1 M HNO_3	5 mA cm^{-2}/ 120 s/ 298 K	dark brown	medium	As figure 3.5a
100 mM Pb(II)/ 1M HNO_3	5 mA cm^{-2}/ 600 s/ 298 K	black	medium	As figure 3.5b
100 mM Pb(II)/ 1 M HNO_3	5 mA cm^{-2}/ 600 s/ 333 K	black	medium/good	As figure 3.7b but thinner
100 mM Pb(II)/ 1 M HNO_3	25 mA cm^{-2}/ 120 s/ 298 K	black	poor	As figure 3.9
100 mM Pb(II)/ 1 M HNO_3	25 mA cm^{-2}/ 120 s/ 333 K	black	medium/good	As figure 3.5a
100 mM Pb(II)/ 1 M HNO_3	25 mA cm^{-2}/ 600 s/ 333 K	black	medium/good	As figure 3.10
500 mM Pb(II)/ 1 M HNO_3	1 mA cm^{-2}/ 1500 s/ 298 K	black	medium/good	As figure 3.8a
500 mM Pb(II)/ 1 M HNO_3	5 mA cm^{-2}/ 120 s/ 298 K	black	medium/good	As figure 3.5a
500 mM Pb(II)/ 1 M HNO_3	5 mA cm^{-2}/ 300 s/ 298 K	black	medium/good	As figure 3.8b
500 mM Pb(II)/ 1 M HNO_3	5 mA cm^{-2}/ 600 s/ 298 K	black	medium/good	As figure 3.7a
500 mM Pb(II)/ 1 M HNO_3	5 mA cm^{-2}/ 300 s/ 333 K	black	very good	As figure 3.8b but thinner
500 mM Pb(II)/ 1 M HNO_3	5 mA cm^{-2}/ 600 s/ 333 K	black	very good	As figure 3.8b
500 mM Pb(II)/ 1 M HNO_3	25 mA cm^{-2}/ 120 s/ 298 K	black	medium	Poorly defined small centers
500 mM Pb(II)/ 1 M HNO_3	25 mA cm^{-2}/ 120 s/ 333 K	black	good	As figure 3.8b
500 mM Pb(II)/ 0.1 M HNO_3	1 mA cm^{-2}/ 1500 s / 298 K	black	good	As figure 3.11
500 mM Pb(II)/ 0.1 M HNO_3	5 mA cm^{-2}/ 300 s/ 298 K	black	good	As figure 3.11
500 mM Pb(II)/ 0.1 M HNO_3	5 mA cm^{-2}/ 300 s/ 333 K	black	medium/good	As figure 3.12

Table 3.1: Characteristics of lead dioxide deposits electroplated using various conditions. Au disk substrate. Definition of adhesive quality see section 2.6.1 (Table 2.3)

From the table, it can be seen that PbO_2 with hemispherical crystals morphology especially prepared from low concentration of Pb(II) in 1 M HNO_3 at 298 K were not strongly adhered on gold substrate. Most of them were classified as medium adhesion. With increasing the concentration of Pb(II) in the deposition solution, the adhesive property of the deposits was slightly improved.

Deposits with cracks and holes which were prepared at high current density (as in figure 3.9) had poor adhesion on gold substrates. They were easily removed by scrapping with tissue. Meanwhile, the top layer of the porous PbO_2 deposit as in figure 3.10 was quite fragile and easily removed when scrapping with tissue but its lower base was quite adherent on the gold surface.

Temperature has a significant role in improving the adhesive quality of the deposits. Basically, deposits prepared at 333 K had good adhesion on gold and the most adhered PbO_2 was prepared at this elevated temperature and from high concentration of Pb(II) using low current density either in 1 M HNO_3 or 0.1 M HNO_3. It is believed that by increasing the deposition temperature the nucleation density increases as well as the deposition rate; these factors lead to a well formed thin layer or foundation for the growth of subsequent PbO_2 layers and as the results the adhesion of the deposits is greatly enhanced.

Deposits prepared at room temperature with low concentration of acid had better adhesive quality on gold substrate than with 1 M HNO_3 at the same deposition temperature. Higher temperature for the deposition of the PbO_2 deposits from 0.1 M HNO_3 did not have a significant effect on improving the adhesion property than that at room temperature. In fact, the deposits prepared at 298 K from low acid concentration solution had a better adhesion than deposition at 333 K.

3.4 Chemical Stability Study

To be useful, an electrode coating must be stable to abrasion (as discussed in section 3.3), corrosion and chemical reactions. The lack of stability of PbO_2 electrodes has been the main problem in producing a good and long lasting anode material. In this study, the stability of the PbO_2 electrodes on open circuit and during electrolysis in different electrolytes was investigated.

3.4.1 Stability of PbO_2 in Sulfuric Acid

The stability of PbO_2 layers on open circuit was investigated by immersing them in a solution of 1 M sulfuric acid. Thin layers of the PbO_2 prepared from 30 mM Pb(II) in 1 M HNO_3 using 5 mA cm^{-2} for 150 s at 298 K were used in this study. Figure 3.13 shows the morphology of the layers before immersion. It was found that these PbO_2 layers dissolved quickly in 1 M H_2SO_4.

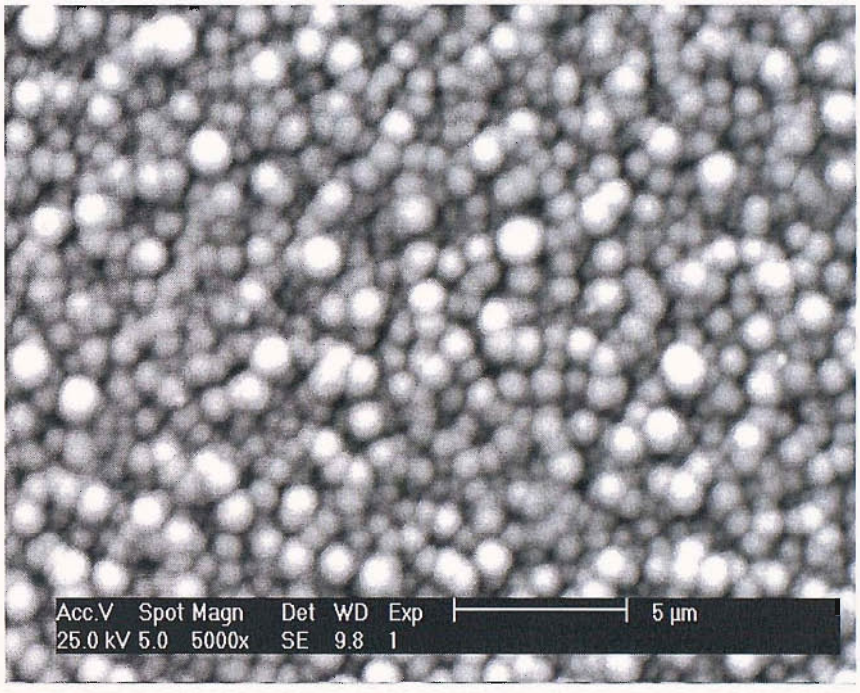

Figure 3.13: SEM of PbO_2 coating before immersion in any solution. PbO_2 layer deposition conditions: 30 mM $Pb(NO_3)_2$ + 1 M HNO_3, 5 mA cm^{-2} for 150s , 298 K.

It is believed that the dissolution of the PbO_2 could occur by two mechanisms (i) via a soluble Pb(IV) species and (ii) by the chemical oxidation of water to oxygen by the PbO_2. Both reactions probably contribute and, in sulfuric acid, a few lead sulfate crystals can be seen on the surface by electron microscopy after immersion for 3 hours as seen in figure 3.14, implying that some reduction of the PbO_2 layer is occuring. The reduction is, however, slow and dissolution was complete after 1 day and no $PbSO_4$ crystals were seen when dissolution was complete.

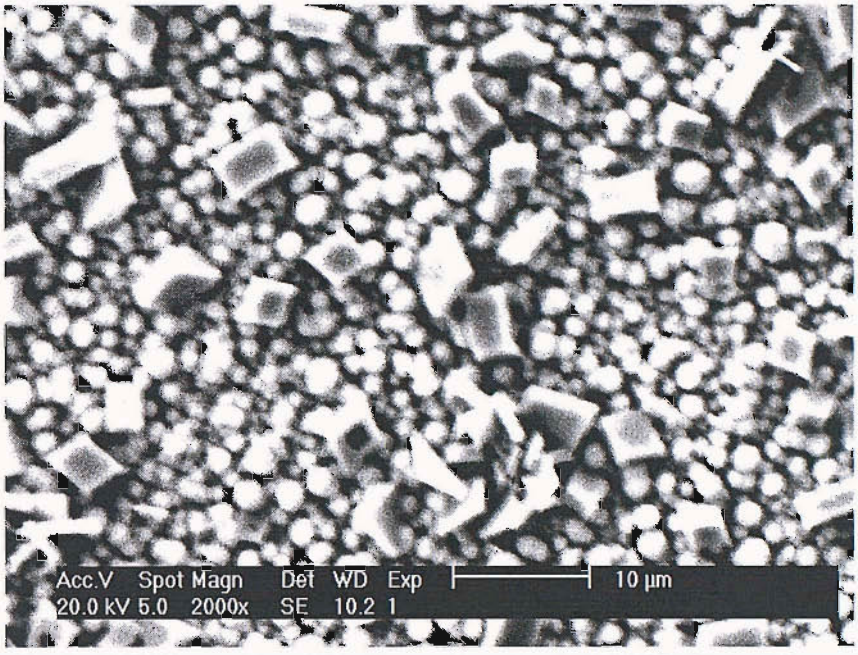

Figure 3.14: SEM of PbO_2 coating after immersion in 1 M H_2SO_4 for 3 hours PbO_2 layer deposition conditions: 30 mM $Pb(NO_3)_2$ + 1 M HNO_3, 5 mA cm^{-2} for 150s , 298 K.

The effect of adding dimethyl sufoxide (DMSO), a compound capable of being oxidized, to the sulphuric acid solution on the stability of the PbO_2 layers was also investigated. The PbO_2 layers used in this study were prepared under the same conditions as the study for sulphuric acid alone. Figure 3.15 shows the morphology of the PbO_2 layers after immersion in 50 mM DMSO + 1 M H_2SO_4 on open circuit for 10 min.

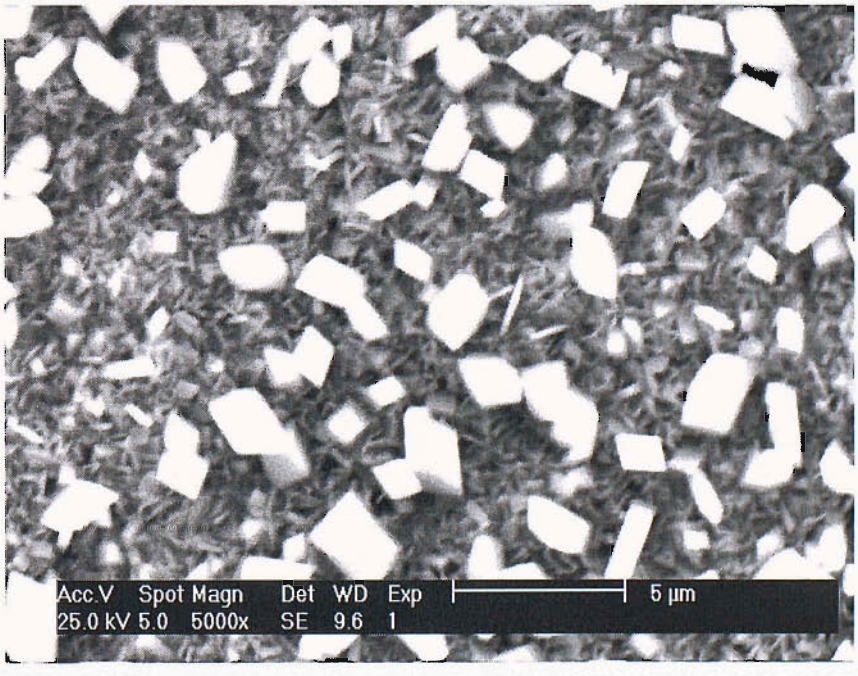

Figure 3.15: SEM of PbO_2 coating after immersion in 50 mM DMSO + 1 M H_2SO_4 for 10 min. PbO_2 layer deposition conditions: 30 mM Pb(II) + 1 M HNO_3, 5 mA cm^{-2} for 150s , 298 K.

It can be seen that the hemispherical morphology is totally destroyed by immersion in this solution. The whole of the structure is extensively corroded and there is a substantial population by crystals with the shape typical of lead sulfate. The whole layer disappeared in less than 3 hours. Clearly, the process of $PbSO_4$ formation was accelerated by the addition of DMSO in the solution as the reaction in Scheme 1 is rapid.

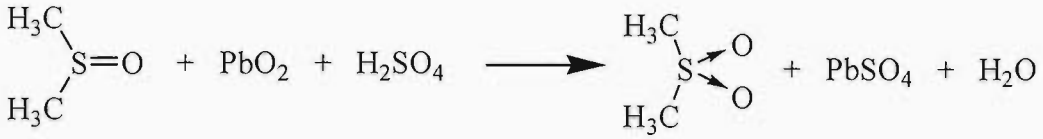

Scheme 1

It is believed that the DMSO solution has quickly absorbed through the voids and spaces offered by the existing gaps between crystals of the layers. The spontaneous chemical reaction shown in Scheme 1 is taking place.

EDAX analysis was carried out on the SEM images of the PbO_2 layers before and after immersion in 50 mM DMSO + 1 M H_2SO_4 as seen in figure 3.13 and 3.15. This is to identify the presence of sulfur compounds on the surface. Figure 3.16 shows the EDAX analysis for both surfaces.

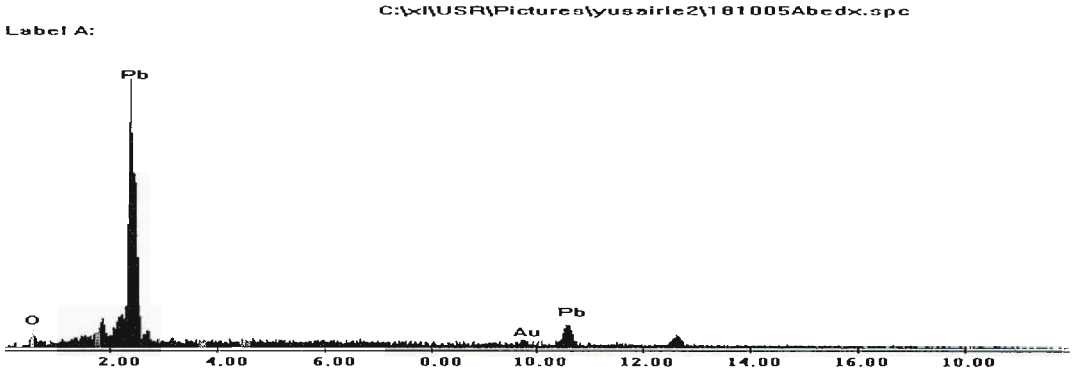

(a)

Energy / keV

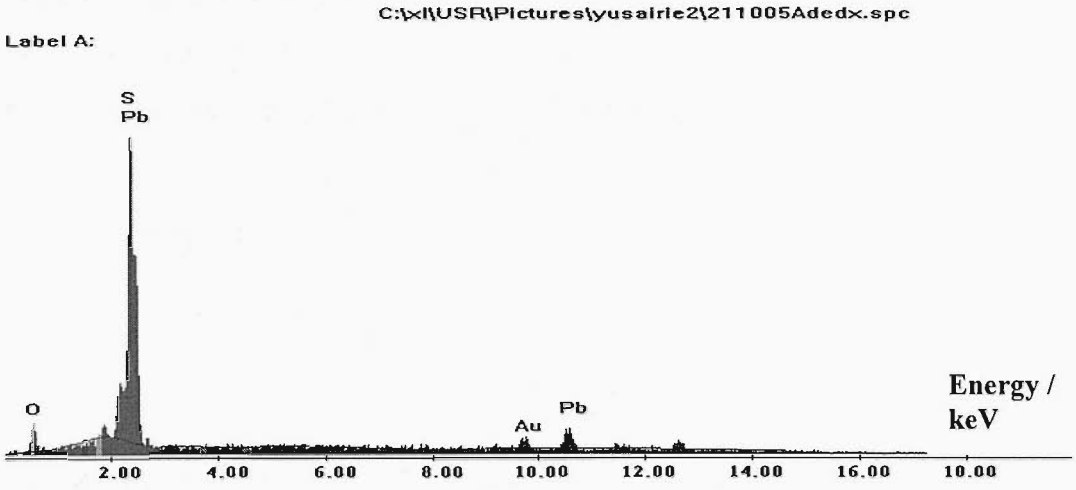

(b)

Figure 3.16: EDAX analysis of PbO_2 deposits (a) before and (b) after immersion in 50 mM DMSO + 1 M H_2SO_4 for 10 minutes.

Table 3.2 compares the atomic percent of the elements present from both images (before and after immersion in 50 mM DMSO + 1 M H_2SO_4 as in figure 3.13 and 3.15). EDAX analysis has some limitations to be considered; such as lack of efficiency for the detection of elements lighter than sodium [153]. For example, from the table, the ratio of Pb/O for PbO_2 deposit should be 1:2, but this is not the case. It should be noted that the quantitative analysis by EDAX is not accurate for light elements such as oxygen; and furthermore the detection efficiency is low when lighter element is compared with other element which is much higher in atomic weight such as Pb. Nonetheless, from the analysis, the transformation of the PbO_2 crystals to $PbSO_4$ crystals after immersion in sulphuric acid solution containing DMSO is confirmed by the detection of high sulfur content for the image of figure 3.15.

Element	**Pb**	**O**	**Au**	**S**
Before (Atomic %)	80.2	9.7	9.9	0.2
After (Atomic %)	60.9	11.8	10.8	16.5

Table 3.2: Elemental content in atomic percent of EDAX measurements for PbO_2 deposits before and after immersion in 50 mM DMSO + 1 M H_2SO_4.

Further experiments in 1 M H_2SO_4 were carried out using two other organic compounds, 3-thiophenecarboxylic acid and 3-methylpyridine. The chemical oxidations on PbO_2 for both organic compounds in 1 M H_2SO_4 are shown in scheme 2 and scheme 3. However, the dissolution processes of the PbO_2 in sulphuric acid with the presence

of these organic compounds are slower than when the reactant is DMSO. The formation of lead sulfate crystals over a period of hours can clearly be confirmed by SEM when the reactions are carried out in aqueous sulfuric acid.

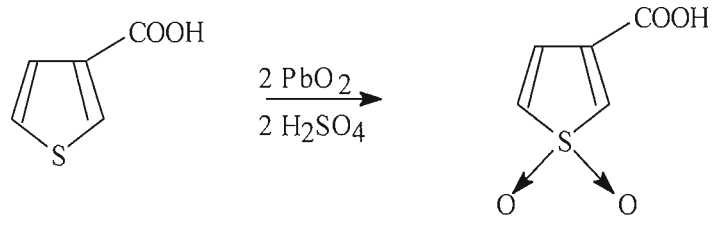

3-thiophenecarboxylic acid 3-thiophenecarboxylic acid sulfone

Scheme 2

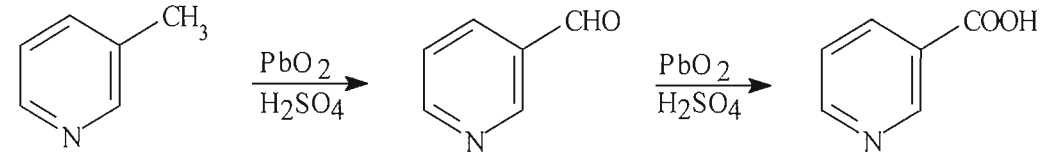

3-methylpyridine (3-picoline) Pyridine-3-carbaldehyde Nicotinic acid

Scheme 3

The stability of the PbO_2 layers in sulphuric acid was greatly increased when the coatings having the best adhesion and resistance to abrasion were used. As described in section 3.3, the most adhesive coatings were prepared from 0.5 M $Pb(NO_3)_2$ + 1 M HNO_3 at a temperature of 333 K using a low current density.

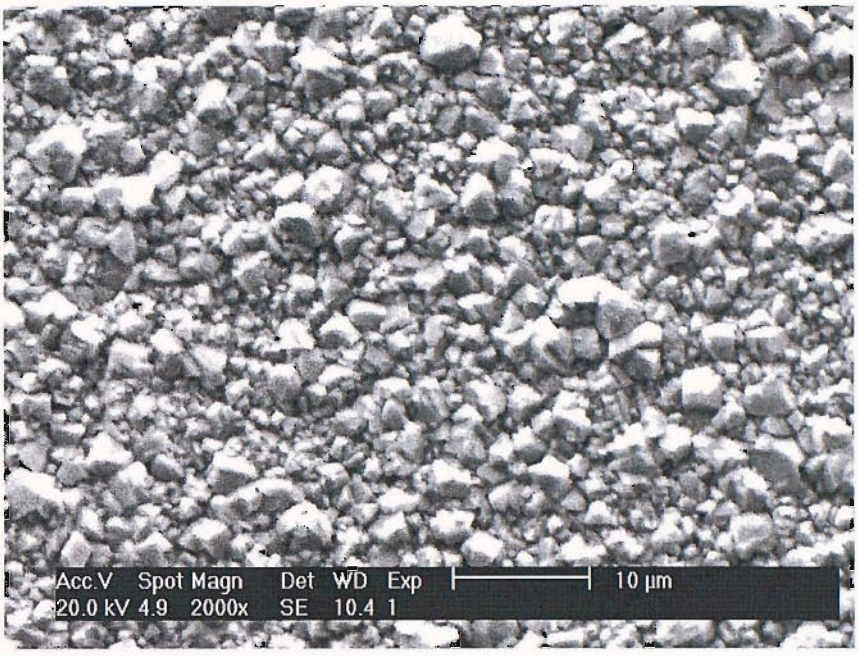

(a)

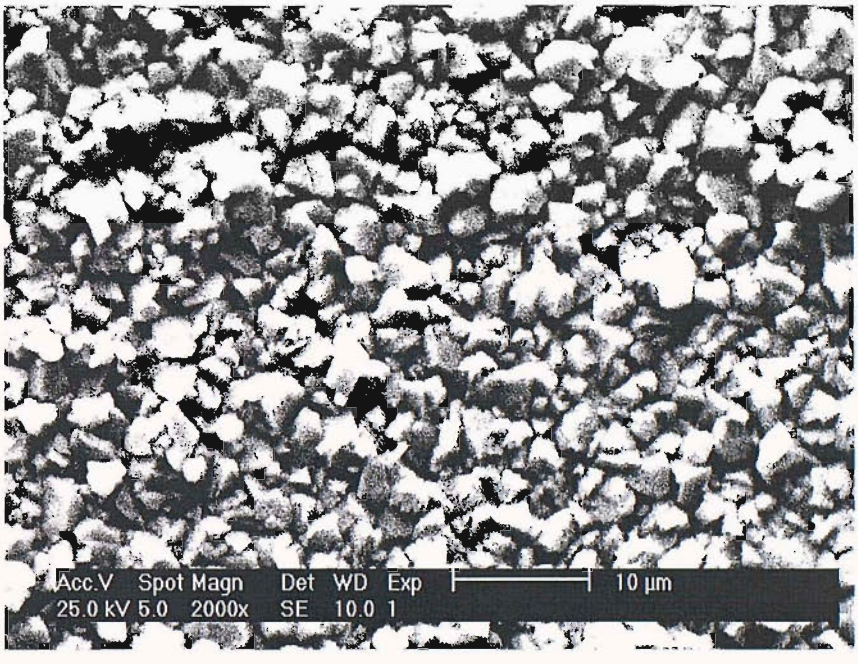

(b)

Figure 3.17: SEM of PbO_2 taken at the middle of the deposit (a) before and (b) after immersion in 50 mM DMSO + 1 M H_2SO_4 for 3 hours. PbO_2 layer deposition conditions: 500 mM $Pb(NO_3)_2$ + 1 M HNO_3, 5 mA cm^{-2} for 600s , 333 K.

These PbO_2 deposits with the closely packed angular crystals structure as shown in figure 3.17(a) probably have the same chemistry but the rates of the changes are much slower. For example, such a coating took 7 days to dissolve in 1 M H_2SO_4 and after immersion in 50 mM DMSO + 1 M H_2SO_4 for 3 hours, the morphology was still the same as before immersion and only a limited number of lead sulfate crystals were

observed by SEM as seen in figure 3.17(b). It is believed that the surface area and porosity of the deposit is a critical factor in determining the kinetics of dissolution/reduction of the PbO_2 layer. It was found that the PbO_2 layers with loose, cracking and lifting up structures were liable to be rapidly reduced by DMSO in sulfuric acid solution, forming $PbSO_4$. These types of PbO_2 layers are not stable on open-circuit and not suitable to be used as the anode for long electrolysis process.

The influence of electrode potential on the stability of the PbO_2 deposits was also examined. In one experiment, a PbO_2 deposit (ie: prepared from 30 mM Pb(II) with hemispherical crystals as shown in figure 3.5a) was held in 1 M sulfuric acid at + 1.70 V for 3 days (slow oxygen evolution was observed) and no change to the surface was seen by SEM. In a second experiment, a PbO_2 deposit was held at + 1.65 V (so that DMSO oxidation occurred) in a solution of 50 mM DMSO + 1 M H_2SO_4 for 3 hours. An anodic current density of 5-7 mA cm^{-2} passed throughout the electrolysis but, again, SEM analysis showed no change to the morphology or thickness of the deposit during the electrolysis. Clearly, when operating at potentials positive to the formal potential of the PbO_2/Pb(II) couple, the deposits become much more stable.

3.4.2 Stability in Different Electrolytes

The stability of PbO_2 layers electrodeposited onto gold in other media were tested by immersing them in various solutions on open-circuit for various periods of time and then examining them by scanning electron microscopy.

Table 3.3 summarizes a comparison of PbO_2 electrodes prepared from a solution, 30 mM Pb(II) + 1 M HNO_3, at 298 K and using a current density of 5 mA cm^{-2} for 300 s in different electrolytes with and without the presence of DMSO. In the solutions of aqueous acid without DMSO, the deposits were observed to change from black to brown within a few hours and while the SEM showed no change in structural type, the hemispheres decreased in size and the voids between centers became more prominent. After 4 days, the coating had dissolved completely and the shiny surface of the gold substrate recovered.

Solution	Observations
1 M H_2SO_4 (pH~0)	Deposit dissolves during 4 days. Deposit color: black-brown to Au (of metal). A few cubic crystals observed by SEM after 1 day.
1 M $HClO_4$ (pH~0)	Deposit dissolves during 4 days. Deposit color: black-brown to Au (of metal). No change in morphology by SEM.
1 M Na_2SO_4 (pH~7)	Unchanged > 10 days but eventually dissolves.
1 M H_2SO_4 + 50 mM DMSO	Dissolves within 3 hours. Square crystals of $PbSO_4$ observed on SEM within few minutes.
1 M $HClO_4$ + 50 mM DMSO	Dissolves within 6 hours but no change in morphology observed by SEM.
1 M Na_2SO_4 + 50 mM DMSO	Stable > 10 days but eventually dissolves.

Table 3.3: Observations on the behaviour of PbO_2 layers during immersion in aqueous solutions at room temperature. Deposits formed from a solution, 30 mM Pb(II) + 1 M HNO_3, 298 K and using a current density of 5 mA cm^{-2} for 300 s.

As discussed earlier in section 3.4.1, the PbO_2 electrodes were not stable on open-circuit in sulfuric acid solution. The presence of DMSO has accelerated the dissolution process of PbO_2. In perchloric acid, the presence of DMSO also accelerates the dissolution of the PbO_2 but the process is not as fast as in sulfuric acid and the hemispherical morphology of the deposits remains; in perchloric acid solutions, Pb(II) is soluble and in the sulfuric acid media, the precipitation of $PbSO_4$ provides an addition driving force for the oxidation of DMSO. Several oxygen-transfer reactions on the PbO_2 deposits were reported to proceed more rapidly when H_2SO_4 was used as the supporting electrolyte instead of $HClO_4$ [154].

It was found that, from the table, the PbO_2 layers were the most chemically stable in sodium sulphate solution than in the two aqueous acid solutions. The dissolution of the layers was incomplete even after 10 days. The DMSO does not accelerate the dissolution in the sodium sulfate solution. Proton is essential to the chemical oxidations by the PbO_2. A spontaneous chemical reaction between the PbO_2 and DMSO is not unexpected as lead dioxide is a known oxidizing agent used in organic synthesis. It is believed that pH of the supporting electrolytes plays a major role in determining the chemical stability of the PbO_2 deposits.

3.5 Electrocatalytic Activity Study

The oxidation of DMSO was used as a model compound to investigate the electrocatalytic activity of the PbO_2 deposits. The DMSO is expected to oxidize in a two-electron process to dimethyl sulfone ($DMSO_2$) [137]. A large number of voltammograms were recorded for 50 mM DMSO in aqueous solutions of sulfuric acid, perchloric acid and sodium sulfate. Throughout, the voltammograms were recorded by scanning the potential in a positive direction from + 1400 mV vs SCE; this negative limit was chosen because it is well positive to the potential where reduction of the PbO_2 to $PbSO_4$ commences; the reduction is observed as a well formed cathodic peak as recorded by cyclic voltammetry shown in section 3.1. In the early stages of the investigation, the voltammograms appeared to be irreproducible and only sometimes showed the well formed oxidation wave reported by Johnson et al [17,76,81.155,156]. Indeed, in some experiments the voltammetric response changes with time. As the investigation proceeded, it became clear that the voltammogram was sensitive to both the conditions for deposition of the PbO_2 and the electrolyte as well as the treatment of the coating during the experiments. As to be expected from the previous sections periods on open circuit were particularly damaging to the PbO_2 coated electrodes.

Figure 3.18 and 3.19 illustrate the former case. They show the voltammograms of two different PbO_2 electrodes in 1 M H_2SO_4 and 50 mM DMSO + 1 M H_2SO_4. Figure 3.18 shows the voltammetric response of the PbO_2 deposits prepared from 500 mM Pb(II) at room temperature which have hemispherical clusters and made up of small centers with gaps in the structure as shown in figure 3.7a, while figure 3.19 shows the voltammograms of the PbO_2 with the angular crystallite structure shown in figure 3.7b which have been prepared at 333 K. It can be seen from the voltammograms, the potential when the current density for the oxidation of DMSO is 12 mA cm^{-2} ($E_{j=12}$) for the former is at +1.73 V while for the latter is at +1.80 V. This indicates that the PbO_2 prepared at 298 K has higher catalytic activity than that of the PbO_2 electrodes prepared at 333 K. It is believed that the morphology of the electrodes and particularly the exposed surface area have significant contribution to the catalytic activity of the PbO_2.

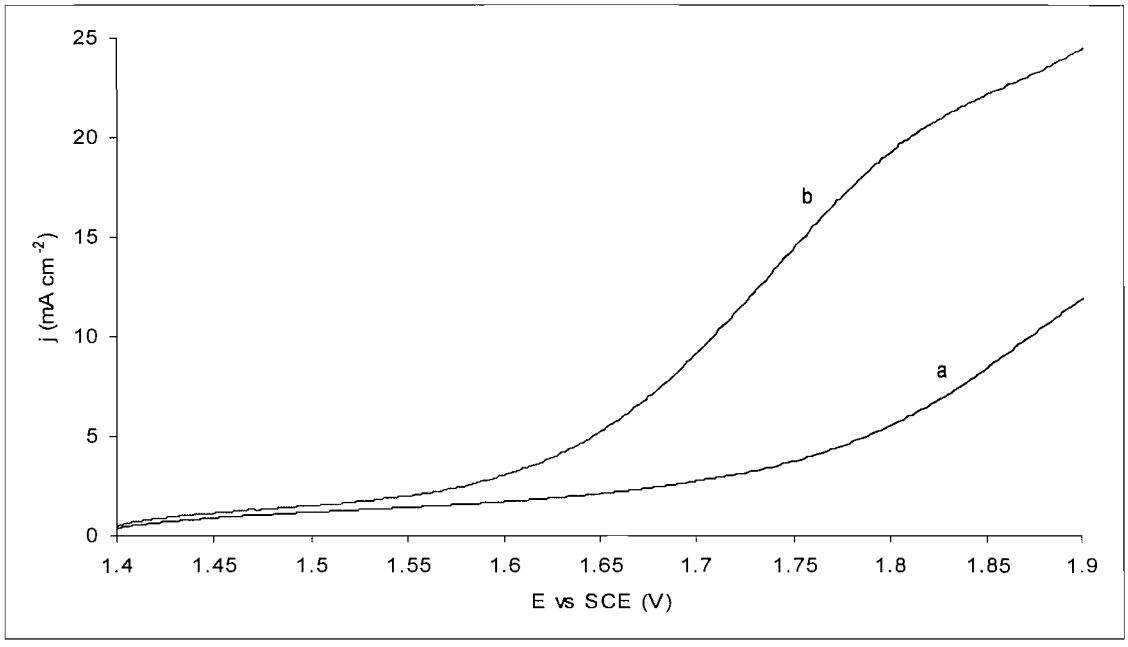

Figure 3.18: Voltammograms for a PbO_2 electrode in (a) 1 M H_2SO_4 and (b) 50 mM DMSO + 1 M H_2SO_4. Temperature 298 K. Potential scan rate: 50 mV s^{-1}. PbO_2 layer deposited from 500 mM $Pb(NO_3)_2$ + 1 M HNO_3, 5 mA cm^{-2} for 600 s, 298 K.

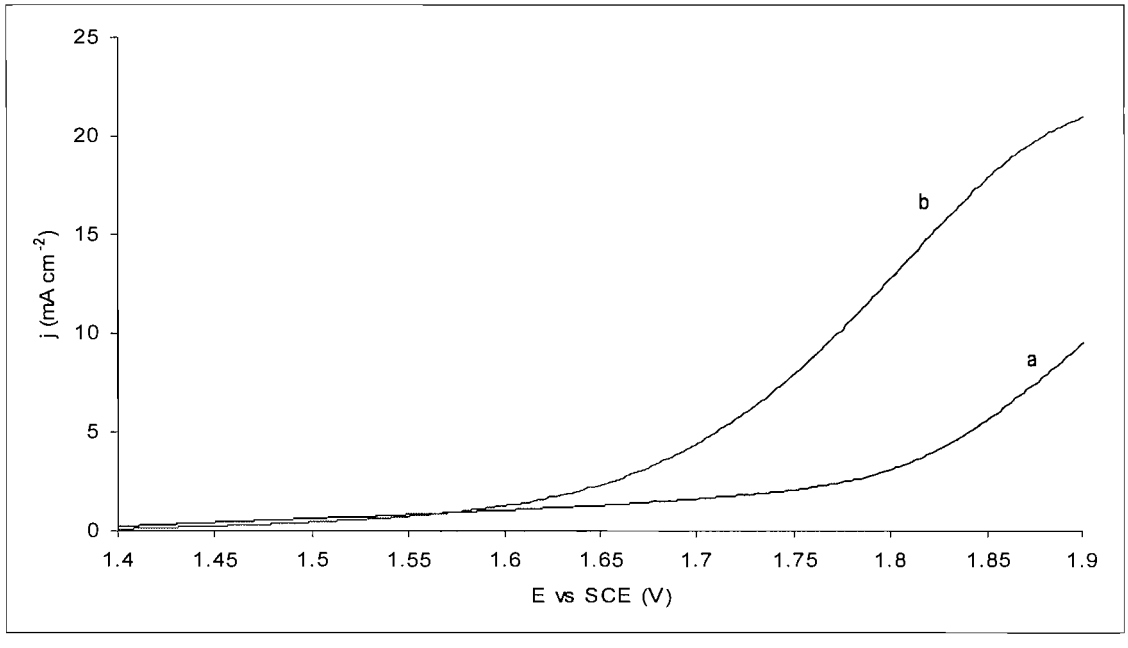

Figure 3.19: Voltammograms for a PbO_2 electrode in (a) 1 M H_2SO_4 and (b) 50 mM DMSO + 1 M H_2SO_4. Temperature 298 K. Potential scan rate: 50 mV s^{-1}. PbO_2 layer deposited from 500 mM $Pb(NO_3)_2$ + 1 M HNO_3, 5 mA cm^{-2} for 600 s, 333 K.

Meanwhile, figure 3.20 illustrates the latter case. It shows the voltammetric responses of PbO_2 electrodes which have hemispherical crystals as shown in figure 3.5a. When a voltammogram was recorded immediately after this PbO_2 electrode was immersed in 50 mM DMSO + 1 M $HClO_4$, $E_{j=12}$ appeared at +1.73 V. But after

standing in sulfuric acid for 10 min, the $E_{j=12}$ was shifted to +1.65 V. The activity for the oxidation of DMSO was more apparent after standing for 40 min, a well formed oxidation wave was observed, the $E_{j=12}$ appeared at +1.56 V. The development of the oxidation wave with time occurred in all acidic solutions but was more rapid in sulfuric acid than in perchloric acid; it did not occur in 1 M Na_2SO_4.

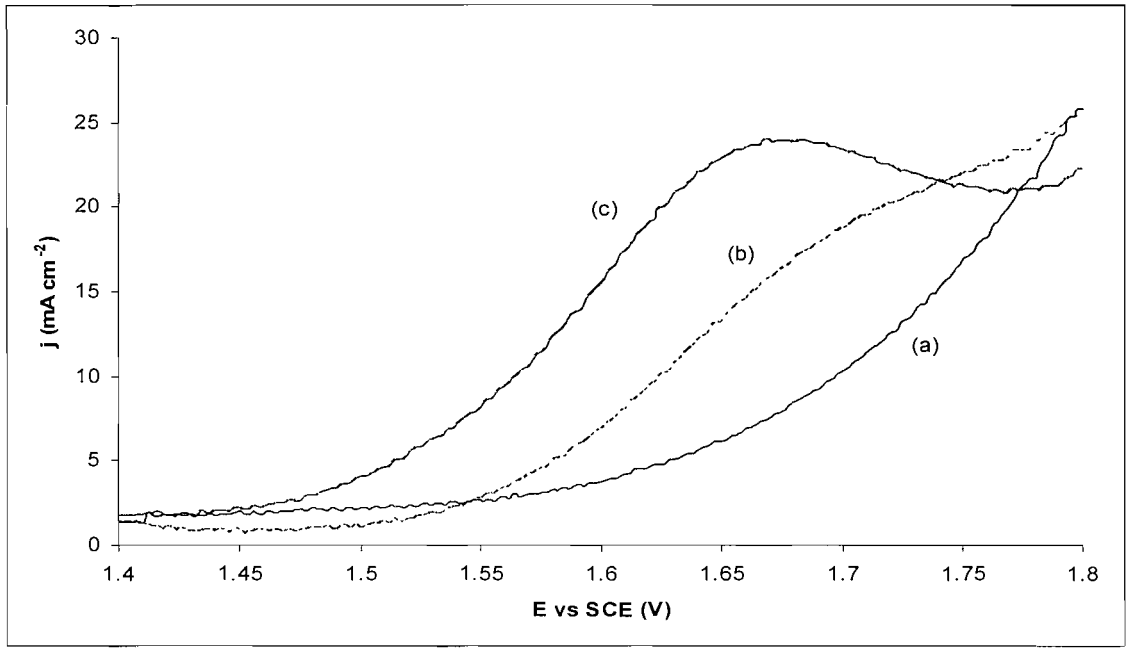

Figure 3.20: Voltammograms for a PbO_2 electrode in 50 mM DMSO + 1 M $HClO_4$ after immersion in 1 M H_2SO_4 for (a) 0 , (b) 10 min and (c) 40 min. Temperature 298 K. Potential scan rate : 50 mV s^{-1}. PbO_2 layer deposited from 30 mM $Pb(NO_3)_2$ + 1 M HNO_3, 5 mA cm^{-2} for 300 s, 298 K.

The increase in activity appeared to be associated with an increase in the surface area of the PbO_2 as the layer corrodes. The development of the wave was most rapid if the voltammetry was carried out in 50 mM DMSO + 1 M H_2SO_4. Hence, the most active anodes also corresponded to the PbO_2 layers that were corroded as in figure 3.15 and it is clear that such layers have a very high surface area. Of course, on a longer time scale the oxidation wave was lost again as the deposits dissolved.

3.6 Macroporous PbO_2

As discussed in section 1.5, a variety of three-dimensional and porous electrodes can be formed in order to have high surface area and high mass transfer

coefficient and hence high rate for electrochemical reactions. Electrodeposition of PbO_2 on flat gold substrates using high current density led to the production of porous deposits (ie: cauliflower-like structure) as shown in figure 3.10 (see page 66). Even though this type of deposit has higher catalytic activity than flat or plain deposit, it is quite fragile, especially the top layer of the deposit which is easily removed with tissue paper. Porous PbO_2 can also be prepared using anodic electrodeposition from a stationary high internal phase emulsion (HIPE) [145]. The porous deposits produced by this technique have a distinct structure consisting of 10 – 50 μm high pyramidal aggregates, pitted with smaller pores with diameters ranging from 0.5 to 2 μm. Nevertheless, this type of porous PbO_2 is not uniform and not well organized. Also, it has low electroactive surface area due to its low porosity. Therefore, in this study, a colloidal templating electrodeposition technique (as described in chapter 2) was employed to produce highly ordered macroporous deposits with small spherical pores and high porosity in order to increase the electrochemically accessible specific surface area of the electrodes. Bartlett and co-workers [148] used this technique in preparing highly ordered macroporous PbO_2 films on gold and indium tin oxides (ITO) substrates. They found the macroporous PbO_2 frameworks were highly polycrystalline, self-supporting and free from defects.

Figure 3.21 shows a SEM micrograph of a macroporous β–PbO_2 film electrodeposited on gold from plating solution containing 100 mM $Pb(NO_3)_2$ + 1 M HNO_3 using a constant current density 5 mA cm^{-2} for 75 s at 298 K. The deposition charge used was calculated to be 0.38 C cm^{-2}. The PbO_2 was grown through a template consisting of a self assembled multilayer of 500 (± 20) nm diameter polystyrene spheres.

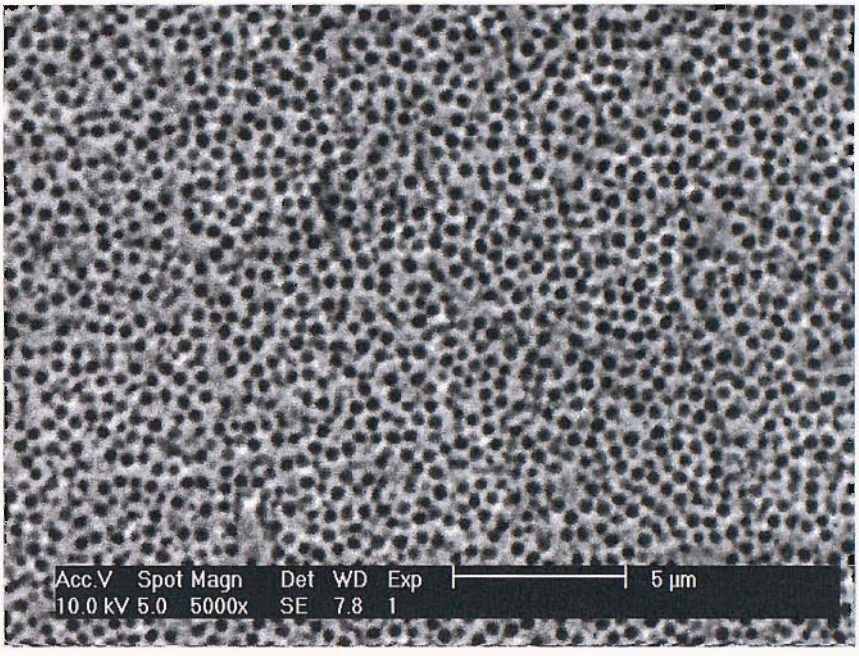

Figure 3.21: SEM image of a macroporous β–PbO_2 film grown at from 100 mM Pb(II) in 1 M HNO_3 using 5 mA cm^{-2} at 298 K through a template of 500 nm diameter polystyrene spheres.

The SEM image shows that the spherical voids, left in the PbO_2 film after the removal of the polystyrene spheres by dissolution in toluene, are arranged in random and dense structure of uniformly-sized pores; resulting in a honeycomb-like structure. From the figure, the measured average pore center to pore center distance from the image is ~ 500 nm, which is the same as the diameter of the original spheres used to prepare the templates. This indicates that the PbO_2 film does not suffer any shrinkage after the removal of the polystyrene template by the toluene.

The thickness of the film was estimated to be 0.88 µm or 1.76 layers. The thickness of the film can be controlled by varying the charge passed for the deposition [157]. The macroporous film produced was good with respect to adhesion to the surface of the gold substrate. The colour of the porous film was dark brown. But when illuminated with white light, the film shows readily visible diffractive colours ranging from blue to red, depending upon the viewing angle. This is an indicator of the formation of a highly ordered pore structure within the film with a pore diameter in the range of the wavelength of visible light [158].

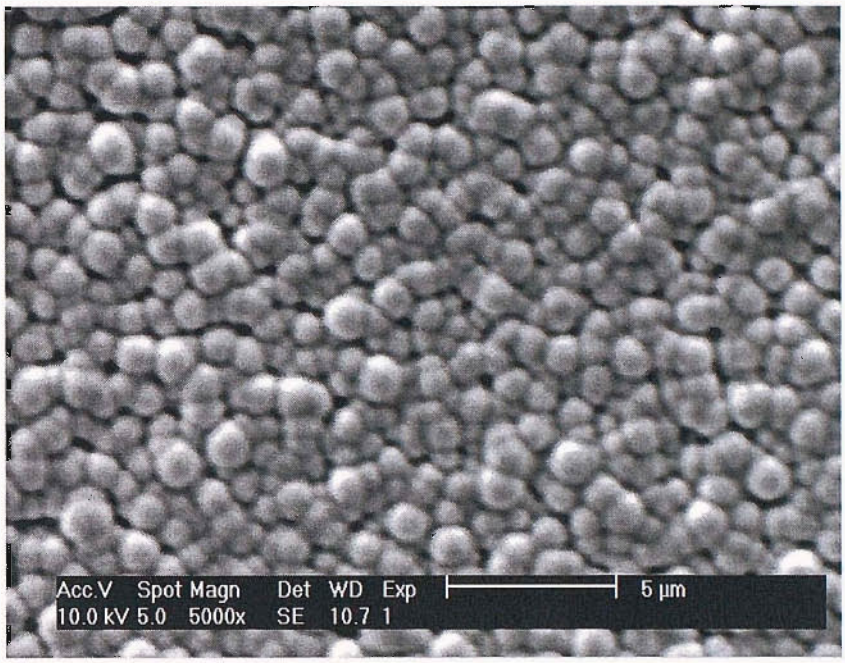

Figure 3.22: SEM image of a plain β–PbO_2 film deposited on gold from 100 mM Pb(II) in 1 M HNO_3 using 5 mA cm^{-2} for 75 s at 298 K. Deposition charge, Q : 0.38 C cm^{-2}.

For comparison, a non-templated or plain PbO_2 film was deposited on an identical 1 mm diameter gold substrate using the same deposition solution and deposition charge as used for the porous. The thickness of the plain PbO_2 was calculated to be 0.5 µm corresponding to a faradaic efficiency for the deposition process of 90 %. Figure 3.22 shows the SEM image of the plain PbO_2. The image shows that the film is quite smooth with hemispherical crystals and non-porous.

The electrocatalytic activity of the porous and plain PbO_2 for the oxidation of DMSO in sulfuric acid was investigated. Figure 3.23 shows voltammetric response of the two electrodes recorded at 50 mV s^{-1} in 1 M H_2SO_4 containing 50 mM DMSO. Although the two electrodes have the same amount of PbO_2 deposited on them, from the figure it can be seen that the catalytic activity for the oxidation of DMSO at the macroporous PbO_2 is greater than the plain PbO_2. $E_{1/2}$ potential for the DMSO oxidation occurs at 1.56 V at the macroporous PbO_2 and at 1.70 V at the plain PbO_2.

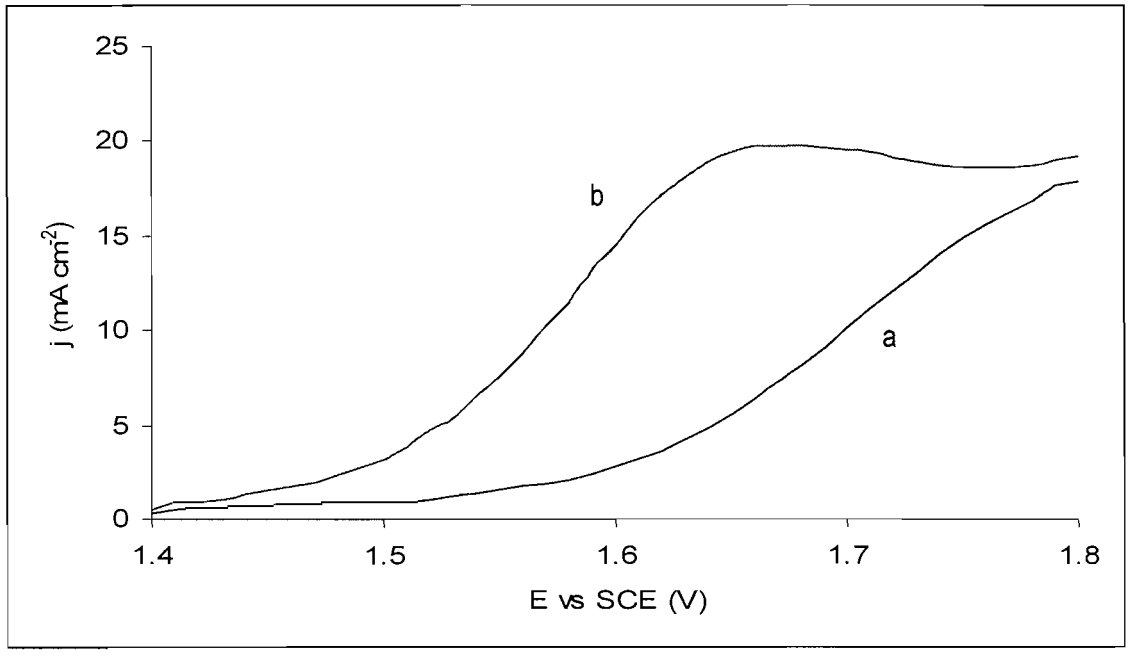

Figure 3.23: Voltammetric responses for DMSO oxidation on (a) plain and (b) macroporous β–PbO_2. Electrolytic solution: 50 mM DMSO + 1 M H_2SO_4. Deposition charge: 0.38 C cm^{-2}; deposition solution: 100 mM Pb(II) + 1 M HNO_3. Scan rate: 50 mV s^{-1}.

It is believed that the porous PbO_2 film has higher surface area and more active sites for the oxidation of DMSO taking place than the plain PbO_2. The combination of the increased specific surface area of the PbO_2 electrodes together with the accessibility of active sites has greatly enhanced the electrocatalytic activity for DMSO oxidation.

Unfortunately, this macroporous PbO_2 is not stable on open circuit in acidic solutions. The PbO_2 corrodes to Pb(II) and transforms to $PbSO_4$. The presence of DMSO accelerates the dissolution process and the transformation process of PbO_2 to $PbSO_4$ is fast. Figure 3.24 shows a SEM image of a corroded macroporous PbO_2 film with the presence of $PbSO_4$ crystals after immersion in 50 mM DMSO + 1 M H_2SO_4 for 10 minutes. This is consistent with the stability study of the plain PbO_2 on open circuit as discussed earlier in section 3.4.

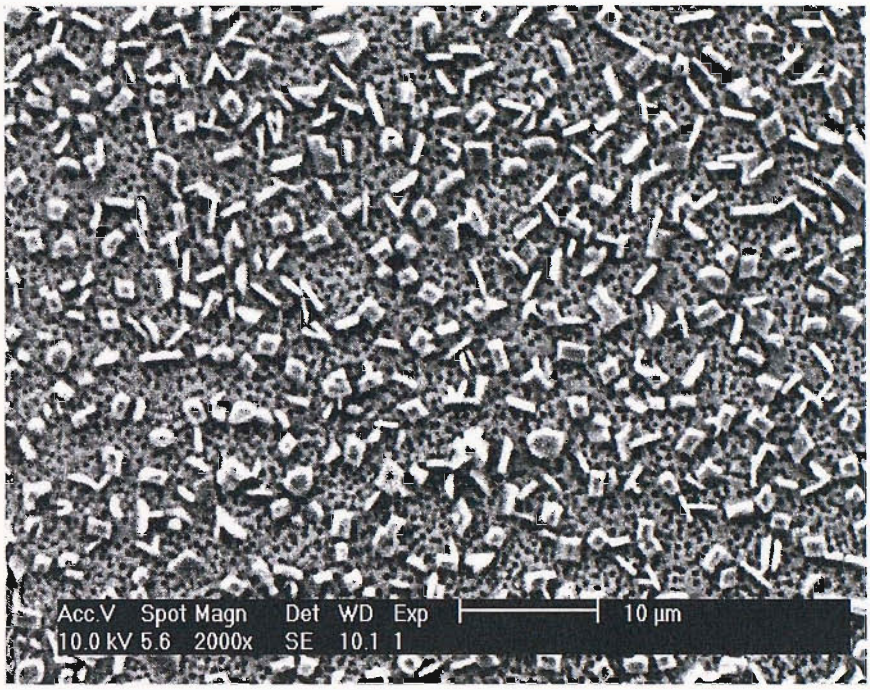

Figure 3.24: SEM image of a corroded macroporous β–PbO_2 film after immersion in 50 mM DMSO + 1 M H_2SO_4 for 10 minutes.

3.7 Deposition of α-PbO_2 Electrodes

Previously, this chapter has solely discussed the characteristics and the catalytic activity β-PbO_2 deposits. While β-PbO_2 can be easily prepared from Pb(II) solution in strong acid, the α-PbO_2 is readily prepared from slightly acidic or alkaline solution as mentioned in section 1.3. Grigger et al. [159] have reported a detail description of the α-PbO_2 deposition bath using alkaline lead tartrate. Very little study has been carried out concerning the deposition or the behaviour of α-PbO_2 compared to β-PbO_2 [84,159,160-162] although it is known to exhibit a lower oxygen overvoltage [162]. Therefore, in this study, the characteristics and catalytic activity of α-PbO_2 were investigated.

Figure 3.25 shows scanning electron micrographs of α-PbO_2 prepared from 500 mM $Pb(OAc)_2$ in 1 M sodium acetate solution using the same deposition conditions as β-PbO_2 shown earlier in figure 3.5b. From these two figures as a comparison, the α-PbO_2 deposit has a more compact and smooth structure compared to the more porous β-PbO_2. The more porous structure of the latter produces less adherent deposit on the substrate compared to the α-PbO_2.

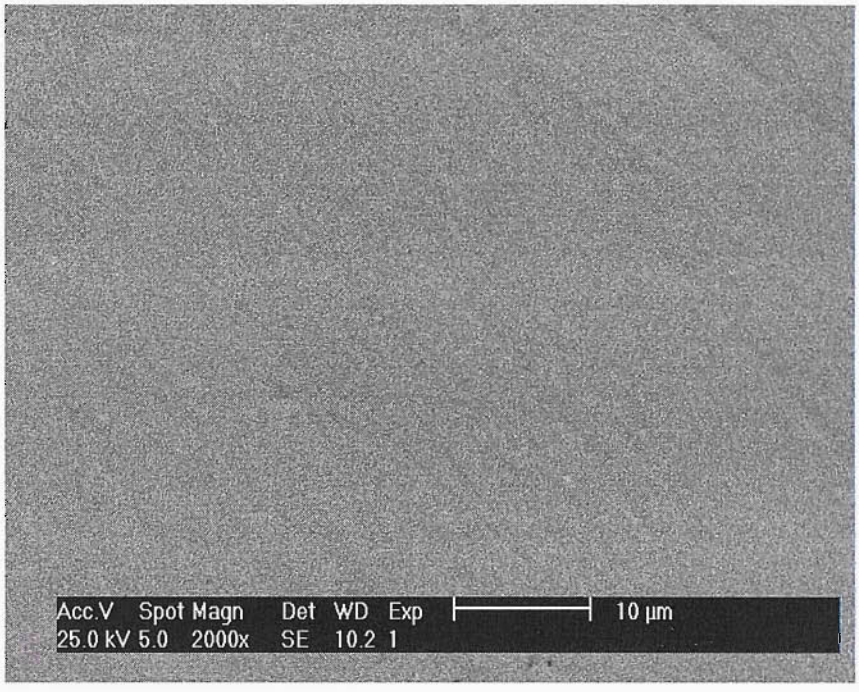

Figure 3.25: SEM image of α-PbO_2 deposited on gold from 500 mM $Pb(OAc)_2$ + 1 M NaOAc using constant current density of 5 mA cm^{-2} for 300 s at 298 K.

The α-PbO_2 prepared using a current density less than 5 mA cm^{-2} gave a very good deposit in terms of appearance and adhesion on the gold substrate. The deposit was black, uniform across the surface, dense and shiny; and the adhesion on gold was very good. The same appearance of the deposit has been reported by Lartney [161]. Hampson and Bushrod [162] have suggested that the current density for the α-PbO_2 preparation must be less than 5 mA cm^{-2} in order to avoid the production of highly stressed, flaky and poorly adherent deposits.

3.7.1 Stability of α-PbO_2 Deposits in Different Electrolyte Solutions

Table 3.4 compares the stability of α-PbO_2 in different supporting electrolyte solutions. All the deposits were prepared from a solution containing 500 mM $Pb(OAc)_2$ + 1 M NaOAc at 298 K and using a current density of 2.5 mA cm^{-2}.

The observations in the table indicate that the α-PbO_2 deposits are not stable for a long time on open circuit in any supporting electrolytes tested. In all media, the α-PbO_2 appears to react with water to give a Pb(II) species. For example, in 1 M NaOH, the α-PbO_2 appears to undergo a very fast dissolution rate to soluble Pb(II). The deposit completely dissolves in less than 1 hour in this strong alkaline solution (pH 14). But,

Feng and Johnson [160] reported earlier that the α-PbO_2 prepared from 2 M NaOH saturated with PbO (s) on stainless steel were very stable in strongly alkaline media.

Solution	**Observations**
1 M H_2SO_4	Dissolves within 2 days. A lot of 'square' crystals on the surface believed to be $PbSO_4$ after 3 hours and all the surface covered by the $PbSO_4$ crystals in 2 days observed by SEM
1 M $HClO_4$	Dissolves within less than 1 day ; Pb(IV) soluble in $HClO_4$
1 M Na_2SO_4	Dissolves within 2-3 days. Less $PbSO_4$ observed than in 1 M H_2SO_4
1 M NaOH	Completely dissolves within less than 1 hour

Table 3.4: Observations on the behaviour of α-PbO_2 deposits during immersion in different aqueous solutions at room temperature.

In the presence of DMSO, the dissolution process of the α-PbO_2 deposit is much faster than in the supporting electrolyte solutions without DMSO. For example, such a deposit took about 6 hours to completely change from PbO_2 to $PbSO_4$ in solution containing 50 mM DMSO + 1M H_2SO_4. The deposit was badly affected by the solution after immersion for a short time (eg: 30 minutes) as can be seen in figure 3.26a and as comparison to the freshly prepared deposit as similar as shown in figure 3.25. It can be seen that the surface consists of closely packed $PbSO_4$ crystals. The spontaneous chemical reaction taking place is shown in Scheme 1.

After being immersed at open circuit in the solution for a longer time (ie: 6 hours), almost all the surface have been transformed to 'square' crystals of lead sulphate as shown in figure 3.26b. In other solutions containing DMSO such as perchloric acid and sodium sulphate, the presence of DMSO has also accelerated the reduction process of the α-PbO_2 to Pb(II).

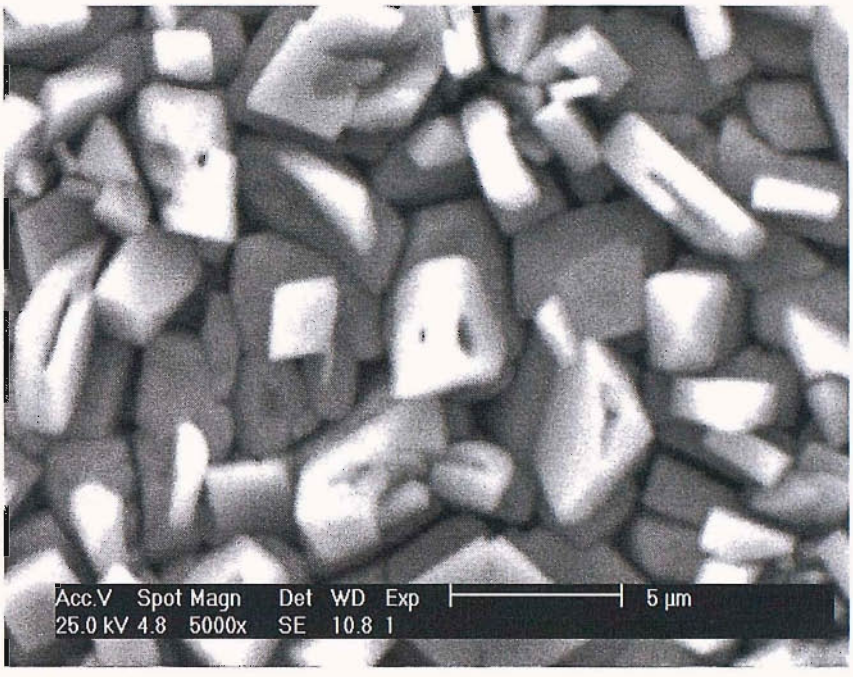

(a)

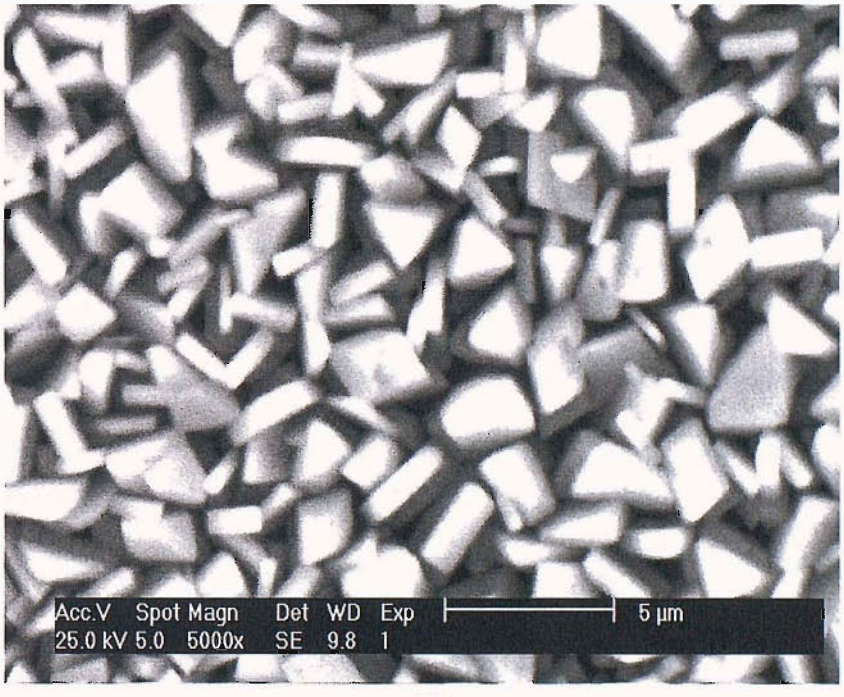

(b)

Figure 3.26: SEM images of α-PbO_2 deposits after immersion in 50 mM DMSO + 1 M H_2SO_4 for (a) 30 minutes and (b) 6 hours at room temperature.

The presence of $PbSO_4$ crystals is confirmed by EDAX analysis as can be seen in figure 3.27 and table 3.5.

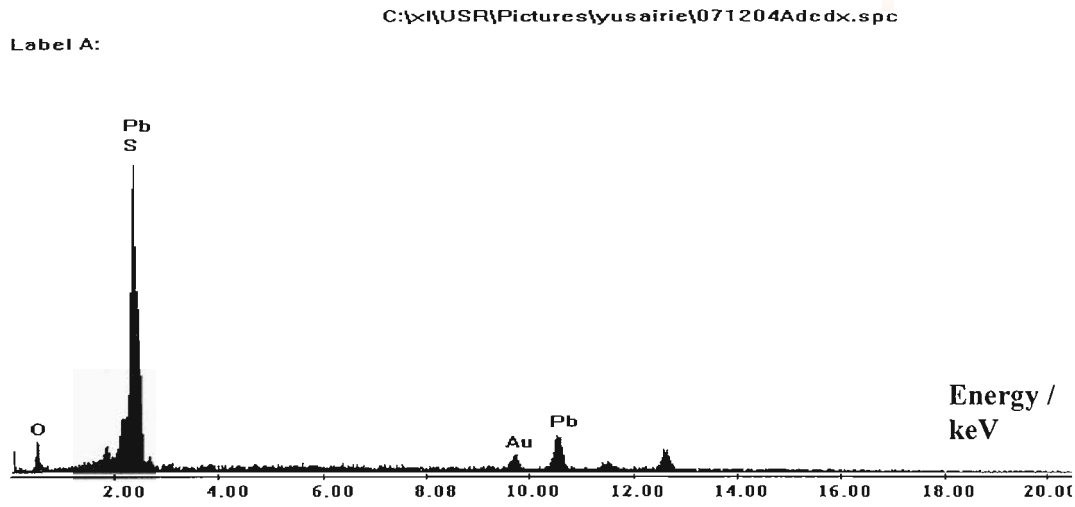

Figure 3.27: EDAX analysis of α-PbO_2 deposits after immersion in 50 mM DMSO + 1 M H_2SO_4 for 6 hours.

Element	Pb	O	Au	S
Atomic %	44.3	18.5	13.3	23.9

Table 3.5: Elemental content in atomic percent of EDAX measurements for α-PbO_2 deposits after immersion in 50 mM DMSO + 1 M H_2SO_4 as shown in figure 3.26b.

3.7.2 Electrocatalytic Activity of α-PbO_2 for DMSO Oxidation

A cyclic voltammetry of the α-PbO_2 electrode for DMSO oxidation was carried out in 1 M H_2SO_4 and scanned from +1.40 to +1.80 V. The electrode was prepared from 500 mM $Pb(OAc)_2$ in 1 M NaOAc at 2.5 mA cm^{-2} for 300 s at room temperature.

Figure 3.28 shows the performance of the electrode after immersion in 50 mM DMSO + 1 M H_2SO_4 for various periods of times. It was found that the freshly prepared α-PbO_2 electrode was inactive for the oxidation of DMSO. There was no wave below +1.60 V only the onset of O_2 evolution > +1.60 V.

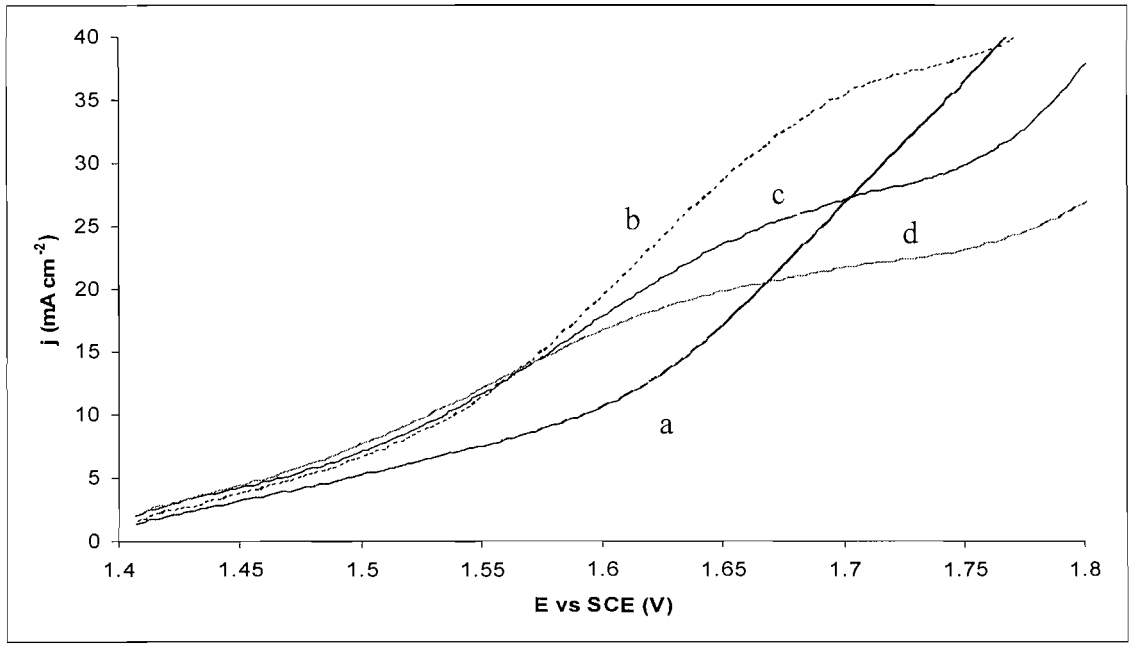

Figure 3.28: Comparison of voltammetric response (positive scan) for 50 mM DMSO at α-PbO_2 after immersion for (a) 0 min (b) 1 min (c) 10 min and (d) 50 min in 50 mM DMSO + 1M H_2SO_4 at room temperature. Electrolyte: 1 M H_2SO_4 Scan rate: 50 mV s^{-1}

After 1 minute in the solution, the α-PbO_2 electrode has quickly dissolved to Pb(II) through the chemical reaction as shown Scheme 1. It is believed that the surface area of the electrode has changed and increased after the immersion and this phenomenon led to the higher catalytic activity for the DMSO oxidation. $E_{1/2}$ has shifted to less positive potential (ie: +1.57 V). The $E_{1/2}$ s for the electrode immersed in the same solution for 10 min and 50 min have remained the same.

The limiting current density (j_L) of the electrode, however, has reduced with time of immersion. As can be seen in the figure, the limiting current densities for the DMSO oxidation of the α-PbO_2 electrode after immersion for 1 min, 10 min and 50 min were 38 mA cm^{-2} , 28 mA cm^{-2} and 22 mA cm^{-2}, respectively. The reduction of limiting current densities is believed to be associated with the reduction of the geometric area of the α-PbO_2 electrode. With increasing of immersion time of the electrode in the solution, more α-PbO_2 surface have transformed to $PbSO_4$ crystals as can be seen in figure 3.26a and 3.26b. The $PbSO_4$ crystals formed on the surface are inactive and their presence has reduced the active surface area of the electrode for DMSO oxidation to take place. In some systems involving chemistry of adsorbed species, there is always the suspicion that the surface is being poisoned by reaction intermediates or impurities, thus the current density can decay over a period of times [163].

3.7.3 Macroporous α- PbO_2

Highly ordered macroporous α-PbO_2 can also be prepared using the colloidal templating technique as used for the preparation of macroporous β-PbO_2 as discussed earlier in section 3.6. Bartlett et al [148] used the same technique in preparing macroporous α-PbO_2 from lead acetate solution. They reported that the structure of the macroporous determined by X-ray diffraction was highly polycrystalline orthorhombic and consistent with the crystal structure of non-templated α-PbO_2 films.

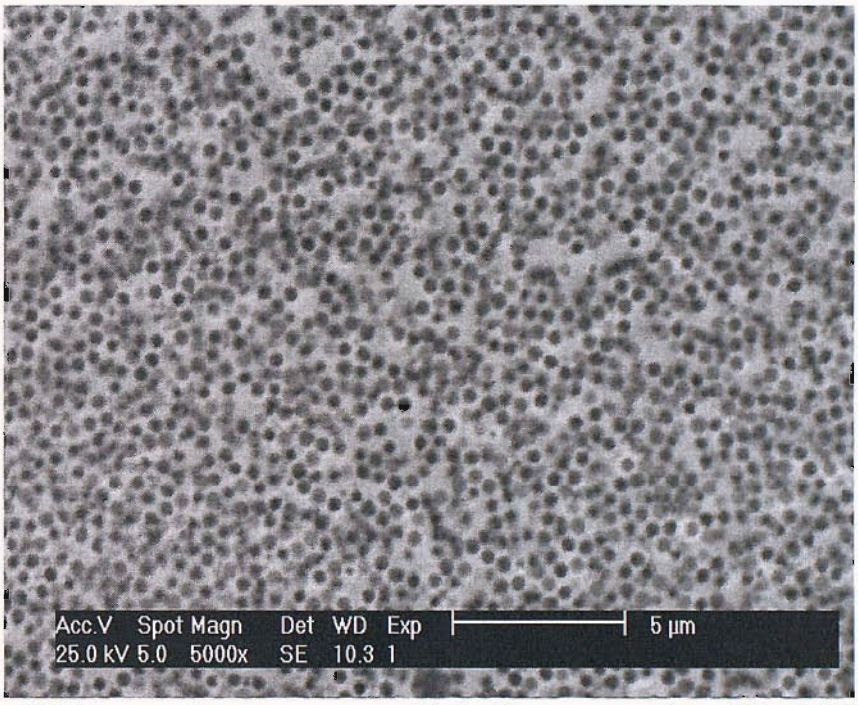

Figure 3.29: SEM image of a macroporous α-PbO_2 film grown at from 100 mM $Pb(OAc)_2$ + 1 M NaOAc using constant current density of 5 mA cm^{-2} for 60 s at 298 K through a template of 500 nm diameter polystyrene spheres.

Figure 3.29 shows a SEM image of macroporous α-PbO_2 film deposited through a 500 nm diameter template using a deposition charge of 0.30 C cm^{-2}. The film was black in colour, quite adherent on the gold substrate, smooth and uniform. The film thickness was calculated to be ~ 0.70 µm. The pore diameter from the image is in good agreement with the diameter of the polystyrene spheres used to form the template.

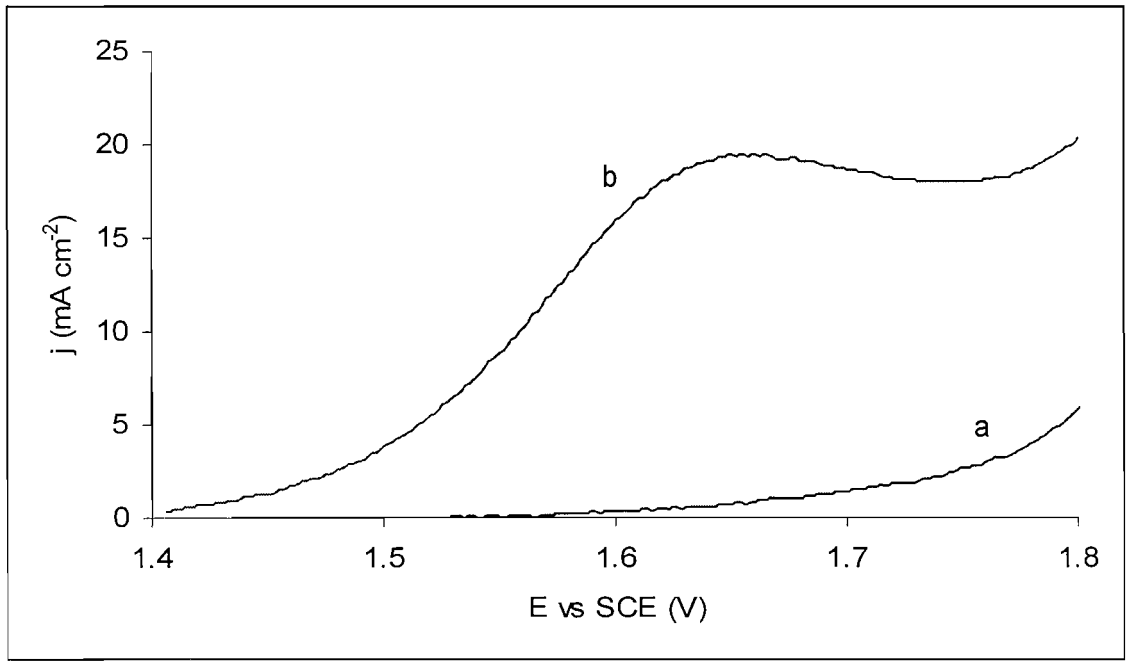

Figure 3.30: Voltammetric responses for macroporous α-PbO_2 in (a) 1 M H_2SO_4 and (b) 50 mM DMSO + 1 M H_2SO_4. Deposition charge: 0.30 C cm^{-2}; deposition solution: 100 mM $Pb(OAc)_2$ + 1 M NaOAc. Scan rate: 50 mV s^{-1}.

Figure 3.30 shows voltammetric responses for macroporous α-PbO_2 film in two sulfuric acid solutions with and without DMSO. It clearly shows that with the presence of DMSO, the voltammetric response clearly shows a well-formed wave for the oxidation of DMSO to $DMSO_2$ occurring at $E_{1/2}$ = +1.56 V. However, without DMSO in the solution, a rapid increase in current at > +1.70 V indicates only the evolution of O_2 is occurring at the macroporous film. It is believed that with high porosity, the film has a significant surface area for the DMSO oxidation to take place. Therefore, the oxidation of DMSO occurs at a relatively less positive potential well before the potentials for O_2 evolution.

Even so, the macroporous α-PbO_2 film has a good activity for the DMSO oxidation, its stability in aqueous acid solution is poor. Figure 3.31 shows a SEM image of destroyed macroporous α-PbO_2 film after a few cycles in 50 mM DMSO + 1 M H_2SO_4 solution. It shows that some places of the film electrode were badly affected by the solution. It was also found that dissolution occurred in the absence of DMSO although this is not consistent with a paper in the literature [148] which claimed the macroporous α-PbO_2 was mechanically robust and chemically stable in sulphuric acid.

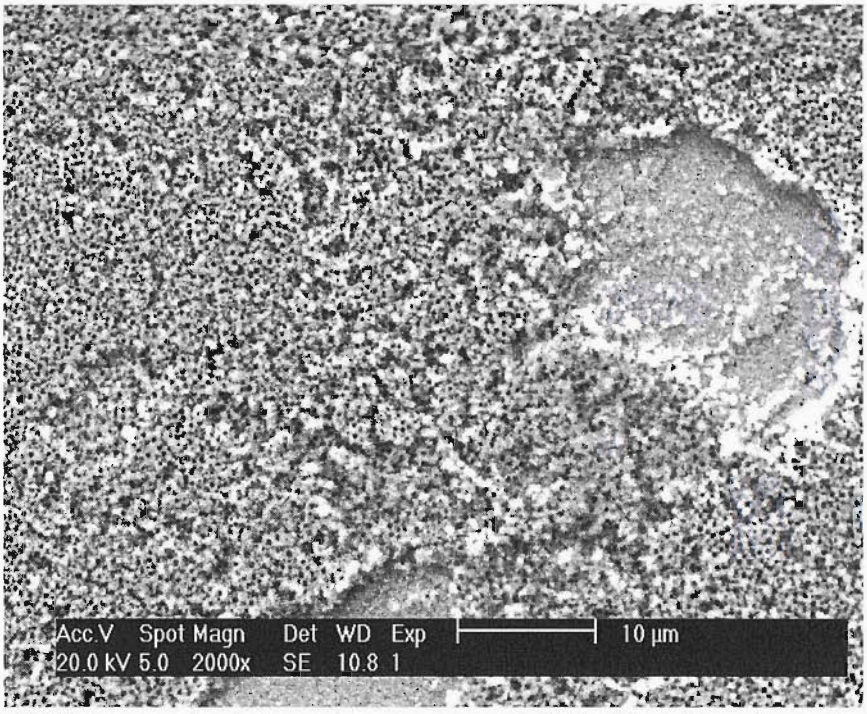

Figure 3.31: SEM image of a destroyed macroporous α-PbO_2 film after a few potential cycles in 50 mM DMSO + 1 M H_2SO_4.

Conclusions

The overall objective of this study was to seek stable and active PbO_2 electrodes that may be used for the oxidation of organic compounds. It was envisaged that the activity of the electrodes can be increased by doping with dopant ions or using high surface area forms such as microstructured layers of PbO_2 deposits. This chapter concerns the preparation and characteristics of pure α- and β- PbO_2. It was found that cyclic voltammetry studies for the deposition and dissolution of PbO_2 on/from gold substrate were consistent with the extensive existing literature [87,94,95,119,123,131].

However, a number of new conclusions have resulted from the study:

- The structure of the PbO_2 deposits on a µm scale is strongly dependent on the deposition conditions. Small changes to the electrolyte, Pb(II) concentration, current density and temperature lead to significant changes in structure.
- More stable PbO_2 deposits can be prepared by using low current density, high concentration of Pb(II) and high deposition temperature. They correspond to the low area surfaces with close packed angular crystals deposits.
- All α- and β- PbO_2 deposits dissolve slowly in all acid solutions left, investigated on open circuit. The deposits were more stable in Na_2SO_4.

- With the presence of DMSO in the acid solutions, destruction of the deposits is rapid on open circuit especially in sulfuric acid; due to chemical reaction as shown below:

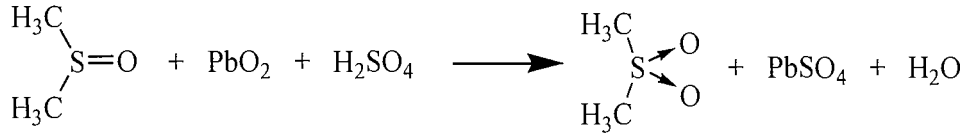

Chemical change is more rapid with the formation of an insoluble Pb^{2+} salt eg: $PbSO_4$.

- α- and β- PbO_2 deposits are more stable during electrolysis than on open circuit.
- β- PbO_2 deposits are more stable in all electrolyte solutions than α- PbO_2 deposits on open circuit.
- The least stable deposits are more active towards DMSO oxidation than the most stable deposits due to their higher surface area.
- Highly ordered macroporous α- and β- PbO_2 films prepared through polystyrene templates are active for the oxidation of DMSO; due to their high surface area. Unfortunately, they are not stable particularly in the presence of an oxidisable organic compound on open circuit.

Chapter 4: Doped PbO_2 on gold

4.0 Introduction

There is a great interest in the improvement of pure PbO_2 electrode as an anode material so that it has a high electrocatalytic activity. It is demonstrated in chapter 3 that the most stable, pure PbO_2 exhibits a low electrocatalytic activity toward an anodic reaction (ie: DMSO oxidation) in acidic media. The electrocatalytic activity of β-PbO_2 as an anode material can be significantly enhanced by doping with other metal ions. There have been a number of studies investigating the influence of foreign ions incorporated within PbO_2 deposits on the oxidation of various inorganic and organic compounds such as Mn(II), Cr(III), DMSO, toluene, phenol, EDTA, cyanide and 3-thiophenecarboxylic acid [80,81,137-139]. Unfortunately, most of the studies were carried out using very thin films of PbO_2 which had been prepared from dilute solutions of Pb(II), usually in aqueous perchloric acid. These are conditions far from those recommended for the fabrication of stable β-PbO_2 anodes. Also the studies largely relate to analytical applications where current densities are low. Many potential applications, for example in synthesis or effluent treatment, require stability and activity at current densities up to 250 mA cm^{-2} in a range of electrolytes.

Hence, in this program the objective was to reinvestigate the catalysis of electrochemical oxidations by dopants in thick and more stable β-PbO_2 anode coatings prepared from high concentration of Pb(II) (ie: 500 mM Pb) in strongly acidic media on a gold substrate. While bulk gold is clearly not a practical substrate for industrial electrodes, a gold underlayer has been proposed for PbO_2 coatings on Ti [114]. Another objective was to define the conditions where such doped PbO_2 electrodes could be used with satisfactory performance. Various metallic ions were used as the potential dopant ions in this study such as transition metals (ie: Ag, Fe, Ni) and group (V) metal ion (ie: Bi).

4.1 Doping with Transition Metal Ions

Three transition metal ions; silver, iron and nickel, were selected as the dopant ions in order to investigate the influence of each dopant on the properties of PbO_2,

especially its catalytic activity. DMSO was used as the reactant to study the electrocatalytic activity of each doped PbO_2 deposits.

10 mM of each dopant was added into a deposition solution containing 500 mM Pb(II) + 1M HNO_3. The electrodeposition of each doped PbO_2 was carried out onto a gold disc substrate (area: 0.11 cm^2) using a current density of 5 mA cm^{-2} for 300 s at room temperature. All the prepared doped PbO_2; so-called 'Ag-doped PbO_2', 'Fe-doped PbO_2' and 'Ni-doped PbO_2' were black in colour with smooth appearance by eye. SEM images taken at the center of each doped PbO_2 were compared with the image of undoped or pure PbO_2 prepared under the same conditions.

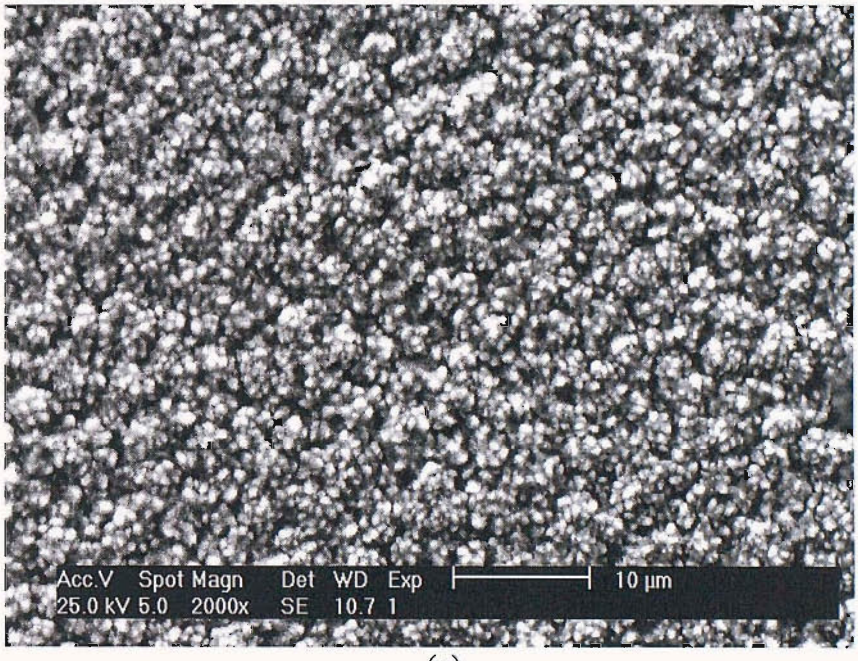

(a)

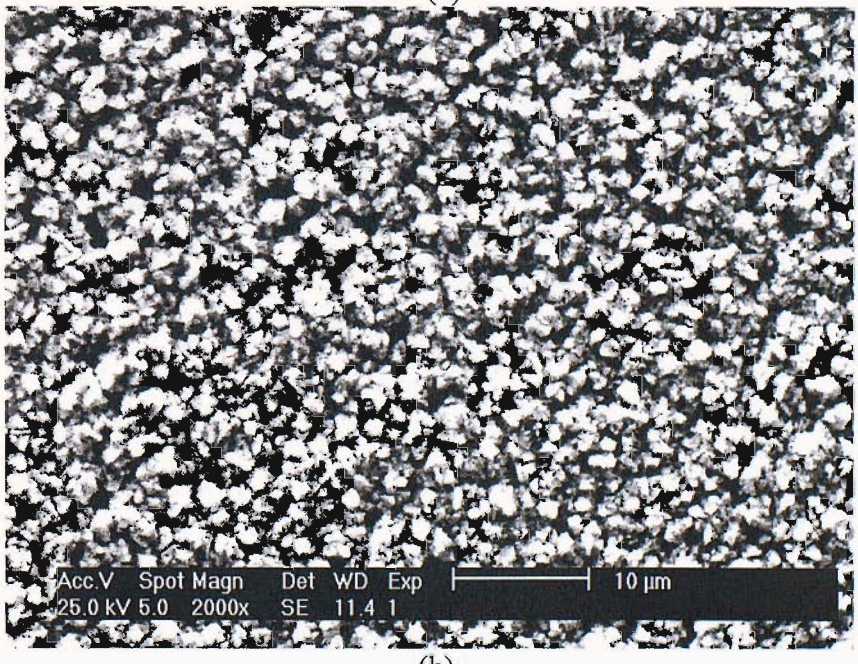

(b)

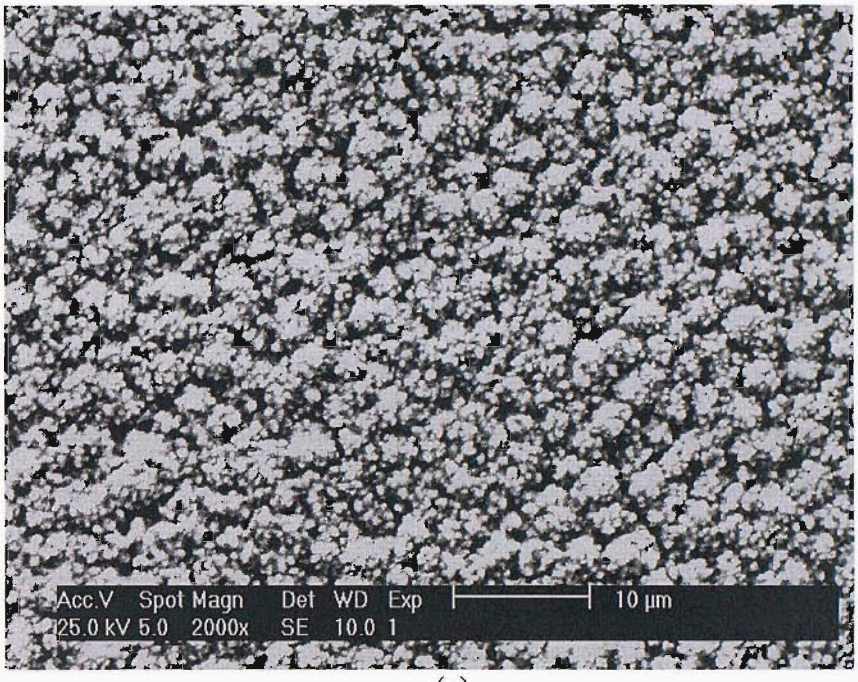

(c)

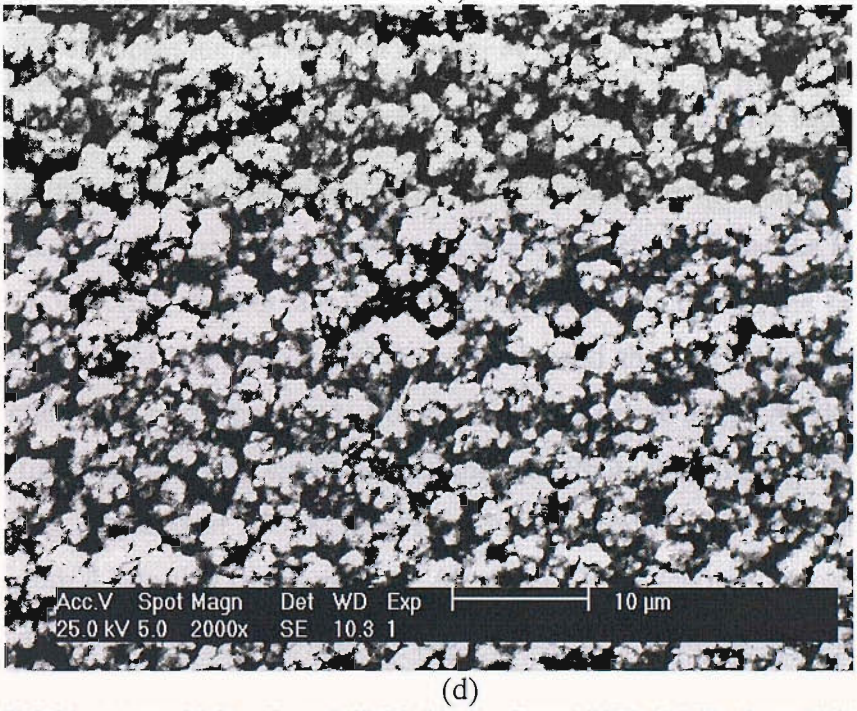

(d)

Figure 4.1: SEM images of (a) undoped PbO_2 (b) Ag-doped PbO_2 (c) Fe-doped PbO_2 and (d) Ni-doped PbO_2 prepared using a current density of 5 mA cm^{-2} for 300 s at 298 K. Deposition solution: 10 mM M^{n+} + 500 mM Pb(II) + 1 M HNO_3

Figure 4.1 shows the SEM images for all the PbO_2 deposits; undoped (figure 4.1a), Ag-doped PbO_2 (figure 4.1b), Fe-doped PbO_2 (figure 4.1c) and Ni-doped PbO_2 (figure 4.1d). It was found that the addition of 10 mM Fe(III) in the deposition solution did not change the morphology of the pure PbO_2 as shown in figure 4.1c. However, the addition of Ag(I) or Ni(II) in the same amount as the Fe(III) has slightly

changed the structure of the PbO_2 deposits from hemispherical centers with small crystallites to more angular aggregates as shown in figure 4.1b and figure 4.1d which represent Ag-doped PbO_2 and Ni-doped PbO_2, respectively.

EDAX analysis was done on all doped PbO_2 deposits and summarized in Table 4.1. The average of each dopant to Pb(IV) ratio are calculated based on 5 sites across the whole surface (middle and edges) as determined by EDAX. The table indicates that the level of dopant ion in the PbO_2 deposit was very low with a ratio of M/Pb below 0.010. Velichenko et al [164] reported that a high content of Fe was found to be incorporated into the PbO_2 if prepared in lower concentration of supporting electrolyte (ie: 0.1 M HNO_3) rather than in high acidic concentration.

Doped PbO_2	**M/ Pb ratio**
Ag-doped PbO_2	0.003
Fe-doped PbO_2	0.010
Ni-doped PbO_2	0.002

Table 4.1: Ratio of dopant ion to Pb(IV) in average of doped PbO_2 deposits determined by EDAX. All deposits prepared from 10 mM M^{n+} + 500 mM Pb(II) + 1 M HNO_3 at 298 K and a current density of 5 mA cm^{-2}. (M refers to each particular metal added in the bath solution)

The preparation of doped PbO_2 deposits at elevated temperature (ie: 333 K) using the same deposition conditions as for the pure PbO_2 showed that the addition of 10 mM Ag(I) or Fe(III) did not significantly change the structure of the pure PbO_2. Images taken by SEM for both doped deposits showed that the both deposits had angular structure as the undoped PbO_2. For example, the image of the Ag-doped PbO_2 as shown in figure 4.2b is very similar to the undoped PbO_2 as in figure 4.2a. But, the Ni-doped PbO_2 prepared at 333 K showed a partial conversion from the angular deposit of figure 4.2 to that of figure 4.1a. All doped PbO_2 deposits prepared at this temperature showed good adhesion and some resistance to abrasion as was the case with pure PbO_2.

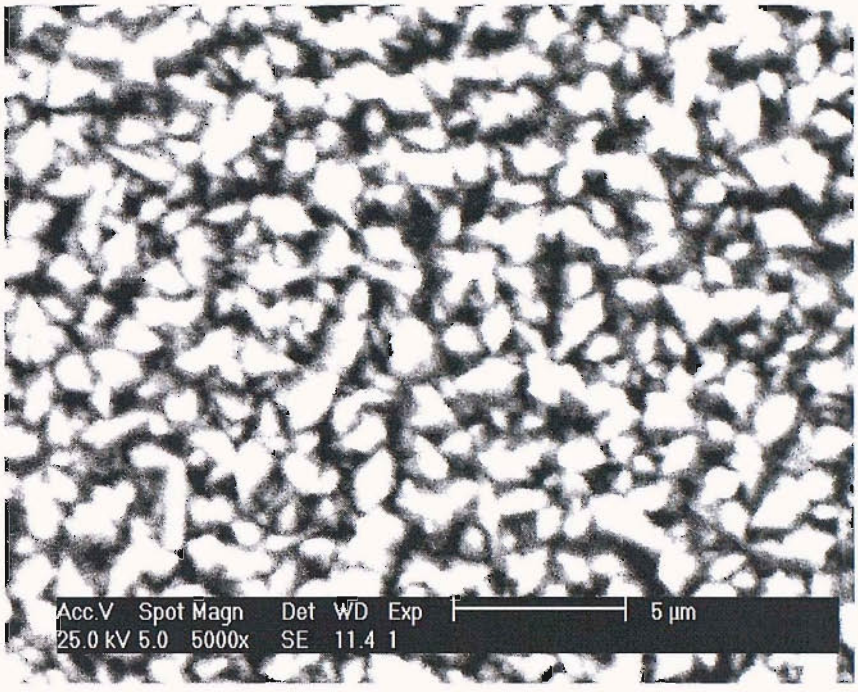

(a)

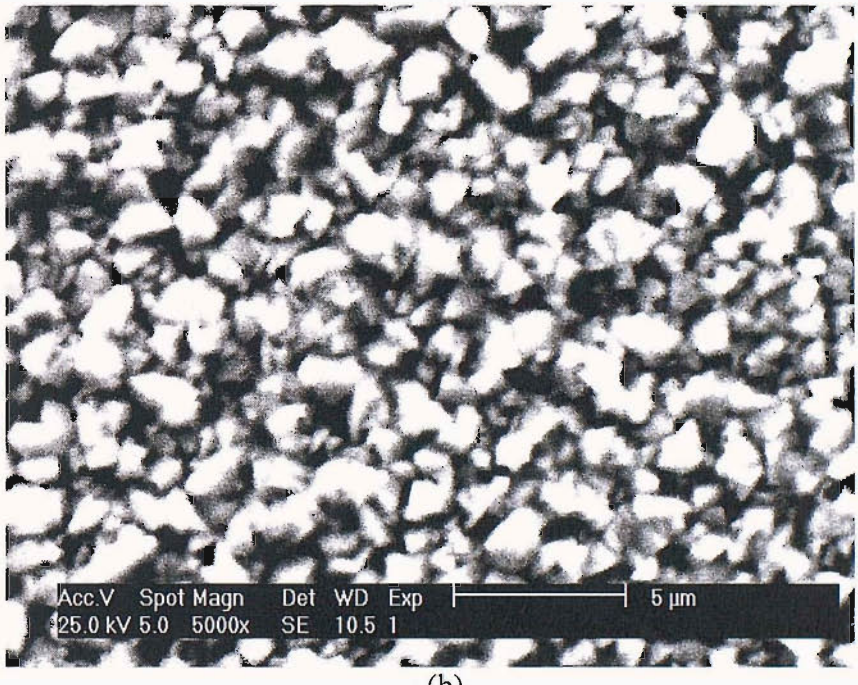

(b)

Figure 4.2: SEM images of (a) undoped PbO_2 and (b) Ag-doped PbO_2 prepared using a current density of 5 mA cm^{-2} for 300 s at 333 K. Deposition solutions: (a) 500 mM Pb(II) + 1 M HNO_3 (b) 10 mM Ag(I) + 500 mM Pb(II) + 1 M HNO_3.

4.1.1 Electrocatalytic Activity of Doped PbO_2

The electrocatalytic activity of the doped PbO_2 electrodes prepared using a current density of 5 mA cm^{-2} at 298 K was investigated for the oxidation of 50 mM DMSO in 1 M H_2SO_4. Figure 4.3A – D show voltammograms for undoped and the

doped PbO_2 electrodes in the sample solution at 298 K. The voltammograms shown in figure 4.3A to 4.3D correspond to the images shown in figure 4.1a to 4.1 d, respectively.

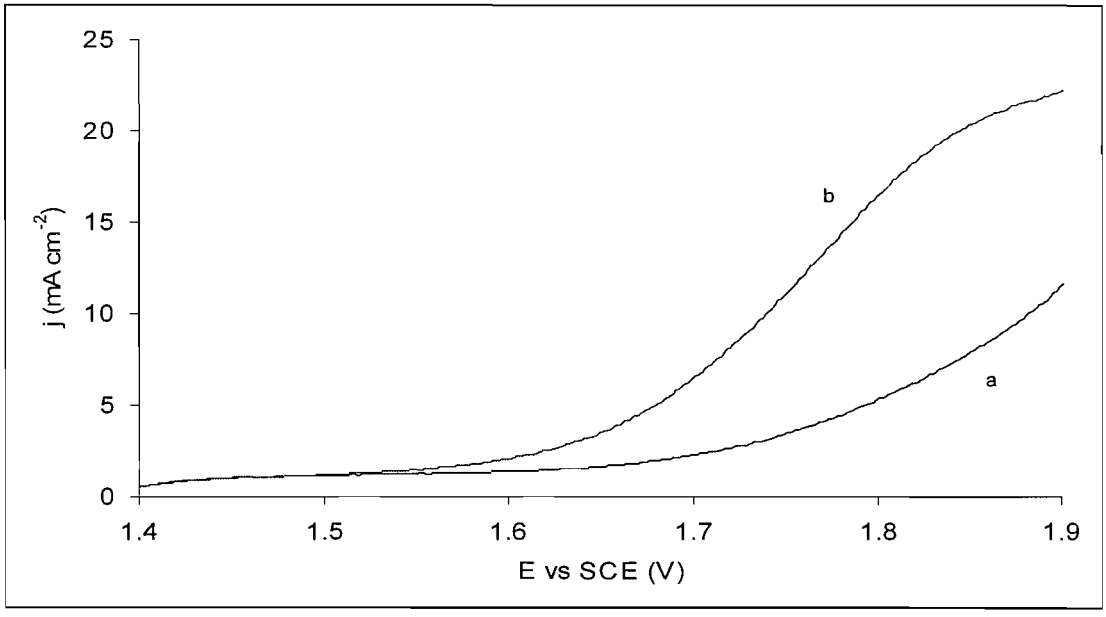

(A)

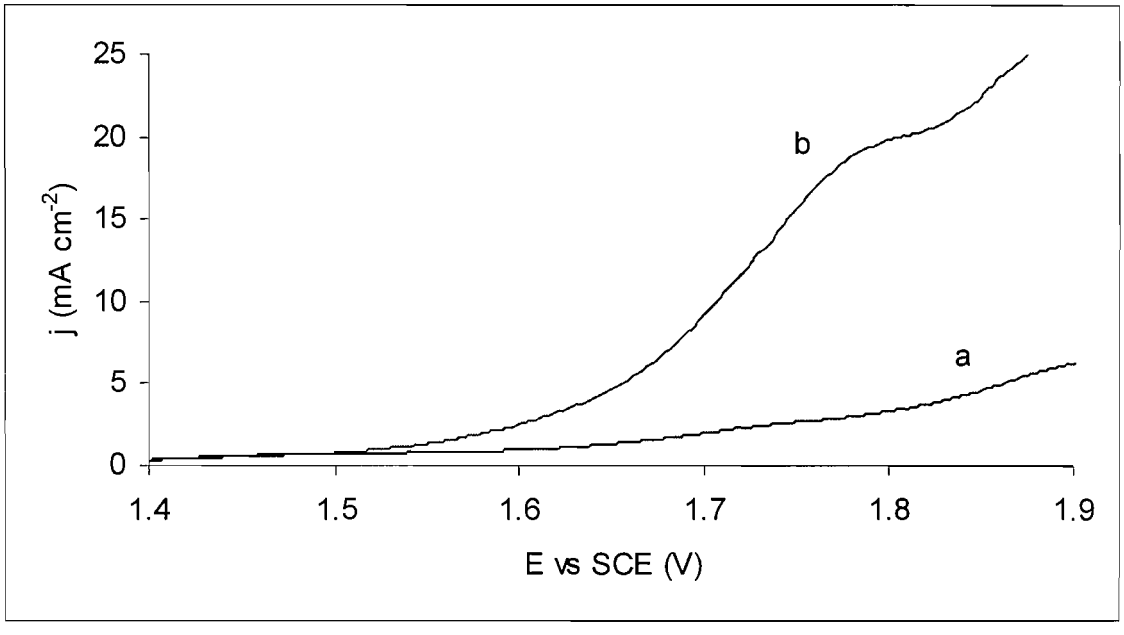

(B)

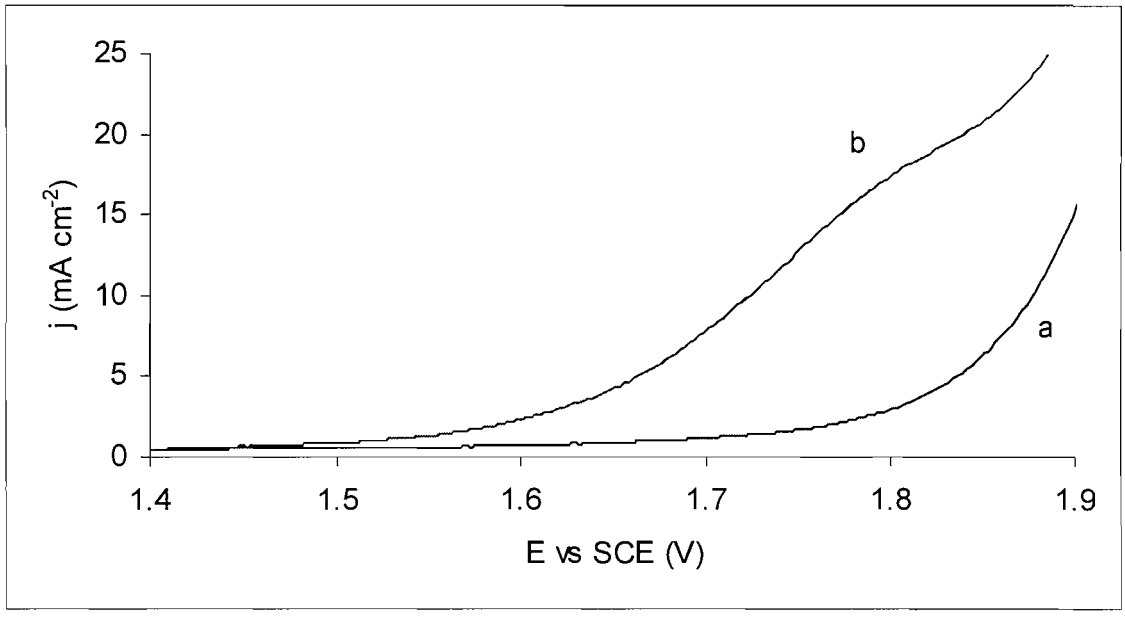

(C)

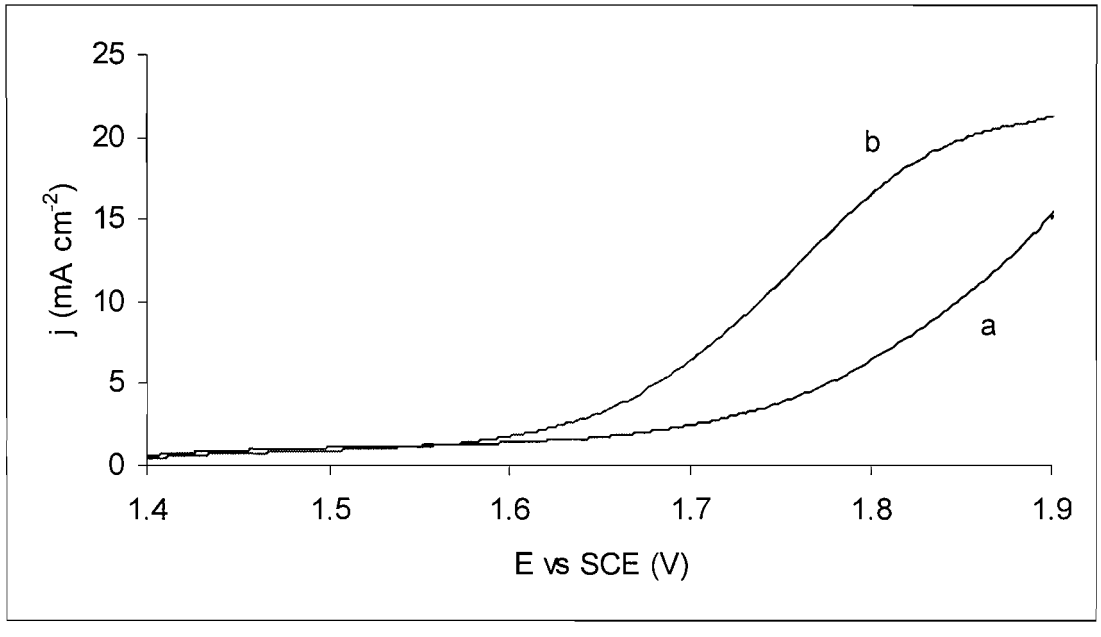

(D)

Figure 4.3: Voltammograms of (A) undoped PbO_2 (B) Ag-doped PbO_2 (C) Fe-doped PbO_2 and (D) Ni-doped PbO_2 in (a) 1 M H_2SO_4 and (b) 50 mM DMSO + 1 M H_2SO_4. Scan rate: 50 mV s^{-1}.

All deposits gave a wave for the oxidation of DMSO with a limiting current density of ca. 16 mA cm^{-2} as expected for mass transport controlled oxidation. It was found that $E_{1/2}$s for the oxidation of DMSO at Ag-doped PbO_2 and Fe-doped PbO_2 occurred at less positive potentials +1.71 V and +1.73 V, respectively as compared to +1.75V for the undoped. But, the incorporation of Ni(II) into the PbO_2 matrix did not

have significant effect on the oxidation of DMSO. However, Ni-doped PbO_2 deposit is more favourable for O_2 evolution as seen in figure 4.3D than other deposits.

4.2 Group (V) Metal Dopant

Two metallic ions in this group (ie: Bi^{3+} and As^{3+}) are the most widely studied in the preparation of doped PbO_2 for the anodic oxidation reactions. It was found that the As-doped PbO_2 electrodes exhibit the O-transfer activity which is greater than that of pure PbO_2 electrodes but not as great as for Bi-doped PbO_2 electrodes [139].

In this study, the generation of active PbO_2 electrodeposited from acidic solutions of Pb(II) containing Bi(III) has been emphasized. 10 mM of Bi(III) was added into a solution containing 500 mM Pb(II) + 1 M HNO_3. The electrodeposition of Bi-doped PbO_2 was carried out using similar preparation conditions as for other doped PbO_2 (as discussed earlier in section 4.1). It was found that Bi-doped PbO_2 deposit was dark grey in colour when deposited at 298 K but it became more greyish when higher temperature (ie: 333 K) was used for the deposition. It is believed that the change in colour of the deposit is strongly dependent on the content of bismuth present in the deposits. More bismuth was detected on Bi-doped PbO_2 prepared at 333 K than 298 K as determined by EDAX (as shown in table 4.2). This shows that deposition temperature has a significant effect on bismuth content incorporated within the PbO_2 deposits.

Bi-Doped PbO_2	Average of Bi/ Pb ratio
Deposited at 298 K	0.10
Deposited at 333 K	0.19

Table 4.2: Bi(III) content of PbO_2 deposits prepared at different temperatures, determined by EDAX. Deposition solutions: 10 mM Bi(III) + 500 mM Pb(II) + 1 M HNO_3. Deposited using a current density of 5 mA cm^{-2} for 300 s.

Figure 4.4 shows a SEM image of Bi-doped PbO_2 deposited using the same deposition conditions as the preparation of other doped PbO_2 as discussed earlier in section 4.1. Comparison of SEM images of all doped deposits (as in figure 4.1b for Ag-doped, 4.1c for Fe-doped, 4.1d for Ni-doped and 4.4 for Bi-doped PbO_2) shows that the presence of bismuth in the deposition solution has more significantly changed the structure of the PbO_2 deposits from hemispherical centers with small crystallites to more obvious hemispherical structure with more closely packed deposits as in

figure 4.4 than other dopant ions with the same concentration of added ions (ie: 10 mM).

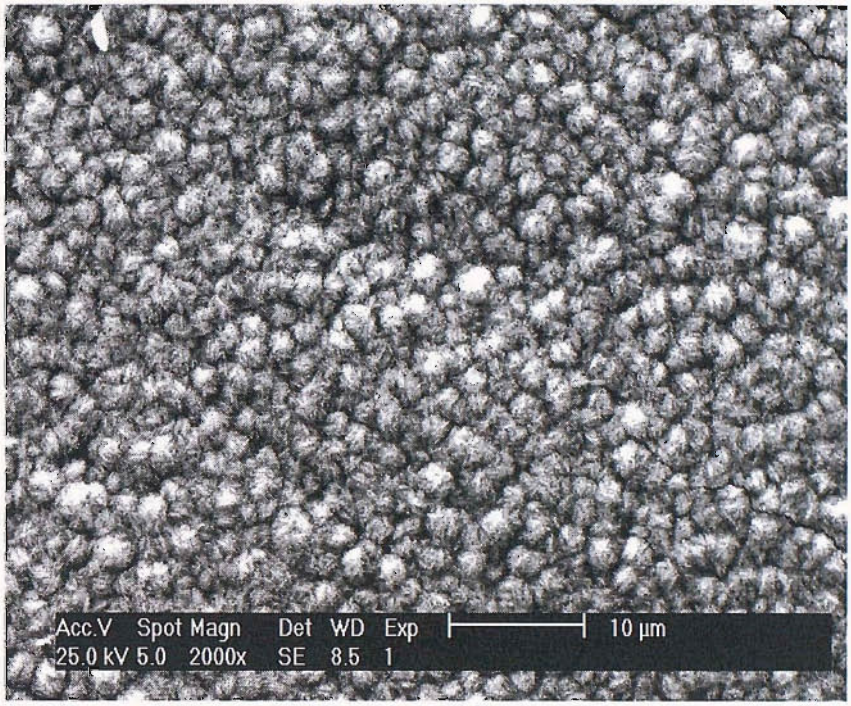

Figure 4.4: SEM image of Bi-doped PbO_2 prepared from 10 mM Bi(III) + 500 mM Pb(II) in 1 M HNO_3 at 298 K.

The electrodeposition of Bi-doped PbO_2 at an elevated temperature (ie: 333 K) is particularly interesting. It can be seen in figure 4.5 to consist of closely packed and rather uniform sized hemispheres completely different from angular structure observed for the undoped PbO_2 deposited under the same conditions, see figure 4.2a. There are also fewer voids between the centers compared with the structures shown in figure 4.1 (deposited at 298 K for undoped and doped PbO_2).

This deposit showed good adhesion and some resistance to abrasion. It is more adherent on gold substrate than Bi-doped PbO_2 or other PbO_2 deposits deposited at 298 K but less adherent than pure PbO_2 deposited at 333 K.

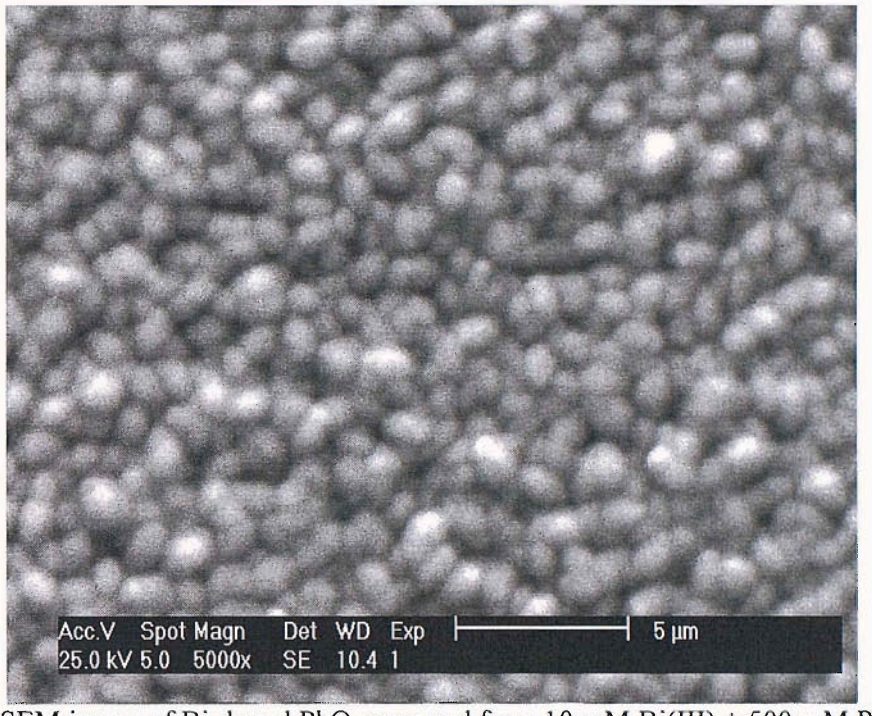

Figure 4.5: SEM image of Bi-doped PbO_2 prepared from 10 mM Bi(III) + 500 mM Pb(II) in 1 M HNO_3 at 333 K.

The electrocatalytic activity of Bi-doped PbO_2 electrodes deposited from 10 mM Bi(III) + 500 mM Pb(II) in 1 M HNO_3 using a current density of 5 mA cm^{-2} at 298K and 333 K was investigated and compared for the oxidation of DMSO. Figure 4.6A and 4.6B show the voltammograms for Bi-doped PbO_2 prepared at 298 K and 333 K, respectively in 1 M H_2SO_4 and 50 mM DMSO + 1 M H_2SO_4. The voltammograms were both recorded at 298 K.

It was found that the catalytic activity of the Bi-doped PbO_2 prepared at higher temperature is greater than at the deposit prepared at room temperature. $E_{1/2}$ for the oxidation of DMSO at Bi-doped PbO_2 prepared at 333 K occurred at +1.62 V but at Bi-doped PbO_2 deposit prepared at 298 K occurred at more positive potential (ie: +1.66 V). It is believed that the presence of different content of bismuth on the surface of the PbO_2 electrodes has led to the difference in the activity of the deposits for the oxidation of DMSO. The more active PbO_2 deposit corresponds to the higher content of bismuth present. The content of bismuth for both deposits was determined by EDAX and shown earlier in table 4.2. It is believed that Bi(III) could be possibly co-deposited as Bi(V) in the slightly defect structure of the β-PbO_2. It is speculated that the Bi(V) sites in the Bi-doped PbO_2 surface can absorb OH· generated by anodic discharge of H_2O and then used for the O-transfer reactions, in this case DMSO to $DMSO_2$.

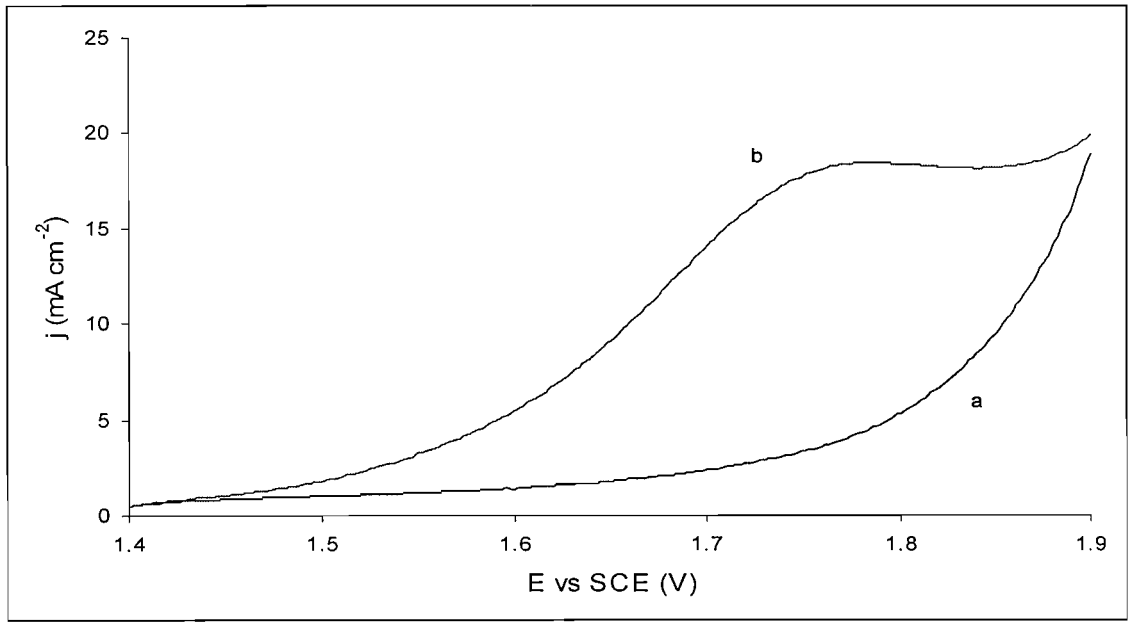

(A)

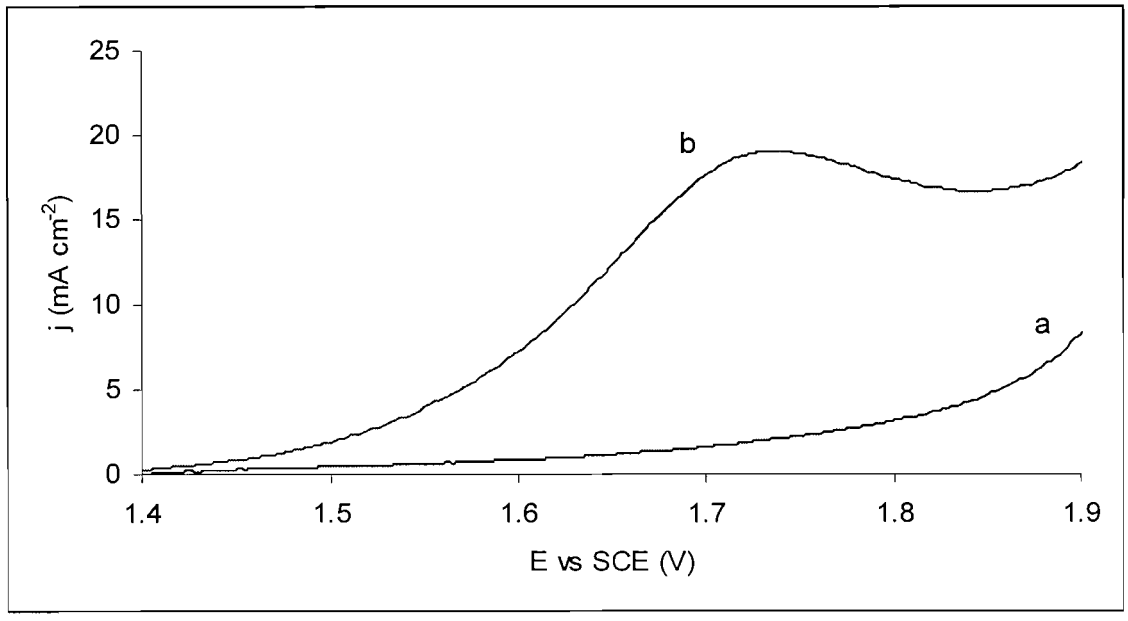

(B)

Figure 4.6: Voltammograms for Bi-doped PbO_2 electrodes prepared at (A) 298 K and (B) 333 K in (a) 1 M H_2SO_4 and (b) 50 mM DMSO + 1 M H_2SO_4. Potential scan rate: 50 mV s^{-1}. Bi-doped PbO_2 deposited from 10 mM Bi(III) + 500 mM Pb(II) + 1 M HNO_3 using a current density of 5 mA cm^{-2} for 300 s.

Comparison with voltammograms recorded for other dopant ions (ie: transition metal ions) as shown in figure 4.3 reveals that bismuth is the best catalyst candidate to be incorporated within the PbO_2 deposits for the oxidation of DMSO. This is consistent with the earlier study done by especially Johnson et al

[80,139,155,165]; that Bi(III) in the PbO_2 deposits was an effective catalyst for oxidations of organic and inorganic compounds such as DMSO and Mn(II).

4.2.1 Influence of Bi(III) Concentration

The influence of added Bi(III) concentration on the electrodeposition of Bi-doped PbO_2 was investigated. Various concentrations of Bi(III) in the range of 1 – 100 mM were added into the deposition solutions containing 500 mM Pb(II) + 1 M HNO_3. Results of Bi:Pb ratio at the center of Bi-doped PbO_2 deposits determined by EDAX are summarized in table 4.3. The results show that the amounts of Bi incorporated with PbO_2 deposits are increased with the increase in Bi(III) concentration in the deposition solutions.

Concentration of Bi(III) added	Average of Bi/Pb ratio
1 mM	0.06
10 mM	0.19
30 mM	0.36
100 mM	0.47

Table 4.3: Bi/Pb ratio analysed by EDAX for Bi-doped PbO_2 deposits prepared from different concentration of added Bi(III) into solution containing 500 mM Pb(II) + 1M HNO_3.Deposition conditions: 5 mA cm^{-2}, 300 s, 333 K.

The morphology of the Bi-doped PbO_2 has changed from angular crystals to hemispherical crystals with increasing Bi(III) concentration in the deposition solutions. The addition of 1 mM Bi(III) did not substantially change the morphology of PbO_2 from that in the absence of dopant as shown in figure 4.2a. The morphology has remained angular as shown in figure 4.7a; similar to the morphology of pure PbO_2 deposited under the same conditions (ie: 5 mA cm^{-2}, 333 K). The colour of the deposit was also black similar to the pure PbO_2.

However, the addition of a higher Bi(III) concentration (ie: 10 mM) has drastically changed the structure of the PbO_2 deposits from angular to hemispherical crystals as shown in figure 4.7b. The colour of the deposit was dark grey. But, the increase of Bi(III) to > 30 mM has produced a lighter coloured deposit. Also, the deposit with a ratio Bi:Pb of 0.36 - 0.47 (as determined by EDAX) had lost its physical integrity; it was easily removed from the gold substrate and the SEM showed both cracking and lifting of the hemispherical deposit from the gold substrate as in

figure 4.7c and 4.7d when 30 mM Bi(III) and 100 mM Bi(III), respectively added in the deposition solutions. With high content of Bi in the deposits, there are possibilities of the formation of another phase such as Pb-Bi_2O_3. Hence, the addition of 10 mM Bi(III) is considered an appropriate amount for the production of a physically stable Bi-doped PbO_2 deposit.

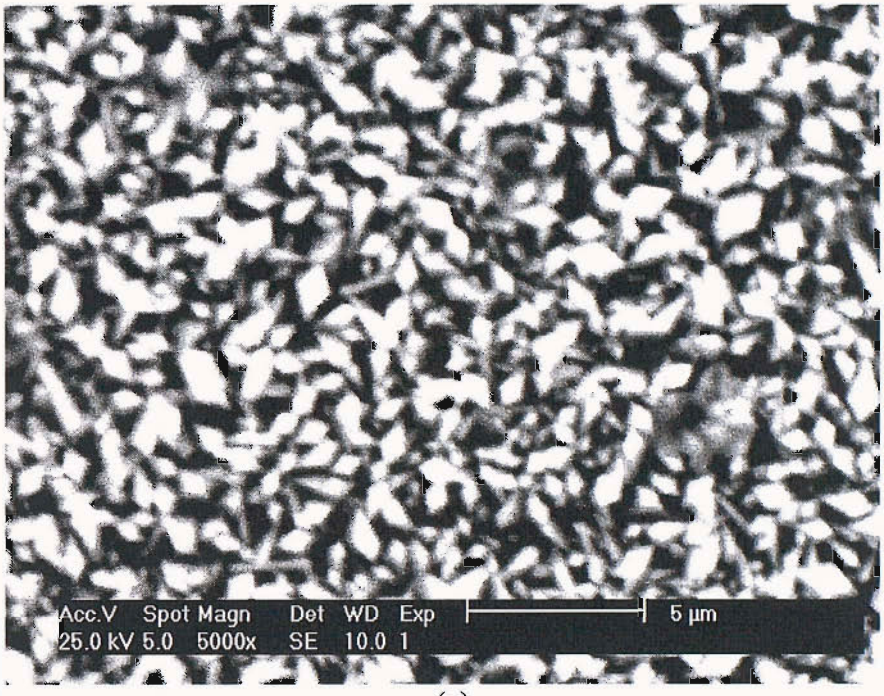

(a)

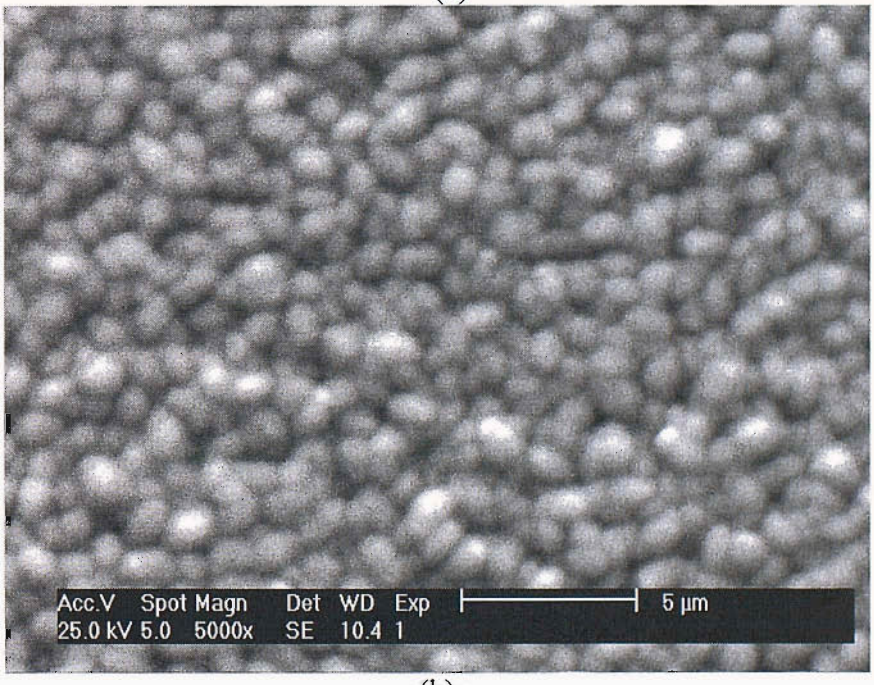

(b)

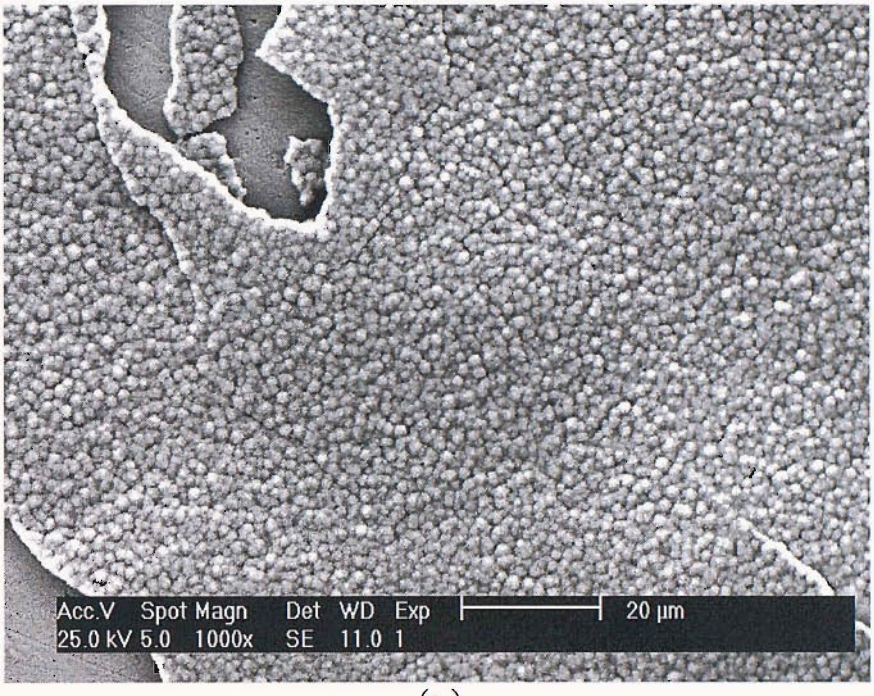

(c)

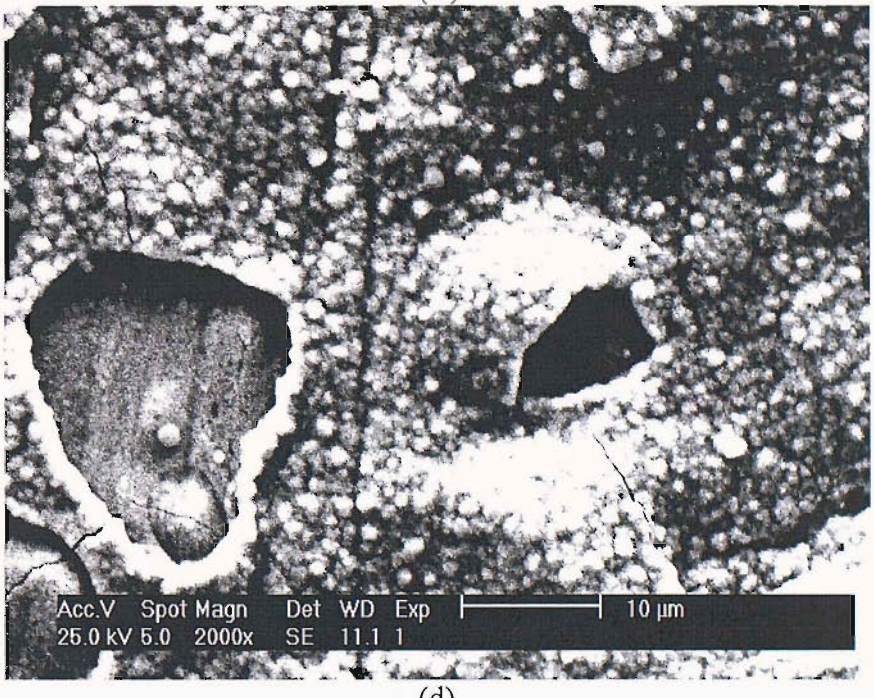

(d)

Figure 4.7: SEM images of Bi-doped PbO_2 prepared from solution containing 500 mM Pb(II) + 1 M HNO_3 with the addition of (a) 1 mM Bi(III) (b) 10 mM Bi(III) (c) 30 mM Bi(III) and (d) 100 mM Bi(III). Deposition conditions: 5 mA cm^{-2}, 300 s, 333 K.

4.2.2 Voltammograms with Bi-doped PbO_2 Prepared from Different Bi(III) Concentration.

A series of experiments on the oxidation of DMSO was carried out to study the influence of added Bi(III) into the deposition solutions on the catalytic activity of

PbO_2 electrodes. The catalytic activity for the DMSO oxidation was assessed by recording voltammogram from +1.40 V to +1.90 V. Figure 4.8 compares current-potential curves for the oxidation of 50 mM DMSO in 1 M H_2SO_4 at 298 K on three different PbO_2 deposits with 50 mV s^{-1} scan rate. They are an undoped PbO_2 electrode prepared from 500 mM Pb(II) + 1 M HNO_3, a Bi-doped PbO_2 electrode prepared from 2 mM Bi(III) + 500 mM Pb(II) + 1 M HNO_3 and a Bi-doped PbO_2 electrode prepared from solution containing 10 mM Bi(III) + 500 mM Pb(II) in 1 M HNO_3.

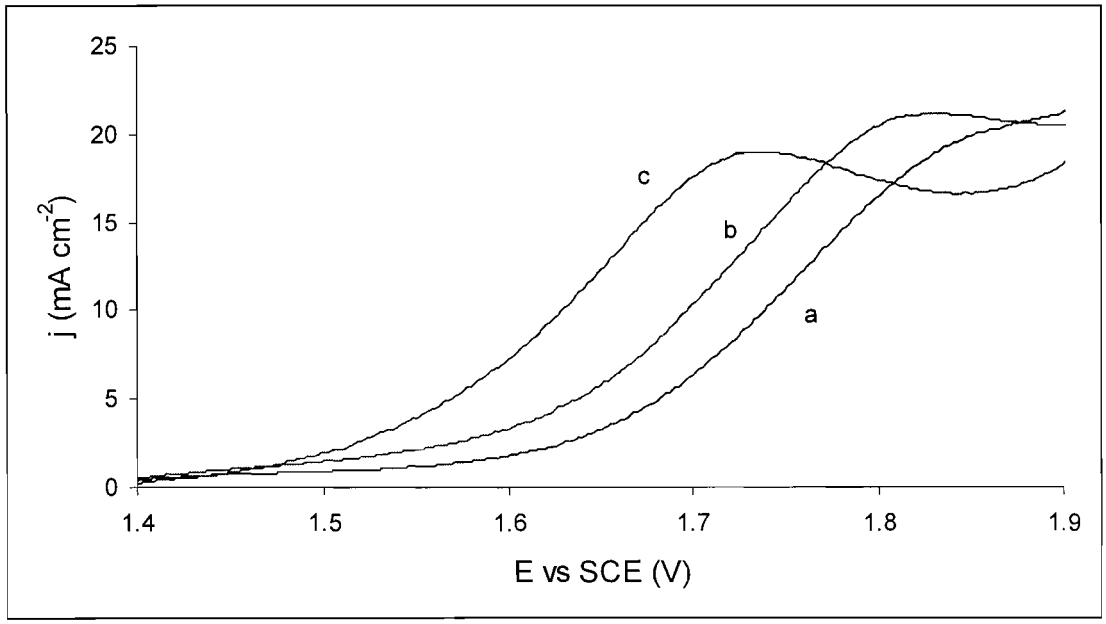

Figure 4.8: Voltammograms of PbO_2 deposits prepared from 500 mM Pb(II) + 1 M HNO_3 containing (a) 0 mM (b) 2 mM and (c) 10 mM Bi(III) in 50 mM DMSO + 1 M H_2SO_4. Deposition conditions: 5 mA cm^{-2}, 300s, 333 K. Scan rate: 50 mV s^{-1}.

It is clearly shown that the anodic wave for the oxidation of DMSO to $DMSO_2$ at both Bi-doped PbO_2 electrodes occurred at less positive potentials if compared to undoped PbO_2 which occurred at ca. +1.75 V. It was also found that the catalytic activity of the PbO_2 electrodes increases with increasing Bi(III) added into the deposition solution. $E_{1/2}$ for the oxidation DMSO at Bi-doped PbO_2 prepared from lower Bi(III) concentration (ie: 2 mM) occurred at +1.70 V; however, when the addition of Bi(III) was increased to 10 mM in the deposition solution; the resulting PbO_2 electrode gave higher activity for DMSO oxidation with $E_{1/2}$ at +1.62 V. This indicates that the amount of bismuth incorporated into the PbO_2 deposits played a major role in the activity of the electrodes.

Overall, the results show that the Bi-doped PbO_2 electrodes prepared by electrodeposition from 10 mM Bi(III) + 500 mM Pb(II) in 1 M HNO_3 using a current density of 5 mA cm^{-2} and a temperature of 333 K represented the best compromise between physical integrity and activity and gave consistent results over a period of hours.

4.2.3 Anodic Oxidations of Selected Organic Compounds at Bi-doped PbO_2

Figure 4.9 shows voltammograms recorded from +1.40 V to +1.90 V for 3 selected organic compounds; dimethylsulfoxide (DMSO), 3-thiophenecarboxylic acid (3-TCA) and 3-picoline at Bi-doped PbO_2 electrodes. All the organic solutions were prepared at concentration of 50 mM in 1 M H_2SO_4. The Bi-doped PbO_2 electrodes were prepared from solution containing 10 mM Bi(III) + 500 mM Pb(II) in 1 M HNO_3 using a current density of 5 mA cm^{-2} at 333 K.

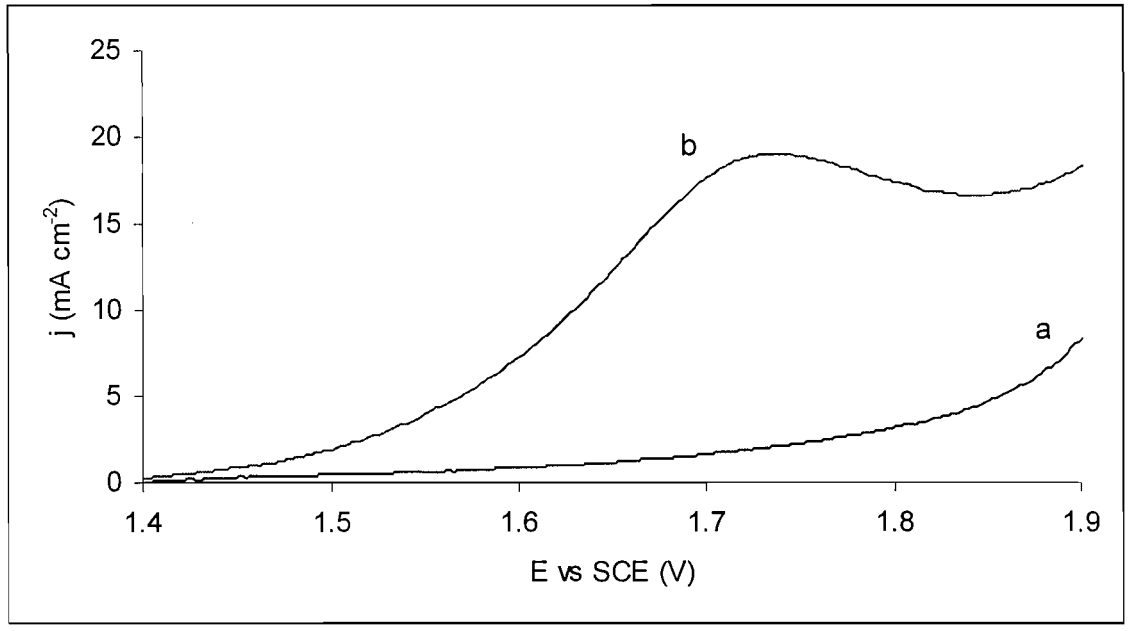

(A)

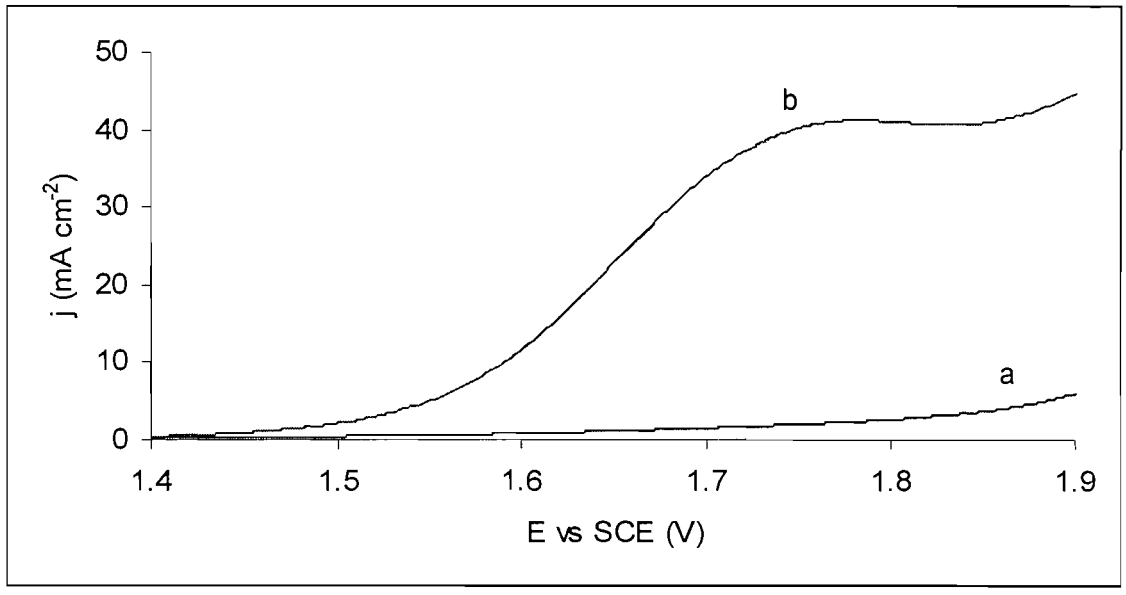

(B)

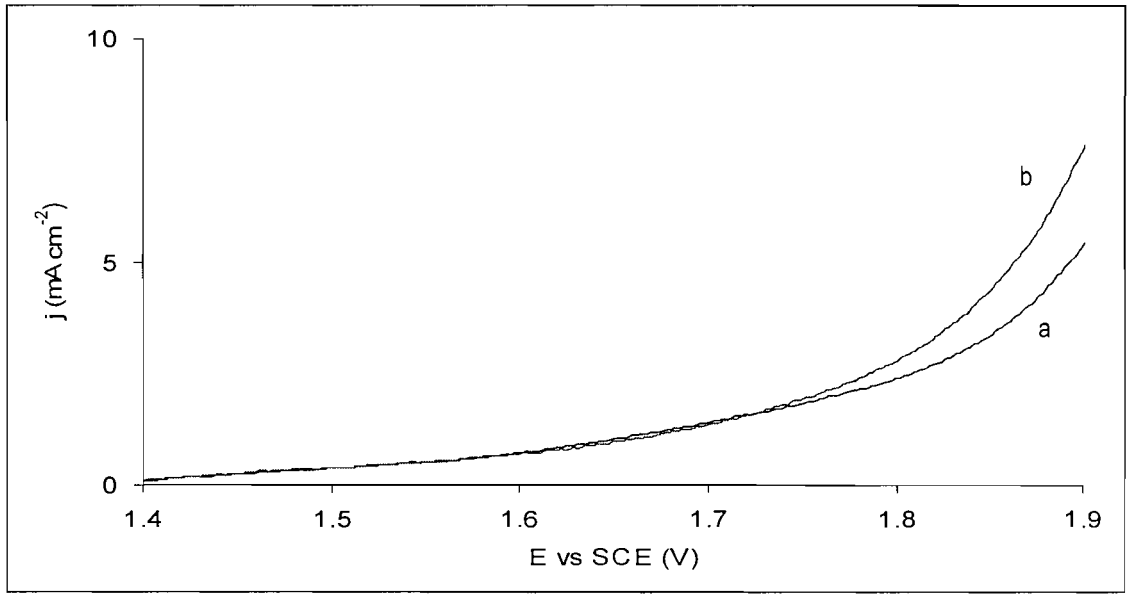

(C)

Figure 4.9: Voltammetric response for (A) dimethyl sulfoxide (B) 3- thiophene carboxylic acid; and (C) 3-picoline at Bi-doped PbO_2 in 1 M H_2SO_4. Scan rate: 50 mV s^{-1}; concentration of reactant: (a) 0 mM and (b) 50 mM.

It can clearly be seen from figure 4.9A and 4.9B that both organic sulphur-containing compounds (ie: DMSO and 3-TCA) were oxidized to their products (ie; $DMSO_2$ and 3-TCA sulfone) at the Bi-doped PbO_2 electrodes. $E_{1/2}$ values for both oxidation waves occurred at about the same potential (ie: +1.62 V). However, limiting current densities recorded for both voltammograms are different; ca. 18 mA cm^{-2} for solution containing DMSO and ca. 36 mA cm^{-2} for 3-TCA. It is believed to

be due to the number of electron involved for the oxidation reactions for each organic compound; 2 electrons for DMSO and 4 electrons for 3-TCA according to equation 1.13 (ie: $j_L=nFk_mc$).

But, the oxidation of 3-picoline to its products either pyridine-3-carbaldehyde or nicotinic acid as shown in scheme 3 (see page 75), does not occur at the Bi-doped PbO_2 electrodes as no oxidation wave was recorded as shown in figure 4.9C. It was reported earlier [80] that some organic compounds such as formaldehyde and cyanide (CN^-) are not oxidized at a substantial rate at Bi-doped PbO_2. These results show that organic sulphur-containing compounds are more readily oxidized at Bi-doped PbO_2 than other organic compounds.

4.2.4 Bi-doped PbO_2 Electrodes Prepared from Low Concentration of Pb(II)

An investigation into the catalytic activity of the Bi-doped PbO_2 deposits prepared from low concentration of Pb(II) in 1 M HNO_3 was also carried out. Figure 4.10 compares the SEM images of undoped and Bi-doped PbO_2 deposits which have been prepared from low concentration of Pb(II) (ie: 30 mM) at 298 K. With the presence of 10 mM Bi(III) in the deposition solution, the resulting oxide has bigger hemispherical crystals and more dense deposit (as shown in figure 4.10b) as compared to undoped PbO_2 deposits (as shown in figure 4.10a) which have been prepared under the same conditions except no addition of Bi(III). A difference was also observed in their colours; undoped was dark brown while Bi-doped PbO_2 was very black in colour. Basically, the adhesion for both deposits on gold substrates is only moderate. They are quite easily removed by alumina slurries but not by wiping with tissues.

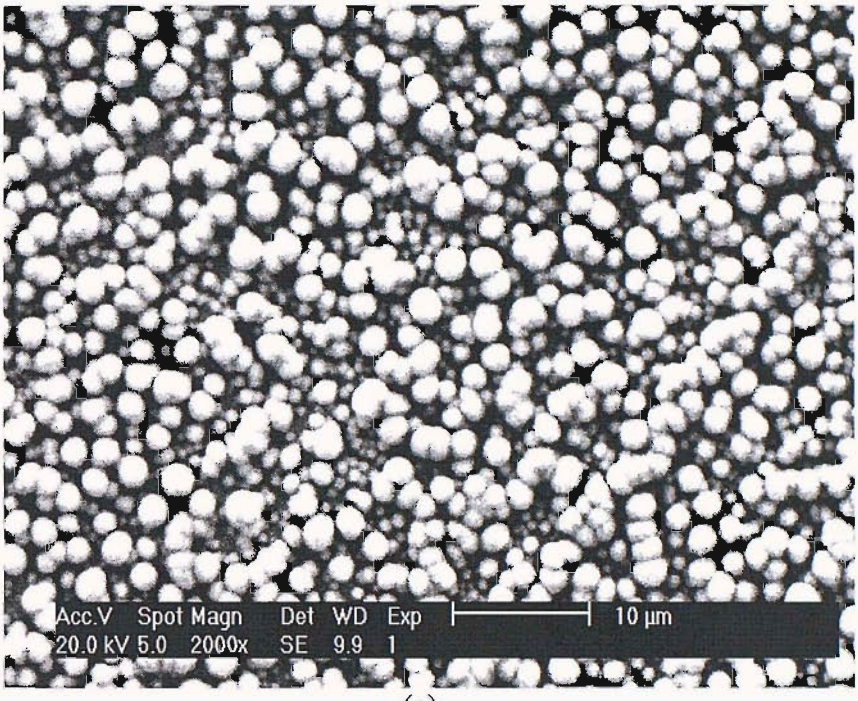

(a)

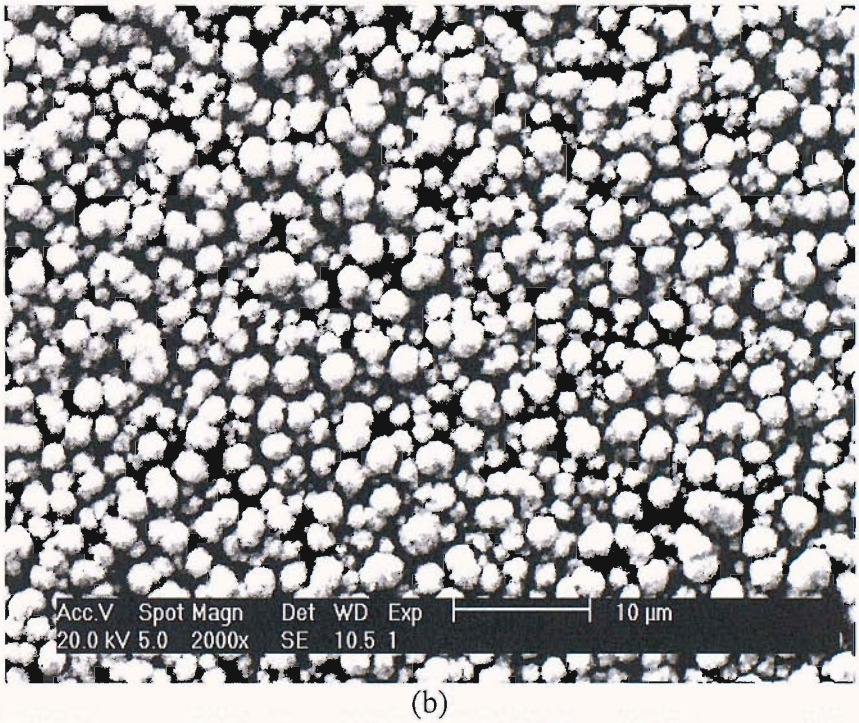

(b)

Figure 4.10: SEM images of (a) undoped PbO_2 and (b) Bi-doped PbO_2 prepared from low concentration of Pb(II) in 1 M HNO_3. Preparation conditions: 5 mA cm^{-2}, 300 s, 298 K

The catalytic activity for both deposits was tested and compared for the oxidation of DMSO. Voltammetric responses for the oxidation of DMSO at both deposits were recorded from +1.40 to +1.90 V as shown in figure 4.11 for the undoped and in figure 4.12 for the Bi-doped PbO_2. It is apparent that half wave potential ($E_{1/2}$) for the oxidation of DMSO at undoped PbO_2 occurred at higher

potential (ie: +1.72 V) while at Bi-doped PbO_2, the $E_{1/2}$ value appeared at +1.57 V. This indicates that the PbO_2 deposits incorporated with bismuth has greater catalytic performance than the undoped PbO_2. The presence of bismuth has a significant effect on the catalytic activity of PbO_2 electrodes.

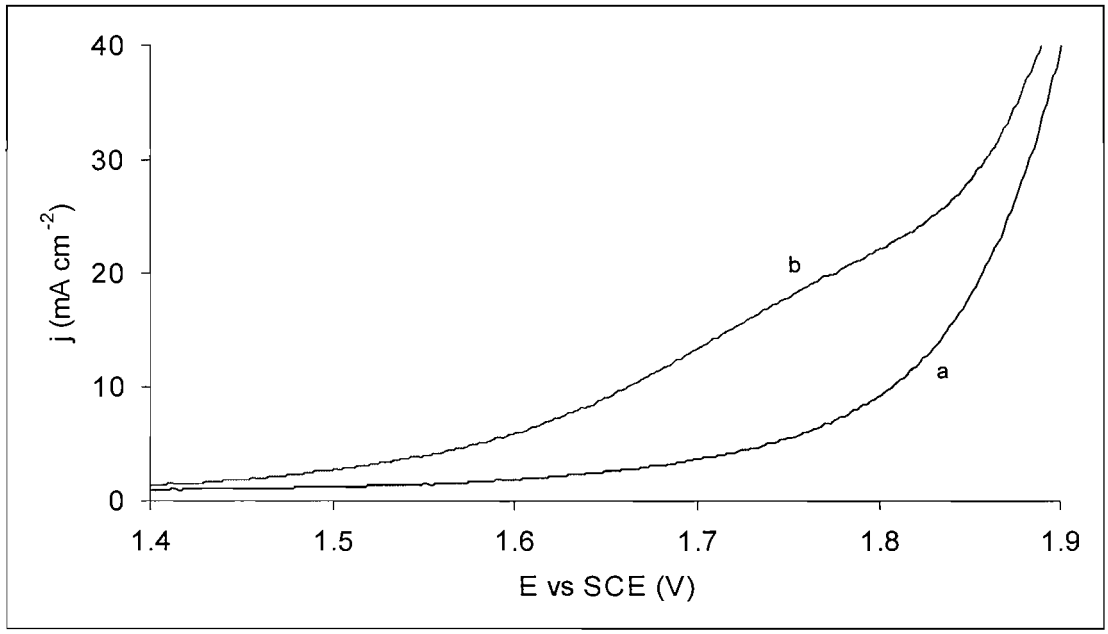

Figure 4.11: Voltammograms of (a) 1 M H_2SO_4 and (b) 50 mM DMSO + 1 M H_2SO_4 at undoped PbO_2 corresponding to SEM image in figure 4.10a. Scan rate: 50 mV s^{-1}

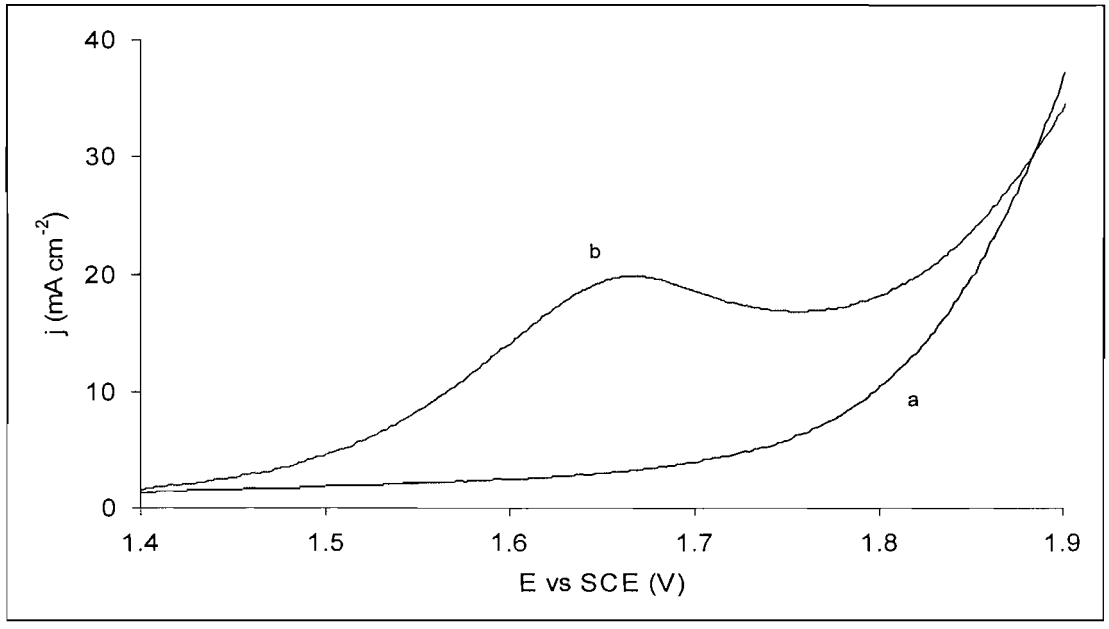

Figure 4.12: Voltammograms of (a) 1 M H_2SO_4 and (b) 50 mM DMSO + 1 M H_2SO_4 at Bi-doped PbO_2 electrodes corresponding to SEM image in figure 4.10b. Scan rate: 50 mV s^{-1}

Comparison of $E_{1/2}$ values for the oxidation of DMSO at different Bi-doped PbO_2 electrodes was also carried out and the results are shown in table 4.4. The results reveal that the Bi-doped PbO_2 electrodes prepared from low concentration of Pb(II) (ie: 30 mM) has greater activity for the anodic oxidation reaction of DMSO than other Bi-doped PbO_2 electrodes prepared from high concentration of Pb(II). This effect is believed to be attributed to the increase in density of bismuth incorporated within the PbO_2 matrix and these sites acted as the adsorption sites for the oxidation to take place. The average ratio of Bi:Pb of each deposit as determined by EDAX is shown in the table. With decreasing Pb(II) concentration in the deposition solution, more bismuth (believed to be Bi(V)) was incorporated within the PbO_2 matrix. It has been reported that the increase in the doping level of Bi-doped PbO_2 electrodes to Bi(V):Pb(IV) = 0.40 result in a decrease of the $E_{1/2}$ for the oxidation of DMSO to $DMSO_2$ to minimum of +1.57 V (vs SCE) [166].

Deposition Solution	**Deposition Conditions**	**SEM image**	**Average of Bi:Pb ratio**	**$E_{1/2}$ (V) for DMSO → $DMSO_2$**
10 mM Bi(III) + 30 mM Pb(II)	5 mA cm^{-2} 300 s 298 K	as in figure 4.9b	0.35	+1.57 (as in figure 4.11)
10 mM Bi(III) + 500 mM Pb(II)	5 mA cm^{-2} 300 s 298 K	as in figure 4.4	0.19	+1.66 (as in figure 4.6A)
10 mM Bi(III) + 500 mM Pb(II)	5 mA cm^{-2} 300 s 333 K	as in figure 4.5	0.10	+1.62 (as in figure 4.6B)

Table 4.4: Results of catalytic performance and Bi:Pb ratio in average of Bi-doped PbO_2 electrodes prepared from 1 M HNO_3 under different conditions. (Bi:Pb ratio determined by EDAX)

The higher catalytic activity is also associated with the morphology of the Bi-doped PbO_2 deposits. The electrodeposition of Bi-doped PbO_2 from a low concentration of Pb(II) has produced more loose structure of hemispherical crystals with significant voids as shown in figure 4.10b than Bi-doped PbO_2 deposits prepared from high concentration of Pb(II) which more dense and closely packed as shown in figure 4.4 (deposited at 298 K) and in figure 4.5 (deposited at 333 K). The loose structure of the deposits has offered more adsorption sites for the adsorption of the reactant (ie: DMSO) than the dense deposits.

Even though the Bi-doped PbO_2 electrodes prepared from 30 mM Pb(II) has greater catalytic activity, the adhesion of the Bi-doped PbO_2 deposits on gold substrates is not as good as compared to the deposits prepared from high concentration of Pb(II) containing the same amount of Bi(III) (ie: 10 mM) either at 298 K or at 333 K.

4.2.5 Stability of Bi-doped PbO_2 Electrodes

An investigation into the stability of Bi-doped PbO_2 on open circuit in sulphuric acid was carried out. In this study deposits prepared from low concentration of Pb(II) (ie: 30 mM) in 1 M HNO_3 with the presence of 10 mM Bi(III) were used as the electrodes.

Figure 4.13 shows SEM images of Bi-doped PbO_2 deposits before and after immersion in sulphuric acid containing DMSO on open circuit. The morphology of a freshly prepared Bi-doped PbO_2; deposited from low concentration of Pb(II) in 1 M HNO_3 containing 10 mM Bi(III) using a current density of 5 mA cm^{-2} at 298 K, is very dense with hemispherical crystals as shown in figure 4.13a. But, after immersion for 30 min in 50 mM DMSO + 1 M H_2SO_4 for 30 min on open circuit, the morphology has changed to less dense hemispherical crystals with the presence of a few cubic crystals believed to be lead sulphate as seen in figure 4.13b. The change of morphology is due to the dissolution process of the deposit when immersed in the acidic solution on open circuit and also the reduction of PbO_2 to $PbSO_4$ as shown in scheme 1. On the other hand, the rate of reduction is substantially slower than with the undoped PbO_2.

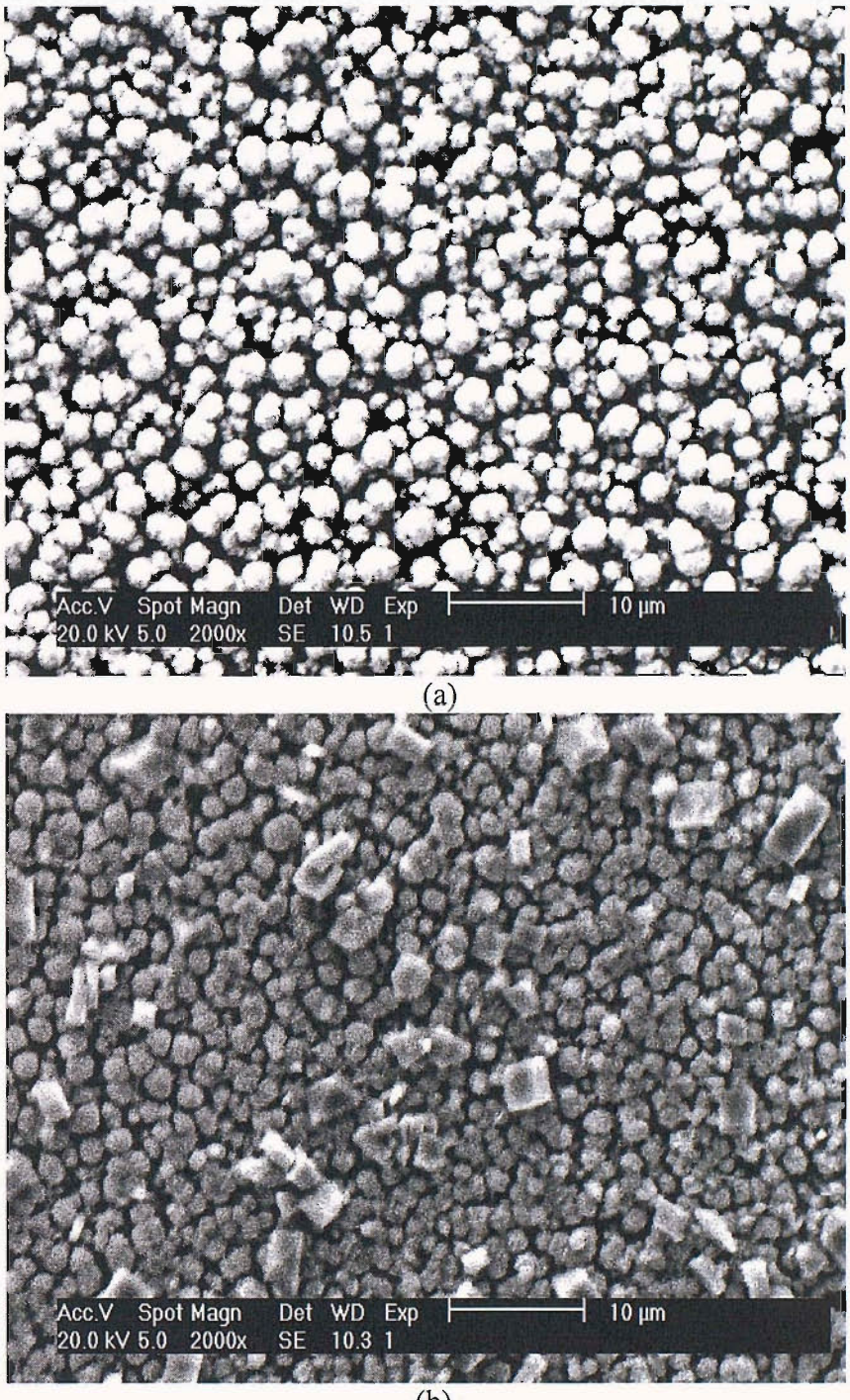

Figure 4.13: SEM images of Bi-doped PbO_2 deposits prepared from 10 mM Bi(III) + 30 mM Pb(II) in 1 M HNO_3 (a) before and (b) after immersion in 50 mM DMSO + 1 M H_2SO_4 for 30 min. Preparation conditions: 5 mA cm^{-2}, 300 s, 298 K

Meanwhile, as reported earlier for the undoped, the catalytic activity of the Bi-doped PbO_2 for the oxidation of DMSO also changes with time after immersion in the sulphuric acid on open circuit. The development of oxidation waves before and after immersion on open circuit is shown in figure 4.14. $E_{1/2}$ value for the oxidation of DMSO is shifted from +1.57 V (before immersion) to +1.54 V (after immersion). The

increase in activity appeared to be associated with an increase in the surface area of the Bi-doped PbO_2 as the layer corrodes. But the limiting current is unchanged as expected for a mass transfer controlled reaction.

However, the Bi-doped PbO_2 electrodes are again much more stable in the sulphuric acid solution containing DMSO if the voltammetric experiments or electrolyses are carried out at potentials positive to the formal potential of the PbO_2/Pb^{2+} couple (ie: E ~ +1.40 V) and the electrodes must not be left in the solution at any time on open circuit.

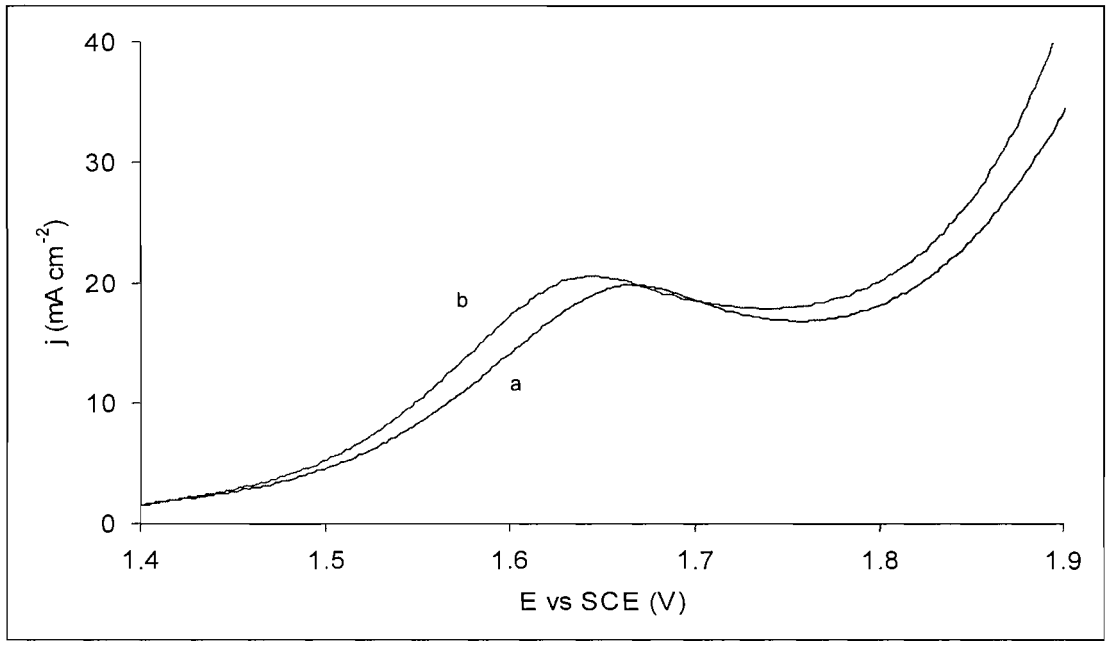

Figure 4.14: Voltammetric responses for 50 mM DMSO + 1 M H_2SO_4 at Bi-doped PbO_2 electrodes after immersion in 50 mM DMSO + 1 M H_2SO_4 for (a) 0 min (b) 30 min. Scan rate: 50 mV s^{-1}

Figure 4.15 shows the reproducibility of the oxidation waves of DMSO for 1st and 10th scans at Bi-doped PbO_2 electrodes which recorded from +1.40 to +1.90 V without any period on open circuit but with a wash between scans. Reproducible results can be easily obtained if the electrodes were immediately washed with deionised water after each scan and there is no period on open circuit.

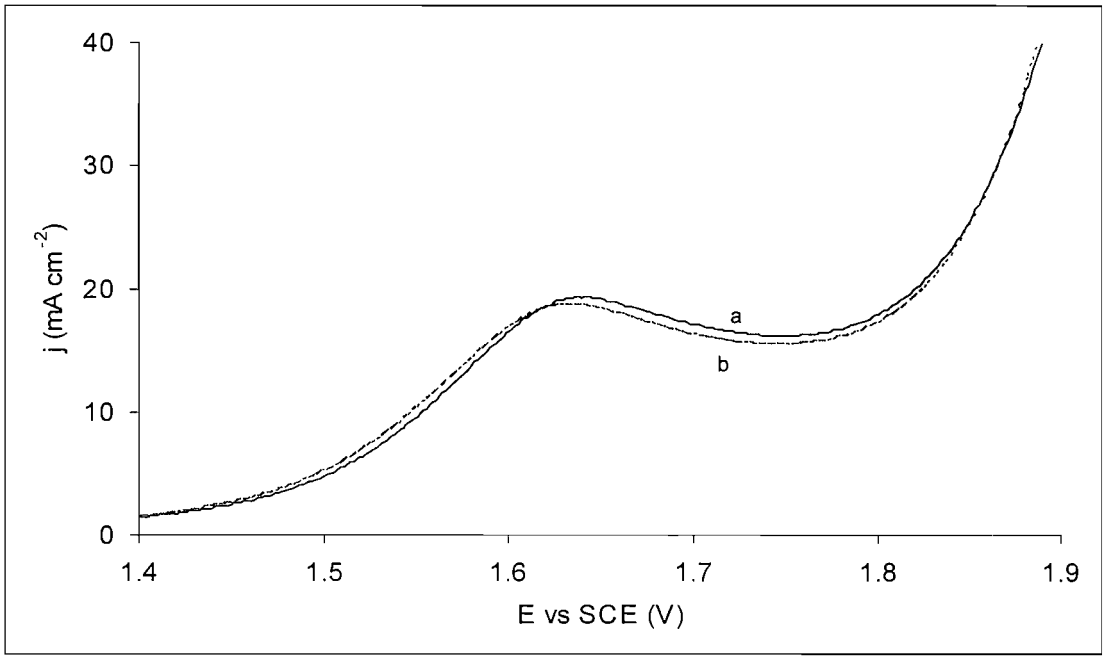

Figure 4.15: Current-potential curves of (a) 1st scan and (b) 10th scan for 50 mM DMSO + 1 M H_2SO_4 at Bi-doped PbO_2 electrodes. Scan rate: 50 mV s^{-1}

Nonetheless, if the scanning is continuously done from +1.40 to +1.90 V and back to +1.40 V and scan again for a few times without taking the electrodes off the solution, limiting currents for the second and consecutive oxidation waves are reduced below the value of the first scan but $E_{1/2}$ values for the oxidation do not change. These observations are shown in figure 4.16. The reduction of the limiting current is believed to be attributed to the present of O_2 bubbles on the electrode surface. The existing of the bubbles has reduced the surface sites for the adsorption of reactant (ie: DMSO) and at the same time for the oxidation of the reactant to take place. Prior to each experiment, the electrodes must be shaken or rotated to remove the bubbles from the electrode surface in order to produce the same limiting current as the first wave. The morphology remained the same as before scanning (as shown in figure 4.13a), as the presence of the bubbles did not affect the structure of the electrodes.

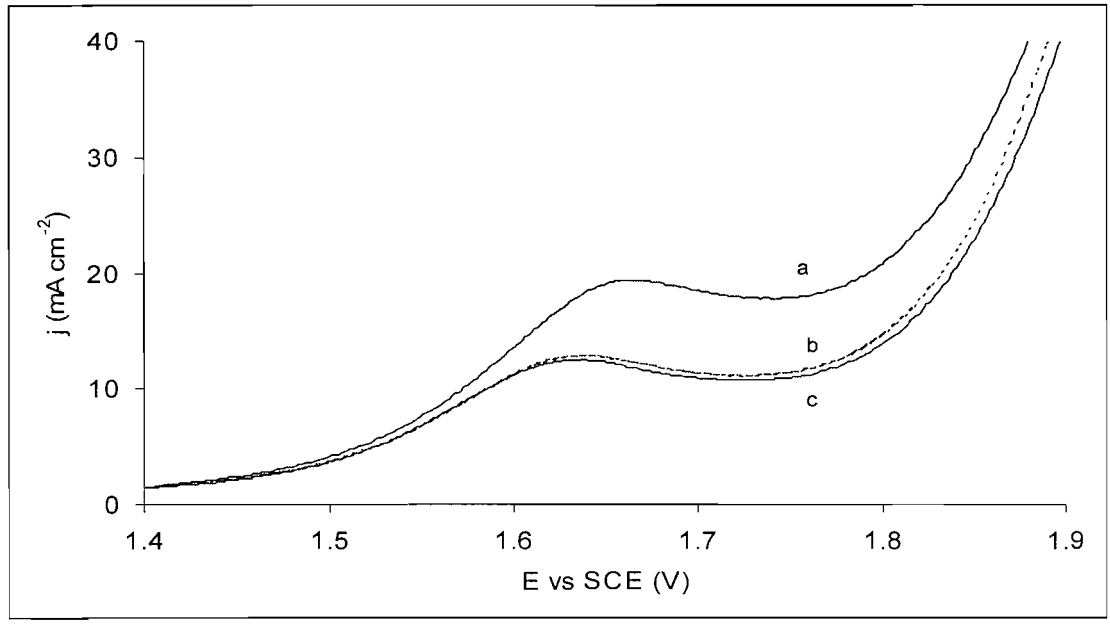

Figure 4.16: Current-potential curves of continuous scanning for 50 mM DMSO + 1 M H_2SO_4 at Bi-doped PbO_2 electrodes. (a) 1st scan (b) 2nd scan and (c) 3rd scan .Scan rate: 50 mV s^{-1}

Further investigation on the stability of the Bi-doped PbO_2 electrodes used electrodes that appeared more stable. These were prepared from high concentration of Pb(II) (ie: 500 mM) in 1 M HNO_3 containing 10 mM Bi(III) using a current density of 5 mA cm^{-2} at 333 K. Sulfuric acid and sodium sulphate were employed as the electrolytes.

Table 4.5 compares half wave potentials ($E_{1/2}$) for the oxidation of DMSO in 1 M H_2SO_4 of the electrodes after immersion for a period of times in 50 mM DMSO + 1 M H_2SO_4 solution and in 50 mM DMSO + 1 M Na_2SO_4 solution on open circuit.

Soaking solution	**Duration**	**$E_{1/2}$ (V) for DMSO → $DMSO_2$**
50 mM DMSO + 1 M Na_2SO_4	0 min	+ 1.62
50 mM DMSO + 1 M Na_2SO_4	15 min	+ 1.62
50 mM DMSO + 1 M Na_2SO_4	60 min	+ 1.62
50 mM DMSO + 1 M Na_2SO_4	24 hours	+ 1.54
50 mM DMSO + 1 M H_2SO_4	0 min	+ 1.62
50 mM DMSO + 1 M H_2SO_4	60 min	+ 1.58
50 mM DMSO + 1 M H_2SO_4	24 hours	NR

Table 4.5: Half wave potentials for 50 mM DMSO in 1 M H_2SO_4 at Bi-doped electrodes before and after immersion in different electrolytes containing 50 mM DMSO. Bi-doped PbO_2 electrodes prepared from 10 mM Bi(III) + 500 mM Pb(II) in 1 M HNO_3 using a current density of 5 mA cm^{-2} for 300s at 333 K. (NR: Not Recorded).

After immersion for 1 hour on open circuit in 1 M Na_2SO_4 containing 50 mM DMSO, the $E_{1/2}$ values recorded were reproducible and still the same (ie: + 1.62 V) as before immersion. However, after immersion for 1 day in the same solution on open circuit, the $E_{1/2}$ for the oxidation of DMSO is shifted to more negative value (ie: + 1.54 V). It is believed that the Bi-doped PbO_2 deposits dissolved slowly in the solution; this process led to the increase of the surface area of the electrodes. The catalytic activity is believed to be increased with increasing surface area which more sites available for oxidation reactions to take place.

But, the Bi-doped PbO_2 electrodes were more vulnerable after standing in 50 mM DMSO + 1 M H_2SO_4 on open circuit. As can be seen in the table, the $E_{1/2}$ value for the oxidation of DMSO is shifted to less positive potential after the electrodes were left in the solution for 1 hour. After immersion for 1 day, no oxidation wave was recorded as all the Bi-doped PbO_2 deposits dissolved completely as observed by the naked eye. These changes were considered to result from corrosion of the Bi-doped PbO_2 deposits. It is shown that the corrosion of the electrodes is faster in sulphuric acid than in sodium sulphate solutions. The same phenomena also occurred on undoped PbO_2 as discussed earlier in chapter 3.

In view of these observations, the Bi-doped deposits are much more stable on open circuit in sodium sulphate than in sulphuric acid solutions. The deposits easily corrode when left in the sulphuric acid solution containing DMSO on open circuit. However, the Bi-doped PbO_2 electrodes are more stable when on load or operating at $E > +1.40$ V vs SCE in the sulphuric acid solution. The electrochemical properties of the Bi-doped PbO_2 deposits on gold are expected to be unchanged as a consequence of lengthy applications to anodic electrolysis of DMSO solutions when operating at constant potential which above the potential of the reduction of PbO_2 (eg: +1.70 V) and without being left on open circuit in acidic solutions. It should be noted that the voltammograms for DMSO oxidation at all undoped and doped PbO_2 deposits in this study were reproducible.

Conclusions

Bi-PbO_2 deposits prepared from solution containing Bi(III) in nitric acid solution leads to substantial doping of the deposits by bismuth (believed to be Bi(V))

with consequent changes to the structure and an increase in the usefulness of the electrodes as anodes for the oxidation of organic compounds especially sulphur-containing compounds (ie: DMSO, 3-TCA). The best compromise between stability and catalytic activity for the anodic oxidation of DMSO was found for Bi-doped PbO_2 electrodes prepared form 10 mM Bi(III) + 500 mM Pb(II) in 1 M HNO_3 using a current density of 5 mA cm^{-2} at a temperature of 333 K. Other dopants tested (ie: Ag^{+}, Fe^{3+} and Ni^{2+}) had insignificant effect on the structure or catalytic performance of the PbO_2 electrodes.

The conclusion of the catalytic activity of bismuth incorporated into PbO_2 by previous workers, especially Johnson et al [17,76,81,83,121,137,155,156,160,167], was confirmed. But they appear to overestimate the stability of their pure and doped PbO_2 deposits and do not recognize the spontaneous chemistry between reactant/electrolyte and electrodes that can occur at open circuit. Their researches, however, were largely related to the application of the PbO_2 deposits in analytical chemistry. Generally, they always prepare very thin PbO_2 deposits from dilute solutions of Pb(II) for their analytical studies using conditions far from those recommended for the fabrication of stable PbO_2 anodes and used for shorter periods of time. They are also concerned with the voltammetry of much more dilute solutions of the organic compounds, typically < 10 mM; the same changes to the PbO_2 deposits could occur but the reduction reactions of the deposits are occurring more slowly than in solutions containing higher concentration of organic compounds (in this case 50 mM DMSO). In addition, it may be that they prepare a fresh deposit for every experiment.

It was also found that the Bi-doped PbO_2 electrodes were more stable on open circuit in sulphuric acid solution containing DMSO than the pure PbO_2 electrodes. The Bi-doped PbO_2 electrodes also are much more stable when standing in sodium sulphate solution than in sulphuric acid solution.

Chapter 5: Electrodeposition of PbO_2 on Titanium

5.0 Introduction

In Chapter 3 and 4, all the data were for the electrodeposition of pure and doped PbO_2 on gold substrates. It was demonstrated that the PbO_2 electrodes can be easily deposited anodically on the gold substrates but the structure of the deposit depended strongly on the deposition conditions. Gold is clearly not a practical and an economical substrate for industrial applications although it may be used as an undercoat on cheaper materials. Titanium (Ti) is the preferred material for industrial electrodes since it is more economical and more complex cell can be easily designed for the industrial applications.

The disadvantage of Ti is the presence of a passive oxide layer (ie: TiO_2) on the Ti surface which makes the deposition of PbO_2 more difficult to achieve. A Ti disk is naturally covered with the TiO_2 layer which forms spontaneously in air on bare Ti. TiO_2 has a high electrical resistivity and therefore creates a high potential barrier to electron transfer. Therefore, the voltage loss within the electrode is high and its practical application is not good. Hence, some pre-treatments on the Ti surface must be done prior to PbO_2 deposition to control the TiO_2 in order to make the Ti conducting and useful as the substrate.

Preliminary experiments were carried out using Ti disc substrates (area: 0.20 cm^2) as shown in figure 2.7b. All experiments were carried out with two samples simultaneously, so that the reproducibility within one batch could be verified.

5.1 Pre-treatments of Ti Surface

Pre-treatment of the Ti surface is the critical step prior to PbO_2 deposition because it is essential to remove the insulating layer (ie: TiO_2) as mentioned above and also to produce a uniform rough surface. The latter is important for the production of an adherent and a stable deposit.

Figure 5.1 shows a SEM image of Ti disc substrate before undergoing any pre-treatments. The surface is clearly smooth although with a few imperfections. The Ti disc was first roughly abraded using silicon carbide paper P1200 and followed by

polishing the disc by alumina slurries and then rinsing with deionised water as described in Chapter 2. This removes some of the imperfections, see figure 5.2.

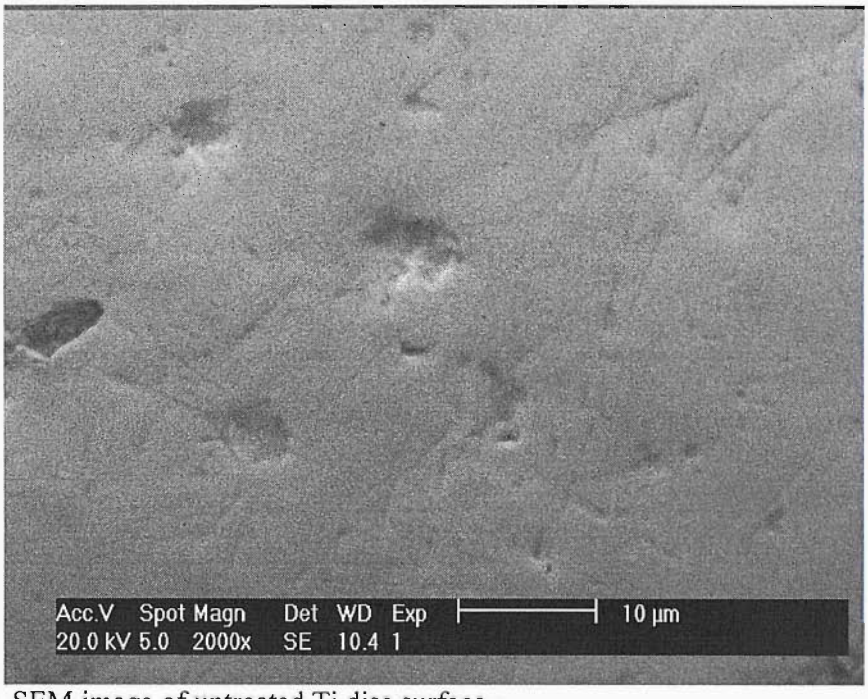

Figure 5.1: SEM image of untreated Ti disc surface.

Although, the surface seemed to be flat with a mirror finish after polished as observed by the naked eye, several stripes and scratches were still present as shown by SEM image in figure 5.2.

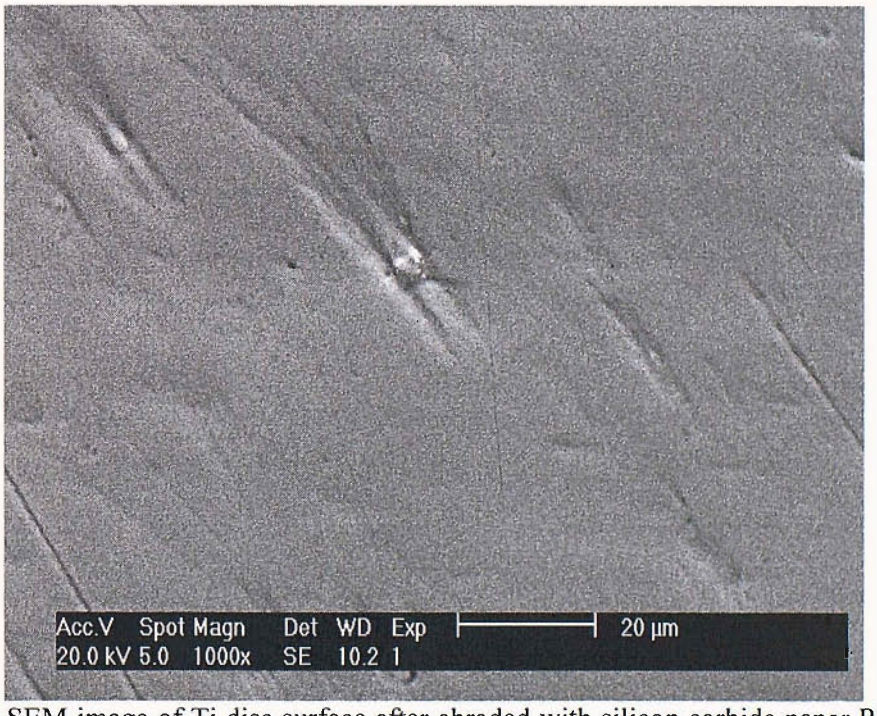

Figure 5.2: SEM image of Ti disc surface after abraded with silicon carbide paper P1200 and polished by alumina slurries.

In general, the Ti discs were chemically etched to make them rougher and more conductive. There are two types of etching solutions used in this study (ie: oxalic acid and hydrochloric acid) which they were mostly used by earlier workers for the treatment of Ti surface. Table 5.1 shows a number of titanium pre-treatments used by the earlier workers prior to oxide coating (usually precious metal eg: DSA). Most authors first treated their Ti substrates by sandblasting. With sandblasting, the etching process could be done in a shorter time.

Sandblasting	**Etching Solution**	**Etching Temperature (K)**	**Etching Time (min)**	**Ref.**
Yes	0.8 M oxalic acid	373	10	168
Yes	1.1 M oxalic acid	373	5	169
Yes	0.8 M oxalic acid	358	15 - 60	110
Yes	11.5 M HCl	> 367	5	170
Yes	10 M HCl	333 - 373	15 - 90	110
Yes	11.5 M HCl	373	0.5 - 3	171
No	**1.6 M oxalic acid**	**373**	**120**	**171**
No	**8 M HCl**	**333**	**120 - 240**	**171**
No	11.5 M HCl	363	60	111

Table 5.1: Various pre-treatments of titanium substrates prior to deposition found in the literature.

In this study the pre-treatments of the Ti disc were carried out without sandblasting and using etching baths recommended by Lipp [171]. Both etching solutions (ie: oxalic acid and HCl) were used and tested for the treatment of the Ti disc surface.

It was found that the etching process of the Ti disc substrate using 1.6 M oxalic acid at boiling point for 2 hours has significantly produced a very rough surface or so called 'stormy-sea' surface with many small craters as seen in figure 5.3. The resulting Ti surface was very similar to the treated Ti wire produced by Lipp using the same technique. The colourless etching solution turned to brown solution indicating the formation of titanium (IV) oxalate.

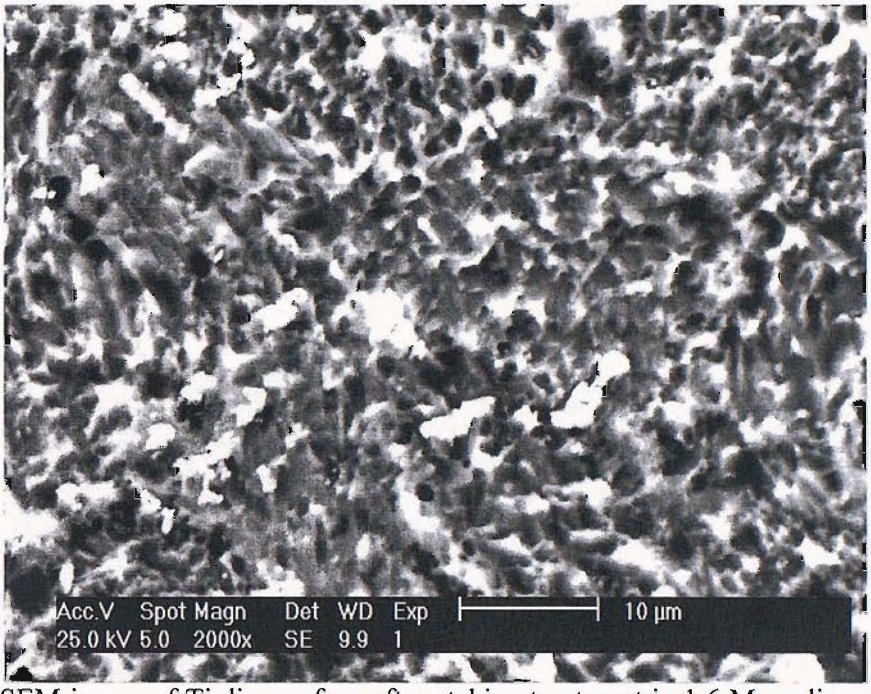

Figure 5.3: SEM image of Ti disc surface after etching treatment in 1.6 M oxalic acid at 373 K for 2 hours.

The same surface was also analysed by EDAX. The only peaks appeared are those for Ti as seen in figure 5.4, indicating that the only metal present on the surface is titanium. The absence of oxygen cannot be confirmed since the sensitivity of the EDAX to oxygen is very low.

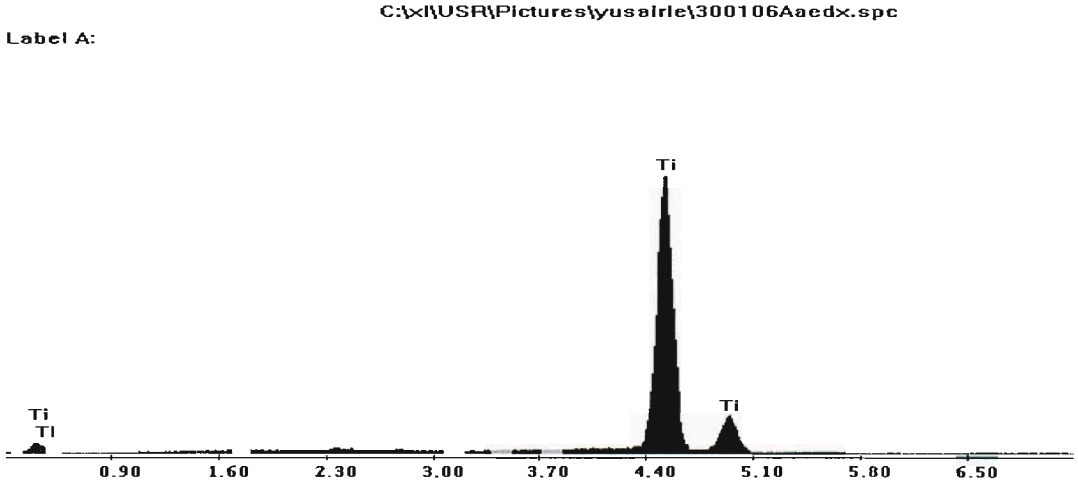

Figure 5.4: Spectrum of the treated Ti disc surface corresponding to SEM image of figure 5.3 as determined by EDAX.

It was also found that the etching rate of the Ti surface in 1.6 M oxalic acid is strongly dependent on the etching temperature and etching time. The resulting Ti surface was found to be smoother when treated in the same etching solution and for the same etching time but at lower etching temperature (ie: 353 K) as shown in figure 5.5. A less rough Ti surface would also be produced when etching time is shortened to less than 30 minutes if etched in the same solution (ie: 1.6 M oxalic acid) at 373 K.

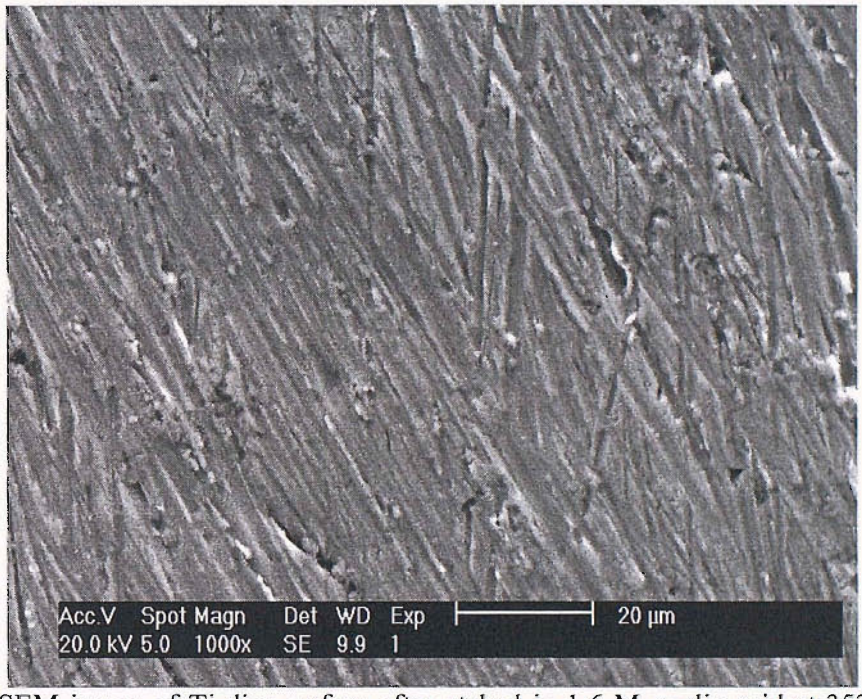

Figure 5.5: SEM image of Ti disc surface after etched in 1.6 M oxalic acid at 353 K for 2 hours.

The use of hydrochloric acid as the etching agent for the treatment as recommended by Lipp, however, did not produce 'stormy-sea' surface. The treatment with 8 M HCl for 3 hours at 333 K produced a less smooth surface with 'scratch-like' features as shown in figure 5.6. This result is not in a good agreement with Lipp. Even though the etching temperature was increased to 373 K, a quite similar surface structure has been produced for the treatment with 8 M HCl for 30 min. These observations show that 8 M HCl is not strong enough to etch the Ti surface at 333 K and if higher temperature was used with 8 M HCl, the etching time must be prolonged in order to produce high surface roughness. The colourless HCl solution has changed to yellowish solution during the etching process indicating the formation of $TiCl_4$.

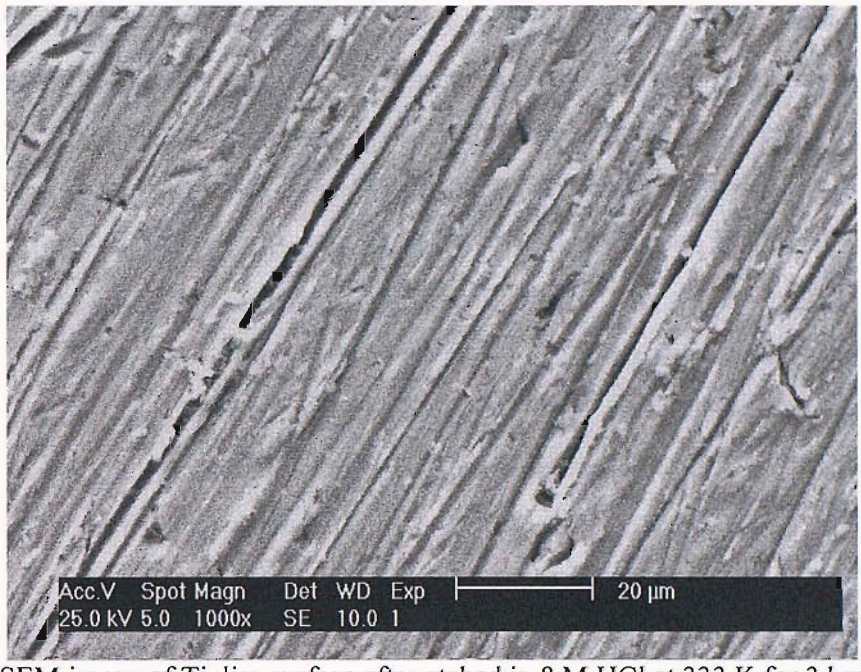

Figure 5.6: SEM image of Ti disc surface after etched in 8 M HCl at 333 K for 3 hours.

As a result of these experiments, oxalic acid was chosen as the preferred etching agent for this study. Even though, in practice the oxalic acid is not as easy as HCl to be handled since it does precipitate when cool or at low temperature, but it has produced a good and uniform rough surface of Ti substrate for the deposition of PbO_2 deposits when used at 373 K for 1 – 2 hours.

5.2 Deposition of β-PbO_2 on Ti

As discussed in Chapter 3, high concentration of Pb(II) (ie: 500 mM) in 1 M HNO_3 was a more favourable condition for the deposition of PbO_2 onto gold substrate than low concentration of Pb(II) (ie: 30 mM or 100 mM). A fast deposition and > 90% of current efficiency were demonstrated with the use of 500 mM Pb(II) for the deposition of PbO_2 on gold. Therefore, the same concentration of Pb(II) was used in the preparation of PbO_2 on Ti substrates (designated as PbO_2/Ti)

5.2.1 Deposition from 1 M HNO_3

Prior to deposition, a cyclic voltammetry experiment was carried out in order to investigate the behaviour of Ti substrate in 1 M nitric acid solution containing 500 mM Pb(II). The cyclic voltammetry experiment was done on clean and rough Ti surfaces as shown in figure 5.3.

Figure 5.7 shows a cyclic voltammogram for lead dioxide deposition/dissolution from solution containing 500 mM Pb(II) + 1 M HNO_3 onto the Ti substrates. On the positive going scan, an increase in current is observed immediately after E > 0.0 V; this is attributed to the formation of oxide layer of Ti (ie: TiO_2). The TiO_2 is constantly formed on the Ti surface up to ca E = +2.0 V (as seen in the figure). The fast increase in current after E = +2.0 V is due to the deposition of PbO_2; and the deposition is observed until ca +1.60 V on the negative going scan. This indicates that the PbO_2 is deposited onto a layer of TiO_2 and the kinetics of nucleation and deposition are slower on Ti dioxide than Au.

Meanwhile, the dissolution of PbO_2 back to Pb(II) is seen slowly occurring at ca +1.00 V on the reverse scan; and the reduction peak appears at ca +0.30 V. Again PbO_2 dissolution is inhibited by the TiO_2 underlayer. These observations are in good agreement with earlier works in the literature [87] for the deposition of PbO_2 on Ti surface but using 1 M $HClO_4$ instead of 1 M HNO_3. The charge balance calculated from the figure for the deposition and reduction of PbO_2 in 1 M HNO_3 is < 70 %. A probable explanation for this is the incomplete conversion of PbO_2 to Pb(II) during the timescale of the voltammetric experiment.

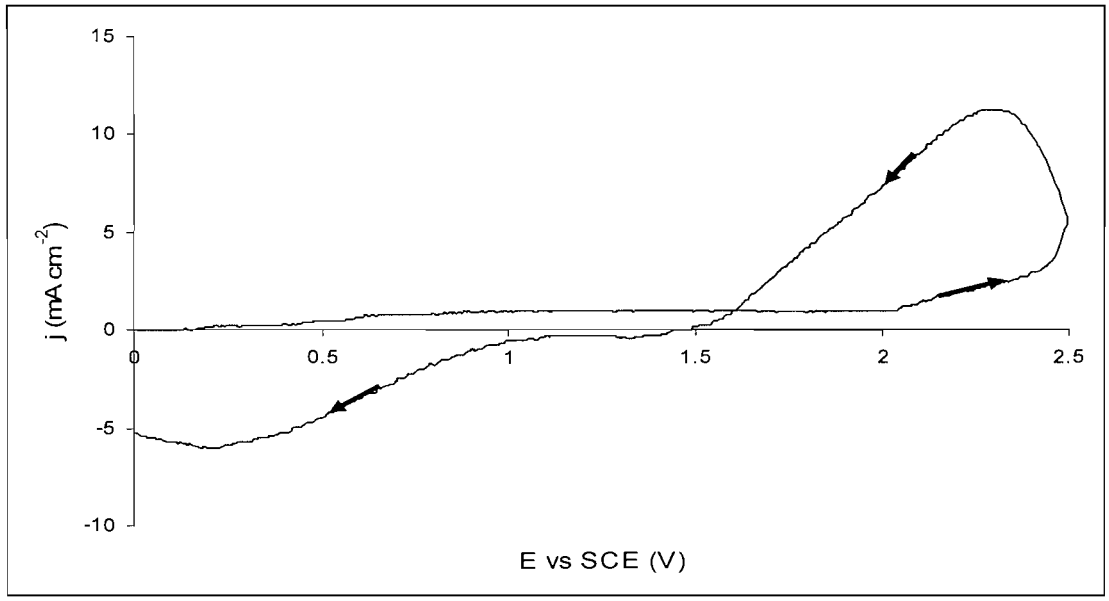

Figure 5.7: Cyclic voltammogram at a Ti surface during a cyclic potential scan in 500 mM Pb(II) + 1 M HNO_3. Scan rate: 50 mV s^{-1}

A different cyclic voltammogram was recorded for the deposition and dissolution of PbO_2 on/from on gold substrate using the same deposition solutions as shown earlier in Chapter 3 (see figure 3.3b). With gold electrodes, the deposition occurred at less positive potential (ie: E ~ +1.70 V) while the reduction peak of PbO_2

was sharp and well defined appearing at ca +1.11 V. However, with Ti electrodes the separation of deposition and dissolution peaks is much higher. It also observed from the cyclic voltammetry profiles that the rate of PbO_2 deposition on gold is higher than on Ti substrates. This is due to the formation of the passive oxide layer, TiO_2. The TiO_2 produced on the Ti substrate behaves as a poor conductor and can disturb the electrodeposition of PbO_2 [17,133]. It has been reported [87] that the charge for the TiO_2 formation is greater than the charge for Au oxidation and the charge for the formation of PbO_2 on gold is always higher than on Ti with an equivalent positive limit.

Besides the formation of oxide layers on the substrates, the topography of the substrates is also believed to be significantly contributing to the different behaviour for the deposition and dissolution of PbO_2. The situation when the deposition of PbO_2 taking place on a rough surface (in this case on treated Ti) is very different from the deposition on well defined smooth substrate such as gold.

Several PbO_2 depositions on the Ti substrates were then carried out using 500 mM Pb(II) in 1 M HNO_3 using different deposition conditions. The aim of this study was to investigate the appearance, morphology and adhesion of the produced PbO_2 deposits on Ti substrates.

Deposition Conditions	**Appearance and Comments**
5 mA cm^{-2} , 10 min , 298 K	Not all surface covered, very dark brown
5 mA cm^{-2} , 30 min , 298 K	All surface covered with rice-like crystals, not smooth. Medium adhesion
10 mA cm^{-2} , 10 min , 298 K	All surface covered, smooth, shiny, uniform, dense and compact with small crystallites. Very good adhesion.
10 mA cm^{-2} , 30 min , 298 K	All surface covered, black, uniform across the surface with angular crystals structure. Very good adhesion.
10 mA cm^{-2} , 30 min , 333 K	A few craters on the surface, black, not shiny, not homogeneous. Medium Adhesion.
20 mA cm^{-2} , 5 min , 298 K	All surface covered, very smooth, black, uniform across the surface, shiny, dense and close packed small angular crystals. Very good adhesion.
20 mA cm^{-2} , 5 min , 313 K	A few craters and lumps across the surface, less shiny than at 298 K. Medium adhesion.
20 mA cm^{-2} , 5 min , 333 K	All surface covered, black, not smooth, not shiny, a lot of craters and lumps across the surface. Medium adhesion.

Table 5.2: Characteristics of PbO_2 film deposits on treated Ti substrates prepared using various deposition conditions. Deposition solution: 500 mM Pb(II) + 1 M HNO_3.

Table 5.2 summarizes the characteristics of PbO_2 film deposits prepared from 1 M HNO_3 containing 500 mM Pb(II) using various deposition conditions. From the table, it can be seen that the deposition of PbO_2 on Ti substrates is strongly dependent on the current density and temperature employed.

At low current density (ie: 5 mA cm^{-2}), the deposition occurs at a slow rate partly because of the contribution to the charge passed from the oxidation of the Ti surface. It produces the surface shown in figure 5.8a.

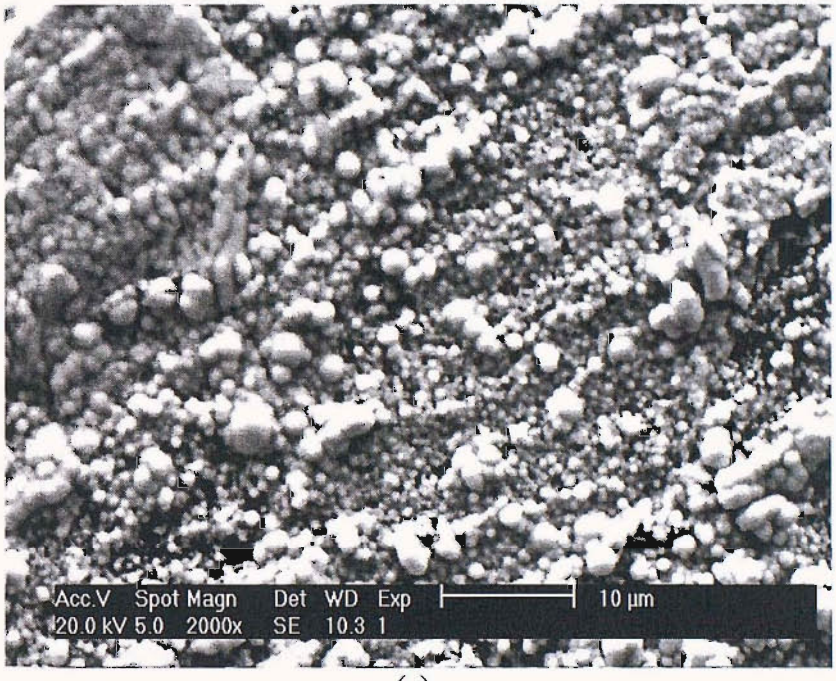

(a)

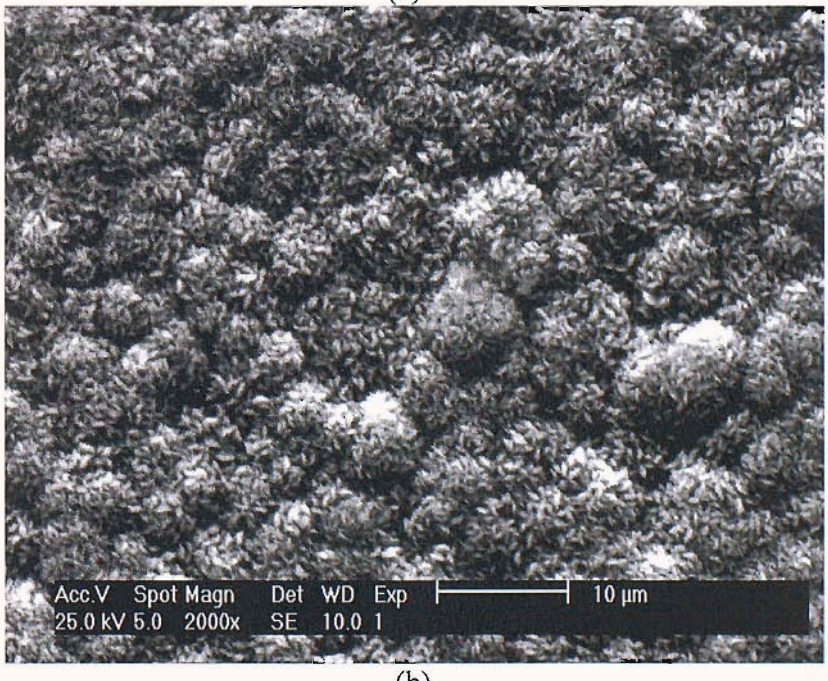

(b)

Figure 5.8: SEM images of PbO_2 deposits prepared using a current density of 5 mA cm^{-2} for (a) 10 min and (b) 30 min at 298 K. Deposition solution: 500 mM Pb(II) + 1 M HNO_3.

Comparing this SEM with figure 5.3 (surface before deposition), it appears that the Ti surface is covered by PbO_2 hemispheres but the size is very non-uniform and EDAX in figure 5.9 clearly shows the presence of Ti suggesting that in some areas the PbO_2 layer is very thin. Non-uniform deposition is occurring. It seems that the deposition of PbO_2 was not uniform throughout the surface since the Ti surface has many imperfections (see figure 5.3). A longer deposition time was required in order to cover all Ti surface as shown in figure 5.8b after deposition process at 5 mA cm^{-2} for 30 minutes. Even though the whole surface was covered by PbO_2, the deposit was not smooth and the adhesion on the substrate was not good.

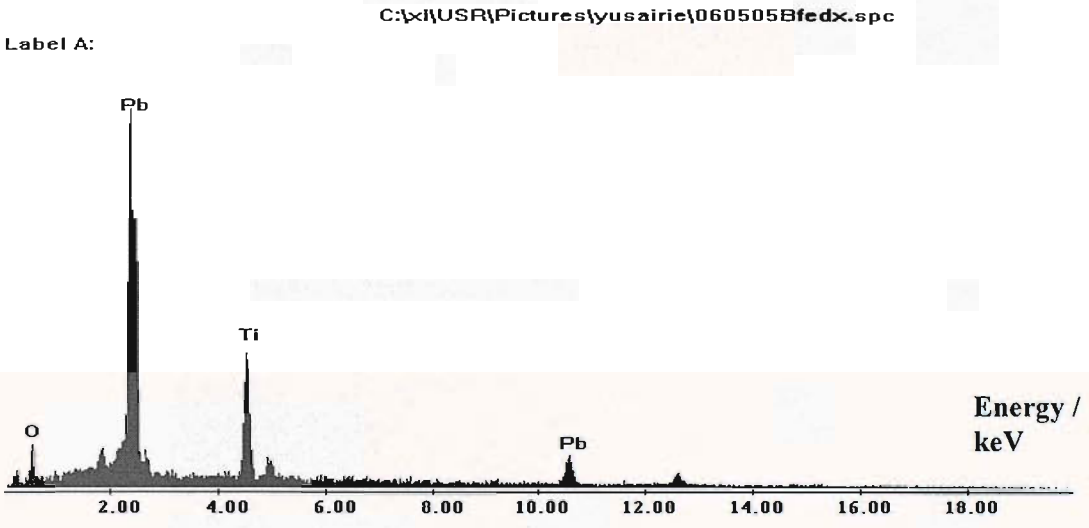

Figure 5.9: EDAX spectrum of PbO_2 deposit prepared using a current density of 5 mA cm^{-2} for 10 min at 298 K on Ti substrate.

However, if the current density is increased to > 10 mA cm^{-2} so that the deposition rate is also increased and the deposits improve in appearance. The deposition at 20 mA cm^{-2} needs less than 5 minutes to cover the whole surface of the Ti. The resulting deposit was shiny, uniform and very smooth with small crystallites as shown in figure 5.10. The adhesion of the deposit on Ti substrate was also very good.

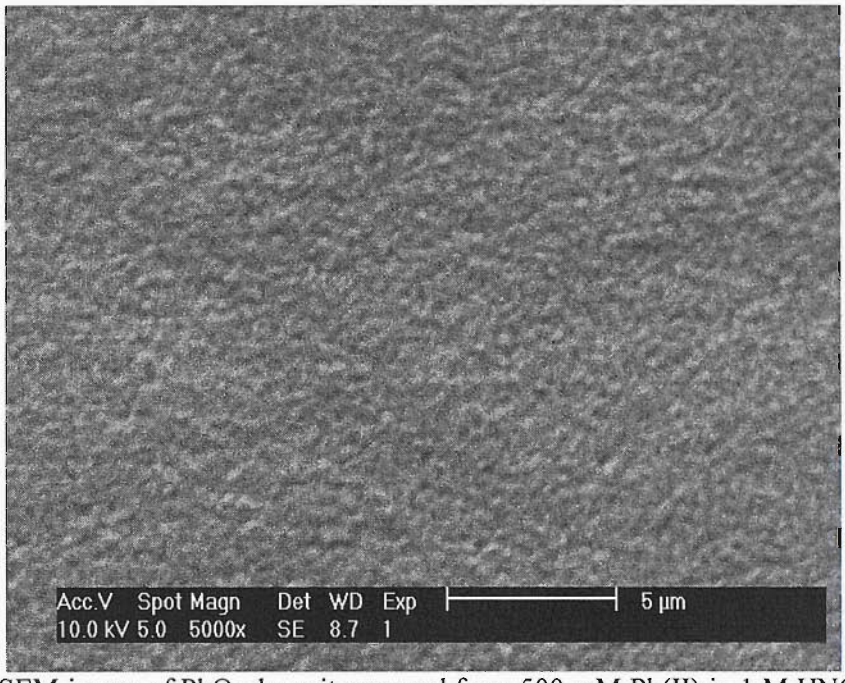

Figure 5.10: SEM image of PbO_2 deposit prepared from 500 mM Pb(II) in 1 M HNO_3 using a current density of 20 mA cm^{-2} for 5 min at 298 K.

The influence of temperature on the deposition of PbO_2 was also investigated. A nice and very smooth appearance of PbO_2 on Ti was observed when the deposition process was carried out at room temperature as shown in figure 5.11a.

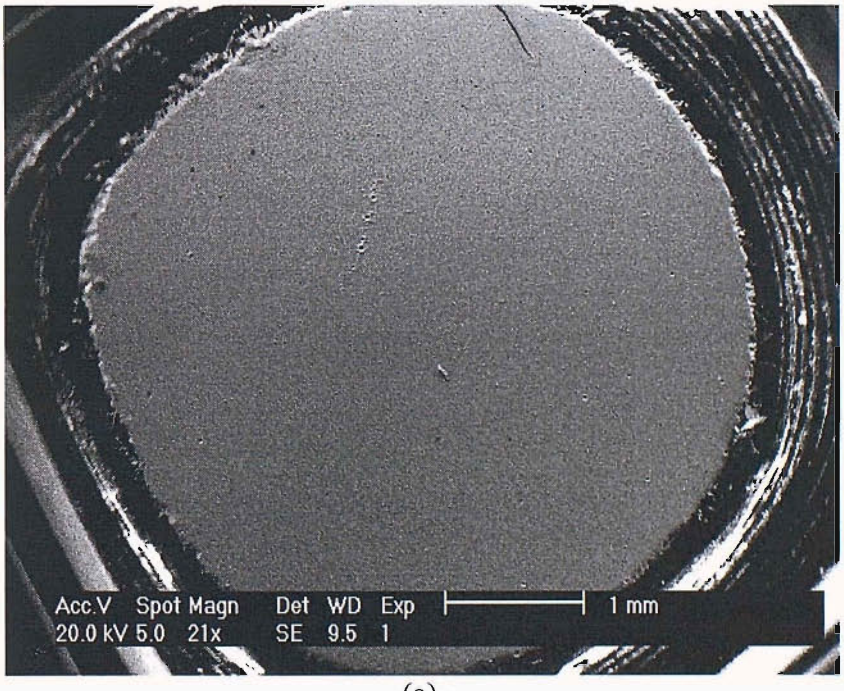

(a)

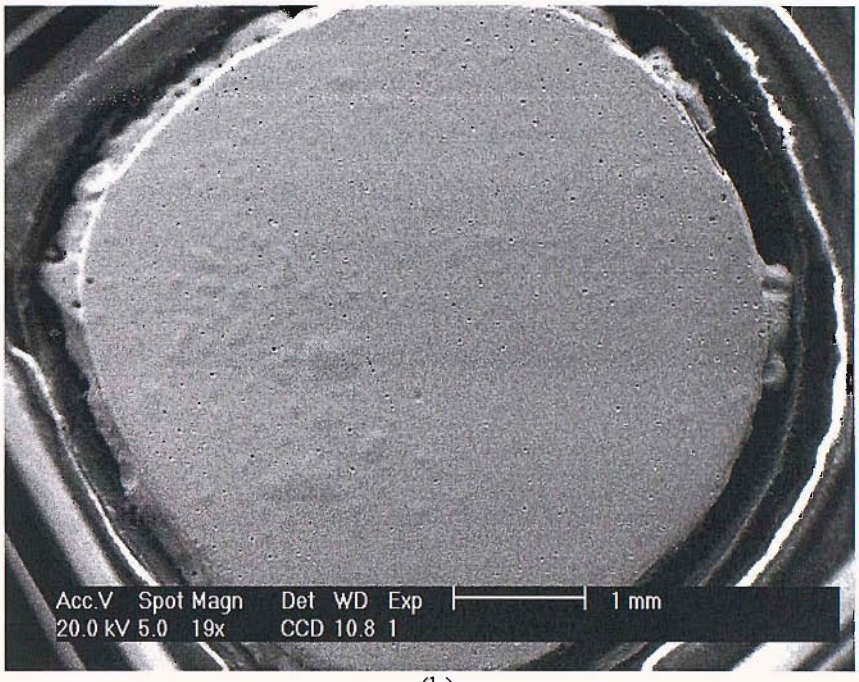

(b)

(c)

Figure 5.11: SEM images of PbO_2 on Ti substrates deposited at (a) 298 K (b) 313 K and (c) 333 K using a current density of 20 mA cm^{-2} for 5 min. Deposition solutions: 500 mM Pb(II) + 1 M HNO_3.

At elevated temperature (either 313 K or 333 K), although all Ti surface was covered by the PbO_2, the deposits had some craters and lumps presence on the surface. These defects are believed to be attributed to the presence of O_2 bubbles during deposition at these elevated temperatures. More craters and lumps present across the surface when deposited at 333 K as shown in figure 5.11c than at 313 K as

in figure 5.11b. This shows that increasing the temperature is not beneficial to the production of a good PbO_2 on Ti.

Unfortunately, even though the PbO_2 deposits prepared from 1 M HNO_3 especially at 298 K were very smooth and very good adhesion on Ti substrate their conductivity was poor. The electrical response during scanning for the oxidation of DMSO at all the produced PbO_2 was low and poor with erratic readings. It is believed that the low response due to the formation of a thick layer of TiO_2 during anodic deposition in 1 M HNO_3.

5.2.2 Deposition from 0.1 M HNO_3

Again, prior to PbO_2 deposition from this low concentration of nitric acid, a cyclic voltammogram scanning from +0.0 to +2.0 V and then back to +0.0 V was recorded to study the behaviour of Ti electrode in 0.1 M HNO_3 containing 500 mM Pb(II). Figure 5.12 shows the cyclic voltammogram of Ti electrode for the deposition and dissolution of PbO_2. It was observed that in 0.1 M HNO_3, the deposition initiated at less positive potential (ie: ca. +1.60 V) and the reduction peak appeared at more positive potential (ie: +0.90 V) than that in 1 M HNO_3. A higher current was also observed for the deposition of PbO_2 as shown in the figure than the deposition charge of PbO_2 in 1 M HNO_3 as shown in figure 5.7.

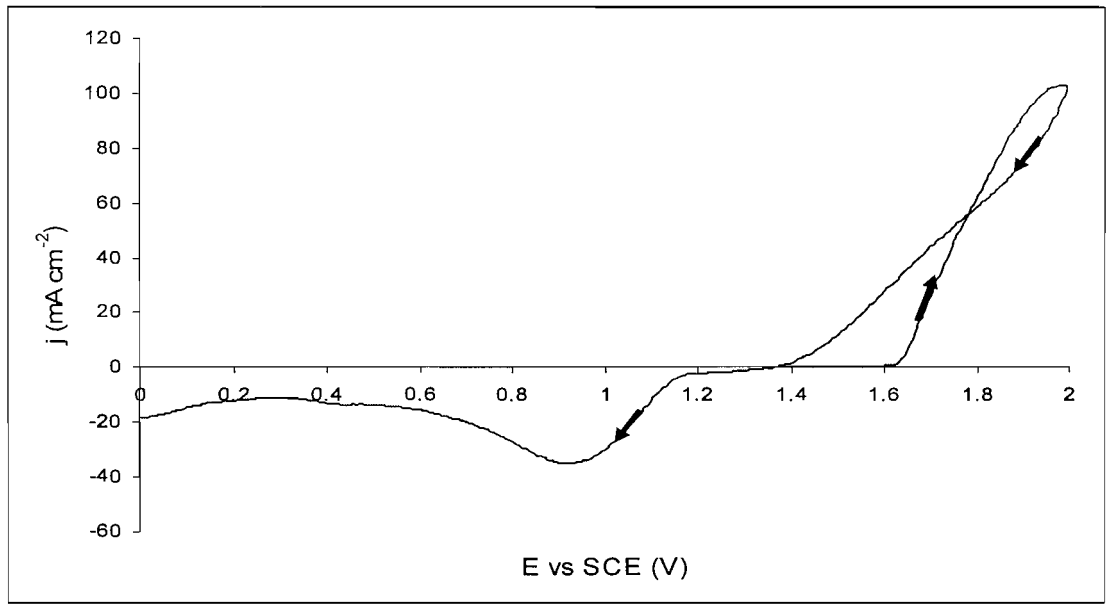

Figure 5.12: Cyclic voltammogram at a Ti surface during a cyclic potential scan in 500 mM Pb(II) + 0.1 M HNO_3. Scan rate: 50 mV s^{-1}

The increase in current is associated with the increasing of the PbO_2 thickness. This shows that more PbO_2 was deposited from 0.1 M HNO_3 solution than 1 M HNO_3. Therefore, 0.1 M HNO_3 is more favourable solution for the deposition of PbO_2 on Ti substrates as indicated by a negative shift in the deposition potential as compared to 1 M HNO_3. Furthermore, high current was recorded for the deposition in 0.1 M HNO_3 and this is evidence for less formation of TiO_2. There are two competing processes occur during anodic scan on Ti surface especially at high potential (ie: E > +1.70 V); the oxidation of Pb(II) to PbO_2 and the formation of TiO_2. The dissolution of the PbO_2 remains slow and the reduction peak is still broad with reduction continuing throughout the sweep. The charge balance is also poor. The voltammograms were very reproducible.

The deposition of PbO_2 from 0.1 M HNO_3 on Ti substrates was carried out using two different current densities (ie: 5 mA cm^{-2} and 20 mA cm^{-2}) at room temperature. It was found that at low current density the deposition process was slow which all Ti surface was covered by PbO_2 in more than 30 minutes. The resulting deposit was inhomogeneous, not shiny and lumpy as shown in figure 5.13. The deposition at 20 mA cm^{-2} has also produced the same morphology but the deposition rate was fast at this current density which all the Ti surface was covered in less than 10 minutes.

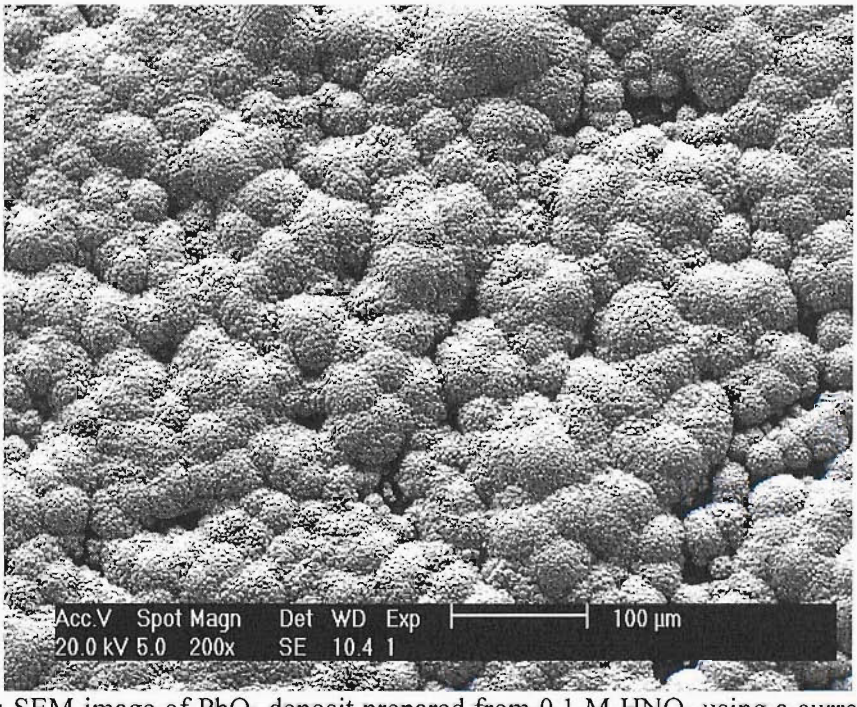

Figure 5.13: SEM image of PbO_2 deposit prepared from 0.1 M HNO_3 using a current density of 5 mA cm^{-2} for 30 min at 298 K.

The PbO_2/Ti electrodes prepared from 0.1 M HNO_3 had an acceptable resistance. But the adhesion of the deposit on the Ti substrate was not good. It has been reported [17] the addition of fluoride ions in the bath solution has improved the adhesion of PbO_2 on Ti. Therefore, in this study, sodium flouride was added in the bath solution containing 500 mM Pb(II) + 0.1 M HNO_3 to investigate the influence of F^- ions. The resulting PbO_2 deposit containing fluoride is designated as F-PbO_2.

Cyclic voltammetry experiment was carried out to study the behaviour of Ti electrode in 500 mM Pb(II) + 0.1 M HNO_3 solution containing 40 mM F^- ions. Figure 5.14 shows a cyclic voltammogram of Ti for the deposition and dissolution of F-doped PbO_2. Comparing this figure with figure 5.12 (without F^- in the bath solution) shows that the presence of F^- ions in the bath solution has shifted the deposition potential to more positive (ie: +1.70 V) while the reduction peak appeared at more negative potential (ie: +0.80 V). Comparison of both figures, the current efficiency is higher for figure 5.14 (for the deposition of PbO_2 with the presence of fluoride ions) than figure 5.12 for PbO_2 without F^- ions. It is believed that less O_2 evolves during the deposition of F-doped PbO_2 than PbO_2. Amadelli and Velichenko [172] observed the decrease of surface oxygen using X-Ray photoelectron spectroscopy (XPS) for the deposition of PbO_2 which the decrease was attributable to the effect of F^-.

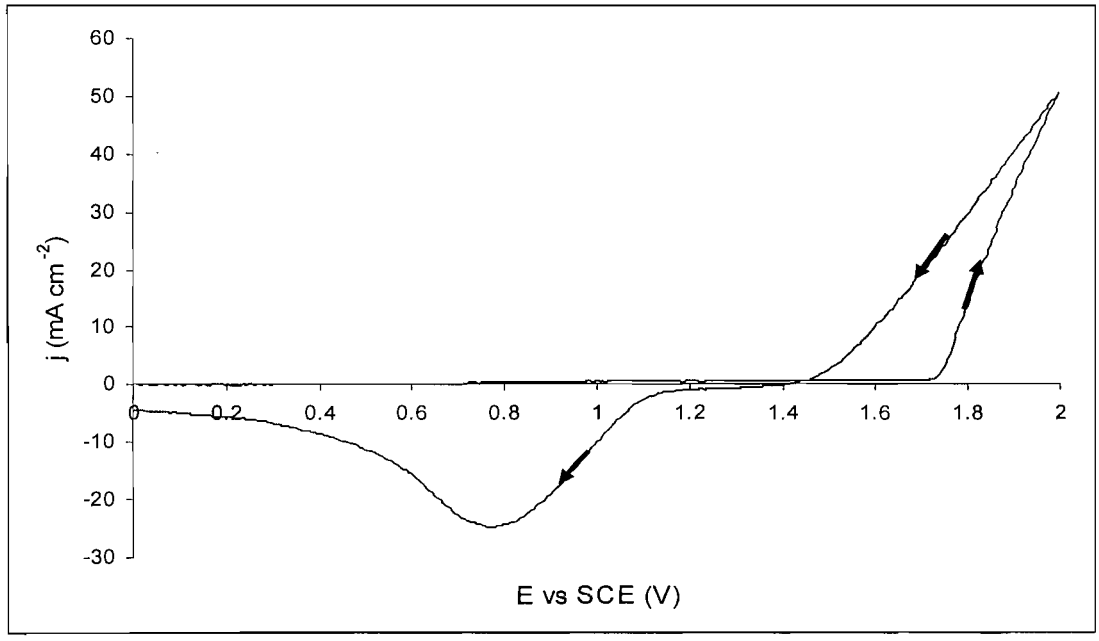

Figure 5.14: Cyclic voltammogram at a Ti surface during a cyclic potential scan in 40 mM NaF + 500 mM Pb(II) + 0.1 M HNO_3. Scan rate: 50 mV s^{-1}

The deposition of PbO_2 with the presence of fluoride in 0.1 M HNO_3 on Ti substrates was carried out using a current density of 5 mA cm^{-2} for 30 min at 298 K. Figure 5.15a shows a SEM image of the F-PbO_2 deposit. The deposit was found to be more uniform and smoother than without F^- as shown earlier in figure 5.13.

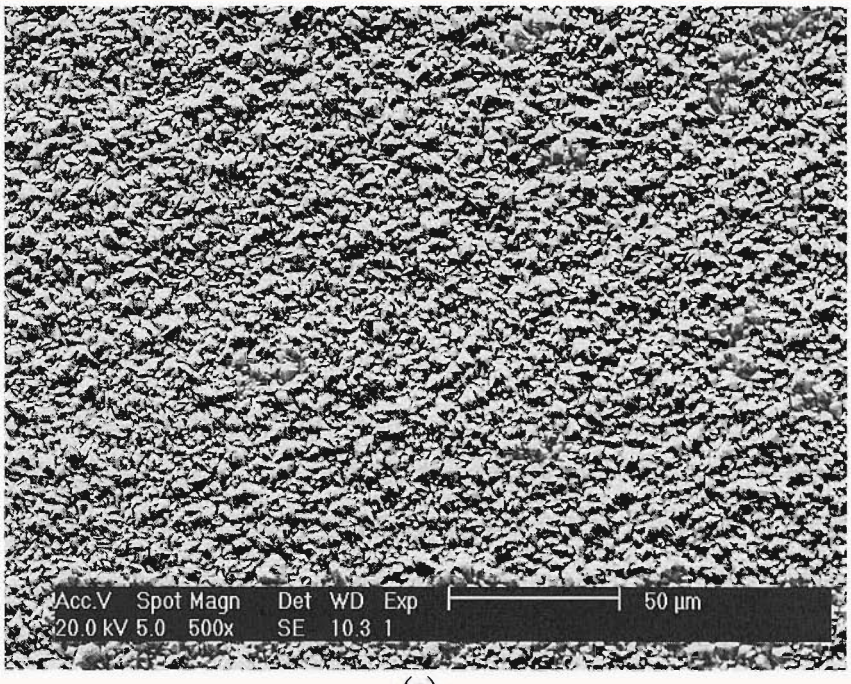

(a)

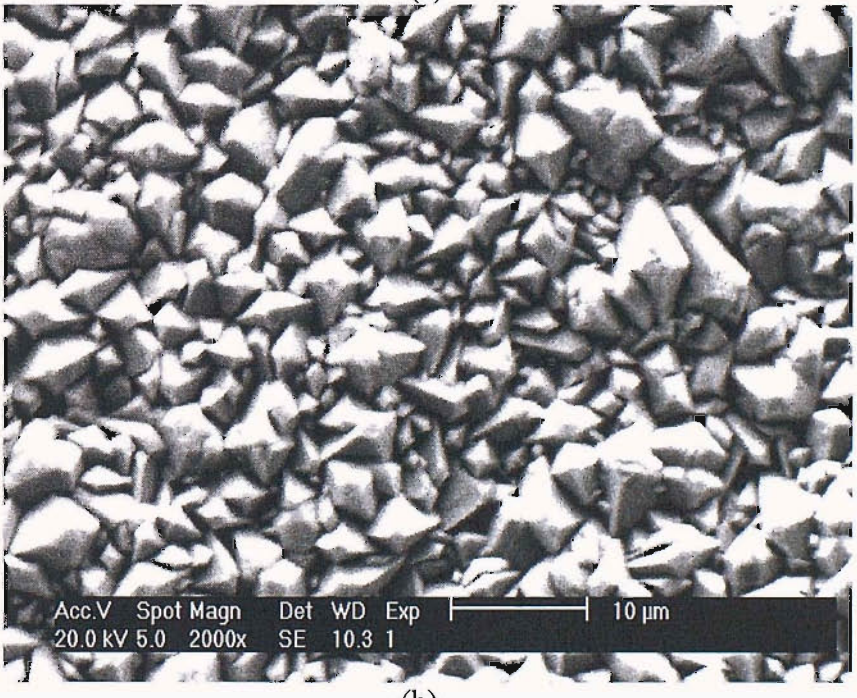

(b)

Figure 5.15: SEM images of F-doped PbO_2 prepared onto Ti substrate by applying constant current density of 5 mA cm^{-2} for 30 min at 298 K.

As can be seen at larger magnitude as the SEM image in figure 5.15b, the deposit consists of dense and close packed angular crystals. Comparison with PbO_2

deposit prepared without F^- under the same conditions as shown in figure 5.13 reveals that the presence of F^- ions in the bath solution has modified and improved the morphology of the PbO_2 deposits. With the addition of F^- in the bath solution, more uniform and homogeneous deposit was produced and this is probably due to less O_2 was formed during deposition as compared to without F^- in the bath solution.

It was found that the produced F-PbO_2 deposit was good in adhesion on Ti and the deposit had high electrical response. Indeed, the F-doped PbO_2 electrode is more active than PbO_2 electrode for the oxidation of DMSO which will be discussed in section 5.4.

5.2.3 Studies of Ti Surface Oxidation.

This study was carried out in order to confirm the difference oxidation process of Ti surface in 1 M HNO_3, in 0.1 M HNO_3 and in 0.1 M HNO_3 with the presence of F^-. Figure 5.16 shows the current – potential responses of Ti surface oxidation process in the three different nitric acid solutions. The readings were taken from figure 5.7 for Ti oxidation in 1 M HNO_3 and figure 5.12 for Ti oxidation in 0.1 M HNO_3 and figure 5.14 for Ti oxidation in 0.1 M HNO_3 solution containing F^- ions, starting from 0.0 V and up to potential prior to PbO_2 deposition occurs (ie: ~ +1.60 V)

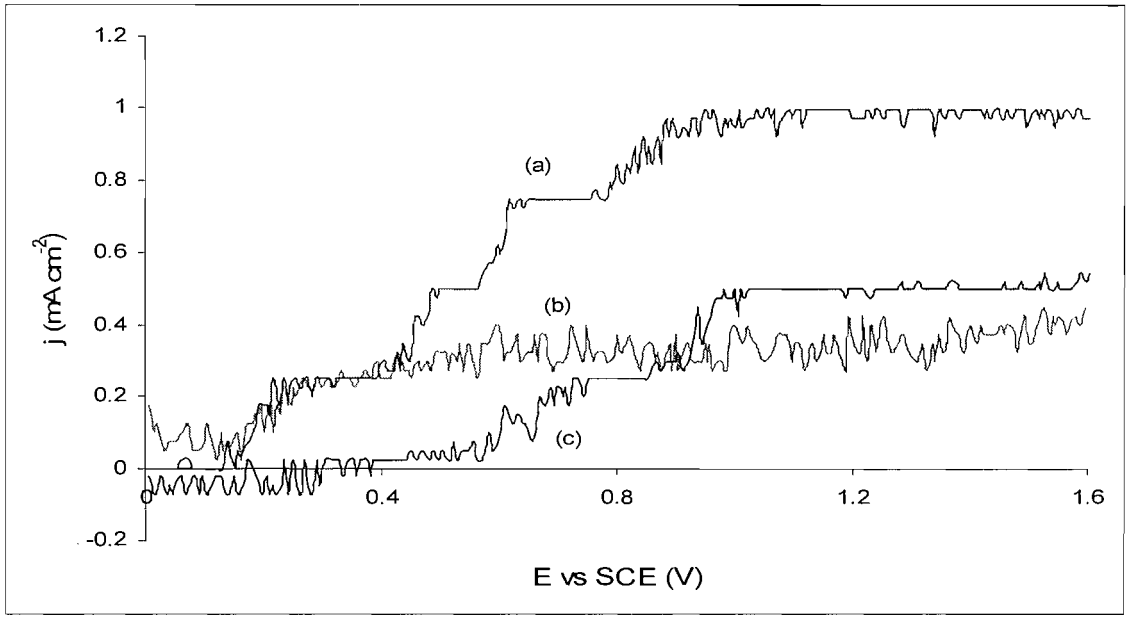

Figure 5.16: Comparison of voltammograms of Ti substrate in different concentration of nitric acid (a) 1 M (b) 0.1 M and (c) 0.1 M + 40 mM F^-. Scan rate: 50 mV s^{-1}.

It shows that more Ti oxidation occurs in 1 M HNO_3 than in 0.1 M HNO_3. This confirms that more TiO_2 was formed on the Ti surface in 1 M HNO_3 prior to PbO_2 deposition than in 0.1 M HNO_3. This means that in 1 M HNO_3, the PbO_2 is deposited on a thicker layer of TiO_2 than if the deposition of PbO_2 is carried out in 0.1 M HNO_3. The thicker layer of TiO_2 formed on the Ti surface leads to a decrease in conductivity.

Meanwhile the presence of F^- ions in 0.1 M HNO_3 has reduced the formation of TiO_2 layer further as shown by curve c (below ca. +1.0 V). This indicates that in 0.1 M HNO_3 solution with the presence of F^-, the PbO_2 coating is deposited on a very thin layer of TiO_2. It is believed that the TiO_2 layer formed is thinner than the TiO_2 layer formed in 0.1 M HNO_3 solution without F^- ions present. Therefore, the deposition of PbO_2 coatings on Ti substrate from 0.1 M HNO_3 solution containing F^- ions tends to produce more conducting deposits than without F^- in the deposition solution. The voltammograms plotted for figure 5.16 were noisy because their readings were taken from expanded scales of figure 5.7, figure 5.12 and figure 5.14.

5.3 Doped PbO_2 on Ti

In chapter 4, the preparation and characteristics of doped PbO_2 deposits on gold substrates were discussed. It was demonstrated that bismuth was the best dopant for the incorporation with PbO_2 electrodes as assessed by the voltammetry for the oxidation of DMSO. The Bi-doped PbO_2/Au electrodes were prepared from 1 M HNO_3 solution containing 500 mM Pb(II) + 10 mM Bi(III).

Unfortunately, in this case the deposition of PbO_2 on Ti substrates from 1 M HNO_3 solution is most likely to produce a high electrical resistance deposit due to the formation of thick layer of TiO_2 in between Ti substrate and PbO_2 as discussed in section 5.2. Some depositions using a solution of 10 mM Bi(III) + 500 mM Pb(II) in 1 M HNO_3 were carried out using a current density of 5 mA cm^{-2} at 298 K. It was found that the resulting Bi-PbO_2 deposit was not well adhered on the Ti substrates with some cracks and lumps as shown in figure 5.17. Furthermore, its electrical response was very low, consistent with pure PbO_2/Ti prepared from the same concentration of nitric acid (ie: 1 M HNO_3). The low electrical response is believed to be due to the formation of a thick layer of TiO_2 during the deposition of the Bi-PbO_2 layer on the Ti surface.

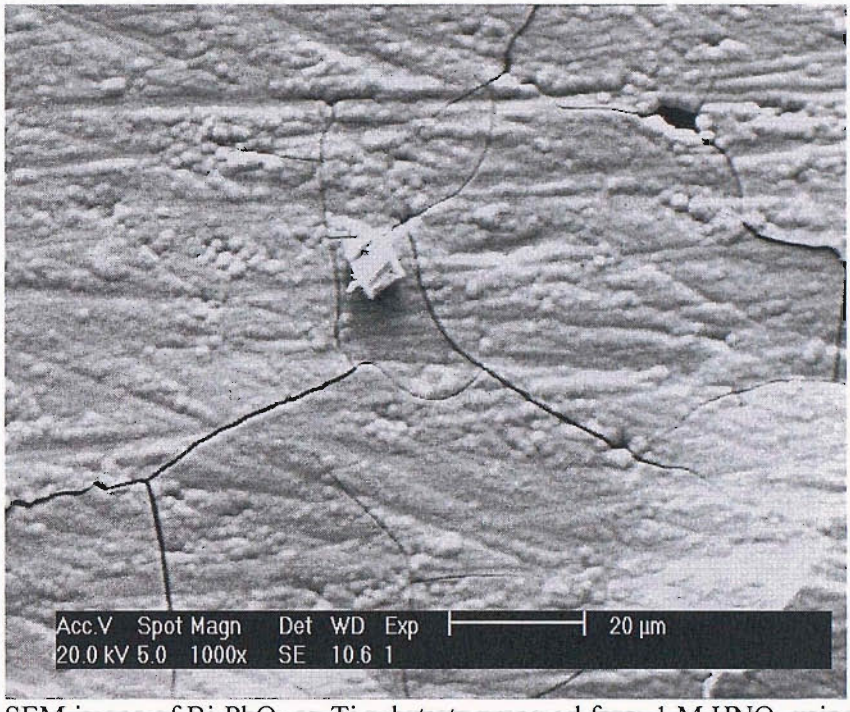

Figure 5.17: SEM image of Bi-PbO_2 on Ti substrate prepared from 1 M HNO_3 using a current density of 5 mA cm^{-2} at 298 K.

Nevertheless, the preparation of Bi-PbO_2/Ti was not feasible from 0.1 M HNO_3 containing 500 mM Pb(II) + 10 mM Bi(III). This is because Bi^{3+} is hydrolysed in this lower acidity solution.

Hence, another potential dopant ion (ie: Fe^{3+}) was incorporated into PbO_2 deposit. The deposition solution containing Fe(III) was easily prepared in either 0.1 M HNO_3 or 1 M HNO_3. But, again the deposition from high concentration of nitric acid is not a favourable condition. Therefore, the doping of PbO_2 with Fe was carried out from 0.1 M HNO_3 solution. As mentioned earlier in section 5.2, the addition of F^- ions has improved the morphology and adhesion of PbO_2 onto Ti substrates. Thus, sodium flouride was also added in the deposition solution together with 10 mM Fe(III) + 500 mM Pb(II) in 0.1 M HNO_3. The resulting deposit is designated as Fe-F-PbO_2/Ti.

Figure 5.18 shows the SEM image of Fe-F-PbO_2/Ti deposit prepared from 0.1 M HNO_3 solution containing 10 mM Fe(III) + 40 mM NaF + 500 mM Pb(II) using a current density of 10 mA cm^{-2} for 15 min at 298 K. The deposit was very smooth with dense angular crystals. It is apparent that the morphology of the deposit is quite similar to the F-PbO_2 deposit prepared at 5 mA cm^{-2} for 30 min at 298 K as shown in figure 5.15. The F-PbO_2 deposit produced at higher current density (ie: 10 mA cm^{-2}) at 298 K was not smooth as shown in figure 5.19a. But with the addition of Fe in the

deposition solution, the deposition at 10 mA cm^{-2} led to the production of a uniform and smooth deposit as shown in figure 5.19b.

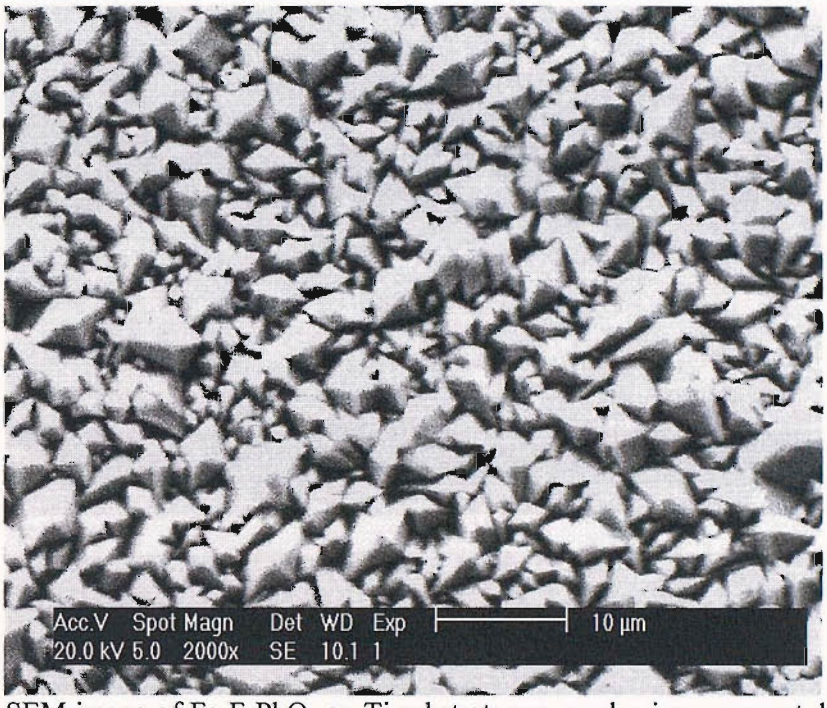

Figure 5.18: SEM image of Fe-F-PbO_2 on Ti substrate prepared using a current density of 10 mA cm^{-2} for 15 min at 298 K.

The use of higher current density for the deposition leads to fast coverage of Ti surface by PbO_2 deposit. At 10 mA cm^{-2} the deposition of Fe-F-PbO_2 was fast with all Ti surface covered in less than 10 minutes. Meanwhile, if low current density (ie: 5 mA cm^{-2}) is used for the deposition of Fe-F-PbO_2, a longer time (~ 30 min) is required to cover the whole Ti surface. The presence of Fe on the deposit was detected by EDAX as shown in table 5.3. The adhesion of the Fe-F-PbO_2 onto Ti substrates was very good.

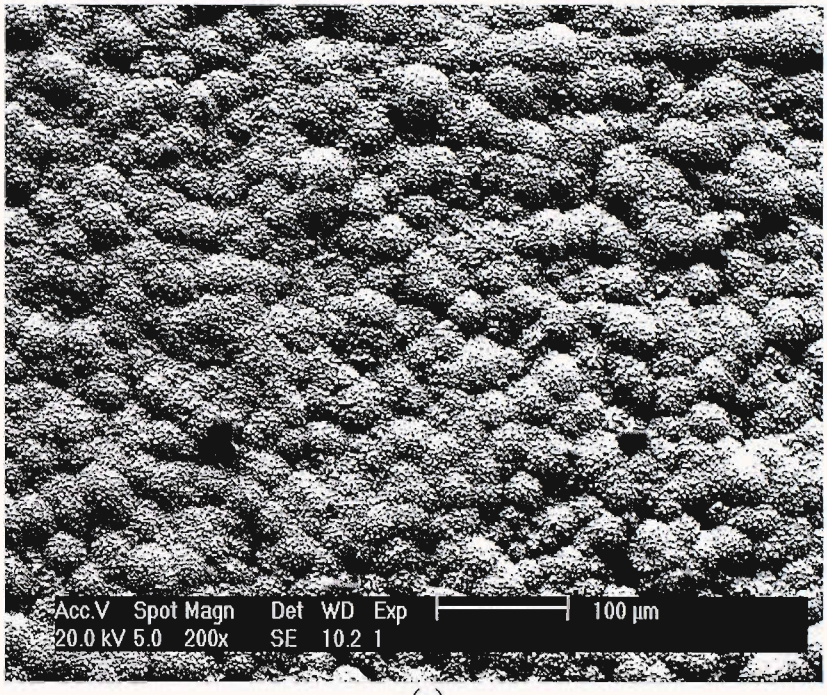

(a)

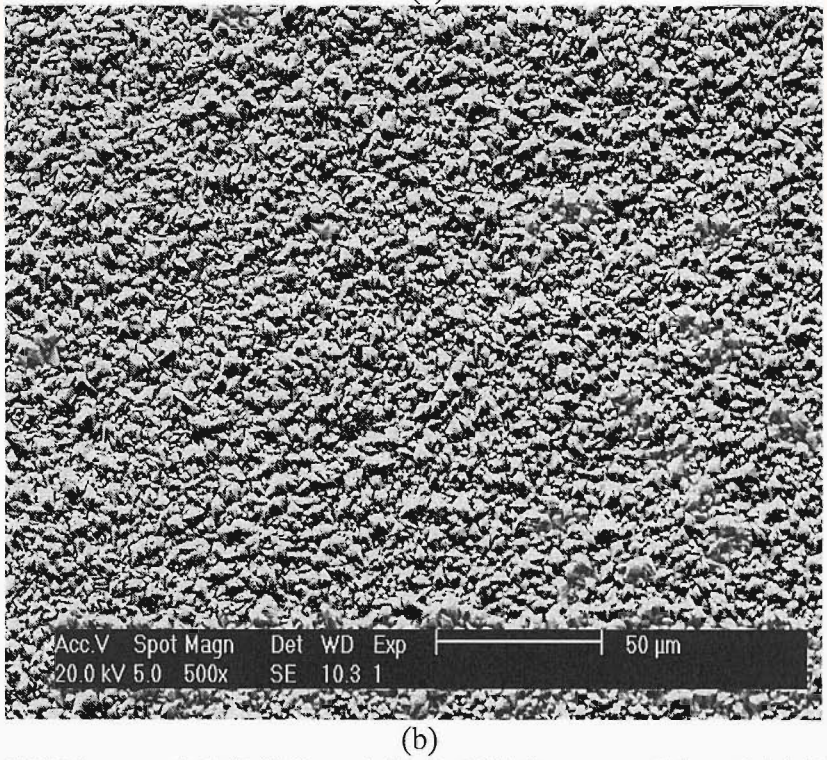

(b)

Figure 5.19: SEM image of (a) F-PbO_2 and (b) Fe-F-PbO_2 prepared from 0.1 M HNO_3 using a current density of 10 mA cm^{-2} for 15 min at 298 K onto Ti substrates.

Nonetheless, the preparation of Bi-PbO_2 electrodes onto Ti substrates become possible if a conducting interlayer or underlayer is deposited earlier on the Ti substrates before Bi-PbO_2. It has been reported [17] that F-PbO_2 prepared from 0.1 M HNO_3 (image as shown in figure 5.16) could be used as the interlayer before the deposition of Bi-PbO_2. Therefore, the Bi-PbO_2 is deposited onto F-PbO_2/Ti which

acts as the new substrate for Bi-PbO_2. The resulting deposit is designated as Bi-PbO_2/ F-PbO_2/Ti.

Element	Average in Atomic percent
Oxygen ,O	38.9
Fluorine , F	4.4
Iron , Fe	4.3
Lead, Pb	52.4

Table 5.3: Elemental analysis of Fe-F-PbO_2 deposit determined by EDAX.

In this study it was found that the Fe-F-PbO_2 prepared from 0.1 M HNO_3 can also be used as the interlayer for the deposition of Bi-PbO_2 deposit on Ti substrates. As mentioned earlier, the Fe-F-PbO_2 was successfully prepared at 10 mA cm^{-2} with smooth and uniform distribution of angular crystals across the Ti surface. Once the interlayer (ie: Fe-F-PbO_2) covered the whole Ti surface, the deposition of Bi-PbO_2 can be carried out from solution of 1 M HNO_3 containing Pb(II) and 10 mM Bi(III). There were two different concentrations of Pb(II) containing 10 mM Bi(III) tested in this study; 30 mM and 500 mM. The resulting deposits are designated as Bi-PbO_2/ Fe-F-PbO_2/Ti.

A successful deposition of Bi-PbO_2 on Fe-F-PbO_2/Ti from solution containing 500 mM Pb(II) was carried out using a low current density (ie: 0.5 mA cm^{-2}) at 298 K. The deposit produced was very smooth and uniform across the surface (as in figure 5.20a) with less angular crystals as clearly shown at higher magnification as in figure 5.20b.

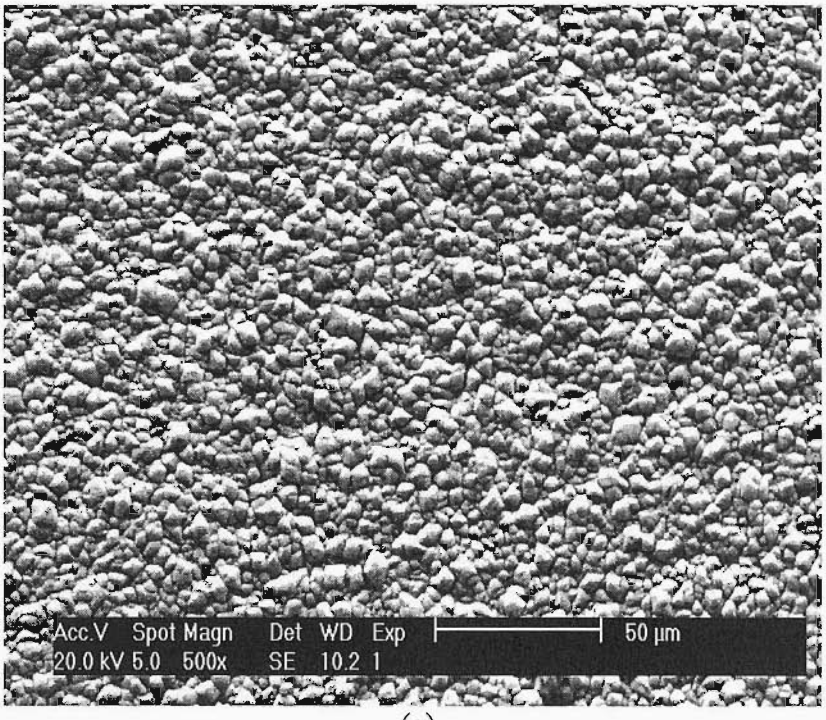

(a)

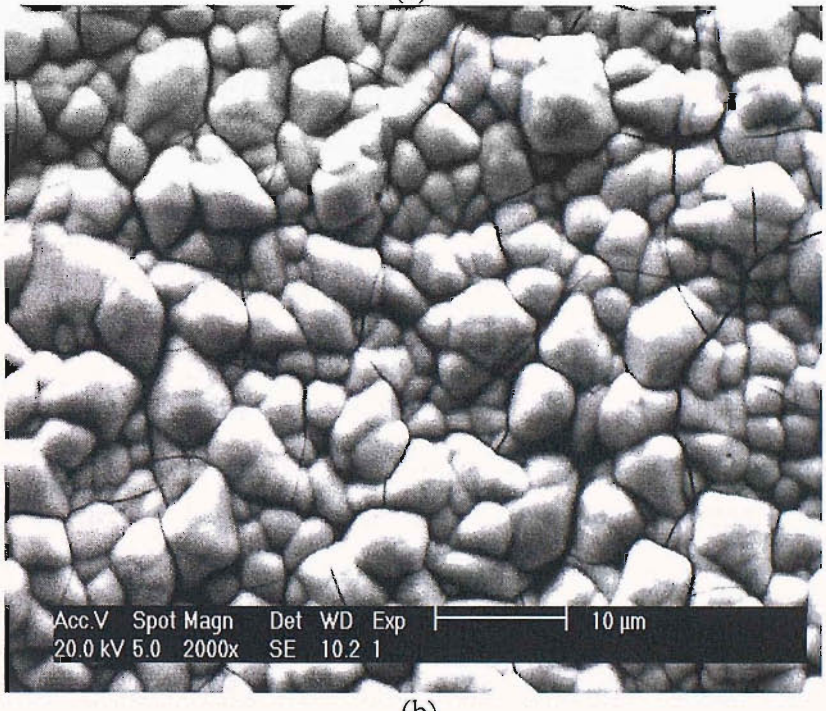

(b)

Figure 5.20: SEM images of Bi-PbO_2 on Fe-F-PbO_2/Ti deposited from 10 mM Bi(III) + 500 mM Pb(II) in 1 M HNO_3 using a current density of 0.5 mA cm^{-2} for 30 min at 298 K.

At higher current density employed (ie: > 1 mA cm^{-2}) the resulting deposits tend to crack and were not smooth as shown in figure 5.21. It is believed that a slow deposition of Bi-PbO_2 onto a rough surface of Fe-F-PbO_2 substrate is required in order to produce a smooth deposit by using a very low current density. This shows

that current density has a significant effect in the formation of a smooth and well-adhered Bi-PbO_2 onto Fe-F-PbO_2/Ti.

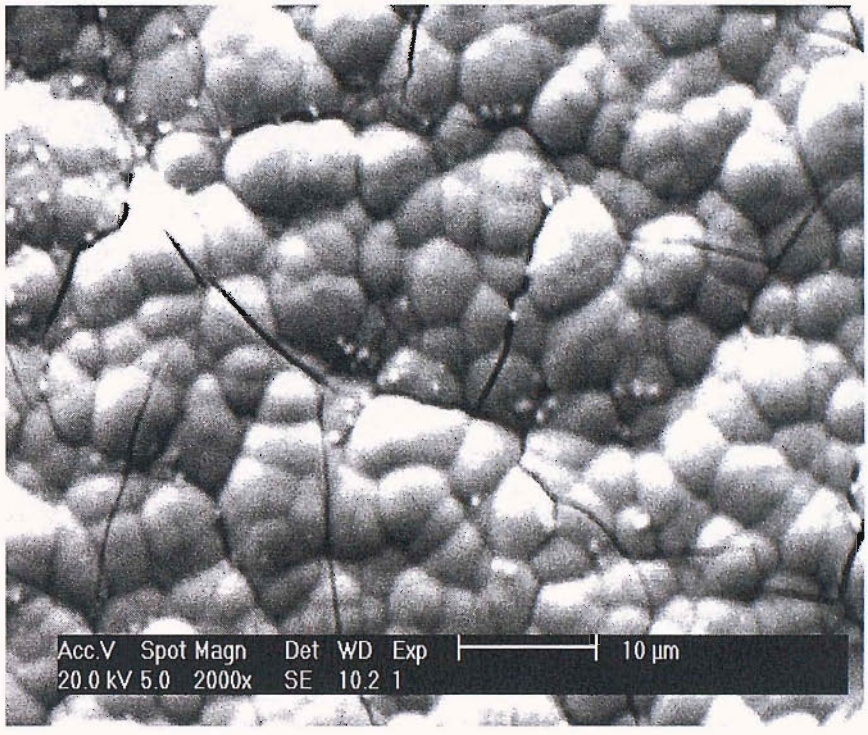

Figure 5.21: SEM image of Bi-PbO_2 electrode on Fe-F-PbO_2/Ti prepared from 10 mM Bi(III) + 500 mM Pb(II) in 1 M HNO_3 using a current density of 2.5 mA cm^{-2} at 298 K.

The deposition of Bi-PbO_2 on Fe-F-PbO_2/Ti from low concentration of Pb(II) (ie: 30 mM) in 1 M HNO_3 containing 10 mM Bi(III) was also investigated. The deposition was carried out using a very low current density (ie: 0.5 mA cm^{-2}) for 30 min at 298 K. The resulting deposit is shown in figure 5.22. It was found that the morphology of the deposit is different than the Bi-PbO_2 deposit prepared from high concentration of Pb(II) as shown in figure 5.20. The Bi-PbO_2 deposit in figure 5.22 is uniform across the surface with 'snail-like' crystals but not close-packed deposit. The deposit was moderately adhered on the Fe-F-PbO_2 substrate.

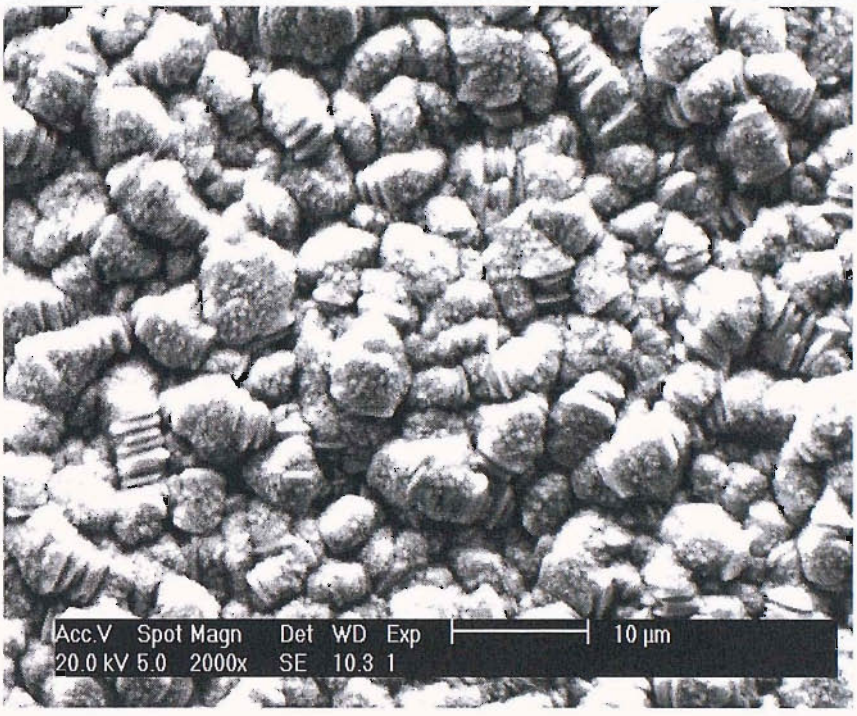

Figure 5.22: SEM image of Bi-PbO_2 electrode on Fe-F-PbO_2/Ti prepared from 10 mM Bi(III) + 30 mM Pb(II) in 1 M HNO_3 using a current density of 0.5 mA cm^{-2} at 298 K.

The content of bismuth incorporated into PbO_2 deposit prepared from low concentration of Pb(II) was found to be higher than Bi-PbO_2 deposit prepared from 500 mM Pb(II). Table 5.4 compares the Bi:Pb ratio of Bi-PbO_2 deposits prepared from different concentrations of Pb(II) as determined by EDAX.

Deposition solution	**Average of Bi:Pb**
10 mM Bi(III) + 30 mM Pb(II) + 1 M HNO_3	0.35
10 mM Bi(III) + 500 mM Pb(II) + 1 M HNO_3	0.14

Table 5.4: Bi:Pb ratio of Bi-PbO_2 electrodes prepared on Fe-F-PbO_2/Ti from different Pb(II) concentration at 298 K using a current density of 0.5 mA cm^{-2} for 30 min.

It was demonstrated in chapter 4 that the amount of bismuth incorporated with PbO_2 deposited onto gold substrates had a significant effect on the oxidation of organic compounds especially sulphur-containing compounds. The catalytic activity of the produced Bi-PbO_2/Fe-F-PbO_2/Ti electrodes prepared from different concentrations of Pb(II) will be discussed later in section 5.4.

5.4 Catalytic Activity of PbO_2/ Ti Electrodes

The catalytic activity of the prepared PbO_2 (doped and undoped) electrodes for O_2 evolution and oxidation of DMSO was investigated.

5.4.1 Anodic Evolution of O_2

Figure 5.23 shows a comparison of the residual voltammetric responses for several PbO_2 electrodes deposited on Ti substrate in 1 M H_2SO_4. The PbO_2 electrodes were prepared from 0.1 M HNO_3 solution containing 500 mM Pb(II) + 40 mM NaF for F-PbO_2 electrode on Ti; from 0.1 M HNO_3 solution containing 500 mM Pb(II) + 40 mM NaF + 10 mM Fe(III) for Fe-F-PbO_2 electrode on Ti and from 1 M HNO_3 solution containing 500 mM Pb(II) + 10 mM Bi(III) for Bi-PbO_2 electrode on Fe-F-PbO_2 substrate. It is quite apparent in the figure that smaller background currents are obtained in the region E > 1.8 V for F-PbO_2/Ti (curve a) and Fe-F-PbO_2/Ti (curve b) in comparison to curve c of Bi-PbO_2/Fe-F-PbO_2/Ti electrode.

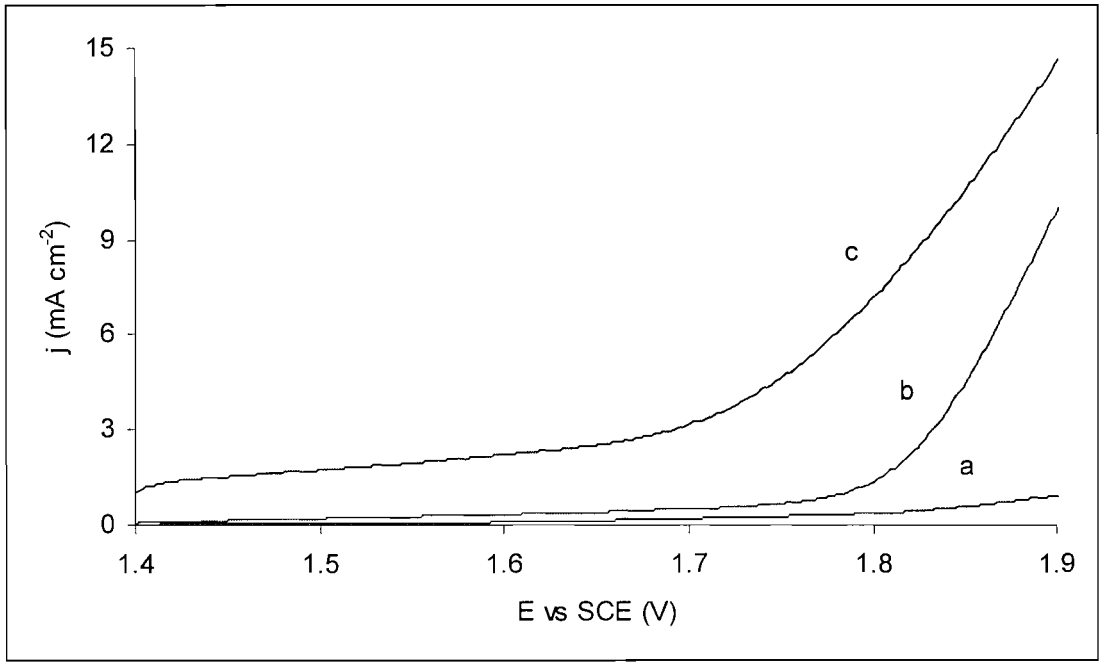

Figure 5.23: Voltammetric response for O_2 evolution at various electrodes in 1 M H_2SO_4. Scan rate: 50 mV s^{-1}; positive scan. Electrode: (a) F-PbO_2/Ti (b) Fe-F-PbO_2/Ti and (c) Bi-PbO_2/Fe-F-PbO_2/Ti

It has been reported [173] that the O_2 evolution is always inhibited at fluoride modified lead dioxide electrode. The presence of Fe in the PbO_2 deposits can be seen to show similar properties to F^-. Meanwhile the incorporation of bismuth into PbO_2 deposits has a great effect on the evolution of O_2. It is believed that the incorporation of active sites (ie: Bi) into the PbO_2 electrode has increased the rate of anodic

discharge of H_2O. The same observation was observed for the O_2 evolution at Bi-PbO_2 on gold as shown earlier in chapter 4 (see figure 4.6A). Indeed the Bi-PbO_2 coatings show a significant current positive to +1.40 V.

5.4.2 Voltammetric Response of Dimethyl Sulfoxide (DMSO)

Anodic oxidation of dimethyl sulfoxide to dimethyl sulfone ($DMSO_2$) was again used for comparison of PbO_2 electrodes activities. The voltammetric response of $(CH_3)_2SO$ in 1 M H_2SO_4 is shown in figure 5.24 for pure PbO_2/Ti, F-PbO_2/Ti, Fe-F-PbO_2/Ti and Bi-PbO_2/Fe-F-PbO_2/Ti respectively. It was found that the presence of flouride in the oxide film has substantially increased the activity for DMSO oxidation (see curve b in the figure) besides its beneficial adhesion effect. It is believed that a very thin layer of TiO_2 was formed on the Ti substrate if F^- ions present in the deposition solutions as demonstrated earlier in figure 5.16. But without F^- ions in the deposition solution, a thicker layer of TiO_2 was formed and this TiO_2 leads to low electrical response for pure PbO_2 as shown by curve a.

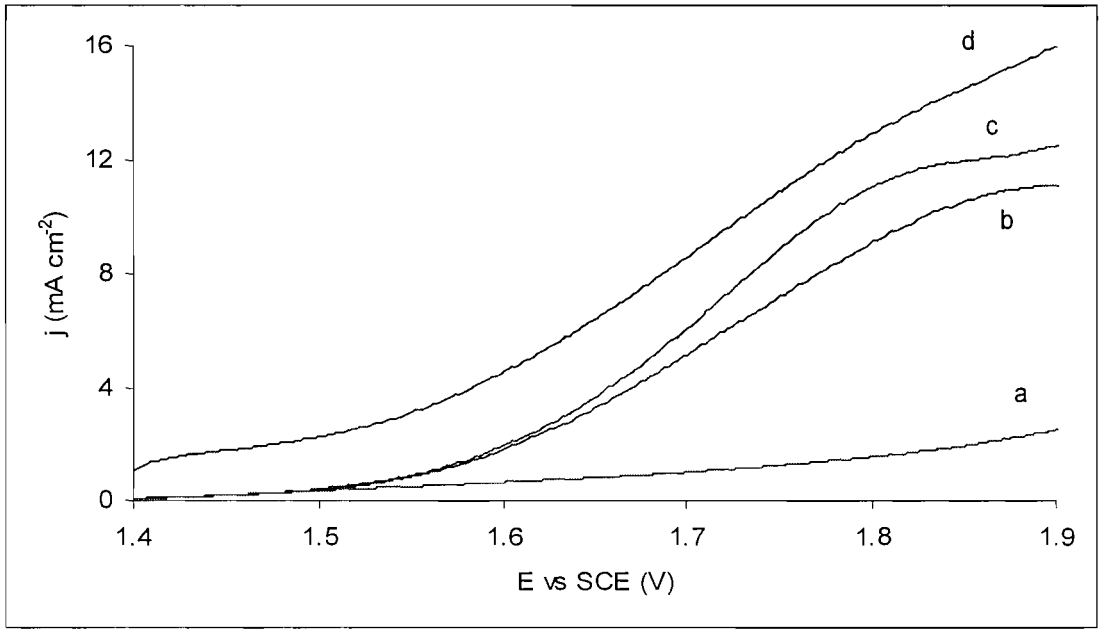

Figure 5.24: Voltammetric response of 50 mM DMSO at various PbO_2 electrodes in 1 M H_2SO_4. Scan rate: 50 mV s^{-1}. Electrode: (a) pure PbO_2/Ti (b) F-PbO_2/Ti (c) Fe-F-PbO_2/Ti and (d) Bi-PbO_2/Fe-F-PbO_2/Ti

The addition of 10 mM Fe(III) in the deposition solution together with F^- ions has slightly increased the activity of PbO_2 electrodes as shown by curve c. The presence of Fe was confirmed by EDAX and shown in table 5.3. It is believed that

more active sites are available on Fe-F-PbO_2 electrode for the oxidation of DMSO than the F-PbO_2 electrode. It was demonstrated earlier in chapter 4 that the incorporation of Fe into PbO_2 deposits prepared onto gold substrate has greater catalytic activity than pure PbO_2 on gold. This indicates that Fe has a significant effect on increasing the catalytic activity of PbO_2 electrodes.

Curve d in the figure represents the voltammetric response for DMSO at Bi-PbO_2 electrodes prepared on Fe-F-PbO_2/Ti substrate. The Bi-PbO_2 electrode was prepared from 1 M HNO_3 solution containing 10 mM Bi(III) + 500 mM Pb(II). It is readily apparent that the activity of Bi-PbO_2 is somewhat greater than Fe-F-PbO_2 and F-PbO_2 electrodes and significantly greater than that of pure PbO_2 electrode. Bi-PbO_2 electrode on gold substrate also has been reported to be more active than other doped PbO_2 electrodes (ie: Ag-PbO_2, Fe-PbO_2, Ni-PbO_2 and Cu-PbO_2) towards DMSO oxidation [174]. This means that the response of DMSO at PbO_2 electrodes is independent on the substrate materials used.

The catalytic activity of Bi-PbO_2 electrodes prepared from low concentration of Pb(II) was also investigated. The electrode was prepared from 1 M HNO_3 solution containing 10 mM Bi(III) + 30 mM Pb(II) on Fe-F-PbO_2/Ti substrate. Figure 5.25 shows the voltammetric responses of the Bi-PbO_2 in 1 M H_2SO_4 and 50 mM DMSO + 1 M H_2SO_4.

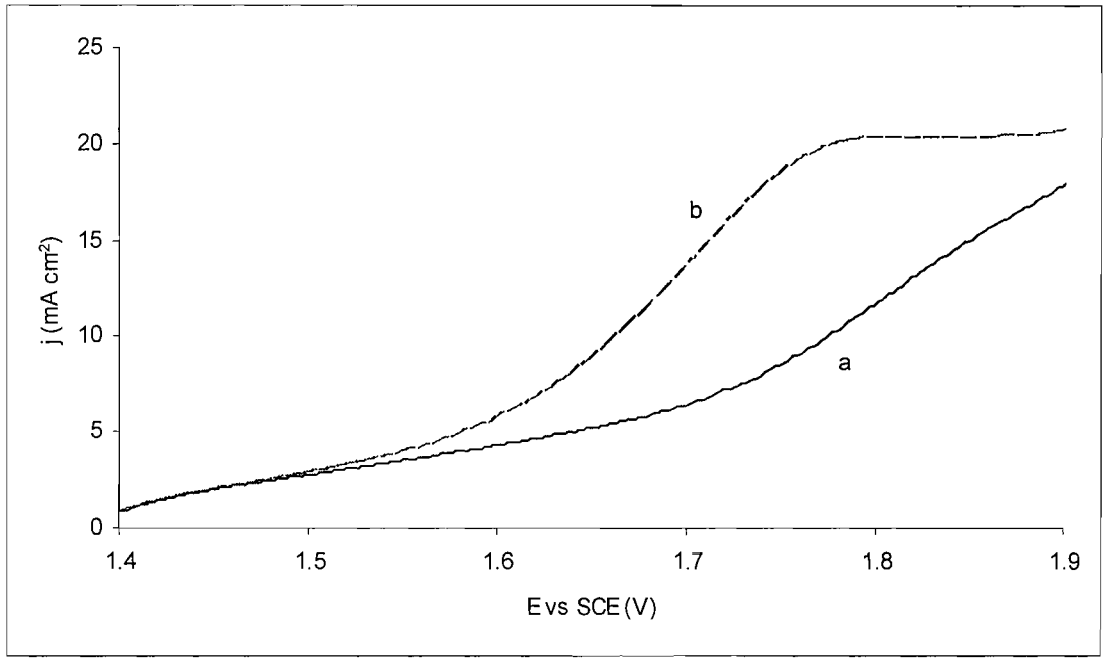

Figure 5.25: Voltammetric response of (a) 1 M H_2SO_4 and (b) 50 mM DMSO + 1 M H_2SO_4 at Bi-PbO_2 prepared from 10 mM Bi(III) + 30 mM Pb(II) in 1 M HNO_3 on Fe-F-PbO_2/Ti.

It is clearly seen that the Bi-PbO_2 electrode prepared from low concentration of Pb(II) is active for the oxidation of DMSO as well the O_2 evolution. Comparing curve b of this figure with curve d in figure 5.24 (DMSO oxidation at Bi-PbO_2 electrode prepared from 500 mM Pb(II)) reveals that the Bi-PbO_2 electrode prepared from 10 mM Bi(III) + 30 mM Pb(II) in 1 M HNO_3 has greater catalytic activity for the oxidation of DMSO than the Bi-PbO_2 electrode prepared from 10 mM Bi(III) + 500 mM Pb(II) in 1 M HNO_3. The O_2 evolution is also higher at Bi-PbO_2 electrode prepared from low concentration of Pb(II) as shown by curve a in figure 5.25 than at Bi-PbO_2 electrode prepared from high concentration of Pb(II) as seen in figure 5.23 (curve c). It is believed that the amount of bismuth in the PbO_2 deposits has a significant effect on the activity of the prepared Bi-PbO_2 electrodes. As shown earlier in table 5.4, the ratio of Bi:Pb detected by EDAX for Bi-PbO_2 electrode prepared from 30 mM Pb(II) is higher than for Bi-PbO_2 electrode prepared from 500 mM Pb(II) with the same amount of Bi(III) present in both deposition solutions. Therefore, the incorporation of bismuth into PbO_2 deposits plays a major role in enhancing the catalytic activity of PbO_2 deposits.

Voltammetric data for DMSO oxidation at various film electrodes are summarized in table 5.5. It shows that the O_2 was evolved most rapidly at the Bi-PbO_2 electrode prepared from 30 mM Pb(II) which contains high amount of bismuth. The potential where the difference of current density between DMSO oxidation and background is 5 mA cm^{-2} or $E_{j=5mA\ cm^{-2}}$ occurred at less positive potential at the same Bi-PbO_2 electrode as compared to other electrodes. Although the electrode is more active for the oxidation of DMSO than other electrodes but the competing reaction (ie: O_2 evolution) is also increased at this electrode. Hence, a major challenge is the optimization of electrode activity for the oxidation reactions without undue increases in the simultaneous background signal for O_2 evolution. It is apparent that the Bi-PbO_2 electrode prepared from 10 mM Bi(III) + 500 mM Pb(II) in 1 M HNO_3 has a good activity for the oxidation of DMSO and a reasonable current for O_2 evolution.

Surface (Substrate)	**I_{bkd} (mA cm^{-2})**	**$E_{j=5\ mA\ cm^{-2}}$ (V vs SCE)**
Pure PbO_2 (Ti)	0.1	NR
F-PbO_2 (Ti)	0.2	1.75
Fe-F-PbO_2 (Ti)	0.4	1.72
Bi-PbO_2 (Fe-F-PbO_2/Ti) prepared from 10 mM Bi(III) + 30 mM Pb(II) + 1 M HNO_3	6.5	1.66
Bi-PbO_2 (Fe-F-PbO_2/Ti) prepared from 10 mM Bi(III) + 500 mM Pb(II) + 1 M HNO_3	2.8	1.68

Table 5.5: Summary of voltammetric response data for oxidation of 50 mM DMSO at various film electrodes on Ti substrates in 1 M H_2SO_4. I_{bkd}: background current density measured at 1.70 V; NR: negligible reactivity

5.5 Stability of PbO_2/ Ti Deposits

The stability of PbO_2 deposits on open circuit was investigated by immersing them in a solution of 1 M sulfuric acid containing DMSO. The F-PbO_2 deposits with very good adherent on Ti substrates were used as the sample electrodes in investigating the stability on open circuit. The electrodes were prepared from 40 mM NaF + 500 mM Pb(II) in 0.1 M HNO_3 using 5 mA cm^{-2} for 30 min at 298 K.

Figure 5.26a shows the morphology of the deposits before immersion. The deposits consist of dense angular crystals and uniform across the surface. After 1 day in the solution on open circuit, the morphology of the whole deposits was totally changed to cubic crystals as shown in figure 5.26b. It is believed that the F-PbO_2 deposits were completely reduced to $PbSO_4$. High amount of Sulfur (ie: 22 in Atomic %) was present on the image in figure 5.26b as detected by EDAX.

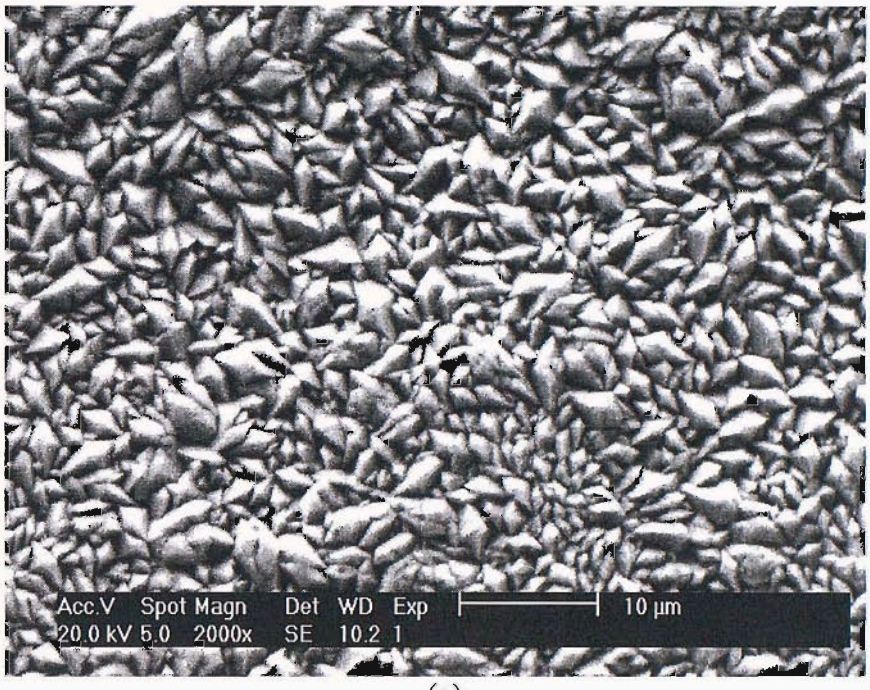

(a)

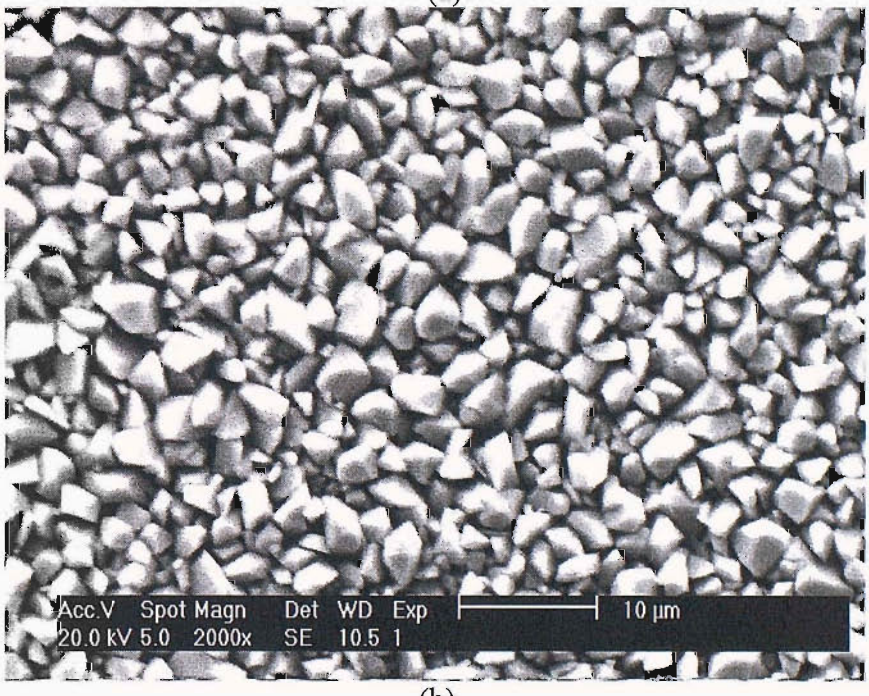

(b)

Figure 5.26: SEM images of F-PbO_2 deposits (a) before and (b) after immersion for 1 day in 50 mM DMSO + 1 M H_2SO_4.

The same phenomena have occurred on PbO_2 electrodes deposited on gold substrates after left standing in the same solution on open circuit. This indicates that the stability of the produced PbO_2 deposits in aqueous solution on open circuit does not dependent on the substrate materials used. This is because the spontaneous chemical reaction occurs between the electrode surface and the solution. The chemical reaction taking place between the electrode and solution is shown below.

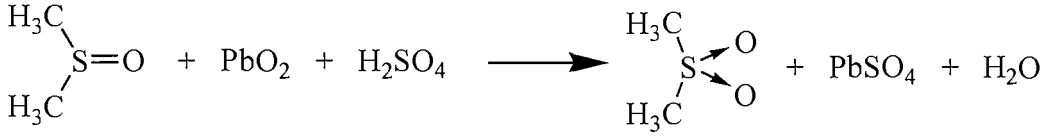

Nevertheless, the PbO_2 electrodes on Ti substrates were much more stable when operating at potentials positive to the formal potential of the PbO_2/Pb(II) couple. The morphology has remained the same as shown in figure 5.26a after electrolysis at E + 1.70 V for a few hours. Therefore, the active PbO_2 electrodes on Ti substrates such as Fe-F-PbO_2 or Bi-PbO_2/Fe-F-PbO_2 can be successfully used as anode materials for the oxidation of organic compounds especially sulphur-containing compounds provided that the electrodes must not be left standing for a long time on open circuit in the electrolytic solution.

5.6 Deposition of PbO_2 on Expanded Ti Mesh

The electrodeposition of PbO_2 onto expanded Ti mesh was also carried out. The Ti mesh as shown in figure 2.4 was a gift from Dexmet Corporation with product code 5.4 Ti 5-031. Meshes with dimensions of 3 cm x 5 cm x 0.0118 cm were firstly treated in a boiling solution of 1.6 M (or 20 % w/v) oxalic acid for 2 hours. This etching process was carried out in order to remove TiO_2 from the Ti mesh and also to make the mesh surface rough.

Figure 5.27a and 5.27b show SEM images of the Ti mesh before and after etched in the oxalic acid solution. It is clearly seen that the Ti mesh was totally changed from smooth surface to very rough or 'stormy-sea' surface.

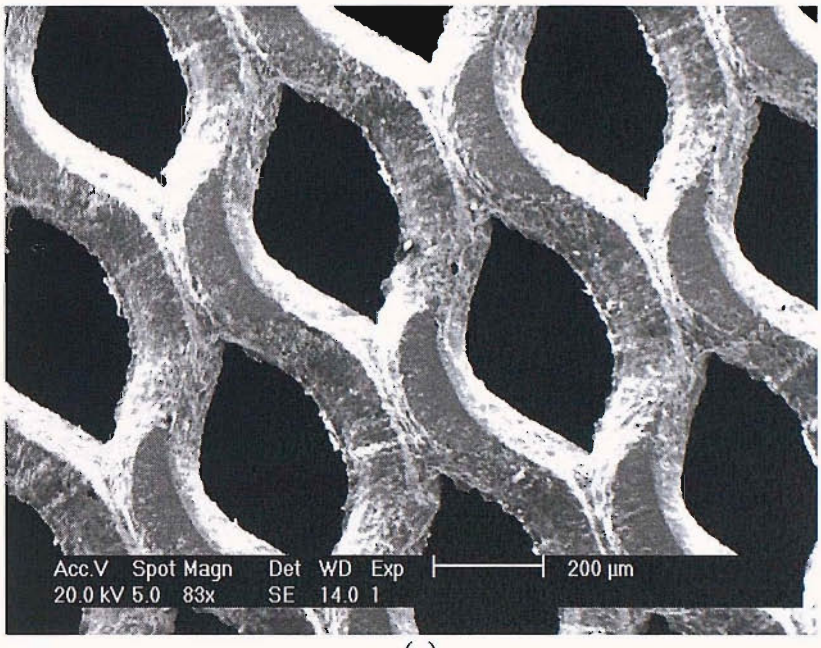

(a)

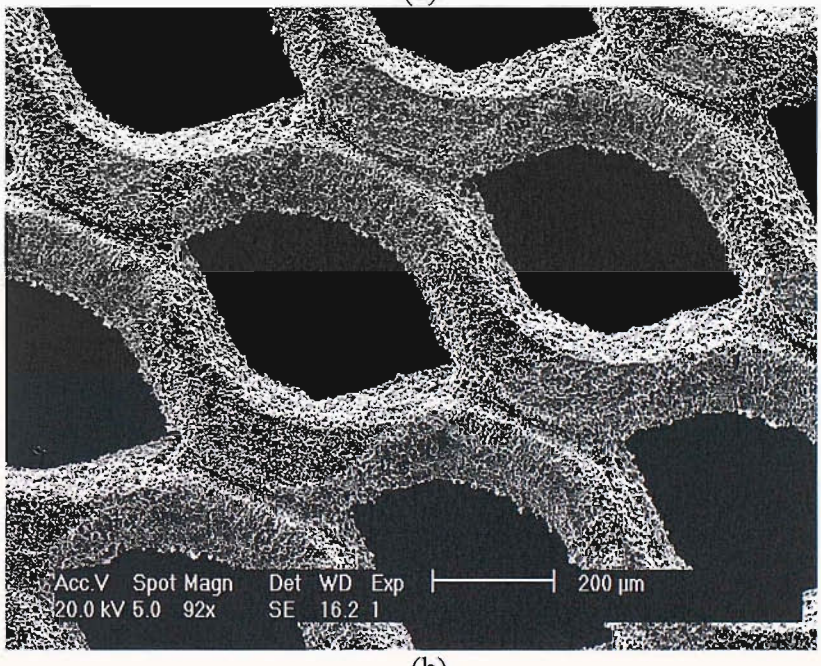

(b)

Figure 5.27: SEM images of Ti mesh (a) before and (b) after treated in 1.6 M oxalic acid for 2 hours at 373.

The difference is more clearly seen at higher magnitude as shown by SEM images in figure 5.28a for the Ti mesh before pre-treatment and figure 5.28b for after pre-treatment in the etching solution. The resulting 'stormy-sea' surface is uniform across the whole Ti surface (ie: both sides). The resulting Ti mesh surface after the etching treatment is similar to the Ti disc surface (see figure 5.3) treated under the same conditions.

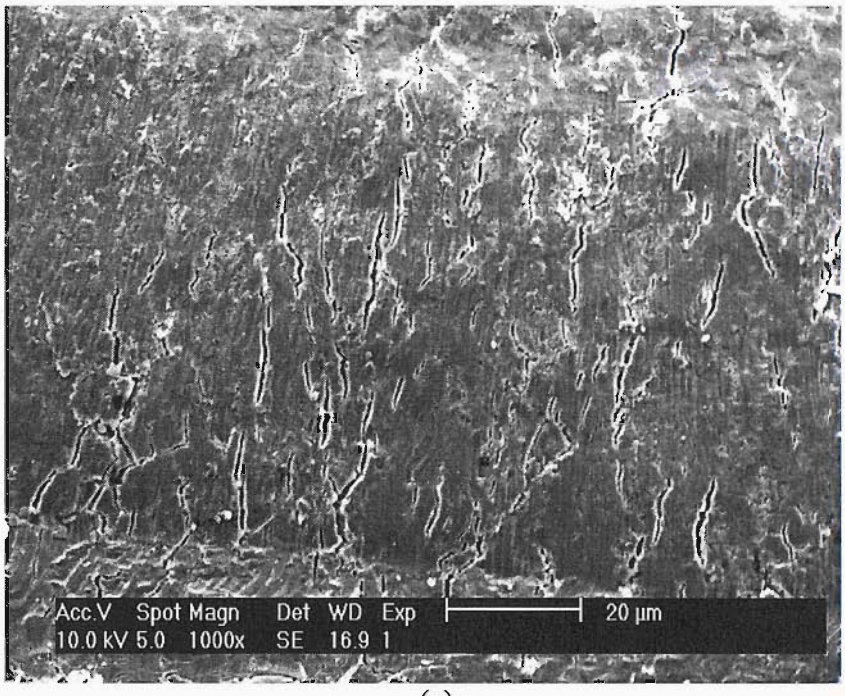

(a)

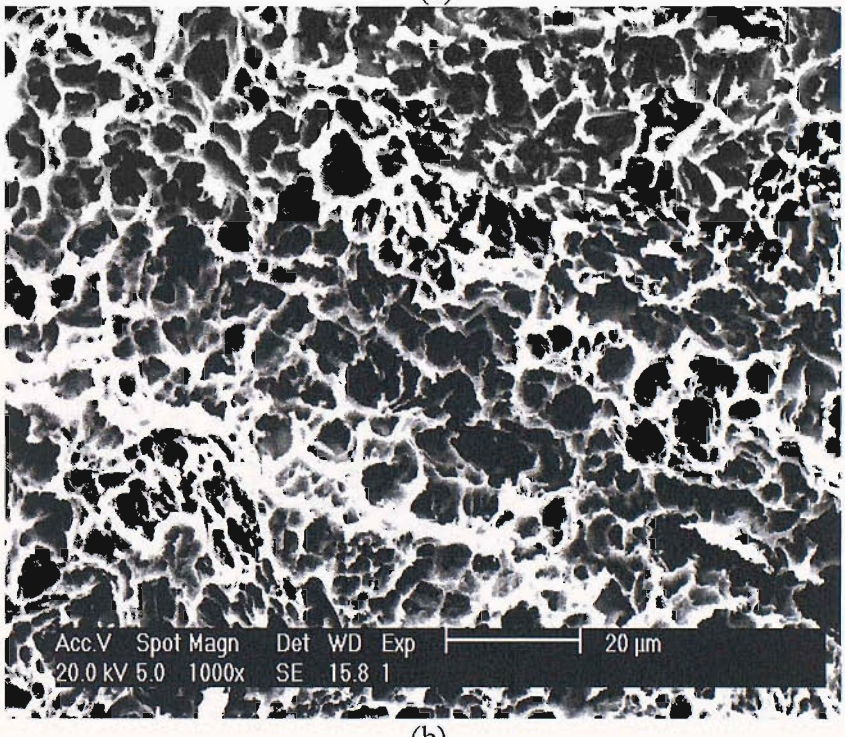

(b)

Figure 5.28: SEM images of Ti mesh (a) before and (b) after etched in 1.6 M oxalic acid for 2 hours at 373 K.

The deposition of the most active and stable PbO_2 electrode (ie: Bi-PbO_2 on Fe-F-PbO_2/Ti substrate) was carried out on the treated Ti mesh. The preparation of the Bi-PbO_2 electrode is based on the experiment carried out earlier on the treated Ti disk substrate. The treated Ti mesh was firstly deposited by an interlayer or Fe-F-PbO_2 layer. The interlayer was prepared from 0.1 M HNO_3 solution containing 10

mM Fe(II) + 40 mM NaF + 500 mM Pb(II) and using a current density of 5 mA cm^{-2} for 30 min at 298 K. The electrodeposition was carried out in a beaker cell as shown in figure 2.9. Figure 5.29 shows the SEM images of the resulting interlayer deposit on Ti mesh substrate at low magnitude (figure 5.29a) and high magnitude (figure 5.29b).

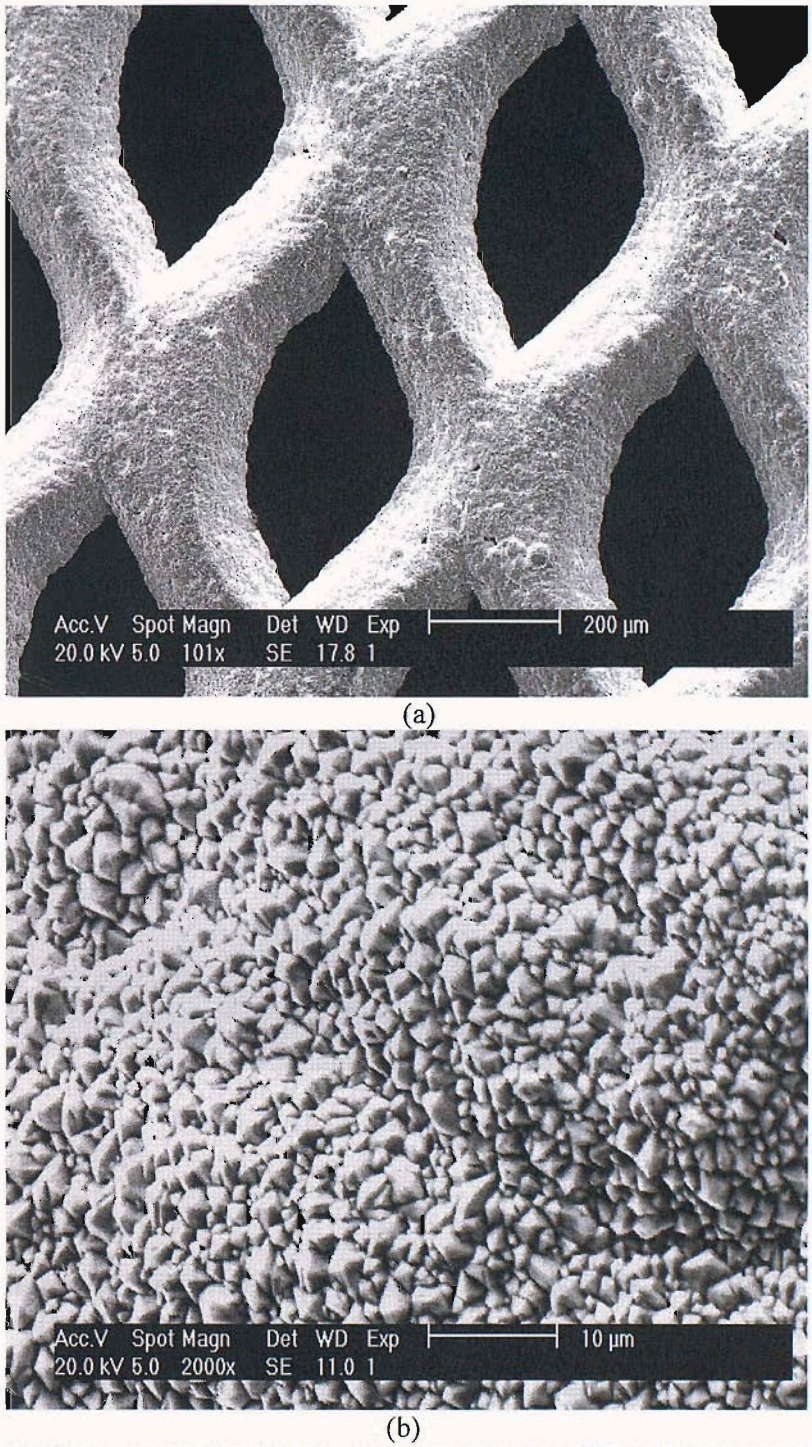

Figure 5.29: SEM images of Fe-F-PbO_2 deposit on treated Ti mesh prepared from 0.1 M HNO_3 solution containing 10 mM Fe(II) + 40 mM NaF + 500 mM Pb(II) using a current density of 5 mA cm^{-2} for 30 min at 298 K.

As clearly seen almost all the Ti mesh surface was covered by the interlayer deposit. The deposit consists of dense angular crystals which is similar to Fe-F-PbO_2 deposit on Ti disc substrate prepared under the same conditions.

A thick layer of Bi-PbO_2 was then deposited on top of the Fe-F-PbO_2 layer from 1 M HNO_3 solution containing 10 mM Bi(III) + 500 mM Pb(II) using a current density of 1 mA cm^{-2} for 240 min at 298 K. Figure 5.30 shows the SEM image of the Bi-PbO_2 deposit on Fe-F-PbO_2/Ti substrate. The Bi-PbO_2 morphology consists of dense and close-packed of less angular crystals. The resulting deposit was uniform at both sides of the Ti mesh and the adhesion was very good. The Bi:Pb ratio was in the range of 0.11 – 0.15 on both sides of the mesh deposit as determined by EDAX.

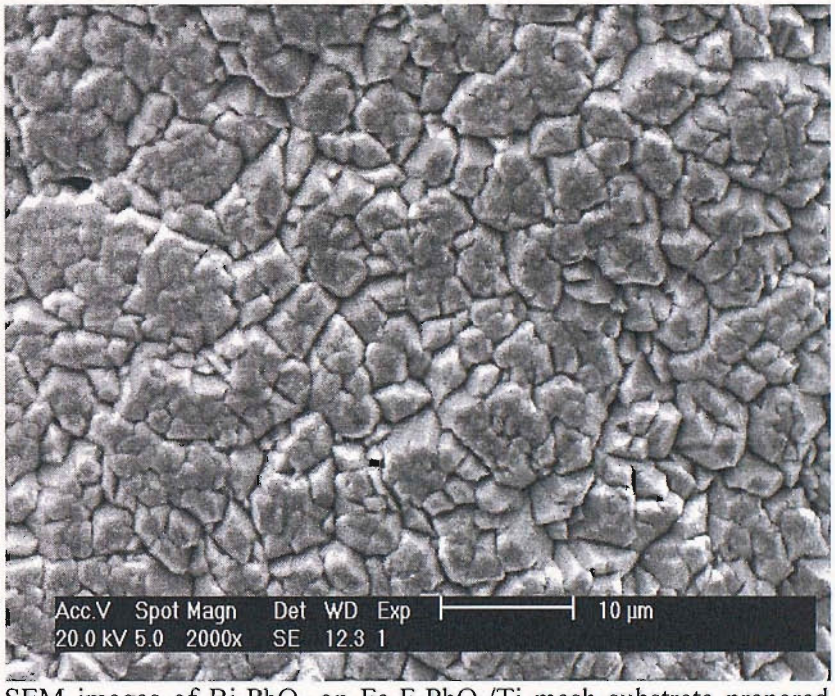

Figure 5.30: SEM images of Bi-PbO_2 on Fe-F-PbO_2/Ti mesh substrate prepared from 1 M HNO_3 solution containing 10 mM Bi(III) + 500 mM Pb(II) using a current density of 1 mA cm^{-2} for 240 min at 298 K.

5.6.1 Voltammetric Response of DMSO at Bi-PbO_2/Fe-F-PbO_2/Ti Mesh Electrode

Figure 5.31 shows the voltammetric response of 50 mM DMSO in 1 M H_2SO_4 at Bi-PbO_2 electrode prepared on Fe-F-PbO_2/Ti mesh from 1 M HNO_3 solution containing 10 mM Bi(III) + 500 mM Pb(II) using a current density of 1 mA cm^{-2} for 240 min at 298 K (morphology as shown in figure 5.30). The oxidation was carried out in a small beaker cell as shown earlier in figure 2.9. The mesh PbO_2/Ti electrodes

(A_{geo}: 1.6 cm^2) have an approximately 8 times larger total surface area than the disk electrode (A: 0.2 cm^2). It was found that the voltammetric response was basically the same as on the disk electrode. This shows that the deposition of a conducting Bi-PbO_2 electrode from 1 M HNO_3 onto Ti mesh substrate can be carried out with the assistance of an interlayer coating (ie Fe-F-PbO_2). The deposition of Bi-PbO_2 onto three dimensional substrate (ie: mesh) has produced a quite similar characteristics as on two dimensional substrate (ie: disc) if deposited under the same preparation conditions.

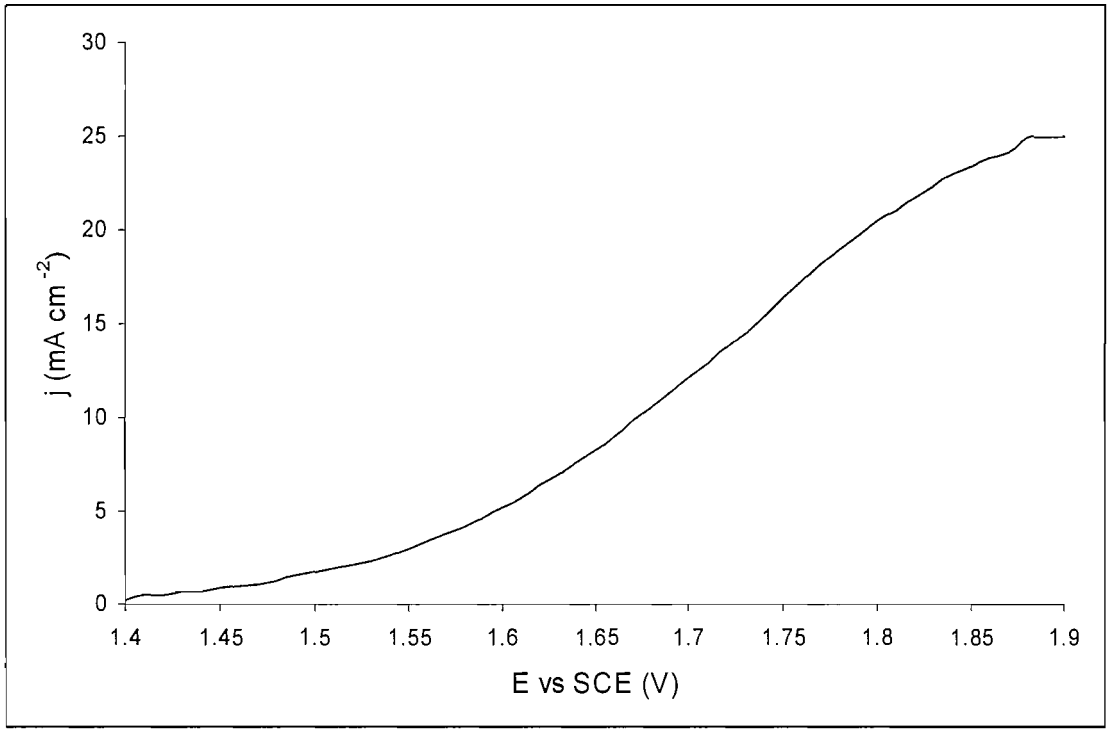

Figure 5.31: Voltammetric response of 50 mM DMSO at Bi-PbO_2/Fe-F-PbO_2/Ti mesh electrode in 1 M H_2SO_4. Scan rate: 50 mV s^{-1}. A_{geo}: 1.6 cm^2

5.6.2 Decolouration of Dyes at Bi-PbO_2/Fe-F-PbO_2/Ti Mesh Electrode

A preliminary study of the decolouration of various dyes at the fabricated PbO_2 on Ti mesh was carried out. The anode used was Bi-PbO_2/Fe-F-PbO_2/Ti mesh with total surface area ~ 25 cm^2 as discussed in section 5.6. The decolouration experiments were carried out in a beaker cell as shown in figure 2.9. There were four dye samples tested; reactive blue 4 (RB4), methyl orange, bromothymol blue and cresol red. Figure 5.32 shows the molecule structure of each dye. Each dye solution was prepared at 1 x 10^{-4} M in 100 mL of 0.5 M H_2SO_4.

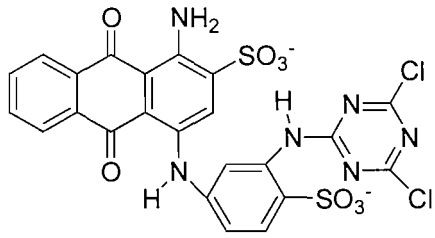

reactive blue 4

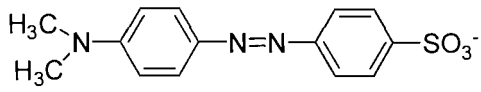

methyl orange

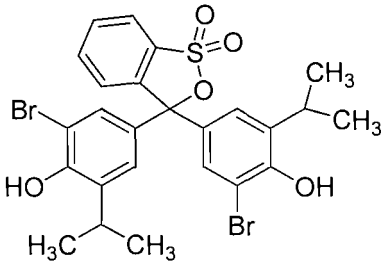

bromothymol blue

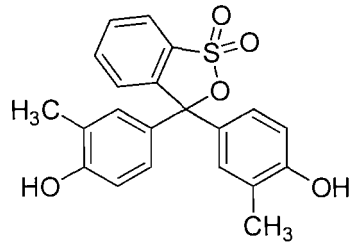

cresol red

Figure 5.32: Structure of dyes used in this study.

Table 5.6 shows initial current density of each dye solution at Bi-PbO_2/Fe-F-PbO_2/Ti mesh electrode in 0.5 M H_2SO_4 at four different potentials (ie: +1.70 V, +1.80 V, +1.90 V and +2.40 V). It was found that the current density increases with increasing potential for each dye. It is believed that the increase in current density partly results from an increase in rate or number of electrons involved in the oxidation of reactant but more importantly the evolution of O_2 at the electrode. It has been suggested that more active oxidizing radical species are formed at higher potential which promote faster dye decomposition [175]. But, at a very high potential (ie: E = + 2.40 V), most of the current passed was used for the O_2 evolution. A vigorous evolution of O_2 at Bi-PbO_2 electrode was seen when the potential was + 2.40 V and this led to the high increase in current density recorded. The current efficiency for the oxidation of reactant at this high potential is then very low but probably rapid oxidation could occur due to the efficient mass transport produced by the O_2 evolution. Further study on the degradation of the dyes at different potentials could be carried out and monitored.

Potential applied, E (V)	Initial current density, j (mA cm^{-2})			
	RB4	Methyl Orange	Bromothymol Blue	Cresol Red
+ 1.70	0.6	0.7	0.4	0.3
+ 1.80	1.6	1.5	1.5	1.0
+ 1.90	3.0*	2.7*	2.8*	2.8*
+ 2.40	33.2¤	15.6¤	19.2¤	14.4¤

Table 5.6: Initial current density vs potential of Bi-PbO_2 electrode in 0.5 M H_2SO_4 solution containing different dyes. (*) slow O_2 evolution observed, (¤) vigorous O_2 evolution observed.

Complete oxidation of the dyes is complex reactions involving many electrons as shown in equation 5.1, 5.2, 5.3 and 5.4 for reactive blue 4, methyl orange, bromothymol blue and cresol red respectively.

$$C_{23}H_{14}Cl_2N_6O_8S_2 + 64H_2O - 132e^- \rightarrow 23CO_2 + Cl_2 + 6NO_3^- + 2SO_4^{2-} + 142H^+ \quad \textbf{(5.1)}$$

$$C_{14}H_{14}N_3O_3S^- + 38H_2O - 86e^- \rightarrow 14CO_2 + 3NO_3^- + SO_4^{2-} + 90H^+ \quad \textbf{(5.2)}$$

$$C_{27}H_{27}Br_2O_5S^- + 53H_2O - 132e^- \rightarrow 27CO_2 + Br_2 + SO_4^{2-} + 133H^+ \quad \textbf{(5.3)}$$

$$C_{21}H_{18}O_5S + 41H_2O - 98e^- \rightarrow 21CO_2 + SO_4^{2-} + 100H^+ \quad \textbf{(5.4)}$$

Decolouration, however, only requires cleavage of the conjugated system in the molecule and this is often achieved at an early stage of the oxidation process. Hence, it may only involve a few electrons.

With the cell and anodes employed, the time for 99% completion of a mass transport controlled reaction may be estimated from the equation:

$$\frac{c_{(t)}}{c_{(0)}} = \exp - \frac{k_m A t}{V} \quad \textbf{(5.5)}$$

where $c_{(0)}$ is the initial concentration of reactant, $c_{(t)}$ the concentration after time t, k_m the mass transport coefficient, A the total surface area of the anode, t the electrolysis time and V the volume of the solution.

Assuming a value of $k_m = 10^{-3}$ cm s^{-1}, the time calculated for 99% completion is approximately one hour. In reality, k_m may be lower and hence electrolysis times of a few hours may be expected. Also assuming mass transport control and complete oxidation, the limiting current density (j_L) for the oxidation of the dyes (1×10^{-4} M) is of the order.

$$\mathbf{j_L = nFk_mc} \qquad \textbf{(5.6)}$$
$$= \sim 1 \text{ mA cm}^{-2}$$

Hence, even at + 1.90 V, oxygen evolution contributes substantially to the current. The decolouration of all dyes was carried out using a constant potential at E = +1.90 V. Table 5.7 shows the results of the decolouration process of each dye in 0.5 M H_2SO_4 at Bi-PbO_2/Fe-F-PbO_2/Ti mesh electrode prepared from 1 M HNO_3 solution containing 10 mM Bi(III) + 500 mM Pb(II) on Fe-F-PbO_2/Ti mesh substrate (as SEM image shown earlier in figure 5.30) using a current density of 1 mA cm^{-2} for 240 min at 298 K.

Electrolysis time, t (min)	**Current density, j (mA cm^{-2})**			
	Reactive Blue 4 (dark blue)	**Methyl Orange (orange)**	**Bromothymol Blue (dark orange)**	**Cresol Red (red orange)**
0	3.0	2.7	2.8	2.8
15	2.9	1.4	2.8	2.7
30	2.9	1.1	2.6	2.7
60	2.8*	0.8	2.6	2.7
120		0.6	2.4	2.7
180		0.5	2.4*	2.6*
240		0.5		
300		0.5*		
Time to decolourize	~ 1 hour	~ 5 hours	~ 3 hours	~ 3 hours

Table 5.7: Current density vs time of electrolysis of four different dyes at Bi-PbO_2/Fe-F-PbO_2/Ti mesh using constant potential (E =+1.90 V). (*) completely decolourised

The decolouration of reactive blue 4 dye occurred within 1 hour while the other dyes took more than 3 hours to be decolourised. The current densities recorded throughout the decolouration of all dyes except methyl orange were quite constant during the whole electrolysis as shown in the table. This indicates that some of the current were used for O_2 evolution. However, for methyl orange, the current densities have greatly reduced with respect to electrolysis time. It is believed that more oxidation of this dye occur at the Bi-PbO_2 electrode as a slower production of O_2 was seen during the decolouration process of this dye as compared to other dyes. But, the time to be decolourised was longer than other dyes and this is probably the molecule of methyl orange adsorbed longer on the electrode before being oxidised or decolourised than other dye samples.

Table 5.8 compares the charge passed during the electrolyses with the theoretical charge for complete oxidation of the dyes (assuming no O_2 evolution). It can be seen that although decolouration is complete, total oxidation cannot have occurred. Studies of the products at this stage of oxidation as well as monitoring of TOC would be interesting but was not attempted. Likewise more complete electrolysis could be considered. At this stage in the project, the main issue was the stability of the PbO_2 coatings.

	Reactive Blue 4	**Methyl Orange**	**Bromothymol Blue**	**Cresol Red**
Charge Required for Complete Oxidation (C)	99	65	99	74
Total Charge Passed, Q (C)	10	14	27	29

Table 5.8: Comparison of theoretical charge for complete oxidation with charge passed during electrolysis for the decolouration of each dye at Bi-PbO_2/Fe-F-PbO_2/Ti mesh electrode applied at constant potential of E = +1.90 V.

An investigation on the chemical stability of the Bi-PbO_2/Fe-F-PbO_2/Ti mesh electrode during the electrolysis was also carried out. Figure 5.32a shows a SEM image of the electrode before electrolysis and figure 5.32b represents the image after electrolysis of reactive blue dye in 0.5 M H_2SO_4 for 1 hour at constant potential of E = +1.90 V. It is clearly seen that there is no change in the morphology of the electrode and no cubic crystals of $PbSO_4$ is seen on the image. The same morphology was observed by the SEM after electrolysis in 0.5 M H_2SO_4 for a few hours containing

other tested dyes. These observations show that the electrode was stable towards chemical reaction in sulphuric acid solution during the electrolysis process.

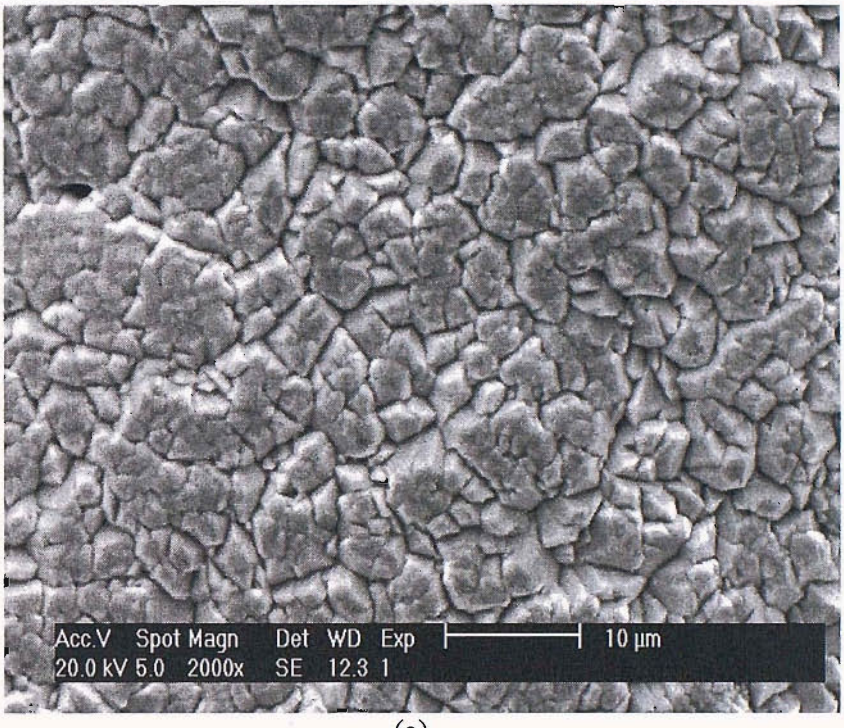

(a)

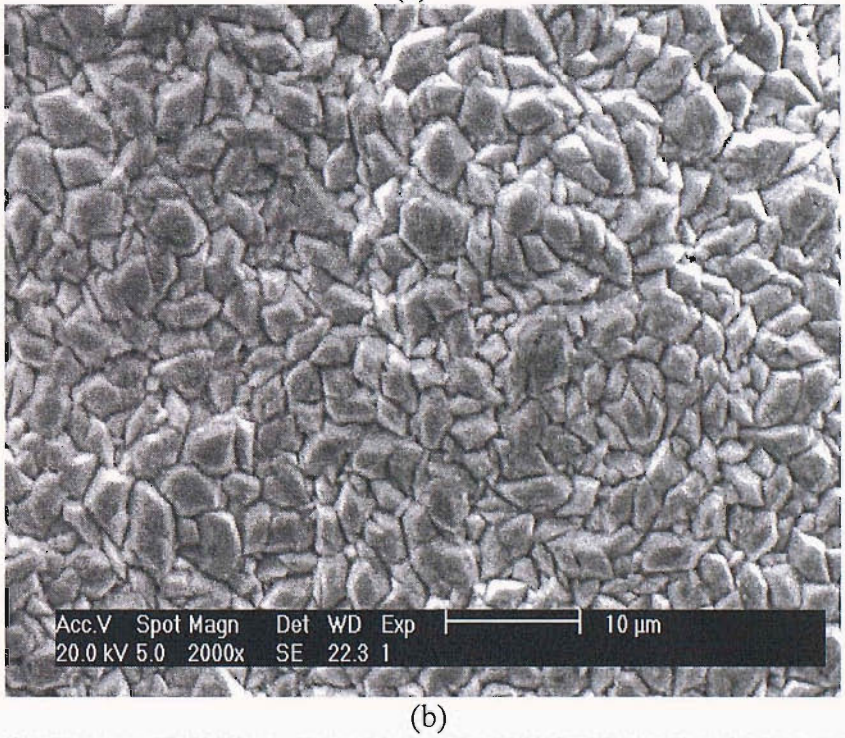

(b)

Figure 5.32: SEM images of Bi-PbO_2 electrode on Fe-F-PbO_2/Ti mesh substrate (a) before and (b) after electrolysis at constant potential E = +1.90 V for the decolouration of 1 x 10^{-4} M reactive blue (RB4) dye in 0.5 M H_2SO_4 for 1 hour.

Nevertheless, the electrode was found to be reduced or corroded if left standing on open circuit in sulphuric acid solution. Figure 5.33 shows the SEM image

of the Bi-PbO_2/Fe-F-PbO_2/Ti mesh after 1 hour immersion on open circuit in 0.5 M H_2SO_4 solution containing reactive blue dye. The image shows that the morphology of the electrode has changed from close-packed of angular crystals (see figure 5.32a) to more loose structure with the presence of cubic crystals believed to be $PbSO_4$. This indicates that the PbO_2 dissolves in the sulphuric acid as Pb(II) and forming $PbSO_4$ with sulphate ions as shown earlier in Scheme 1.

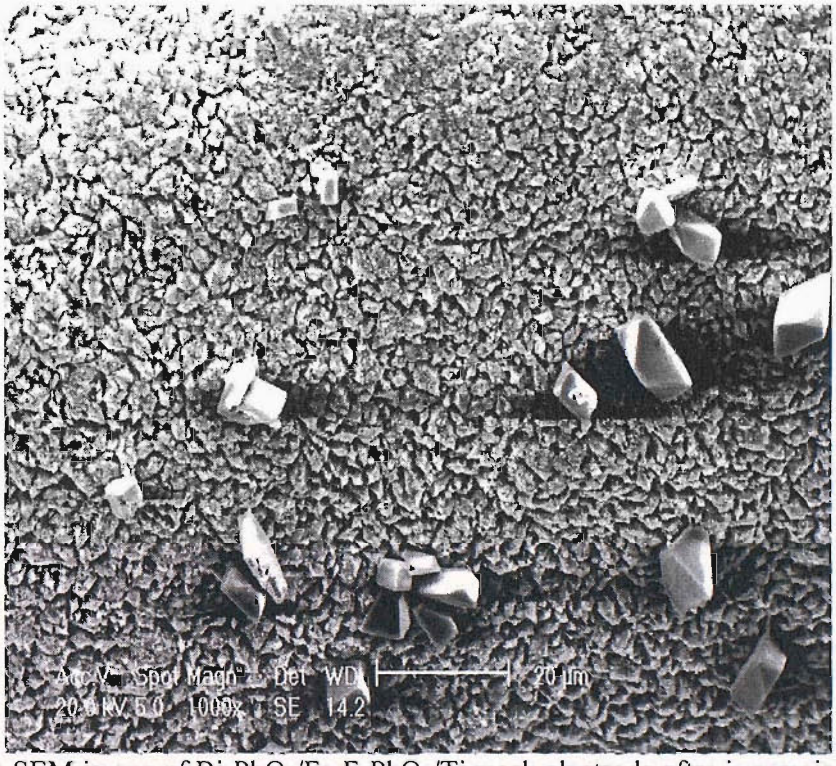

Figure 5.33: SEM image of Bi-PbO_2/Fe-F-PbO_2/Ti mesh electrode after immersion for 1 hour on open circuit in 0.5 M H_2SO_4 solution containing reactive blue dye.

Conclusions

It is concluded that the deposition of PbO_2 deposits onto Ti substrates was not as easily carried out as on gold substrate due to the formation of TiO_2 layer on Ti surface during the deposition process. It is shown that the pre-treatment of the Ti surface by chemical etching process prior to PbO_2 deposition is crucial in order to remove the passive layer of TiO_2 from the surface and to make the surface rough for good adherence of the PbO_2 deposit. The addition of F^- ions has also improved the adhesion quality of the PbO_2 deposits onto Ti substrate.

Cyclic voltammetry studies of the Ti surface oxidation revealed that more TiO_2 was formed during anodic polarization in 1 M HNO_3 than in 0.1 M HNO_3 solution. The presence of F^- ions in 0.1 M HNO_3 solution has reduced further the formation of the TiO_2 layer. A thick layer of TiO_2 on Ti surface led to the decrease in conductivity of the produced PbO_2 deposits.

It is concluded that physically stable, conducting and active PbO_2 electrodes can be electrodeposited on Ti substrates from low concentration of nitric acid of high concentration of Pb^{2+} containing either only NaF or NaF + Fe(III) (ie: F-PbO_2 or Fe-F-PbO_2 electrodes). They also appear ideal as substrates for further electrodeposition of active Bi-PbO_2 electrodes prepared from 1 M HNO_3.

The use of interlayer (ie: Fe-F-PbO_2) between Ti substrates and Bi-PbO_2 electrodes is a successful method in order to make the deposition of conducting and active Bi-PbO_2 electrodes onto Ti possible. The catalytic activity for the oxidation of DMSO increases with increasing Bi content in the PbO_2 deposits, but also for O_2 evolution. Bi-PbO_2 electrode on Fe-F-PbO_2/Ti prepared from 10 mM Bi(III) + 500 mM Pb(II) in 1 M HNO_3 was an adherent and a good deposit with high activity for DMSO oxidation and a low current for O_2 evolution.

The Bi-PbO_2 electrode can also be prepared on three dimensional substrate (ie: Ti mesh) and the interlayer (ie: Fe-F-PbO_2) is required prior to Bi-PbO_2 deposition to make the electrode conducting. The same morphology and electrochemical behaviour were observed for Bi-PbO_2 on Ti mesh as compared to Bi-PbO_2 on Ti disc. The Bi-PbO_2/Fe-F-PbO_2/Ti mesh can also be used for dyes decolouration. It was found that all tested dyes were decolourised at this electrode but at different rates. However, the electrode was not chemically stable after left standing on open circuit in sulphuric acid solution containing dye.

Good adhesion and active PbO_2 films electrodeposited on Ti substrates, as compared to Au, are significant advantages for applications to large-scale electrolytic processes in terms of cost. Even though the produced PbO_2 deposits on Ti substrate was good in adhesion but their stability in aqueous solution on open circuit is not very good and a problem during applications. Hence, the active PbO_2 can be useful as anode materials for the oxidation of organic compounds if they are used at potentials positive to the formal potential of the PbO_2/Pb(II) couple and immediately washed after use and never left standing for a long time on open circuit.

Chapter 6: Conclusions and Further Work

Studies of the electrodeposition of pure and doped PbO_2 from acidic nitrate baths onto both gold and titanium substrates have been extended. It has been shown that the morphology of the PbO_2 deposits depends strongly on the composition of the electroplating bath (concentrations of lead (II) and acid, presence of cationic and anionic dopants) and other deposition parameters such as temperature, current density and deposition time. Properties such as adhesion also depend strongly on the substrate. In fact, good quality PbO_2 deposits were easily achieved on gold but not on titanium. The presence of a pre-existing TiO_2 layer and/or the further formation of a passive layer of TiO_2 at positive potentials leads to PbO_2 coated anodes with a high resistance and poor adhesion. The fabrication of satisfactory PbO_2/Ti anodes required (a) initial etching the Ti substrate in boiling oxalic acid (b) use of a bath with a low nitric acid concentration and addition of F^- ions to minimise anodic formation of TiO_2 during the deposition (c) selection of appropriate additives (F^-, Fe^{3+}), at least for an underlayer in contact with the titanium substrate.

Scanning electron microscopy shows remarkable differences in the morphology of the PbO_2 deposits – uniform angular crystallites, uniform overlapping hemispheres and less ordered morphologies were all observed depending on the conditions. The most stable and adherent PbO_2 deposits on smooth gold substrates were prepared from high concentration of Pb (II) (ie: 500 mM Pb (II)) using a low current density (ie: < 5 mA cm^{-2}) at an elevated temperature (ie: 333 K). However, on Ti substrate, where a rough surface of the substrate is required to produce a good adhesion and long-lasting PbO_2 electrodes, higher charges were essential for uniform layers and a higher current density at room temperature was found to be beneficial. As noted above, etching and the addition of F^- ions in the plating solution also helped in improving the adhesion quality of the PbO_2 on the Ti substrate.

It was confirmed that, in general, the electrocatalytic activity of the PbO_2 electrodes for the oxidation of organic compounds is significantly enhanced with the incorporation of dopant cations and bismuth was found to be the preferred metal. The addition of Bi (III) in the deposition solution has greatly increased the catalytic activity of PbO_2 electrodes for organic oxidations especially sulphur-containing compounds. Bi-PbO_2 on gold was easily produced on gold substrate. The production

of Bi-PbO_2 on gold with optimum activity and stability were prepared from 1 M HNO_3 solution containing 10 mM Bi(III) + 500 mM Pb(II) using a current density of 5 mA cm^{-2} at 333 K. On Ti substrate, an underlayer (either F-PbO_2 or Fe-F-PbO_2) prepared from 0.1 M HNO_3 was necessary before the Bi-PbO_2 coating was plated from 1 M HNO_3. A high resistance Bi-PbO_2/Ti electrode was produced if no underlayer was coated earlier due to a thick layer of TiO_2 formed during the deposition of Bi-PbO_2 from 1 M HNO_3 (bismuth (III) is hydrolysed in 0.1 M HNO_3).

With all PbO_2 coatings, it was found that decomposition occurred when such electrodes were left in an electrolyte solution on open circuit. Decomposition was particularly rapid when the electrolyte contained a species subject to chemical oxidation by PbO_2. The spontaneous decomposition appeared to occur either by very slow dissolution as Pb (IV) or more rapid reduction to Pb (II). The latter was most obvious in sulphuric acid media when cubic $PbSO_4$ crystals were observed by scanning electron microscopy. The rate of decomposition of the PbO_2 layers depended on the electrolyte, morphology of the PbO_2 layer and the additives present. In contrast, the PbO_2 layers were stable when used as anodes or simply when the potential was held at a potential above formal potential of Pb^{2+}/PbO_2 couple. When used as anodes, the PbO_2 coated materials must be removed from the electrolyte, washed with water and dried as soon as the current is interrupted. This is not a convenient strategy in industrial practice; approaches akin to trickle charging could, however, be investigated.

Highly ordered, high porosity and high surface area PbO_2 deposits were successfully produced on gold by deposition into self assembled layers of polystyrene microspheres. It was found that this porous PbO_2 layer led to a high rate for the oxidation of DMSO. This high activity was attributed to more active sites available on the porous structure for the adsorption of reactant and the oxidation to take place. This approach was, however, discontinued because it was considered unlikely that the polystyrene microspheres would form ordered structures on the etched titanium and because the PbO_2 layers rapidly disintegrated on open circuit.

As a first stage to the fabrication of three dimensional PbO_2 anodes, extended area materials were prepared by deposition onto fine Ti meshes. Stacks of such meshes in a flow cell could then form a genuine three dimensional electrode that could find application in effluent treatment. The preferred conditions concluded from the experiments with Ti discs were found to produce satisfactory coated meshes

although it was advantageous to use lower current densities at the meshes (to improve current distribution); uniform coatings with good adhesion and stability could be fabricated. Again, a double coating with an Fe-F-PbO_2 underlayer and Bi-PbO_2 top layer was the preferred approach.

A preliminary study to assess the suitability of these coated mesh electrodes for effluent treatment revealed significant activity for the decolouration of dyes. The decolouration of all four tested dyes was successfully achieved by the direct oxidation at the fabricated Bi-PbO_2/Fe-F-PbO_2/Ti mesh electrodes. Although TOC, COD and intermediate oxidation products was not monitored, preliminary evidence is presented that the oxidation of reactive blue 4 underwent mass transport controlled decolouration with parallel oxygen evolution. In the cases of the other three dyes, there appears to be slow chemical steps in the sequence leading to decolouration. Moreover, the electrodes were stable if handled carefully. Several electrolyses without change to the coating were possible if they were removed and washed immediately each electrolysis was terminated.

The next stage in the development of three dimensional electrodes would be the construction of stacked meshes and an appropriate flow cell. This would permit more rapid electrolysis and allow trials of complete oxidation to be carried out. It would also allow more reliable assessment of the stability of the PbO_2 coated titanium anodes on load by carrying out extended electrolysis runs with monitoring of both the electrolyte for lead (II) and the surface by electron microscopy.

Overall, the goal of stable but active PbO_2 coatings on titanium has been partially achieved but industrially useful anodes will require further development.

References

1. V. Montiel, V. Garcia-Garcia, J. Gonzalez-Garcia, J.R. Perez-Mallol, G. Sanchez-Cano and A. Aldaz, J. New Mater. Electrochem. Systems, 3 (2000) 269

2. K. Juttner, U. Galla and H. Schmieder, Electrochim. Acta, 45 (2000) 2575

3. Ch. Comninellis, Electrochim. Acta, 39 (1994) 1857

4. P. Ribordy, C. Pulgarin, J. Kiwi and P. Peringer, Water Sci. Tech., 35 (1997) 293

5. E. Plattner and C. Comninellis, in "Process Technologies for Water Treatment", Editor S. Stucki, Plenum Press, 1988

6. C. Walling, Acc. Chem. Res., 8 (1975) 125

7. N. Al-Hayek and S. Dore , Environ. Tech. Lett., 6 (1985) 37

8. L.J. Zeman and A.L. Zydney, Microfiltration and Ultrafiltration: Principles and Applications, Marcel Dekker, New York, 1996

9. F. Banata and N. Al-Bastakib, Desalination, 170 (1) (2004) 69

10. G Nakhla, A. Lugowski, J. Patel and V. Rivest, Bioresource Tech., 97 (1) (2005) 1

11. T. Mohammadi and A. Esmaeelifar, J. Membrane Sci., 254 (2005) 129

12. P. Tatapudi and J. M. Fenton, in "Environmental Oriented Electrochemistry", Editor C. A. C. Sequeira, Elsevier, 1994

13. K. Rajeshwar and J. G. Ibanez, Environmental Electrochemistry; Fundamentals and Applications in Pollution Abatement, Academic Press Inc., CA, 1997

14. R. Kotz, S. Stucki and B. Carcer , J. Appl. Electrochem., 21 (1991) 14

15. S. Stucki , R. Kotz, B. Carcer and W. Suter, J. Appl. Electrochem., 21 (1991) 99

16. Ch. Comninellis and C. Pulgrin, J. Appl. Electrochem., 21 (1991) 703

17. J. Feng and D. C. Johnson, J. Electrochem. Soc., 138 (1991) 3328

18. O.J. Murphy, G.D. Hitchens, L. Kaba and C.E. Verostko, Wat. Res., 26 (1992) 443

19. A.M. Polcaro, S. Palmas, F. Renoldi and M. Mascia, J. Appl. Electrochem., 29 (1999) 147

20. J.D. Roogers, W. Jedral and N.J. Bunce, Environ. Sci. Technol., 33 (1999) 1453

21. M.S. Urete-Zanertu, P. Bustos, M.C. Diez, M.L. Mora and C. Gutierrez, Electrochim. Acta, 46 (2001) 2545

22. M. Fleischmann, D. Pletcher and A. Rafinski, J. Appl. Electrochem., 1 (1971) 1

23. C. Zawodzinski, W. Smith and K. Martinez, in " Environmental Aspects of Electrochemistry and Photoelectrochemistry", Editors M. Tomkiewicz, H. Yoneyama, R. Haynes and Y. Hori, The Electrochemical Society, New Jersey, 1993

24. D.F. Steele, Electrochemistry and Waste Disposal, Chem. Br. 27(1991) 915

25. R.W. Coughlin and M. Farooque, Nature, 249 (1979) 301

26. P.M. Dhooge, D.E. Stillwell and S.M. Park, J. Electrochem. Soc., 129 (1982) 1719

27. K. Rajeshwar, J. G. Ibanez and G. M. Swain, J. Appl. Electrochem., 24 (11) (1994) 1077

28. A. T. Kuhn, in "Electrochemistry of Cleaner Environments", Editor J. O. M. Bockris, Plenum Press, New York (1972)

29. L. Szpyrkowicz, J. Naumczyk and F. Zilio-Grandi, Wat. Res., 29 (1995) 517

30. K. Vijayaraghavan, T. K. Ramanujam and N. Balasubramaniam, J. Environ. Eng., 124 (1998) 887

31. A. G. Vlyssides and C. J. Israilides, J. Environ. Sci. Health, A33 (1998) 847

32. J. Naumczyk, L. Szpyrkowicz and F. Zilio-Grandi, Water Sci. Tech., 34 (1996) 17

33. C. J. Israilides, A. G. Vlyssides, M. Loizidou, V.N. Mourafeti and G. Karvouni, Bioresource Technol., 61 (1997) 163

34. US Patents No. 4,316,782; 4,375,395 and 4,541,989

35. P. C. Foller and M. L. Goodwin, Ozone Science and Engineering, 6 (1984) 29

36. S. Stucki, G. Theis, R. Kötz, H. Devantay and H. J. Christen, J. Electrochem. Soc., 132 (1985) 367

37. J. –S. Do and C. –P. Chen, J. Electrochem. Soc., 140 (1993) 1632

38. E. Yeager, Electrochim. Acta, 29 (1984) 1572

39. D. Wabner and C. Grambow, Vom Wasser, 60 (1983) 181

40. R. Tomat and A. Vecchi, J. Appl. Electrochem., 1 (1971) 185

41. R. Tomat and A. Rigo, J. Appl. Electrochem., 6 (1976) 257

42. R. Tomat and A. Rigo, J. Appl. Electrochem., 10 (1980) 549

43. T. Matsue, M. Fujihira and T. Osa, J. Electrochem. Soc., 128 (1981) 2565

44. K. Otsuka, M. Kunieda and H. Yamagata, J. Electrochem. Soc., 139 (1992) 2381

45. I. Yamanaka, T. Akimoto and K. Otsuka, Electrochim. Acta, 39 (1994) 2545

46. R. Tomat, R. Salmaso and S. Zecchin, Electrochim. Acta, 39 (1994) 2475

47. D. Pletcher and F. C. Walsh, Industrial Electrochemistry, Chapman and Hall, London, 1990

48. C. Oloman and A.P. Watkinson, J. Appl. Electrochem., 9 (1979) 1885

49. J.A. McIntyre, Interface, 4 (1995) 29

50. P.C. Foller and R.T. Bombard, J. Appl. Electrochem., 25 (1995) 613

51. F. Alcaide, E. Brillas, P-L. Cabot and J. Casado, J. Electrochem. Soc., 145 (1998) 3444

52. E. Brillas, R.M. Bastida, E. Llosa and J. Casado, J. Electrochem. Soc., 142 (1995) 1733

53. A. Alvarez-Gallegos and D. Pletcher, Electrochim. Acta, 44 (1998) 853

54. T. Harrington and D. Pletcher, J. Electrochem. Soc., 146 (1999) 2983

55. A.M. Couper, D. Pletcher and F.C. Walsh, Chem. Rev., 90 (1990) 837

56. D. Devillers, M.T. Dinh Thi, E. Mahe and Q. Le Xuan, Electrochim. Acta, 48 (2003) 4301

57. M. Gattrell and D.W. Kirk, J. Electrochem. Soc., 140 (1993) 1534

58. L. Marinerc and F.B. Lectz, J. Appl. Electrochem., 8 (1978) 335

59. F. Vigo, L. Avalle and M. De Paz, La Rivista Italiana Sostanze Grasse, 60 (1983) 125

60. D Gandini, P A Michaud, I Duo, E Mahe, W Haenni, A Perret, Ch. Comninellis, New Diamond Carbon Technol., 9 (1999) 303

61. A. J. Saterlay, J. S Foord, R. G Compton, Analyst, 124 (1999) 1791

62. Q Y Chen, M. C Granger, T.E Lister, G. M. Swain, J Electrochem Soc., 144 (1997) 3806

63. F. Okino, H Shibata, S. Kawasaki, H. Touhara, K. Momota, M. Nishitani-Gamo, L Sakaguchi, T Ando, Electrochem Solid State Lett., 2 (1999) 382

64. F. Marken, Y-C. Tsai, A.J. Saterlay, B.A. Coles, D. Tibbets, K. Holt, C.H. Goeting, J.S.Foord and R.G. Compton, J. Solid State Electrochem 5 (2001) 313

65. A. J. Saterlay, S.J. Wilkins, K.B.Holt, J.S. Foord, R.G. Compton and F. Marken, J. Electrochem. Soc., 148 (2) (2001) E66

66. Ch. Comninellis and C. Pulgrin, J. Appl. Electrochem., 23 (1993) 108

67. Ch. Comninellis and A. Nerini, J. Appl. Electrochem., 25 (1995) 23

68. L. Lipp and D. Pletcher, Electrochim. Acta, 42(7) (1997) 1091

69. N. Winograd in ' Laboratory Techniques in Electroanalytical Chemistry', Eds. P.T. Kissinger and W.R. Heineman, Marcel Dekker, New York, 1984

70. J.S. Clarke, R.E. Ehigamusoe and A.T. Kuhn, J. Electroanal. Chem., 70 (1976) 333

71. D. Pletcher and S.J.D. Tait, J. Appl. Electrochem., 11 (1981) 493

72. J. Feng and D.C. Johnson, J. Electrochem. Soc., 137 (1990) 507

73. M. Chettiar and A. P. Watkinson, Can. J. Chem. Eng., 61 (1983) 568

74. H. Sharifian and D.W.Kirk, J. Electrochem. Soc., 133 (1986) 921

75. V. Smith de Sucre and A. P. Watkinson, Can. J. Chem. Eng., 59 (1981) 52

76. Y.-L.Hsiao, J.E.Vitt and D.C.Johnson, J.Electrochem. Soc., 139 (1992) 377

77. I.F. McConvey, K.Scott, J.M.Henderson and A.N. Haines, Chem Eng. Process, 22 (1987) 231

78. N. B. Tahar and A. Savall, J. Appl. Electrochem., 29 (1999) 277

79. B. Fleszar and J. Ploszynska, Electrochim. Acta, 30 (1985) 31

80. D.C. Johnson, H. Chang, J. Feng and W. Wang, in Electrochemistry for Cleaner Environment, eds. J.D. Genders and N.L.Weinberg, The Electrosynthesis Company Inc., New York, 1992

81. K. Kawagoe and D.C. Johnson, J. Electrochem. Soc., 141 (1994) 3404

82. A. T. Kuhn, Editor, 'The Electrochemistry of Lead', Academic Press, London, (1979) 217

83. S.E. Treimer, J. Feng, M.D. Scholten, D.C. Johnson and A.J. Davenport, J. Electrochem. Soc., 148 (12) (2001) E459

84. I. Petersson, E. Ahlberg and B.Berghult, J. Power Sources, 76 (1998) 98

85. D. W. Kirk, H. Sharifian and F.R. Foulkes, J. Appl. Electrochem. 15, (1985) 285

86. N. Vatistas and S. Cristofaro, Electrochem. Commun., 2 (2000) 334

87. J. Lee, H. Varela, S. Uhm and Y. Tak, Electrochem. Commun. 2 (2000) 646

88. S. Abaci, K. Pekmez, T. Hokelek and A. Yildiz, J. Power Sources, 88 (2000) 232

89. A.B. Velichenko, D.V. Girenko, S.V. KoKovalyov, A.N. Gnateko, R.Amadelli and F.I.Danilov, J. Electroanal. Chem., 454 (1998) 203

90. R. Amadelli, L. Armelao, E. Tondello, S. Daolio, M. Fabrizio, C. Pagura and A.B. Velichenko, Appl. Surf. Sci., 142 (1999)200

91. M. Musaini, F. Furlanetto and P. Guerriero, J. Electroanal. Chem., 440, (1997) 131

92. M. Musaini, F. Furlanetto and P. Guerriero, J. Electroanal. Chem., 465 (1999) 160

93. Y. Matsumoto, M. Noguchi and T.Matsunaga, J. Phys. Chem., 103 (1999) 117

94. H. Chang and D.C. Johnson, J.Electrochem.Soc., 136, 1989, 17

95. A.B. Velichenko, D.V. Girenko and F.I. Danilov, J. Electroanal. Chem. 405 (1996) 127

96. D. Velayutham and M. Neol, Electrochim. Acta, 36 (1991) 2031

97. M. Fleishmann and M. Liler, Trans. Faraday Soc., 54 (1958) 1370

98. B.J. Hwang, R. Santhanam and Y.W. Chang, Electroanalysis, 14 (2002)363

99. A.B. Velichenko, R. Amadelli, A. Benedetti, D.V. Girenko, S.V. Kovalyov and F.I. Danilov, J. Electrochem. Soc., 149 (2002) C445

100. M. Ueda, A.Watanabe, T. Kameyama, Y. Matsumoto, M. Sekimoto and T. Shimamune, J. Appl. Electrochem, 25 (1995) 817

101. C. N. Ho and B.J. Hwang, Electrochim. Acta, 38 (1993) 2749

102. J. E. Graves, D. Pletcher, R.L. Clarke and F.C. Walsh, J. Appl. Electrochem., 21 (1991) 848

103. J.E. Graves, D. Pletcher, R.L.Clarke and F.C. Walsh, J. Appl. Electrochem. 22 (1992) 200

104. A. Czerwiński and M. Zelazowska, J. Electroanal. Chem. 410 (1996) 55

105. A. Czerwiński and M. Zelazowska, J. Power Sources, 64 (1997) 29

106. A. H. Ras and J. F. Van Staden, J. Appl. Electrochem. 29 (1999) 313

107. A. de Oliviera-Sousa, M.A.S da Silva, S.A.S Machado, L.A. Avaca and P.de Lima-Neto, Electrochim. Acta, 45 (2000) 4467

108. H.B. Beer, DDR-Pat. 55223.Belg. Pat. 710551

109. Ch. Comninellis and G. P. Vercesi, J. Appl. Electrochem., 21 (1991) 335

110. G.P. Vercesi, J. Rolewicz and Ch. Comninellis, Thermochim Acta, 176 (1991) 31

111. M. Pusphavanam and S.R. Natarajan, Metal Finishing, June 1994, 85

112. J. Gonzalez-Garcia, J. Iniesta, E. Exposito, V. Garcia-Garcia, V. Montiel and A. Aldaz, Thin Solid films, 352 (1999) 49

113. D. Gilroy and R. Stevens, J. Appl. Electrochem., 10 (1980) 511

114. Ch. Comninellis and E. Plattner, J. Appl. Electrochem., 12 (1982) 395

115. H. Devantay, R. Kotz, C. Schuler and S. Stucki, Switer. Pat. 665429

116. D. W. Wabner, H.P.Fritz and R. Huss, Chem. Ing. Technol. 49 (1977) 329

117. J. Gonzalez-Garcia, G. Sanchez-Cano, A. Aldaz, V. Monteil and J.L.G. Fierro, Appl. Surf. Sci., 78 (1994) 457

118. M. E. Heron, D. Pletcher and F.C. Walsh, J. Electroanal. Chem.,332 (1992)183

119. I. –H. Yeo, Y.S. Lee and D.C. Johnson, Electrochim. Acta, 37 (1992) 1811

120. A.B. Velichenko, D.V.Girenko and F.I. Danilov, Electrochim. Acta, 40 (1995) 2803

121. K. Pamplin and D.C. Johnson, J.Electrochem. Soc, 143 (1996) 2119

122. P. Ruetschi, J. Sklarchuk and R.T.Angstadt, Electrochim. Acta, 8 (1963) 333

123. P.K.Shen and X.L.Wei, Electrochim. Acta., 48 (2003) 1743

124. H. Bode, Lead-Acid Batteries, Wiley, New York, 1977

125. R. Amadelli, A. Maldotti, A. Molinari, F.I.Danilov and A.B.Velichenko, J. Electroanal. Chem. 534 (2002) 1

126. D. Pavlov and B. Monahov, J. Electrochem. Soc. 143 (1996) 3616

127. N. Munichandraiah and S. Sathyanarayana, J. Appl. Electrochem. 18 (1988) 314

128. S. Abaci, U. Tamer, K. Pekmez and A. Yildiz, Appl. Surf. Sc. 240 (2004) 112

129. J.C.K. Ho, G. T. Filho, R. Simpraga and B. E. Conway, J. Electroanal. Chem., 366 (1994) 147

130. S.A. Campbell and L.M. Peter, J. Electroanal. Chem., 306 (1991) 185

131. H. Chang and D.C. Johnson, J. Electrochem. Soc., 136 (1989) 23

132. J.B. Cotton, Werkst. Korros., 11 (1960) 152

133. Y. Matsumoto, M. Nogchi and T. Matsunaga, J. Phys. Chem. B, 103 (1999) 7190

134. M. Fleischmann, J.R. Mansfield, H.R. Thirsk and H.G.E. Wilson, Electrochim. Acta., 12 (1967) 967

135. J.Feng, D.C.Johnson, S.N.Lowery and J.J.Carey, J. Electrochem. Soc., 141 (1994) 2708

136. A.B.Velichenko, R.Amadelli, E.A.Baranova, D.V. Girenko and F.I. Danilov, J. Electroanal. Chem., 527 (2002) 56

137. I.-H. Yeo, S. Kim, R.Jacobson and D.C. Johnson, J. Electrochem. Soc., 136 (1989) 1395

138. J. Iniesta, J.Gonzalez-Garcia, E. Exposito, V. Montiel and A.Aldaz, Wat. Res., 35 (2001) 3291

139. I.-H. Yeo and D.C. Johnson, J.Electrochem. Soc., 134 (1987) 1973

140. Y.-L. Hsiao and D.C. Johnson, J. Electrochem. Soc., 136 (1989) 3704

141. U. Casellato, S. Cattarin and M. Musaini, Electrochim. Acta , 48 (2003) 3991

142. M. Musaini, Chem. Commun. 2403 (1996)

143. M. Musaini and P. Guerriero, Electrochim. Acta, 44 (1998) 1499

144. R. Bertoncello, S. Cattarin, I. Frateur and M. Musaini, J. Electroanal. Chem. 492 (2000) 145

145. P.J. Blood, I.J. Brown and S. Sotiropoulus, J. Appl. Electrochem., 34 (2004) 1

146. H. Yan, C.F. Blandford, B.T. Holland, W.H. Smyrl and A. Stein, Chem. Material, 12 (2003)1134

147. A. Stein and R.C. Shroden, Solid State and Material Sc., 5 (2001) 553

148. P.N. Bartlett, T. Dunford and M.A. Ghanem, J. Mat. Chem., 12 (2002) 3130

149. F.C. Walsh, 4th International Symposium on Frontiers of Electrochemistry (SAEST), Madras, 1989

150. G. Tremiliosi-Filho, L.H. Dall Antonia and G. Jerkiewicz, J. Electroanal. Chem., 422 (1997) 149

151. Z. Jusys and S. Bruckenstein, Electrochem. Solid-State Lett., 1 (1998) 74

152. H. Chang and D.C. Johnson, J. Electrochem. Soc., 137 (1990) 3108

153. P.J. Goodhew, J. Humphreys and R. Beanland, 'Electron Microscopy and Analysis', 3rd Ed., Taylor & Francis, 2001, pg.175

154. Y.-L. Hsiao, PhD Dissertation, Iowa State University, Ames, IA, 1990

155. H. Chang and D.C. Johnson, Anal. Chim Acta, 248 (1991) 85

156. J.S. Gordon, V.G. Young and D.C. Johnson, J. Electrochem. Soc., 141 (1994) 3404

157. P.N. Bartlett, P.R. Birkin and M.A. Ghanem, Chem. Comm., (2000) 1671

158. P.N. Bartlett, M.A. Ghanem, I.S. El Hag, P. de Groot and A. Zhukov, J. Mater. Chem., 13 (2003) 2596

159. J.C. Grigger, H.C. Miller and F.D. Loomis, J. Electrochem. Soc., 105 (1958) 100

160. J. Feng and D.C. Johnson, J. Appl. Electrochem., 20 (1990) 116

161. R. Lartney, PhD Thesis, Salford University, 1976

162. N. Hampson and C. Bushrod, Brit. Corrossion J., 6 (1971) 129

163. D. Pletcher in A First Course in Electrode Processes, Alresford Press Ltd., Hampshire, 1991

164. A.B. Velichenko, R.Amadelli, G.L. Zucchini, D.V. Girenko and F.I. Danilov, Electrochim. Acta, 45 (2000) 4341

165. N.D. Popović, J.A. Cox, D.C. Johnson, J. Electroanal. Chem., 455 (1998) 153

166. N.D. Popović, D.C. Johnson, Anal. Chem., 70 (1998) 468

167. W.R. LaCourse, Y.-L. Hsiao, D.C. Johnson, and W.H. Weber, J. Electrochem. Soc., 136 (1989) 3714

168. V.A.Alves, L.A. da Silva, J.F.C. Boodts and S. Trasatti, Electrochim. Acta., 39 (1994) 1585

169. A.I. Onuchukwu and S. Trasatti, J. Appl. Electrochem., 21 (1991) 858

170. American National Standards Institute Report, Number G 53.18 1970 : ASTM Designation: B481 -68

171. L.Lipp, PhD Thesis, University of Southampton, 1996

172. R. Amadelli and A.B. Velichenko, J. Serb. Chem. Soc., 66(11-12) (2001) 835

173. R.Amadelli, L. Armelao, A.B. Velichenko, N.V. Nikolenko, D.V. Girenko, S.V. Kovalyov, F.I. Danilov, Electrochim. Acta, 45 (1999) 713

174. Y. Mohd and D. Pletcher, J. Electrochem. Soc., 152, (2005) D97

175. P.A. Carneiro, M.E. Osugi, C.S. Fugivara, N. Boralle, M. Furlan and M.V.B. Zanoni, Chemosphere, 59 (2005) 431

Appendix A

Estimation of charge required to deposit a PbO_2 film of half a sphere layer thick on 0.008 cm^2 gold substrate:

Diameter of polystyrene sphere: 500 nm

Volume of unstructured PbO_2 = electrode surface area x film thickness
i.e. $= \pi r^2 \times r$ (where r = the radius of the template spheres)
$= 0.008\ cm^2 \times (2.5 \times 10^{-5}\ cm)$
$= 2 \times 10^{-7}\ cm^3$

Number of spheres at the electrode surface
= (electrode surface area/cross-sectional area of a sphere) x 0.9^{i}
$= (0.008\ cm^2 / 1.963 \times 10^{-9}\ cm^2) \times 0.9$
= 3,667,855

Volume of a sphere = $4/3\ \pi r^3 = 6.54 \times 10^{-14}\ cm^3$

Volume of PbO_2 deposit occupied by spheres (Total spheres volume)
= (number of spheres x volume of sphere) / 2
$= (3{,}667{,}855 \times 6.54 \times 10^{-14}) / 2$
$= 1.19 \times 10^{-7}\ cm^3$

Total volume of PbO_2 = unstructured PbO_2 volume – total sphere volume
$= 2 \times 10^{-7}\ cm^3 - 1.19 \times 10^{-7}\ cm^3$
$= 8.1 \times 10^{-8}\ cm^3$

Moles of PbO_2 = (total volume of gold x density) / molecular weight
$= (8.1 \times 10^{-8}\ cm^3 \times 9.3\ g\ cm^{-3}) / 240\ g\ mol^{-1}$
$= 3.14 \times 10^{-9}$ moles

Deposition Q = mnF (where m = moles, n= number of electrons and F = Faraday constant)

$= 3.14 \times 10^{-9}\ mol \times 2 \times 96485\ C\ mol^{-1}$
$= 6.06 \times 10^{-4}\ C$

Therefore, 6.06×10^{-4} C deposition charge is required to deposit half a sphere layer thick (~ 250 nm) of PbO_2 on 0.008 cm^2 gold substrate.

[i]2D hexagonal packing efficiency = 90%